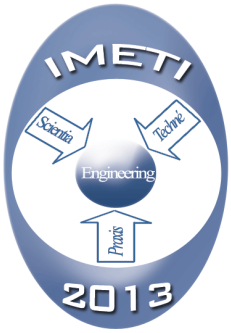

The 6th International Multi-Conference on Engineering and Technological Innovation

July 9 - 12, 2013 – Orlando, Florida, USA

PROCEEDINGS

Post-Conference Edition

Edited by:

Nagib Callaos
Hsing-Wei Chu
Belkis Sánchez
Michael J. Savoie
Andrés Tremante

Organized by

International Institute of Informatics and Systemics

Member of the International Federation for Systems Research (IFSR)

COPYRIGHT

The papers of this book comprise the proceedings of the conference mentioned on the title and the cover page. They reflect the authors' opinions and, with the purpose of timely disseminations, are published as presented and without change. Their inclusion in these proceedings does no necessarily constitute endorsement by the editors.

ISBN: 978-1-936338-92-4 (Post-Conference Edition)

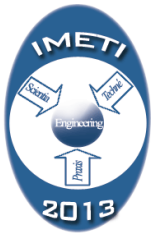

PROGRAM COMMITTEE

Chairs: Hsing-Wei Chu (USA) and C. Dale Zinn (USA)

Adascalitei, Adrian	Gheorghe Asachi Technical University of Iaşi	Romania
Aguilar Torres, Fernando J.	University of Almeria	Spain
Al Obaidy, Mohaned	Gulf College	Oman
Al-Aomar, Raid	Jordan University of Science and Technology	Jordan
Amelink, Catherine	Virginia Tech	USA
Ariwa, Ezendu	London Metropolitan University	UK
Ashraph, Sulaiman	National University of Rwanda	Rwanda
Ayuga Téllez, Esperanza	Polytechnic University of Madrid	Spain
Barberà, Elena	Open University of Catalonia	Spain
Batos, Vedran	University of Dubrovnik	Croatia
Bekiaris, Evangelos	The Centre for Research & Technology, Hellas	Greece
Bönke, Dietmar	Reutlingen University	Germany
Braghin, F.	Politecnico di Milano	Italy
Bubnov, Alexey	Academy of Sciences and the Czech Republic	Czech Republic
Cázares-Rangel, Víctor M.	Autonomous University of Nuevo Leon	Mexico
Chang, Maiga	Athabasca University	Canada
Chang, Wen-Kui	Tunghai University	Taiwan
Chen, Yuhua	University of Houston	USA
Cinquemani, S.	Politecnico di Milano	Italy
Curran, Kevin	University of Ulster	UK
Dawoud, Dawoud S.	Victoria University	Uganda
Elmasry, Sarah	United Arab Emirates University	UAE
Fúster-Sabater, Amparo	Institute of Applied Physics	Spain
Gegner, Jürgen	University of Siegen	Germany
Gohil, Dipakkumar	Sardar Vallabhbhai National Institute of Technology	India
Guerlesquin, Gaël	Université de Technologie Belfort-Montbéliard	France
Haggag, Mahmoud	United Arab Emirates University	UAE
Hepdogan, Seyhun	University of Central Florida	USA
Iovan, Stefan	Romanian Railway IT Company	Romania
Jazar, Reza N.	Royal Melbourne Institute of Technology University	Australia
Jesudoss, Auxeeliya	National University of Rwanda	Rwanda
Jingchao, Chen	University Donghua	China
Juanals, Brigitte	Université Paris Ouest Nanterre La Défense	France
Kobielarz, Magdalena	Wroclaw University of Technology	Poland
Koleva, Maria	Bulgarian Academy of Sciences	Bulgaria
Kothaneth, Shreya	Virginia Tech	USA
Kotnana, Ratnakar	National University of Rwanda	Rwanda
Kuipers, Ulrich	University of Applied Sciences Südwestfalen	Germany

Lahlouhi, Ammar	University of Biskra	Algeria
Lamastra P., Giovanna	IBMEC	Brazil
Lappas, Georgios	Technological Institute of Western Macedonia	Greece
Lefevre, Thierry	CEERD	Thailand
Li, Longzhuang	Texas A&M University	USA
Li, Man-Sze	IC Focus Ltd.	UK
Litvin, Vladimir	California Institute of Technology	USA
López Román, Leobardo	University of Sonora	Mexico
Luh, Guan-Chun	Tatung University	Taiwan
Machado Caldeira, André	Sulamerica	Brazil
Mahdjoub, Morad	Université de Technologie Belfort-Montbéliard	France
Mauntz, Manfred	CMC Instruments GmbH	Germany
Mbobi, Aime Mokhoo	Centennial College	Canada
Medevielle, Jean-Pierre	IFSTTAR	France
Minel, Jean-Luc	Université Paris Ouest Nanterre La Défense	France
Naddeo, Alex	University of Salerno	Italy
Nagai, Yasuo	Tokyo University of Information Sciences	Japan
Ngabonziza, Yves	The City University of New York	USA
Nožička, J.	Czech Technical University in Prague	Czech Republic
Oberer, Birgit	University of Klagenfurt	Austria
Okita, Yuji	Kanazawa Institute of Technology	Japan
Petit, Frédéric	Argonne National Laboratory	USA
Phillips, Steve	FEHRL Knowledge Centre	Belgium
Pillai, Krish	Lock Haven University of Pennsylvania	USA
Pursell, David	University System of Georgia	USA
Rai, Bharatendra K.	University of Massachusetts Dartmouth	USA
Resta, F.	Politecnico di Milano	Italy
Robinson, Ashley	Virginia Tech	USA
Sagot, Jean-Claude	Université de Technologie Belfort-Montbéliard	France
Sala, Nicoletta	University of Italian Switzerland	Italy
Schaetter, Alfred	Pforzheim University	Germany
Schumacher, Jens	University of Applied Sciences Vorarlberg	Austria
Shiraishi, Yoshiaki	Nagoya Institute of Technology	Japan
Siddique, Mohammad	Fayetteville State University	USA
Singh, Harwinder	Guru Nanak Dev Engineering College	India
Skawinska, Eulalia	Poznan University of Technology	Poland
Soares M. María Augusta	IBMEC	Brazil
Staretu, Ionel	Transilvania University of Brasov	Romania
Sulema, Yevgeniya	National Technical University of Ukraine	Ukraine
Suzuki, Hiroshi	GE Energy	Japan
Tam, Wing K.	Swinburne University of Technology	Australia
Thundat, Thomas	University of Alberta	Canada
Velázquez-Araque, Luis	Universidad Nacional Experimental del Táchira	Venezuela
Vinod, D. S.	Sri Jayachamarajendra College of Engineering	India
Vrána, Stanislav	Czech Technical University in Prague	Czech Republic
Yadav, S. M.	Sardar Vallabhbhai National Institute of Technology	India
Zalewski, Romuald I.	Poznan University of Technology	Poland
Zaretsky, Esther	Hebrew University	Israel
Zobaa, Ahmed	University of Exeter	UK

ADDITIONAL REVIEWERS

Abdelatif, Hassini	University of Science and Technology of Oran	Algeria
Abdelhamid, Tamer	Alexandria University	Egypt
Abou-Mesalam, Mamdouh	Atomic Energy Authority	Egypt
Acma, Bulent	Anadolu University	Turkey
Albayrak, Y. Esra	Galatasaray University	Turkey
Alhassan, Mohammad	Purdue University Fort Wayne	USA
Andreev, Rumen	Bulgarian Academy of Sciences	Bulgaria
Baker, John	Johns Hopkins University	USA
Balas, Valentina	Aurel Vlaicu University of Arad	Romania
Barreiro, Joaquín	University of Leon	Spain
Bayraktar, Emin	École Nationale Supérieure Publique d`Ingénieurs	France
Bayraktar, Seyfettin	Yildiz Technical University	Turkey
Bernardino, Jorge	Institute of Engineering of Coimbra	Portugal
Bigan, Cristin	Ecological University of Bucharest	Romania
Bilbao, Josu	IKERLAN	Spain
Bilich, Feruccio	University of Brasilia	Brazil
Bojcetic, Nenad	University of Zagreb	Croatia
Bouslimani, Yassine	University of Moncton	Canada
Branzila, Marius	Gheorghe Asachi Technical University of Iaşi	Romania
Camins, Angel Sevilla	University of Murcia	Spain
Carrió Pastor, M. Luisa	Polytechnic University of Valencia	Spain
Cavaro, Christine	University of Angers	France
Chauhan, K. A.	Sardar Vallabhbhai National Institute of Technology	India
Cheggour, Mohamed	Ecole Normale Superieure	Morocco
Chen, Jing-Heng	Feng Chia University	Taiwan
Chen, Ping-Hei	National Taiwan University	Taiwan
Chiou, Chuang Chun	Da-Yeh University	Taiwan
Chow, James	University Health Network	Canada
Chu, Hsing-Wei	Lamar University	USA
Ciftja, Arjan	SINTEF	Norway
Costa, Costas	Cyprus University of Technology	Cyprus
Cotet, Costel Emil	Polytechnic University of Bucharest	Romania
Csáki, Tibor	University of Miskolc	Hungary
Dijkstra, Jan	Eindhoven University of Technology	Netherlands
Drid, Saïd	University of Batna	Algeria
Elwany, Hamdy	Alexandria University	Egypt
Ersoy, A.	Istanbul University	Turkey
Fidan, Ismail	Tennessee Technological University	USA
Figueroa, José	IBM	USA
Fiorini, Rodolfo A.	Polytechnic Institute of Milan	Italy

Gallucci, Fausto	Eindhoven University of Technology	Netherlands
Ge, Mouzhi	Dublin City University	Ireland
Gheno, Simoni	Federal University of São Carlos	Brazil
Giardina, Marco	University of Neuchatel, Switzerland	Switzerland
Glossman-Mitnik, Daniel	Center for Research in Advanced Materials	Mexico
Glowacki, Miroslaw	AGH University of Science and Technology	Poland
Goel, Arun	National Institute of Technology Kurukshetra	India
Goi, Chai Lee	Curtin University	Malaysia
Gonzalez, Emmanuel A.	Jardine Schindler Elevator Corporation	Philippines
Granovsky, Alex	Moscow State University	Russian Federation
Gu, Fei	Zhejiang University	China
Gujarathi, Ashish M.	Birla Institute of Technology and Science	India
Hardman, John	Florida Atlantic University	USA
Harris, Marilyn	Capella University	USA
Hassini, Abdelatif	University of Oran	Algeria
Hegazy, Mohamed	NARSS	Egypt
Hennequin, Sophie	Ecole Nationale d'ingénieurs de Metz	France
Hirz, Mario	Graz University of Technology	Austria
Hrebicek, Jiri	Masaryk University in Brno	Czech Republic
Huang, Shian-Chang	National Changhua University of Education	Taiwan
Ibrahim, Rahinah	Putra Malaysia University	Malaysia
Jamali Dinan, Fatemeh Sadat	Khajeh Nasir Toosi University of Technology	Iran
Jastroch, Norbert	MET Communications	Germany
Jen, Chun-Ping	National Chung Cheng University	Taiwan
Jha, Ranjana	Netaji Subhas Institute of Technology	India
Jia, Hongjie	TianJin University	China
Jiang, Jinlei	Tsinghua University	China
Kaewarsa, Suriya	Rajamangala University of Technology Isan	Thailand
Kamrani, Ehsan	Polytechnic Montreal	Canada
Kässi, Tuomo	Lappeenranta University of Technology	Finland
Khudayarov, Bakhtiyar	TIIM	Uzbekistan
Kim, Hyun-Jun	Samsung Electronics	South Korea
Komerath, Narayanan	Georgia Institute of Technology	USA
Ksenofontov, Alexandre	Moscow Engineering Physics Institute	Russian Federation
Kunold, Ingo	University of Applied Sciences Dortmund	Germany
Kwak, Jin	Soonchunhyang University	South Korea
Lee, Joo Hwan	Seoul National University	South Korea
Legendre Afnor, Jean-François	AFNOR	France
Lin, Chih-Ting	National Taiwan University	Taiwan
Lin, Chun Yuan	Chang Gung University	Taiwan
Liu, Shuhua	Tsinghua University	China
Liu, Tingyang Lewis	National Kaohsiung Normal University	Taiwan
Lopez de Lacalle, Luis	University of the Basque Country	Spain
Mahdoum, Ali	CDTA	Algeria
Mahmoudi, Saïd	University of Mons	Belgium
Markakis, Euaggelos	Technological Educational Institution of Crete	Greece
Masunov, Artëm E.	University of Central Florida	USA
Medina, Dulce Yolotzin	Metropolitan Autonomous University	Mexico
Mierlus-Mazilu, Ion	Technical University of Civil Engineering Bucharest	Romania
Morel, Eneas N.	National Technological University	Argentina
Moschim, Edson	State University of Campinas	Brazil

NagaLakshmi, Vadlamani	Gandhi Institute of Technology and Management	India
Navas, Luis Manuel	University of Valladolid	Spain
Neaga, Elena Iirna	Loughborough University	UK
Neves, Filipe	LNEG	Portugal
Neves, Luís F. F.	University of Oklahoma	USA
Nicolescu, Cornel Mihai	Royal Institute of Technology of Sweden	Sweden
Nisar, Humaira	Gwangju Institute of Science and Technology	South Korea
Oueslati, Walid	PMLNMH	Tunisia
Pascal, Goureau	ENSEA	France
Pedamallu, Chandra Sekhar	Dana-Farber Cancer Institute	USA
Pieters, Cornelis (Kees)	University for Humanistic	Netherlands
Pieterse, Vreda	University of Pretoria	South Africa
Podaru, Vasile	Military Technical Academy	Romania
Popa, Rustem	University of Galati	Romania
Puslecki, Zdzislaw	Adam Mickiewicz University	Poland
Radneantu, Nicoleta	Romanian-American University	Romania
Raibulet, Claudia	University of Milano	Italy
Rana, Mukhtar Masood	Anglia Ruskin University	USA
Ribakov, Y.	Ariel University Center of Samaria	Israel
Rodriguez F., Miguel A.	Canary Islands Institute of Technology	Spain
Rodríguez L., Gloria I.	National University of Colombia	Colombia
Ros, L.	Polytechnic University of Valencia	Spain
Rot, Artur	Wroclaw University of Economics	Poland
Rudakov, Fedor	Oak Ridge National Laboratory	USA
Safarik, Pavel	Czech Technical University in Prague	Czech Republic
Salay Naderi, Mohammad	University of New South Wales	Australia
Salva, Sebastien	University of Auvergne	France
Sánchez, Caio	University of Campinas	Brazil
Sane, Vijay	American Chemical Society	India
Santulli, C.	Sapienza University of Rome	Italy
Serodio, Carlos	University of Trás-os-Montes and Alto Douro	Portugal
Silva, Daniel Pereira	Tiradentes University	Brazil
Siricharoen, Waralak V.	University of the Thai Chamber of Commerce	Thailand
Sirjani, Mojtaba B.	Norfolk State University	USA
Skoko, Hazbo	Charles Sturt University	Australia
Song, Bo	University of Illinois at Chicago	USA
Spina, Edison	University of Sao Paulo	Brazil
Šraml, Matjaž	University of Maribor	Slovenia
Stematiu, Dan	Technical University of Civil Engineering Bucharest	Romania
Suárez-Ántola, Roberto	Catholic University of Uruguay	Uruguay
Süral, Haldun	Middle East Technical University	Turkey
Sutherland, Trudy	Vaal University of Technology	South Africa
Tobar, Carlos Miguel	Pontifical Catholic University of Campinas	Brazil
Travieso-González, Carlos M.	University of Las Palmas de Gran Canaria	Spain
Tseng, Juin-Ling	Minghsin University of Science and Technology	Taiwan
Tsinarakis, George. J.	Technical University of Crete	Greece
Turcu, Cristina	Stefan cel Mare University of Suceava	Romania
Vaganova, Natalia	SBRAS	USA
Valakevicius, Eimutis	Kaunas University of Technology	Lithuania
Valdez, Pierre	Georgia Institute of Technology	USA
Vega, J. A.	Universidad de Oviedo	Spain

Verstichel, Stijn	Ghent University	Belgium
Virvilaite, Regina	Kaunas University of Technology	Lithuania
Vlasiou, Maria	Georgia Institute of Technology	USA
Vukadinovic, Dinko	University in Split	Croatia
Weeden, Elissa	Rochester Institute of Technology	USA
Wolfengagen, Viacheslav	MSU	Russian Federation
Yindi, Zhao	China University of Mining and Technology	China
Yoon, Changwoo	ETRI	South Korea
Yuan, Huajun	University of Illinois at Chicago	USA
Zabierowski, Wojciech	Technical University of Lodz	Poland
Zwaneveld, Bert	Open University	Netherlands

ADDITIONAL REVIEWERS FOR THE NON-BLIND REVIEWING

Abramchuk, George H.	Measurement Technologies and Advanced Applications	Canada
Ahmadi, Goodarz	Clarkson University	USA
Aktan, Bora	University of Bahrain	Bahrain
Aldape-Pérez, Mario	Instituto Politécnico Nacional	Mexico
Bhatt, Manherlal	S.V National Institute of Technology	India
Bustos Farias, Eduardo	ESCOM-IPN	Mexico
Cano, Gadiro	Universidad Tecnológica de Tlaxcala	Mexico
Car, Zlatan	University of Rijeka	Croatia
Casagni, Michelle	The MITRE Corporation	USA
Cervelli, Janice	University of Arizona	USA
Chung, Lap-Loi	National Center for Research of Earthquake Engineering	Taiwan
Costa, Ivanir	UNIP	Brazil
Cruz-Zaragoza, Epifanio	Universidad Nacional Autónoma de México	Mexico
D`Ambra, Luigi	Università di Napoli Federico II	Italy
Demirkiran, Ilteris	Embry-Riddle Aeronautical University	USA
Deng, Ziliang	Renmin University of China	China
Desai, Hemant	Sardar Vallabhbhai National Institute of Technology	India
Djeffal, Lakhdar	University of Batna	Algeria
Fadare, David	University of Ibadan	Nigeria
Garcia, Abel	Universidad Politecnica de Pachuca	Mexico
Gencel, Osman	Bartin University	Turkey
Gohil, Dipakkumar	Sardar Vallabhbhai National Institute of Technology	India
Golenko-Ginzburg, Dmitriy	Ben Gurion University	Israel
Graziosi, Serena	Politecnico di Milano	Italy
Gruberger, Nira	Ruppin Academic Center	Israel
Higgins, Colm	Queens University Belfast	UK
Hloch, Sergej	Technical University of Košice	Slovakia
Hodgson, Norman	Coherent. Inc.	USA
Hong, Jinglan	Shandong University	China
Houy, Thomas	Telecom Paris Tech	France
Isaza-Narvaez, Claudia	Universidad de Antioquia	Colombia
Jakayinfa, Simeon	Ladoke Akintola University of Technology	Nigeria
Jilek, Miroslav	Czech Technical University in Prague	Czech Republic
Karnitis, Edvins	University of Latvia	Latvia
Kazemi, Ahad	Iran university of Science and Technology	Iran
Kobayashi, Kentaro	Nagoya University	Japan
Korsakiene, Renata	Vilnius Gediminas Technical University	Lithuania

Lashley, Mary	Towson University	USA
Lucassen, G. W.	Personal Care Institute	Netherlands
Manous, Joe	Institute for Water Resources	USA
Menchaca-Campos, Carmina	Universidad Autonóma del Estado de Morelos	Mexico
Mukamurenzi, Solange	National University of Rwanda	Rwanda
Ophir, Dan	Ariel University College	Israel
Pang, Les	University of Maryland University College	USA
Pitkanen, Jani	Kymenlaakso University of Applied Sciences	Finland
Raahemifar, Kaamran	Ryerson University	Canada
Radovic-Markovic, Mirjana	Institute of Economic Sciences	Serbia
Ribas, Emilio Gago	University of Oviedo	Spain
Safarik, Pavel	Czech Technical University in Prague	Czech Republic
Silvernail, Nathan	Embry-Riddle Aeronautical University	USA
Singh, Bikram Jit	National Institute of Technology	India
Stanèeková, Dana	University of Zilina	Slovakia
Sudhir, C. V.	Caledonian College of Engineering	Oman
Summers, Mark	Airbus	UK
Twizere, Celestin	National University of Rwanda	Rwanda
Vargas Sánchez, Nelson A.	Universidad Distrital	Colombia
Whinnem, Eric	Boeing Advanced Technology Center	USA
Yagoub, Mustapha	University of Ottawa	Canada

The 6th International Multi-Conference on Engineering and Technological Innovation: IMETI 2013

HONORARY CHAIR
William Lesso

PROGRAM COMMITTEE CHAIRS
Hsing-Wei Chu
C. Dale Zinn

GENERAL CHAIR
Nagib Callaos

ORGANIZING COMMITTEE CHAIRS
Belkis Sánchez
Andrés Tremante

CONFERENCE PROGRAM MANAGER
María Sánchez

HARDCOPY PROCEEDINGS PRODUCTION CHAIR
María Sánchez

TECHNICAL CONSULTANT ON COMPUTING SYSTEM /
CD PROCEEDINGS PRODUCTION CHAIR
Juan Manuel Pineda

META REVIEWERS SUPPORT
Dalia Sánchez

SYSTEM DEVELOPMENT, MAINTENANCE AND DEPLOYMENT
Dalia Sánchez
Keyla Guédez
Bebzabeth Garcia

OPERATIONAL ASSISTANTS
Marcela Briceño

HELP DESK
Louis Barnes

The 10th International Conference on Cybernetics and Information Technologies , Systems and Applications: CITSA 2013
in the context of
The 6th International Multi-Conference on Engineering and Technological Innovation: IMETI 2013

GENERAL CHAIR
Michael Savoie

ORGANIZING COMMITTEE CHAIR
José Ferrer

PROGRAM COMMITTEE

Chair: Hsing-Wei Chu (USA)

Agrawalla, Raman	Tata Consultancy Services	India
Aguilar, José	University of the Andes	Venezuela
Bubnov, Alexey	Academy of Science of the Czech Republic	Czech Republic
Chang, Tsun-Wei	De Lin Institute of Technology	Taiwan
Głowacki, Mirosław	AGH University of Science and Technology	Poland
Halverson, Ranette	Midwestern State University	USA
Kim, Moo Wan	Tokyo University of Information Sciences	Japan
Kobayashi, Hideo	Mie University	Japan
Leu, Fang-Yie	Tunghai University	Taiwan
Leung, Lin	City University of New York	USA
Li, Xiangdong	City University of New York	USA
Liu, Chuan-Ming	National Taipei University of Technology	Taiwan
Martinez, Christopher	University of New Haven	USA
Mbobi, Aime Mokhoo	Centennial College	Canada
Mori, Kazuo	Mie University	Japan
Müller, Wilmuth	Fraunhofer IITB	Germany
Mundani, Ralf-Peter	Technical University of Munich	Germany
Naito, Katsuhiro	Mie University	Japan
Oya, Hidetoshi	University of Tokushima	Japan
Passos, Nelson Luiz	Midwestern State University	USA
Pawliczek, Piotr	AGH University of Science and Technology	Poland
Portnoy, Jacov	Ben-Gurion University of the Negev	Israel
Priesler, Miri	Ruppin Academic Center	Israel
Ramos, Ana Luísa	University of Aveiro	Portugal
Romanowska-P., Anna	AGH University of Science and Technology	Poland
Simpson, William R.	Institute for Defense Analyses	USA
Sołtys, Zbigniew	Jagiellonian University	Poland
Su, Meng	Penn State University	USA
Thuo, Gikiri	Florida Agricultural and Mechanical University	USA
Zaretsky, Esther	Academic College for Education Givat Washington	Israel

ADDITIONAL REVIEWERS

Abe, Jair Minoro	Paulista University	Brazil
Abramchuk, George (Heorhi)	Natural Science Engineering Research Council	Canada
Al. Obaidy, Mohaned	Gulf College	Oman
Al-khassaweneh, Mahmood	Michigan State University	Jordan
Bai, Xue	Virginia State University	USA
Barnoschi, Adriana	Nicolae Titulescu University of Bucharest	Romania
Bayne, Jay	Meta Command Systems, Inc	USA
Bayraktar, Seyfettin	Yildiz Technical University	Turkey
Bojcetic, Nenad	University of Zagreb	Croatia
Cruz-Cunha, Manuela	Polytechnic Institute of Cávado and Ave	Portugal
De Sitter, Jan	University of Antwerp	Belgium
El-Deeb, Ahmed	American University in Cairo	Egypt
Erkollar, Alptekin	University of Applied Sciences	Austria
Fang, Sheng	Shandong University of Science and Technology	China
Fu, Yujian	A&M University	USA
Gaspar, Alessio	University of South Florida	USA
Goel, Arun	National Institute of Technology	India
Habib, Maki	The American University in Cairo	Egypt
Huang, Chun-Che	National Chi Nan University	Taiwan
Husak, Miroslav	Czech Technical University in Prague	Czech Republic
Imaña, José Luis	Universidad Complutense	Spain
Islier, A. Attila	Eskisehir Osmangazi University	Turkey
Jayasuriya, Terrance D.	IET	Brunei
Jeng, Wei-Min	Soochow University	Taiwan
kang, kyeong	University of Technology Sydney	Australia
Kinsman, Thomas	Rochester Institute of Technology	USA
Lam, Vitus	The University of Hong Kong	Hong Kong
Lee, In Soo	Kyungpook National University	South Korea
Lee, Joohwan	Seoul National University	South Korea
Maekawa, Mamoru	University of Electro-Communications	Japan
Mahanti, Prabhat	University of New Brunswick	Canada
Massiha, G.H.	University of Louisiana at Lafayette	USA
McDonnell, Ciaran	Dublin Institute of Technology	Ireland
Montabert, Cyril	Virginia Polytechnic Institute and State University	USA
Moriyama, Masamitsu	Kinki University	Japan
Naddeo, Alessandro	Università di Salerno	Italy
Nickolov, Eugene	National Laboratory of Computer Virology	Bulgaria
Nutter, Brian	Texas Tech	USA
Ong, Soh Khim	National University of Singapore	Singapore
Rahman, Hakikur	School Net Foundation Bangladesh	Bangladesh
Roehrig, Christof	University of Applied Sciences Dortmund	Germany
Romagni, Susana	Universidad Metropolitana	Venezuela
Salina, Gateano	INFN Roma Tor Vergata	Italy
San Feliu, Tomas	Polytechnic University of Madrid	Spain
Shyr, Wen-Jye	National Changhua University of Education	Taiwan
Silva, Dante	Mapúa Institute of Technology	Philippines
Silva, Paulo Afonso	Military Institute of Engineering	Brazil
Tee, Sim-hui	Multimedia University	Malaysia
Teixeira, Leonor	University of Aveiro	Portugal
Tsaur, Woei-Jiunn	Inderscience Publishers	Taiwan
Valova, Irena	University of Rousse	Bulgaria

Vial, Peter	University of Wollongong	Australia
Wang, Wendy	San Jose State University	USA
Watanabe, Shigeyoshi	The University of Electro-Communications	Japan
Wiriyasuttiwong, W.	Srinakharinwirot University	Thailand
Zhou, Xiaocong	Sun Yat-Sen University	China
Zhuang, Yu	Texas Tech University	USA

ADDITIONAL REVIEWERS FOR THE NON-BLIND REVIEWING

Al-Hilo, Eman A.	University of Kufa	Iraq
Boumerzoug, Zakaria	University of Biskra	Algeria
Fan, Weicheng	Tsinghua University	China
Ferreira, Nuno	Institute of Engineering of Coimbra	Portugal
Figueiredo, Josiel	UFMT	Brazil
Fonseca, Aldemar	Universidad Distrital	Colombia
Fu, Song	Tsinghua University	China
Joe, Sheng-Wuu	Vanung University	Taiwan
Kumngern, Montree	KMITL	Thailand
Luengas, Lely	Pontificia Universidad Javeriana	Colombia
Méndez Rojas, Miguel A.	Universidad de Las Américas Puebla	Mexico
Mustapha, Aida	University of Putra	Malaysia
Nickolov, Eugene	National Laboratory of Computer Virology	Bulgaria
Oblitey, William	Indiana University of Pennsylvania	USA
Shann, Jyh-Jiun	National Chiao Tung University	Taiwan
Simoes, Nielsen	UFMT	Brazil
Smith, David	Indiana University of Pennsylvania	USA
Turoff, Murray	New Jersey Institute of Technology	USA
Yang, Wuu	National Chiao Tung University	Taiwan

Number of Papers Included in these Proceedings per Country

(The country of the first author was the one taken into account for these statistics)

Country	# Papers	%
TOTAL	**32**	**100.00**
China	5	15.63
United States	5	15.63
Japan	4	12.50
Czech Republic	2	6.25
Iraq	2	6.25
Israel	2	6.25
Romania	2	6.25
Canada	1	3.13
Colombia	1	3.13
Finland	1	3.13
France	1	3.13
India	1	3.13
Mexico	1	3.13
Sweden	1	3.13
Taiwan	1	3.13
United Kingdom	1	3.13
Venezuela	1	3.13

Foreword

Engineering activities are based on the development of new Knowledge (*Scientia*), new 'made things' (*Techné*), and/or new ways of working and doing (*Praxis*). *Scientia*, *Techné,* and *Praxis* are three important dimensions of a comprehensive conception of Engineering as a whole. Engineering, as *Scientia*, is mostly developed in academia; as *Techné,* is practiced in industry generating technological innovations; and as *Praxis,* is carried out in technical and non-technical organizations, supporting managerial activities and technical procedures, via methodical and methodological design and implementation. This is why Engineering provides one of the most solid academic and professional substrata for bridging among universities, industries and governments.

Publications and conferences related to Engineering are usually oriented to one of its three dimensions. While this is an adequate thing to do when disciplinary focus is sought, it does not represent Engineering as a whole and it misses the very important synergic relationships among the three kinds of engineering activities mentioned above. This is why a group of scholars, professionals, and consultants, in the field of engineering, considered the possibility of organizing a conference where presentations would not be reduced to one specific Engineering dimension, but would foster the participation of academics, practitioners, and managers in the three dimensions of Engineering, in the same conference, so they can synergistically interact with each other. A consequence of this purpose is the organization of The 6th International Multi-Conference on Engineering and Technological Innovation: IMETI 2013, where submissions were accepted for the presentation of:

- **New knowledge** (Engineering as *scientia*);
- **New products and services**, i.e. technological innovations (Engineering as *techné*);
- **New technical and managerial methods and methodologies** (Engineering as *praxis*);
- **New meta-engineering** (Engineering of Engineering activities) knowledge, innovations, and methodologies.

IMETI 2013 was organized and sponsored by the International Institute of Informatics and Systemics (IIIS, www.iiis.org), member of the International Federation of Systems Research (IFSR). The IIIS is a ***multi-disciplinary organization for inter-disciplinary communication and integration***, which includes about 4500 members. Consequently, a main purpose of the IIIS is to foster knowledge integration processes, interdisciplinary communication, and integration of academic activities. Based on 1) the transdisciplinarity of the systemic approach and its emphasis on *relationships* and *integrating* processes, and 2) the multi-disciplinary support of cybernetics' and informatics' concepts, notions, theories, technologies, and tools, the IIIS has been organizing multi-disciplinary conferences as a platform for fostering inter-disciplinary communication and knowledge integration processes.

Multi-disciplinary conferences are organized by the IIIS as support for both **intra-** and **inter-disciplinary** communication. Processes of intra-disciplinary communication are mainly achieved via traditional paper presentations in corresponding disciplines, while conversational sessions, regarding trans- and inter-disciplinary topics, are among the means used for inter-disciplinary communication. Intra- and inter-disciplinary communications might generate *co-regulative cybernetic loops*, via negative feedback, and *synergic* relationships, via positive feedback loops, in which both kinds of communications could increase their respective effectiveness. Figure 1 shows at least two cybernetic loops if intra- and inter-disciplinary are adequately related. A necessary condition for the effectiveness of Inter-disciplinary communication is an adequate level of **variety** regarding the participating disciplines. *Analogical thinking and learning processes* of disciplinarians depend on it; which in turn are potential sources of the creative tension required for cross-fertilization among disciplines and the generations of new hypothesis. An extended presentation regarding this issue can be found at www.iiis.org/MainPupose.

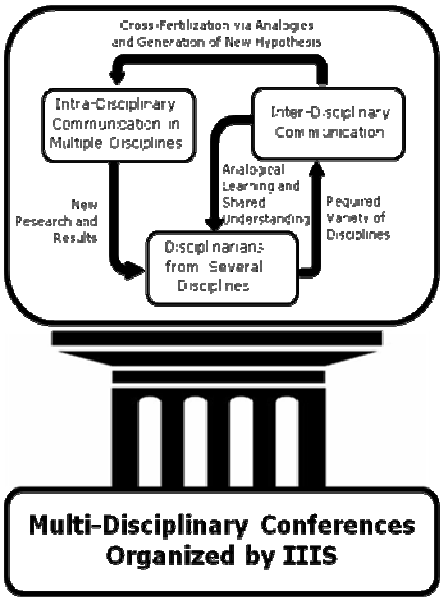

Figure 1

IMETI 2013 was organized jointly with other multi-disciplinary events with the purpose of providing a communicational forum to researchers, engineers, practitioners, developers, consultants, and end-users of computerized, communications, and/or control systems and technologies in the private and the public sectors. This multi-disciplinary forum provides the opportunity to share experience and knowledge by facilitating discussions on current and future research and innovation. Participants can explore the implications of relationships between new developments and their applications to organizations and society at-large. One of the primary objectives of IMETI 2013, and its collocated events, is to promote and encourage interdisciplinary cross-fertilization and knowledge communication. This might foster systemic thinking and practice, including the analogical thinking that characterizes the Systems Approach, which is, in most cases, the required path to logical thinking, scientific hypothesis formulation, and new design and innovation in engineering.

On behalf of the Organizing Committee, I extend our heartfelt thanks to:

1. the 223 members of the Program Committees from 42 countries;
2. the 268 additional reviewers, from 57 countries, for their **double-blind peer reviews**; and
3. the 78 reviewers, from 34 countries, for their efforts in making the **non-blind peer reviews**. (Some reviewers supported both: non-blind and double-blind reviewing for different submissions)

A total of 667 reviews made by 346 reviewers (who made at least one review) contributed to the quality achieved in IMETI 2013. This means an average of 8.55 reviews per submission (78 submissions were received). ***Each registered author had access,***

via the conference web site, to the reviews that recommended the acceptance of their respective submissions. Each registered author could also get information about: 1) the average of the reviewers evaluations according to 8 criteria, and the average of a global evaluation of his/her submission; and 2) the comments and the constructive feedback made by the reviewers, who recommended the acceptance of his/her submission, so the author would be able to improve the final version of the paper.

In the organizational process of IMETI 2013 (including the events organized in its context) about 78 papers/abstracts were submitted. These pre-conference proceedings include about 32 papers, from 17 countries, that were accepted for presentation. We extend our thanks to the invited sessions organizers for collecting, reviewing, and selecting the papers that will be presented in their respective sessions. The submissions were reviewed as carefully as time permitted; it is expected that most of them will probably appear in a more polished and complete form in scientific journals.

This information about IMETI 2013 is summarized in the following table, along with the other collocated conferences:

Conference	# of submissions received	# of reviewers that made at least one review	# of reviews made	Average of reviews per reviewer	Average of reviews per submission	# of papers included in the proceedings	% of submissions included in the proceedings
WMSCI 2013	210	740	1330	1.80	6.33	116	55.24%
IMSCI 2013	104	437	886	2.03	8.52	53	50.96%
IMETI 2013	78	346	667	1.93	8.55	32	41.03%
CISCI 2013	184	693	1771	2.56	9.63	93	50.54%
TOTAL	**576**	**2216**	**4654**	**2.10**	**8.08**	**294**	**51.04%**

We are also grateful to the co-editors of these proceedings for the hard work, energy, and eagerness they displayed preparing their respective sessions. We express our intense gratitude to Professor William Lesso for his wise and opportune tutoring, for his eternal energy, integrity, and continuous support and advice as Honorary President of WMSCI 2013 and its collocated conferences, as well as for being a very caring old friend and intellectual father to many of us. We also extend our gratitude to Professor Belkis Sánchez, who brilliantly managed the organizing process. Special thanks to Dr. C. Dale Zinn, Professors Hsing-Wei Chu, Andrés Tremante, Michael Savoie, and Belkis Sánchez for chairing, or co-chairing the Program and/or the Organizing Committees of IMETI 2013 and/or the events organized in its context.

We also extend our gratitude to the following scholars, researchers, and professionals who accepted to deliver plenary workshops and/or to address the audience of the General Joint Plenary Sessions with keynote conferences.

Workshops, more details (abstracts and short bios) were included in the Conference Program booklet and at http://www.iiis.org/summer2013plenaryevents/

Professor Leonid Perlovsky, Harvard University and The Air Force Research Laboratory, USA, two hours plenary workshop, ***"Mathematical Equivalence of Evolution and Design"***

Professor Louis H. Kauffman, University of Illinois at Chicago, USA, two hours plenary workshop, ***"Circularity, Topology and Cybernetics: Second Order Science"***

Professor T. Grandon Gill, University of South Florida, USA, four hours plenary workshop, ***"Interdisciplinary Research, Education, and Communication through Case Studies and Methodologies"***

Plenary Keynote Speakers, more details more details (abstracts and short bios) were included in the Conference Program booklet and at http://www.iiis.org/summer2013plenaryevents/

Professor Leonid Perlovsky, Harvard University and The Air Force Research Laboratory, USA, "*Musical Emotions: Cognitive function and evolution: A mathematical-psychological theory and experimental evidence."*

Professor Louis H. Kauffman, University of Illinois at Chicago, USA, "*Circularity, Topology and Cybernetics: Second Order Science"*

Professor Stuart A. Umpleby, The George Washington University, USA, "*Expansion of Science."*

Professor Shigehiro Hashimoto, Kogakuin University, Japan, "*An interdisciplinary area of research offers the tool of cross-cultural understanding: cross-cultural student seminar for communication training on biomedical engineering*."

Professor T. Grandon Gill, University of South Florida, USA, *"Complexity, Cybernetics, and Informing Science: Building a Better Mousetrap."*

Dr. Jeremy Horne, President-emeritus, Southwest Area Division, American Association for the Advancement of Science (AAAS), USA, *"Complexity, Cybernetics, and Informing Science: Building a Better Mousetrap"*

Dr. Karl Muller, University of Vienna, Austria and Head of The Wiener Institute for Social Science Documentation: WISDOM, Austria, *"Unfolding and Expanding Science with the Help of the New Science of Cybernetics (NSC)"*

Professor Andreas Ninck, Bern University of Applied Sciences, Switzerland, *"Action Learning: Doing in order to think - Thinking in order to do"*

Professor Richard Segall, Arkansas State University, USA, *"Dimensionalities of Computation: from Global Supercomputing to Data, Text and Web Mining"*

Dr. Mark Donald Rahmes, Harris Corporation, USA, *"A Biometric for Neurobiology of Influence with Social Informatics Using Game Theory"*

Dr. Denise K. Comer, Duke University, USA, **"***Academic Writing for Inter-Disciplinary Communication"*

Professor Thomas Marlowe, Seton Hall University, USA, *"Systemics and Requirements: A Missing Dimension?"*

Dr. Ronald Styron, University of South Alabama, USA, *"Interdisciplinary Education: A Reflection of the Real World."*

Dr. Robert Cherinka and Mr. Joseph Prezzama, MITRE Corporation, USA *"Trending Approaches in Innovation Utilizing Interdisciplinary Methods"*

Dr. Marta White, Georgia State University, USA, "*The Scholarship of Teaching: Inter-Cultural and Inter-disciplinary Communication for Academic Globalization"*

Dr. Kostas Demestichas, National Technical University of Athens, Greece**,** "*Flexible next generation communication networks*"

We also wish to thank all the authors for the quality of their papers, and the Program Committee members and the additional reviewers for their time and their contributions in the respective reviewing processes.

We extend our gratitude as well to María Sánchez, Juan Manuel Pineda, Leonisol Callaos, Dalia Sánchez, Keyla Guédez, Bebzabeth García, Marcela Briceño, Louis Barnes, Sean Barnes, and Freddy Callaos for their knowledgeable effort in supporting the organizational process producing the hard copy and CD versions of the proceedings, developing and maintaining the software supporting the interactions of the authors with the reviewing process and the Organizing Committee, as well as for their support in the help desk and in the promotional process.

Professor Nagib C. Callaos, Ph. D.
IMETI 2013 General Chair
www.iiis.org/Nagib-Callaos

Post-Conference Edition

CONTENTS

Engineering Concepts, Relations and Methodologies

Technological Development and Innovation

Information and Computing Technologies

Interdisciplinary Research, Analogy based Modeling and Problem Solving

Applications of Cybernetics and Informatics in other Scientific and Engineering Disciplines

Disciplinary Research and Development

Engineering Concepts, Relations and Methodologies

Interactive Pre-Simulation Strategies: Engaging Students in Experiential Learning from the Start

Beverly J. D. Bye, EdD, CRNP, CNE, FNE
Associate Professor, Stevenson University
1525 Greenspring Valley Road Stevenson, MD 21153 USA

ABSTRACT

Decrease in clinical nursing facilities created a need to develop supplemental real-life patient scenarios outside of the traditional nursing units. Over the past five years, there has been a dramatic increase in the number of simulation exercises integrated into the clinical aspect of nursing education. However, many students are not engaged and are not effectively participating in the simulation. Many students state they are perplexed and do not understand the purpose of simulation, and often do not take it seriously. The challenge to nurse educators is to develop realistic goals and objectives with a variety of activities that occur prior to the actual simulation experience Debriefing is one of the most important aspects of the simulation activity, but if students are not participating, then the learning is not occurring. The key with simulation is to engage students through the use of various strategies that incorporate visual, auditory, tactile, and cognitive learning. This study investigated the use of interactive pre-simulation strategies such as concept mapping, group discussion, teaching, and body mapping prior to the simulation experience. The focus of this research was on student success and increased knowledge. The most important overall goal is to engage students prior to the simulation experience in a safe, nonthreatening learning environment in order to allay students' fear of failure and ultimately increase knowledge, retention, and critical thinking. Results of the study have implications on the development and integration of innovative teaching pedagogies.

Keywords*:* pre-simulation strategies, pre-instructional activities, simulation, Interactive Pre-Simulation Strategies:

I. INTRODUCTION

Simulation has been proven as an effective and safe methodology in academia that involves active learning. Additionally, simulation has enabled students to link theory and practice, synthesize knowledge, and gain clinical confidence (Rauen, 2004). Simulation is a proven successful learning strategy when students actively participate; therefore, the key is to determine how to gain students' enthusiasm to actively partake in the simulation experience. This research investigated the relationship between pre-simulation strategies and selected student learning outcomes (knowledge) within a medical – surgical nursing course. A quasi-experimental design was used. Students are randomly assigned to and within sections.

II. LITERATURE REVIEW

A review of the literature is lacking with pre-simulation strategies or pre-instructional strategies. For this research pre-simulation strategies is defined as those activities that participants perform prior to the simulation experience. One of the research articles found discussed pre-instructional strategies within a high school biology course to prepare students for the simulation experience by using either formal or informal activities [1]. This study defined the pre-instructional strategies as a formal briefing where all students were influenced by these activities [1].The idea of briefing parallels the idea of debriefing at the conclusion of the simulation experience.

Literature review is necessary to provide for an evidenced-based simulation. [2],[3], [4], [5] assisted with the evidence to suggest symptoms and process for the Gastrointestinal (GI) scenario. It is imperative to provide research in order to provide an accurate and current simulation experience.

III. RESEARCH SETTING: PROCEDURES

Once the IRB approval was obtained, the medical surgical nursing students were introduced to the consent form. The course, Medical Surgical Nursing I, is a required course for all nursing students and is offered in the second semester junior level in the nursing program. The course is offered every spring. The enrollment for the course varies each semester. During the spring semester of 2012, two sections of the course were offered on Thursday and one section on a Monday. The course is a 15-week, four-credit course in the nursing program and consists of a combined lecture and clinical component. Students learn theory and clinical skills to complement the disease process discussed. The course uses a web-enhanced learning platform where content is placed by the instructor on the *BlackBoard* course site for students to review and enhance their learning. The course site is used to provide lecture notes, class material, power point lectures, and taped lectures.

Students in the course attend a two-hour class one day a week with a 12-hour clinical component one day a week. Each class is taught by the same faculty member using the same course syllabus, text book, classroom, online quizzes, and available taped lecture. The online course site for each section is set up similarly with learning modules and videos for students to review for each class. Prior to the Gastrointestinal (GI) module, students were provided with the consent form to sign and were reminded that they did not have to participate.

Sample

The sample used in this research is a sample of convenience. The sample consists of approximately 74 undergraduate junior level nursing students in the medical surgical I nursing course

from a small, comprehensive Mid-Atlantic university. Data collected in the study was obtained from students enrolled in the three sections of the required second semester junior level medical surgical I nursing course. This is the second semester of the junior year and the second class that students are exposed to the simulator (*VitalSim*™) in the classroom. Participation in the study was completely voluntary and will not affect student grades.

Enrolled Nursing Students Background

Nursing students in the first semester of their junior year take three other required nursing courses concurrently with Medical Surgical Nursing I: Research, Psychiatric Nursing, and Obstetrical nursing. Students must pass each course and maintain a 3.0 GPA in order to progress to the next level in the nursing program. Students learn about the various medical, obstetrical, and psychiatric conditions in the three clinical theory courses taken in the second semester junior year. The Research class discusses evidenced-based research that assists the students in their clinical courses.

Selection of Content

The content that was selected was based on utilizing a simulation that was developed with four other faculty members at a simulation seminar. Another rationale for the integration of the GI content (see brief topical outline in Appendix B) was that this is discussed in the first Medical Surgical nursing course since it is a basic concept in all nursing programs, and is necessary to learn in order to pass the nursing boards (NCLEX) which are taken at the successful completion of the nursing program. Additionally, the skills that students gain in this module carry over to the clinical setting.

Simulation Design

The simulation scenario was designed through a collaboration of five medical surgical educators from four different universities. The educators originally met at Johns Hopkins University M-FAST (Maryland Faculty Academy for Simulation Teaching in Nursing) program in January 2012. They reviewed the literature and developed a scenario that was appropriate for all nursing students, but focused the level of the simulation for the medical surgical I nursing student. Throughout the year the educators remained in contact via email and are encouraged to run the same simulation at all four universities. At this time two of the universities have successfully run a pilot of the simulation but did not collect data currently. The goal for all five educators is to collect and compare data in the future.

IV. RESEARCH DESIGN

The design used in this research is a nonequivalent comparison group design. Participants were not randomly assigned to groups, but rather the groups were randomly assigned to the treatments [6]. The treatment was decided by tossing a coin to determine which treatment was assigned to each group. This research involved the use of three different Medical Surgical sections, each section had 4 clinical groups. The GI content was taught by the same instructor to all three classes, but the interventions were randomly selected the following week for each group.

The variables for this study will include the aforementioned two groups (the independent variables) and student knowledge as the dependent variable (see Figure 1).

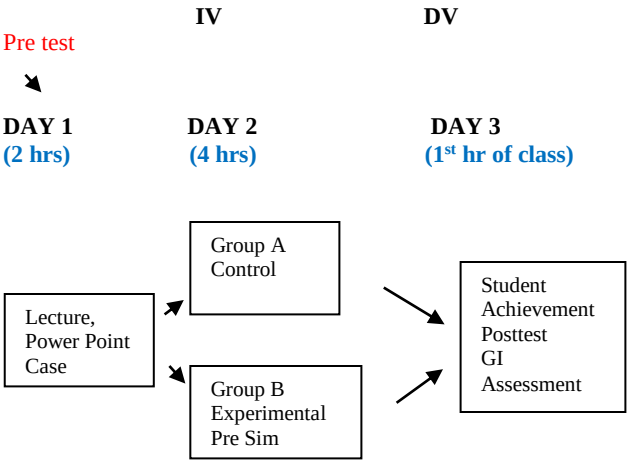

Figure 1. Independent (IV) and Dependent Variables (DV).

Groups and Procedures

All three groups were given a pretest prior to being exposed to GI content which occurred prior to day one since students prepare for class by reviewing the textbook and notes before the content is presented. Students received a power point prior to class lecture and were presented with a case study pertaining to the material. The pre- posttest was given to all students the week after the instructional treatment was administered. Students are made aware that completing the pre test post test and confidence survey have no effect on the student grade or status within the nursing program.

The learning module occurs over two class periods which are each separated by one week and consists of a power point lecture (the same given to each group). Students can download the lecture notes from the online course site at any time prior to or after class. Prior to coming to the second session, all groups were instructed to do the following: 1.) review the course textbook; and 2.) review the case study. Students were encouraged to develop questions needed to ask the case study patient in preparation for respiratory class two session. All students continued to attend their other five classes over the two weeks of the respiratory module, including clinical rotations within health care facilities, either a hospital or rehabilitation center.

Prior to the first day, students were given a pretest consisting of a twenty-five question multiple choice test. The first day was the same for all three sections of students who were instructed by the same educator. Students were provided with an outline of the power point presentation to follow during the class lecture. The class period lasts two hours. Students were assigned to groups. Each student was provided with the case study scenario and encouraged to review the scenario over the next week prior to the second class session in order to be acquainted with the information in the scenario. At the conclusion of day one, students were instructed to review the following: 1.) the lecture notes and power point; 2.) the course textbook; and 3.) the case study.

The Control group (Group A) consisted of nursing students enrolled in the Monday section 01. These students were exposed to the simulation experience the usual way by randomly assigning roles and then orienting them to the room, followed by a period of twenty minutes to allow them time to determine what each participant should be doing and what is the priority of the patient in the scenario. The first day was the same for sections as was previously discussed. The second day of the module

consisted of beginning the class with a clarification of the case scenario. Then students were placed in their groups based on arbitrarily pre-assigned clinical groups that are randomly decided upon by the clinical coordinator. The students then prepared for their roles for the simulation experience. Students were arbitrarily assigned any one of five roles (recorder, previous shift nurse, current nurse, nursing student, and nursing instructor) by drawing a piece of paper out of a hat with their role written on it. The simulation experience lasted approximately twenty minutes. At that time, students needed to assist the patient, the *VitalSim*™ simulator with her condition. Following the simulation experience, students documented their note and were debriefed with the instructor discussing what could have been done better, how they felt, and final results of what they think was happening with the patient. Specific questions were asked of all groups.

The Experimental group (Group B) consisted of nursing students that were randomly selected to participate in this group. These students used the *VitalSim*™ simulator. The respiratory module was divided into two days. The first day was the same for both groups as was previously discussed. The second day of the module consisted of beginning the class with a clarification of the case scenario. Then students were placed in their groups and prepared for their roles for the simulation experience using the *VitalSim*™ simulator. Students were arbitrarily assigned any one of five roles (recorder, previous shift nurse, current nurse, nursing student, and nursing instructor) by drawing a piece of paper out of a hat with their role written on it. The simulation experience with the *VitalSim*™ lasted approximately twenty minutes. At that time, students needed to assist the patient, the *VitalSim*™, with her condition. Following the simulation experience, students documented and were debriefed with the instructor discussing what could have been done better, how they felt, and final results of what they think was happening with the patient. Specific debriefing questions were asked of all groups.

All groups had an opportunity at the beginning of the following class, day three, to ask questions and clarify any information. This session was followed by the posttest. The groups interacted with each other as suggested by Bandura's theory [7]. The same scenario lasting 20 minutes was given to all of groups followed with a debriefing period where students shared their experiences with each other and discussed other interventions that could have been integrated to potentially change outcomes that occurred during the simulation.

V. THREATS TO VALIDITY

There were several threats to validity due to the inability of the researcher to assign the participants to random groups. The threats to validity include: 1.) regression; 2.) maturation; 3.) history; 4.) testing; and instrumentation [8]. More specifically, in this study, the threats to internal validity can incorporate interactions among variables such as selection, history, and testing[9]. If there was a difference between pre –test post- test scores, then the rationale could possibly be due to history versus the intervention [8]. A pretest – posttest gain could be attributed to such variables as history and testing (selection-history or selection-testing interaction) as opposed to the intervention and could pose threats to internal validity [8]. Since the nursing program is small, students may have discussed test questions outside of the classroom, even though they were instructed not to. Additionally, there was a concern that participants learn from the pre-test versus the effect of the intervention. A threat to external validity occurs when the participants are aware of being "guinea pigs" and realize that certain participants are actually part of the experiment. By being a part of the experiment, students may feel like they have to do well or possibly that they really do not care about the content or performing well. Participants might not feel like answering questions honestly or even at all since it does not reflect on their grade.

VI. RESEARCH QUESTION

The following question was proposed:

There will be no significant difference in pre-test post-test scores of the simulation group with the pre-simulation strategies and the group using traditional simulation preparation techniques. $p < 0.05$.

VII. DATA COLLECION: INSTRUMENTS

Data was collected using several tools. The pretest – post test tool was used to evaluate learning gained from the simulation- case-study experience. The pre-test post-test was developed. Data was collected and analyzed using SPSS software and compared with the post test that was given immediately after the experience.

The case study was developed and reviewed by expert educators for completeness. Each group received a copy of the case to preview.

Selection of Simulator

There are several types of fidelity simulators on the market including *Meti-man,* developed by the Medical Educational Technologies, Incorporated in Florida, and Sim-Man, Sim-Baby, and *VitalSim*™ all developed by [9], [10] . This study will incorporate the integration of *VitalSim*™ for a variety of reasons, mainly its ease of use and cost. *VitalSim*™ is much more cost effective than the other two simulators with a cost of between $1900 - $2000 versus $29,000 for *SimMan* and up to $85,000 for *MetiMan* based on recent information from [9]. The *VitalSim*™ enables students to auscultate respiratory, cardiac, and bowel sounds while palpating pulses and taking vital signs. *MetiMan* and *SimMan* add another realm of realism, but are based on a more complicated programming computer versus the simplicity of the *VitalSim*™ computer. Overall, *VitalSim*™ is less cumbersome, less complicated, easier to use, and less costly.

VIII. DATA COLLECTION AND ANALYSIS

Data collection for this study was conducted using a hand written pre-post test and survey collection tool. The data was entered into a statistical analysis package (SPSS) for analysis. A dependent t test was used to look at the difference between the post-test scores among the two study groups. Figure 4 shows an analysis plan for student achievement while Figure 5 shows an analysis plan for student's confidence levels.

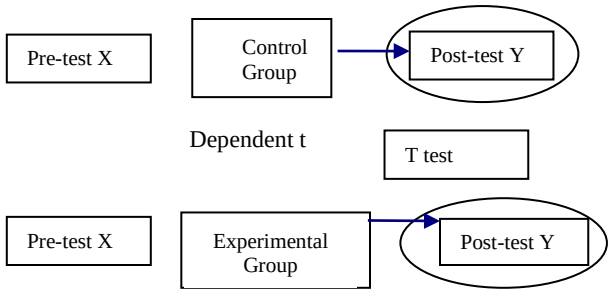

Figure 2. Plan for analysis of student achievement.

IX. LIMITATOINS AND ASSUMPTIONS

The research was conducted acknowledging several limitations and assumptions. The participants were limited to 74 eligible students among three different Medical Surgical sections in the spring 2012 semester. The sample is one of convenience and introduced bias. Therefore, the results are not generalizable beyond this sample of 74 students in the three Assessment courses. It is assumed that all students will agree to participate, but they do not have to. Students were informed that whether they choose to participate or not, there grade will not be affected for the course. The module was taught by one instructor. Although the same instructor taught all three sections and did not determine which group was to receive which treatment until after the lectures were completed, the study was limited to the possible variances in the teaching style among the three classes. Researcher bias may impact the study because of pre-existing beliefs by the researcher of the effects of simulation on learning retention. This research incorporated a student self assessed confidence level report. Although it is assumed that students answered questions truthfully and honestly, the study was limited to the individual differences in student self perception. It is assumed that students honestly answered the pre and post test questions by themselves and were not informed of questions by students completing the quizzes on earlier days. All three classes completed the same pre and posttests, and for example the Monday class could have informed the Thursday class of the questions. It is assumed that students collaborated equally in the case scenarios.

X. DATA OVERVIEW

In this study, the pre-test post-test were administered to the participants at two intervals: at the start of the teaching module and at the conclusion of the teaching module. The tool was a knowledge test based on twenty multiple choice questions.

Knowledge

The pretest – posttest tool was used to evaluate learning gained from the simulation- case-study experience. One method of measuring reliability of a tool is by using the Cronbach coefficient alpha. Using the Cronbach coefficient alpha, the internal consistency of the knowledge prequiz was 0.74. The internal consistency showed that this tool is acceptable to use for the study. According to Nunnaly [11], a Cronbach coefficient alpha of 0.7 or above indicates an acceptable reliability coefficient and shows internal consistency.

The mean pre-test scores for the groups were as follows: the Control group had a mean of 53 and the Experimental group had a mean of 53.8. The experimental group showed improvement in mean scores from the pretest to the post test, but these gains were not statistically significant. The mean gain scores was as follows: the Control group had mean gain scores of -5.6 and the Experimental group had gain score of 4.

XI. RESULTS

This study focused on the use of different pre-simulation instructional pedagogies on knowledge.

Research Hypothesis

This section reports results pertaining to the test of the following null hypothesis: There will be no significant difference in student knowledge based upon the instructional treatment – integration of pre-simulation strategies. Essentially the pre-test scores were similar in both groups. Post hoc comparisons for the two groups showed that there was an increase in knowledge in the Experimental group of + 4 versus the Control group showing a decrease of 5.6.Therefore the null hypothesis was rejected indicating there was a significant difference in post test scores between the Control group and Experimental group. This difference was expected since the students had complained in the past requesting more guidance prior to the simulation experience.

XII. SUMMARY

Descriptive statistics were calculated which revealed that the Experimental group showed an improvement between the pre and post knowledge test. There was a statistical significant difference found between the Control and Experimental groups after the post knowledge test favoring the Experimental group. It appears that the integration of pre-simulation strategies assists students with learning content and additionally students appeared more comfortable during the simulation experience.

XIII. DISCOVERIES

The integration of simulation as a teaching and learning pedagogy has been shown to be effective in teaching all levels of nurses from students to novice nurse to experienced nurses [10], [12]. The use of high fidelity simulation enhances clinical competence such that students are able to learn proper techniques in a safe and nonthreatening realistic environment that are used within the hospital setting [13]. One of the more recent types of simulation strategy is the incorporation of standardized patients, which is similar to an actor. Standardized patients are trained to perform in a certain way for specific training purposes [14] [15]. Simulation using standardized patients assists nursing students to learn new skills and perfect previously learned clinical skills in a safe environment. This study examined pre-simulation strategies (use of activities prior to simulation in order to engage students in the simulation experience) and traditional simulation preparation pedagogy as instructional techniques.

This study supports the relevance of technology integration, namely simulation, within a baccalaureate nursing course. There was a statistical difference in knowledge between the Control and Experimental group demonstrating that there is a need for pre-simulation activities to prepare students better in an engaging manner for the simulation experience. A variety of instructional pedagogies can be utilized, thus challenging educators to select the appropriate teaching method for each specific class.

The improvement of post test scores shows that the Experimental group's instructional treatments assisted students in learning content. Similar studies did not find statistically significant differences in knowledge scores comparing high fidelity simulation and traditional learning groups with medical students [16].

There are several limitations that affect the generalizability of this study. The study cannot be generalizable to all nursing student groups since this study used a small sample size of 74 second semester junior nursing students; however, the results can be generalizable to small size groups at similar nursing schools for second semester nursing students. Only one simulator was used in this result that possibly could limit the use of the results of the study to schools integrating that particular simulator. The focus of this study relied on students being truthful with relation to maintaining test integrity by not sharing the questions with the other sections.

Instrumentation

The instrumentation might have affected the results of the study. Scherer, Bruce, and Runkawatt [16] suggested that instruments such as the knowledge test might have produced different results. It is possible that the knowledge test could be improved with additional items that measured lower level content knowledge to make it easier for the students.

Additionally every section had a student evaluator and the instructor as an evaluator. For each group, an observer tool was completed. During the debriefing phase, the students would discuss what they had observed during the simulation. Additionally pre-selected questions for debriefing were utilized so that consistency was maintained between sections.

Simulation and Use of Actors

In the 1980's, nurse educators incorporated the use of early simulation by using actors to play patients in simulated case scenarios [17]. However, one study was located using standardized patients, or actors that demonstrated positive outcomes with teaching undergraduate nursing students skills [15]. Bosek, Li, and Hicks [15] found that the use of standardized patients may be a promising adjunct to the clinical setting for skill attainment, but more research needs to be done with the use of standardized patients.

Radhakrshnan, Roche, & Cunningham [17] found that the use of simulation assists with the ability of nursing students assessing patients. According to the literature reviewed, simulation demonstrates the ability of students learning in a self-paced risk-free realistic environment with immediate feedback and remediation available at any time [10], [12], [19], [20]. Simulation provides the opportunity to improve and /or learn skills within a safe environment, which is an important educational endeavor. The results of this study suggests that simulation is an important tool for nurse educators in order to provide active learning for their students based on Bandura's theory. Additionally, the type of simulator utilized is important for nurse educators to be able to operate. If the simulator is difficult to use, then nurse educators will not integrate the technology. The more sophisticated the simulator, the less apt the educator will integrate the technology [17]. *MetiMan* is one example of a high fidelity simulator that is complicated and contains complex medical simulation programs. The programs may be too complex for nursing students to work with. For example, nurse educators find the *MetiMan* extremely difficult to work, even just to turn the simulator on and off. It takes several days of training to be able to learn how to turn the simulator (*MetiMan*) on and off, much less program the simulator with appropriate scenarios for nursing students. This study found that an important component to the successful integration of simulation was to align the student's level in the program with the simulation. Educators must remember to assure that the scenario is not too complicated for the student.

XIV. RECOMENDATIONS

The results of the study demonstrate that pre-simulation strategies can enhance the learning experience for the simulation experience by integrating a variety of participative instructional pedagogies. Simulation itself incorporates both Bandura and adult learning theories which provides an interactive learning environment. By providing activities prior to the simulation, students are even more active. The study needs to be replicated with a larger sample size using detailed nursing skills and behavior checklist that could be incorporated within the clinical setting. The addition of the clinical instructor perception of critical thinking would add another dimension to the integration of simulation. In order to assess if simulation assists students to integrate theory into practice, clinical instructors could assess students in the clinical setting to determine if they are able to answer questions effectively in the practice setting.

An important consideration is the ease of use of the simulator since it could be easier to demonstrate to new faculty. In this study, the researcher demonstrated to the students and current new faculty how to use the *VitalSim™* in less than twenty minutes while other simulators, such as the *Metiman*, may require multiple training sessions to learn the series of steps necessary to make the simulator operational. Students were able to continue using the simulator once the research data was collected in order to maintain their clinical assessment skills. Most nursing schools have "Open Skills Lab" where students can practice skills at their own pace which is a perfect opportunity for students to gain and improve basic ausculatory skills such as lung, heart, and bowel sounds. It is recommended that the integration of the *VitalSim™* continues to be used within the nursing curriculum, and that more graduate nurse educator programs train future nurse educators both the benefit and ease of simulation within the classroom setting.

Kardong-Edgren, Lungstrom, and Bendel [20] recently conducted a study integrating two different simulators (*VitalSim™ and SimMan ™*) and found no differences with learning acquisition and satisfaction among baccalaureate nursing students. A suggestion would be to repeat the current study in terms of analyzing confidence levels and knowledge acquisition integrating a post 2 quiz at 1 month and possibly following up with NCLEX pass rates. Currently the author is attempting to collect information regarding NCLEX results that will be available during the summer and fall 2013 since the participants graduated in spring 2013.

Replication of this study using the simulation continuously throughout the same semester could be conducted to determine the effectiveness of simulation. Future research could analyze larger groups with multiple simulation scenarios throughout a variety of nursing courses encompassing several levels of undergraduate nursing students, since the results of this study are only generalizable to this sample and course. It is the goal of the all five of the scenario developers (including the author) to collect and compare data from her own university and then compile the data to ascertain commonalities and themes.

Future studies incorporating different instructional approaches such as a variation of the case study. Another strategy for future research is the integration of instructional pedagogy that would combine both simulation strategies and comparing both simulations with traditional learning strategies. Another question to ask is in what setting does each instructional treatment work best – online or face-to-face in the classroom? Additionally, more research should be conducted with the integration of simulation as an activity completed by one student via videotaping without an instructor present and the effects on student learning and confidence levels. There is still much more work that needs to be conducted in the area of simulation and simulation evaluation.

Another possibility for future research is to compare other schools to see if there are any other factors involved in the improvement of learning. There are so many strategies and instructional pedagogies that could be utilized for preparing students for simulation. The incorporation of virtual online simulation preparation and interactivity via clickers on cell phones would be interesting to investigate since the group of

students that nurse educators are teaching are technology savvy and learn better with the integration of technology.

The future possibilities of simulation integration are endless. The value of simulation versus the clinical setting needs to be explored. Will students possibly gain more from the clinical setting if every student first completes several case study simulations prior to practicing on the clinical unit with real patients under the guidance and supervision of the nursing instructor? The impetus for this is based on the fact that various hospitals have recently purchased simulators for training purposes of hospital personnel. Nurse educators and leaders have adapted new training strategies for new graduates and experienced nurses integrating simulation to demonstrate and test new skills and techniques with the nursing staff.

XV. CONCLUSION

This study together with other research demonstrates that simulation does assist students with increasing their knowledge. The premise behind the simulation scenario was based on several meetings of a group of five nurse educators the met one summer and continued to contact each other via email.

Simulation is currently used in a variety of settings, including education, business, aviation, and healthcare. Instructional technology teachers need to be reminded of the benefits of benefits from simulation in education from preschool through doctoral education and beyond. There are many challenges that educators face when integrating simulation technology in the classroom. Simulation needs to be appropriately introduced to both faculty and students alike [21]. It is important to integrate simulation wisely such that it is realistic and aligns with the curriculum at the appropriate level for the student.

Further research needs to be conducted in order to ascertain best practices with simulation technology, especially with pre-simulation strategies. There is limited empirical evidence to support the effect that simulation has on clinical practice [13] Studies have shown that students value the simulation experience within the safe, interactive learning environment, but there is no robust conclusive quantitative evidence indicating the transfer of knowledge and skills into the clinical practice [13]. Simulation is seen as a potential learning pedagogy to promote safe practice in an ever increasing litigious healthcare environment. According to the National League for Nursing [22], the challenge for nurse educators is to create learning environments that promote clinical competency, "critical thinking, self-reflection, and prepare nurse graduates for practice in a complex, dynamic healthcare environment" (p. 1-2).

Simulation can provide an opportunity for students to gain exposure to increased learning with the integration of debriefing, immediate feedback, and guided reflection. Additionally, these opportunities have enabled students to demonstrate the link between theory and practice, synthesize knowledge and gain clinical confidence [23]. To be effective, simulation should be aligned with goals, skills and knowledge acquisition, competency testing, critical thinking, and best practices while integrating a variety of realistic case scenarios.

Another aspect of learning in the clinical setting is the post conference. Debriefing is an important strategy that is used within simulation learning and is compared to post conference learning [24]. Both the post conference and the simulation debriefing are facilitated by nursing faculty. This study used pre-selected questions for the debriefing in order to maintain consistency across all sections. Lassater [24] stated that students learn by sharing observations during and after the simulation experience. Even the students that are present within the lab can learn by observing others and during debriefing experience whether they are directly participating in the experience and discussion since this is facilitated by the nursing faculty and can be compared to their own simulation experience [25]. Likewise pre-simulation strategies could be compared to the pre-conference where students are prepared for the clinical day.

The current research certainly has proved the value of not only incorporating simulation for the benefit of increasing confidence, but there are also additional benefits that have not been totally explored at this time with relation to the clinical setting. Simulation is now currently being integrated within hospital settings to train nurses and medical residents to learn new skills, techniques, and strategies as new medical equipment is purchased for the hospital setting [25]. Simulation provides a kinesthetic (hands-on) learning strategy within a safe environment. There is a need to push for more simulation studies for cost-saving and life-saving reasons. The most expensive simulators might not be necessary in order to effectively train all personnel. Some lower cost simulators, such as the *VitalSim™* could be purchased as additional simulators so that the medical facility has several simulators, not just one expensive simulator. This would provide learning opportunities for more hospital personnel. The more training, the more lives that could be saved in the long run, especially since simulation has already proven to be an effective learning strategy for skill acquisition, and in this research demonstrated an increase in confidence levels so that nurses will ultimately be able to rely on themselves to make life or death decisions within the clinical setting.

Simulation has proven to be an effective learning strategy for baccalaureate nursing students, not only for skill acquisition, but for increasing confidence levels. Future research will be needed to connect the increase confidence levels with improvement in critical thinking which enables nurses to think quicker in the clinical setting, promoting more effective and efficient life or death decision making. This research proved an important aspect of that decision making algorithm, in addition to demonstrating that simulation would assist students with clinical acquisition. Students will still acquire knowledge, skills, confidence, and critical thinking without always being at the clinical site with the integration of simulation. Additionally, learning time on the clinical site might even prove to be more effective with the use of simulation learning.

The challenge facing all educators, not just nursing educators, today is to implement teaching strategies that promote clinical and theoretical competency while at the same time assisting students in developing critical-thinking skills within a safe environment. There is the potential for simulation to assist with the clinical void in nursing education. With the increasing demand for more clinical sites, simulation may serve as a potential placement for clinical experiences, especially since it can provide consistent learning across all groups by exposing students to the same disease conditions [12], [13] [21], [23]. . The challenge for the educator is to develop realistic case-based scenarios, standardized simulation forms, and reliable testing checklists while making the simulation experience available to students [26]. It is up to the educator to facilitate the integration of the simulation experience.

References

[1] Helms, S. A.. "A case student of a high school science student and the role of pre-instruction activities, goal

orientation, and self-efficacy in learning with simulations." **Dissertation: University of Northern Colorado**.ISBN 978-2010, pp. 1240-1705..

[2] Ahsberg, K., Hoglund, P., Kim, W.H. & von Holstein, C. S. "Impact of aspirin, NSAIDs, warfarin, corticosteroids, and SSRIs on the site and outcome of non-varicealupper and lower gastrointestinal bleeding. " **Scandinavian Journal of Gastroenterology**, Vol 45, No 12, 2010, pp.1404-1415.

[3] Ianni, R. C. & Campbell, E. F.. "Aspirin use in a patient at high risk for GI bleed. "**Clinical Advisor for Nurse Practitioners,** Vol 14, No 2, 2011, p, 66..

[4] Krumberger, J.M. & Roman, L.. "How do you manage an upper GI bleed?" **RN**, Vol 68, No 3, 2005, pp. 34-40, 2.

[5] Wilcox, D M., Cryer, B. L. Henk, H.J., Zarotsky, V., & Zlateva, G. "Mortality associated with gastrointestinal bleeding events: Comparing short-term clinical outcomes of patients hospitalized for upper GI bleeding and acute myocardial infarction in a US managed care setting." **Clinical and Experimental Gastroenterology,** Vol 2, 2009, pp.21-30.

[6] Gay, L.R., Mills, G. E., & Airasian, P. **Educational research: Competencies for analysis and applications** *(8th ed).* Upper Saddle River, New Jersey: Pearson, 2006.

[7] Bandura, A. **Self-efficacy: The exercise of control.** New York: W.H. Freeman. Retrieved on November 14, 2005 from http://tip.psychology.org/bandura.html.1997

[8] Campbell, D. & Stanley, J. **Experimental and quasi-experimental designs for research.** Chicago, IL: Rand-McNally, 1963

[9] Laerdal (2006). Product information. Retrieved December 23, 2006 from http://www.laerdal.com/document.asp?subnodeid=7144017

[10] Nehring, W, M., Ellis, W. E., & Lashley, F. R. "Human patient simulators in nursing education: An Overview.**"Simulation & Gaming**,Vol 32, No 2, 2001, pp. 194-204.

[11] Nunnaly, J. **Psychometric theory**. New York: McGraw-Hill, 1978.

[12] Nehring, W. M. & Lashley, F. R. "Current use and opinions regarding human patient simulators in nursing education: An international survey. " **Nursing Education Perspectives,** Vol 25, No 5, 2004, pp. 244-248.

[13] Murray, C., Grant, M., Howarth, M., & Leigh, J. "The use of simulation as a teaching and learning approach to support practice learning." **Nurse Education in Practice**, Vol 8, No 1, 2008, pp.5-8.

[14] Becker, K., Rose, L., Berg, J.., Park, H., & Shatzer, J. "The teaching effectiveness of standardized patients." **The Journal of Nursing Education**, Vol 45, No 4, 2006, pp. 103-111.

[15] Bosek, M. S., Li, S., & Hicks, F. D. "Working with standardized patients: A Primer." **International Journal of Nursing Education Scholarship,** Vol 4, No1,2007, pp.1-12.

[16] Scherer, Y. K., Bruce, S. A., Graves, B. T., & Erdley, W. S. "Acute care nurse practitioner education: Enhancing performance through the use of clinical simulation." **AACN Clinical Issues,** Vol 14, No 3 ,2003, pp. 331-341.

[17] Radhakrshnan,K., Roche, J., & Cunningham, H. "Measuring clinical practice parameters with human patient simulation: A pilot study." **International Journal of Nursing Education Scholarship,** Vol 4, No 1,, 2007.

[18] Feingold, C., Calaluce, M., & Kallen, M. "Computerized patient model and simulated clinical experiences: Evaluation with baccalaureate nursing students." **Journal of Nursing Education**, *43*(4), Vol 43, No 4, 2004, pp.156-163.

[19] Rauen, C. A. "Simulation as a teaching strategy for nursing education and orientation in cardiac surgery. "**Critical Care Nurse,** Vol 24, No 3, 2004, pp.46-51.

[20] Kardong-Edgren, S; Lungstrom, N., & Bendel, B."VitalSim vs SimMan: Comparing BSN student learning and satisfaction outcomes." Washington State University Poster Presentation, 2008.

[21] Issenberg, S. & Scalese, R. "Simulation in health care education."**Perspectives in Biology and Medicine**, Vol 51, No 1, 2008, pp. 31-36.

[22] National League for Nursing (NLN). "Position statement: A call to nursing education, A call to reform." Retrieved http://www.nln.org/aboutnln/positionstatements/innovation082203.pdf, 2003.

[23] Decker, S., Sportsman, S., Puetz, L, & Billings, L. "The evolution of simulation and its contribution to competency. "**The Journal of Continuing Education in Nursing,** Vol 39, No 2, 2008, pp. 74-80.

[24] Lassatar, K. "Clinical judgment development: Using simulation to create an assessment rubric". **Journal of Nursing Education**, Vol 46, No 11, 2007, pp. 496-504.

[25] Jeffries, P. R."A framework for designing, implementing, and evaluating simulations used as teaching strategies in nursing." **Nursing Education Perspectives**,Vol 26, No 2, 2009, pp. 96-103.

[26] Seropian, M., Brown, K., Gavilanes, J., & Driggers, B. "Simulation: Not just a manikin." **Journal of Nursing Education**, Vol 43, No 4, 2004, pp. 164-169.

.

Microstructure, Mechanical and Anticorrosive Properties of a New Implant Alloy in Simulated Human Body Environment

Silviu I. DROB, Jose M. CALDERON MORENO, Cora VASILESCU, Monica POPA
Romanian Academy, Institute of Physical Chemistry "Ilie Murgulescu", Bucharest, Romania

and

Mihai F. POPA
SC Dentestetics SRL, Bucharest, Romania

ABSTRACT

The corrosion resistance of the new ternary Ti-15Zr-5Nb alloy was correlated with its microstructure, surface structure and composition of its native passive film and of the film formed after 1500 soaking hours in Ringer solutions of different pH values. Nobler passive behaviour of alloy in comparison with Ti was determined due to its more compact passive film (containing TiO_2, Ti_2O_3, ZrO_2 and Nb_2O_5 oxides). EIS spectra depicted a predominantly capacitive behaviour, a passive film formed by two layers. After 1500 soaking hours, XPS, SEM and EDX revealed the same protective oxides and $Ca_3(PO_4)_2$ compound (precursor of hydroxyapatite) deposited on the alloy surface.

Keywords: Ti-15Zr-5Nb Alloy, XRD, XPS, SEM, Passive Films.

1. INTRODUCTION

The alloys designed for implant applications need to have high corrosion resistance and biocompatibility, for a good osseointegration and suitable mechanical properties as modulus, elongation, strength, fatigue limit to avoid osteoclasia [1,2]. Ternary Ti-Zr-Nb alloys are considered as basic systems for the hard tissue implant because all their alloying elements are non-toxic and very resistant to corrosion in the human biofluids. Only Ti-13Nb-13Zr alloy [3-9] has been analysed in more detail: its corrosion and security in lactated Ringer solution [3,8]; its corrosion characterisation in Hank's solution [9]; its electrochemical behaviour and surface chemistry in minimum essential medium (MEM) [7] with and without H_2O_2 addition [4]; long-term immersion tests in Hank's solution [6]; this alloy directly bonds to the bone but this process is slower than the healing period of the bone. The corrosion resistance of Ti-15Zr-4Nb alloy [10-12], Ti-5Nb-13Zr and Ti-20Nb-13Zr alloys [13], Ti-35Nb-xZr (x = 3; 5; 7; 10; 15) alloys [14] also was studied. The most of ternary Ti-Zr-Nb alloys have some limitations and a general effort is underway to obtain new alloys with improved properties.

In this paper, the corrosion resistance (by cyclic and linear polarisation, and long-term monitoring of the open circuit potentials) of the new ternary Ti-15Zr-5Nb alloy was correlated with its microstructure (by optical microscopy and SEM), and morphology (by SEM) and composition (by XPS) of its native passive film and of the protective film formed on the alloy surface (by XPS, SEM and EDX) after 1500 soaking hours in Ringer solutions of different pH values which simulate the severe conditions from the human biofluid in case of the surgery, infections or inflammations [15,16].

2. EXPERIMENTAL

Alloy characterization
The new Ti-15Zr-5Nb alloy was obtained by vacuum melting and re-melting in a FiveCell furnace by semi-levitation mode in a cold crucible. The alloy composition was (wt.%): 0.011% H_2, 0.02% N_2, 0.12% O_2, 0.052% Mg, 0.00235% Ca, 0.00831% Cr, 0.02048% Fe, 0.0077% Ni, 0.0181% Ta, 14.97% Zr, 5.111% Nb, balance Ti.

The alloy microstructure was determined with an optical microscope with polarized light, AXIO IMAGER A1m type and with a scanning electron microscope Zeiss EVO LS10 operating at 30 kV.

The phase identification of the new alloy was carried out by X-ray diffractometry (XRD) with a Rigaku Ultima IV, Diffractometer θ-2θ using CuK_α λ=1.5406 Å radiation over the range $10<2\theta/\text{degrees}<90$ at 40 kV and 30 mA.

Mechanical properties were studied by tensile tests until rupture using an INSTRON 3382 module. The stress-strain curve was recorded; from this curve the main mechanical properties were evinced: Young's modulus (E), ultimate tensile strength (UTS), elongation (EL), and 0.2% yield strength (0.2% YS).

Surface characterization
The composition and microstructure of the native passive film and of the film formed on the alloy surface after long-term soaking (1500 h) in Ringer solution of different pH values were analysed by SEM, EDX, and XPS.

SEM measurements were carried out in a FEI Quanta 3D FEG apparatus working at accelerating voltage of 20 kV, equipped with an energy dispersive X-ray (EDX) spectrometer.

XPS equipment (Quantera SXM) has X-ray source, Al K_α radiation (1486.6eV, monochromatized) and the overall energy resolution is estimated at 0.65 eV by the full width at half maximum (FWHM) of the Au $4f_{7/2}$ line. The errors in the quantitative analysis (relative concentrations) were estimated in the range of ± 10 %, and the accuracy for Binding Energies (*BEs*) assignments was ± 0.2 eV.

Alloy electrochemical characterization

The cylindrical electrodes were cut from as-cast ingots and were grinded with metallographic paper, polished with aluminium oxide to mirror surface, rinsed with bi-distilled water, ultrasonically degreased in acetone and bi-distilled water (for 15 min.), dried in air and fixed in a Stern-Makrides hold system.

The human fluid was simulated by the physiological Ringer solution and the severe functional conditions took into consideration the pH variations of this fluid from acid values [3,15] to alkaline values [16]. Ringer solution composition was (g/L): NaCl – 6.8; KCl – 0.4; $CaCl_2$ – 0.2; $MgSO_4.7H_2O$ – 0.2048; $NaH_2PO_4.H_2O$ – 0.1438; $NaHCO_3$ -1.1; glucose – 1; pH = 7.58; pH = 3.21 was obtained by HCl addition; pH = 8.91 by KOH addition.

The alloy electrochemical behaviour was investigated by potentiodynamic and linear polarisation, and monitoring of the open circuit potentials (E_{oc}) and corresponding potential differences (ΔE_{oc}) in time and with pH values.

The cyclic potentiodynamic polarisation was started at 0.5 V (vs. SCE) below E_{oc} and the potential was increased with a rate of 1 mV/s till +2 V (vs. SCE). From voltammograms, the main electrochemical parameters were determined: E_{corr} - corrosion potential, like zero current potential, E_p – passivation potential at which the current density is constant; $|E_{corr} - E_p|$ difference represents the tendency to passivation; ΔE_p – passive potential range of the constant current; i_p – passive current density.

The linear polarisation was performed for ±100 mV around the open circuit potential with a scan rate of 1 mV/s. VoltaMaster 4 program directly supplied the values of corrosion current densities - i_{corr}, corrosion rates - V_{corr}, polarisation resistances - R_p.

The following open circuit potential differences that can appear because of the pH non-uniformities $\Delta E_{oc}(pH)$ along the metal surface were simulated:

$$\Delta E_{oc1}(pH) = E_{oc}^{pH=3.21} - E_{oc}^{pH=7.58} \quad (1)$$

$$\Delta E_{oc2}(pH) = E_{oc}^{pH=3.21} - E_{oc}^{pH=8.91} \quad (2)$$

$$\Delta E_{oc3}(pH) = E_{oc}^{pH=7.58} - E_{oc}^{pH=8.91} \quad (3)$$

3. RESULTS AND DISCUSSION

Alloy microstructure

The indexed spectra from XRD measurements (Fig. 1) determined a crystalline structure consisting of the hexagonal α phase, with calculated lattice parameters of a = 2.916 Å, c = 4.624 Å and the cubic β phase, with calculated lattice parameter of a = 3.188 Å.

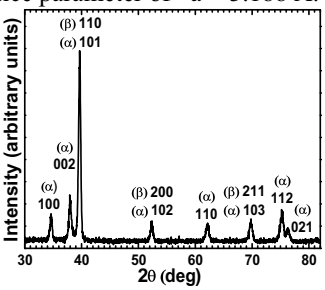

Fig. 1. XRD pattern for Ti-15Zr-5Nb alloy

The alloy microstructural measurements determined from optical (Fig. 2a-b) and SEM (Fig. 2c) micrograph show a bi-phase α + β lamellar microstructure. The darker lamellae in the SEM micrograph (Fig. 2c) correspond to the α phase, and the brighter lamellae correspond to the β phase. The EDX spectra (Fig. 2d) detected the component elements Ti, Nb, and Zr and a very small contribution of O, from the native oxide film, overlapping with the Ti-K peak . The weight ratios Ti/Zr/Nb are 77.6/16.8/5.6.

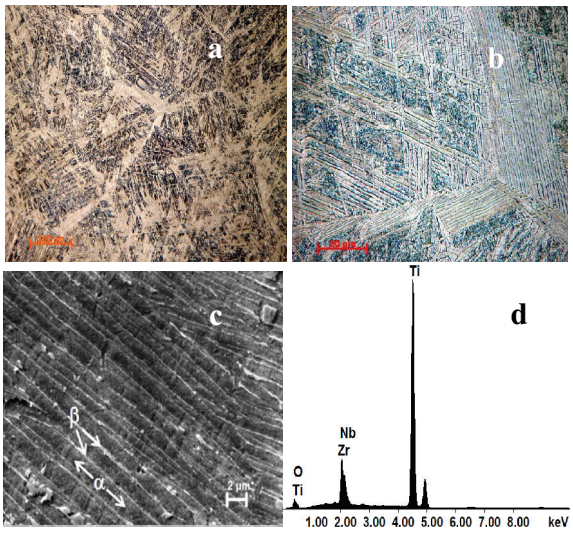

Fig. 2. Optical (a, b) and SEM (c) micrographs of Ti-15Zr-5Nb alloy and EDX spectra (d).

Alloy mechanical properties

The stress-strain tensile curve for Ti-15Zr-5Nb alloy (Fig. 3) shows an elastoplastic behaviour with a plateau of plastic flow before rupture (at about 16% strain). Young's modulus of 82.69 GPa is lower than those of the commercial CP Ti, Ti-6Al-4V ELI and Ti-6Al-7Nb alloys (Table 1). The ultimate tensile strength (UTS) and elongation (EL) for the new Ti-15Zr-5Nb alloy are

comparable with those of the commercial materials (Table 1); The new alloy exhibits good correlation of its mechanical properties with the plasticity.

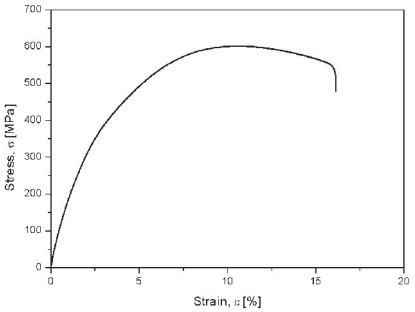

Fig. 3. Stress-strain tensile curve for Ti-15Zr-5Nb alloy

Table 1. Main mechanical properties of Ti-15Zr-5Nb alloy in comparison with commercial materials

Material	E (GPa)	UTS (MPa)	EL (%)	0.2% YS (MPa)
CP Ti [1]	105	344	20	170-244
Ti-6Al-4V ELI [1]	114	860	15	790
Ti-6Al-7Nb[1]	105	1000	12	900
Ti-15Zr-5Nb	82.69	611.94	16.11	376.26

[1] ASM data base

Alloy native passive layer composition by XPS

XPS survey spectrum (Fig. 4) displays the presence of Ti^{3+}, Ti^{4+}, Nb^{5+}, Zr^{4+} ions. XPS deconvoluted spectra (Fig. 5) reveal: the binding energies for Ti 2p doublet peaks (Fig. 5a) which correspond with Ti_2O_3 and TiO_2; binding energies of Nb 3d doublet peaks (Fig. 5b) showing Nb_2O_5 oxide; binding energies of Zr 3d doublet peaks (Fig. 5c) proving the existence of ZrO_2; binding energies for O 1s are formed from two peaks (Fig. 5d) representing O^{2-} and OH^- ions [17,18]. Therefore, the native passive film on the Ti-15Zr-5Nb alloy surface is formed by the protective Ti_2O_3, TiO_2, Nb_2O_5 and ZrO_2 oxides that confer to this film, higher compactness, stability and resistance than those of Ti metal.

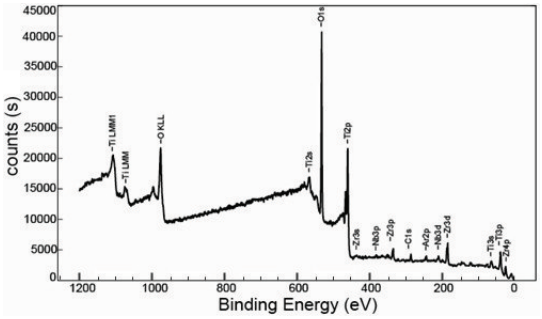

Fig. 4. XPS survey spectrum of native passive film on Ti-15Zr-5Nb alloy surface.

Alloy electrochemical behaviour in Ringer solutions

The representative cyclic potentiodynamic polarisation curves (Fig. 6) of Ti-15Zr-5Nb alloy and of Ti in Ringer solutions of different *p*H values exhibit self-passivation behaviour.

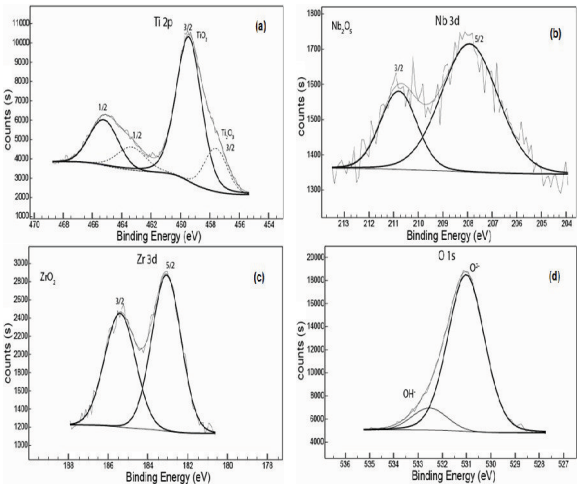

Fig. 5. XPS deconvoluted spectra of native film on Ti-15Zr-5Nb alloy surface.

The data from Table 2 indicate: the shift of the alloy corrosion potential, E_{corr} in electropositive direction in comparison with that of Ti, due to the beneficial effect of Zr and Nb alloying elements which participate with their protective oxides ZrO_2 and Nb_2O_5 to the alloy passive film, compacting this film; these oxides were detected (together with TiO_2 and Ti_2O_3 oxides) by XPS analysis; the current density in the passive potential range, i_p for alloy is lower than that of Ti, suggesting a more stability and resistance of its passive film [19,20]; the tendency to passivation, $|E_{corr} - E_p|$ has lower value for alloy, demonstrating an easier, more rapid, stronger passivation than that of Ti. Both Fig. 6 and Table 2 show a nobler passive behaviour of Ti-15Zr-5Nb alloy in comparison with Ti due to its more resistant, compact passive film.

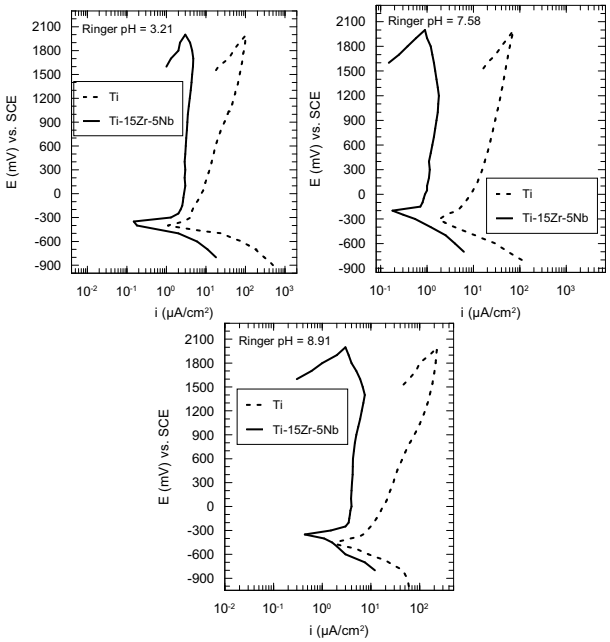

Fig. 6. Cyclic potentiodynamic curves of Ti and Ti-15Zr-5Nb alloy in Ringer solutions at 37^0C.

Table 2. Main electrochemical parameters of Ti and Ti-15Zr-5Nb alloy, obtained in Ringer solutions at 37^0C.

Material	E_{corr} (mV)	E_p (mV)	ΔE_p (mV)	$\lvert E_{corr}-E_p \rvert$ (mV)	i_p ($\mu A/cm^2$)
Ringer pH = 3.21					
Ti	-400.4	-200.2	>2000	200.2	25.1
Ti-15Zr-5Nb	-350.5	-200.1	>2000	150.4	3.9
Ringer pH = 7.58					
Ti	-320.6	-50.3	>2000	270.3	15.2
Ti-15Zr-5Nb	-200.3	0.2	>2000	200.1	1.0
Ringer pH = 8.91					
Ti	-500.7	-200.4	>2000	300.3	18.4
Ti-15Zr-5Nb	-350.2	-200.2	>2000	150.0	4.1

Main corrosion parameters, i_{corr} and V_{corr} from Table 3 present very low values (tens of times smaller) for the alloy in comparison with Ti, confirming a very resistant passive film on the alloy surface. The alloy corrosion rates, V_{corr} are placed in the "Perfect Stable" resistance class and the corresponding total quantities of the ions released in Ringer solution are lower than those of Ti, proving the alloy very reduced toxicity. Polarisation resistances, R_p have higher values (tens of times) for the new alloy in comparison with Ti metal, due to the very high protective capacity of the alloy passive layer. The R_p values of about 10^5 Ω cm^2 for Ti-15Zr-5Nb alloy denote a highly corrosion resistance.

Table 3. Main corrosion parameters of Ti-15Zr-5Nb alloy and Ti, obtained in Ringer solutions at 37^0C.

Material	i_{corr} ($\mu A/cm^2$)	V_{corr} ($\mu m/yr$)	Resistance class	R_p ($k\Omega$ cm^2)
Ringer pH = 3.21				
Ti	0.746	8.625	Very Stable	11.35
Ti-15Zr-5Nb	0.081	0.751	Perfect Stable	330.83
Ringer pH = 7.58				
Ti	0.724	8.326	Very Stable	18.25
Ti-15Zr-5Nb	0.039	0.358	Perfect Stable	397.05
Ringer pH = 8.91				
Ti	1.186	13.700	Stable	13.91
Ti-15Zr-5Nb	0.071	0.657	Perfect Stable	305.14

Open circuit potentials, E_{oc} shift to more electropositive direction both for Ti and Ti-15Zr-5Nb alloy in all three Ringer solutions (Fig. 7), showing the growth and thickening of their passive layer [19,20]. For Ti-15Zr-5Nb alloy, the more electropositive values were registered, which are indicative of a nobler behaviour than that of Ti. The most positive values of E_{oc} were obtained in neutral Ringer solution, proving the best passive resistant state; little more active E_{oc} values were monitored in acid and alkaline Ringer solutions depicting a slightly corrosion susceptibility in these solutions.

The open circuit potential differences, ΔE_{oc} that can appear due to the pH non-uniformities along the alloy surface were calculated in Table 4; very low values were obtained and these potential differences cannot initiate or maintain galvanic cells or local corrosion.

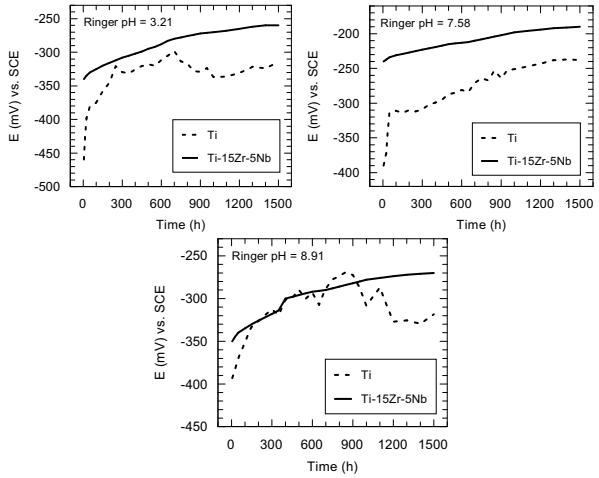

Fig. 7. E_{oc} versus time for Ti and Ti-15Zr-5Nb alloy in Ringer solutions at 37^0C.

Table 4. Open circuit potential differences for Ti-15Zr-5Nb alloy in Ringer solutions at 37^0C.

Time (h)	ΔE_{oc1}(pH) (mV)	ΔE_{oc2}(pH) (mV)	ΔE_{oc3}(pH) (mV)
0	-100.6	+10.1	+110.2
500	-80.1	+10.6	+81.4
1000	-72.3	+8.2	+80.3
1500	-70.5	+10.4	+80.5

Alloy surface analysis after 1500 h in Ringer solutions

SEM micrographs of the Ti-15Zr-5Nb alloy surfaces after 1500 h in Ringer solutions of different pH values (Figs. 8a-c) show the formation of the surface films: sub-micron sized particles are scattered on the alloy surfaces, deposited from the solutions on all the samples. Immersion in Ringer of pH= 3.21 results in a smoother surface (Fig. 9a); increasing the pH value (Figs 8b and c) leads to higher densities of deposited particles. The EDX elemental analysis (an example is given in Fig. 8d) clearly shows the rich oxygen content of the surface, Ca and P.

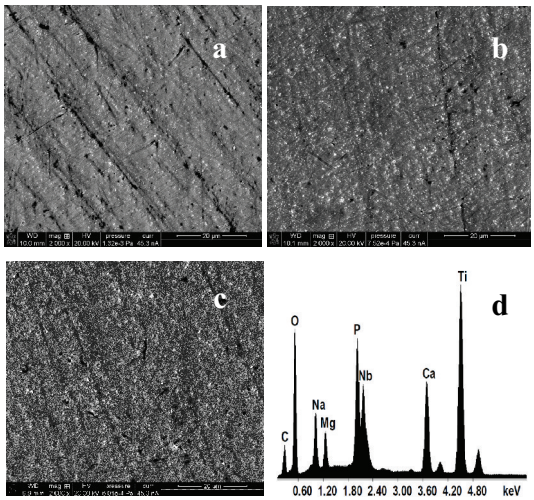

Fig. 8. SEM micrographs of the Ti-15Zr-5Nb alloy surface after immersion in Ringer solution at:a) pH= 3.21; b) pH = 7.58; c) pH = 8.91; d) EDX spectra pH=8.91.

XPS analysis was carried out to determine the Ca/P ratio in the calcium phosphate surface films deposited from the Ringer solutions. XPS survey spectra of the Ti-15Zr-5Nb alloy surface after 1500 soaking hours in Ringer solutions (Fig. 9) reveal the peaks of Ti 2p, Zr 3d, Nb 3d, O 1s, C 1s, P 2p, Ca 2p [17,18], namely the surface film contains the oxides of the alloy constituent elements, carbon as contaminant element, and, in addition, calcium and phosphorous ions [21-25]. The deconvoluted spectra for the main elements are presented in Fig. 10. The peak for Ti 2p was deconvoluted (Fig. 10a) and shows the doublets of Ti_2O_3 and TiO_2 oxides. The peak of Zr 3d distinguishes (Fig. 10b) the ZrO_2 oxide. The peak for Nb 3d represents (Fig. 10c) Nb_2O_5 oxide. The deconvoluted O1s peak evidences (Fig. 10d) OH^- and O^{2-} ions. The peak for P 2p was deconvoluted (Fig. 10e) as $Ca_3(PO_4)_2$ compound. Also, the deconvoluted Ca 2p peak proves (Fig. 10f) the presence of the same $Ca_3(PO_4)_2$ compound. Table 5 presents the element concentrations on the Ti-15Zr-5Nb alloy surface and shows that the Ca/P ratio varies around 1.5 value, the real ratio from $Ca_3(PO_4)_2$ compound. It results that the protective $Ca_3(PO_4)_2$ compound, a precursor of the hydroxyapatite, the main inorganic component of the human bone, was deposited on Ti-15Zr-5Nb alloy surface; consequently, this alloy can stimulate the bone formation.

Table 5. Relative element concentrations of the film on Ti-15Zr-5Nb alloy surface after 1500 soaking hours in Ringer solutions.

pH	C	O	Ti	Zr	Nb	P	Ca	Ca/P
3.21	22.72	55.46	16.60	1.60	0.43	1.28	1.91	1.49
7.58	10.80	63.43	18.94	2.03	0.52	1.71	2.57	1.502
8.91	10.56	63.82	20.74	2.19	0.70	0.80	1.19	1.488

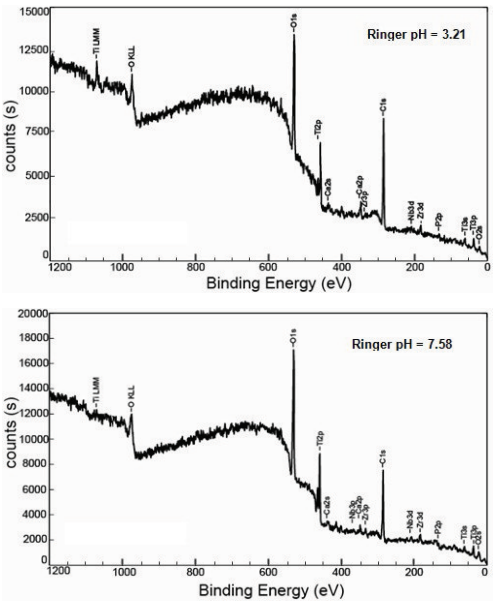

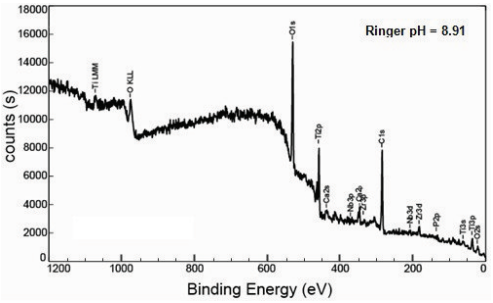

Fig. 9. XPS survey spectra of Ti-15Zr-5Nb alloy surface after 1500 soaking hours in Ringer solutions.

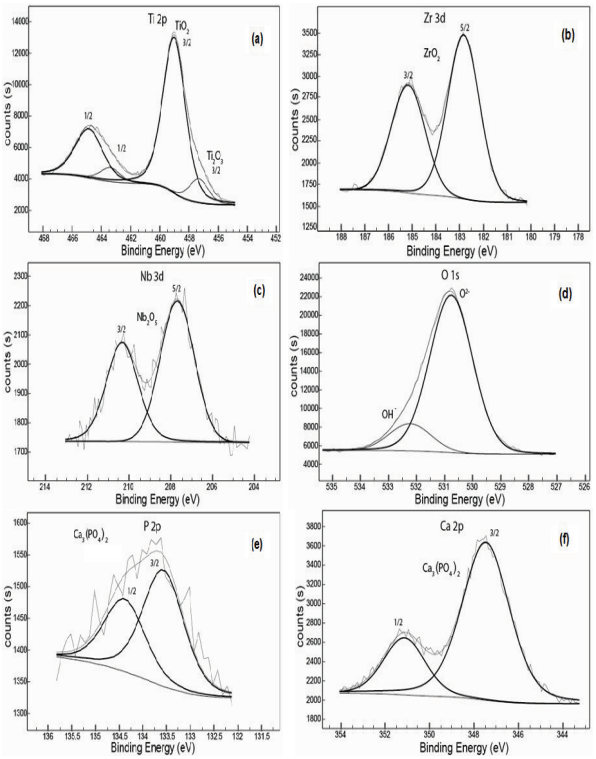

Fig. 10. XPS deconvoluted spectra of: a) Ti 2p; b) Zr 3d; c) Nb 3d; d) O 1s; e) P 2p; f) Ca 2p after 1500 soaking hours in Ringer solution of pH = 8.91.

4. CONCLUSIONS

1. The alloy shows a bi-phase α + β fully lamellar microstructure, without secondary precipitation.
2. More favourable values of the main electrochemical parameters, a nobler passive behaviour of Ti-15Zr-5Nb alloy in comparison with Ti were determined due to the alloy more resistant, compact passive film (containing high protective TiO_2, Ti_2O_3, ZrO_2, and Nb_2O_5 oxides).
3. The main corrosion parameters, i_{corr} and V_{corr} presented very low values (tens of times smaller) for the alloy than those for Ti, confirming a very resistant passive film on its surface; polarisation resistances have higher values (tens of times) for the new alloy in comparison with Ti

metal, denoting the higher protective capacity of the alloy passive film.

5. The open circuit potentials demonstrated a nobler behaviour of Ti-15Zr-5Nb alloy than that of Ti.

6. After 1500 soaking hours in Ringer solutions, SEM, EDX and XPS measurements revealed the existence of the protective Ti_2O_3, TiO_2, ZrO_2, and Nb_2O_5 oxides and of $Ca_3(PO_4)_2$ compound deposited on Ti-15Zr-5Nb alloy surface.

Acknowledgments

This work was supported by Romanian UEFISCDI, project number IDEI 278/2011. Thanks are also due to Dr. P. Osiceanu and Chem. E. I. Neacsu from Institute of Physical Chemistry, Bucharest for XPS analysis.

5. REFERENCES

[1] Q.M. Hu, S.J. Li, Y.L. Hao, R. Yang, B. Johansson, L. Vitos, Phase stability and elastic modulus of Ti alloys containing Nb, Zr, and/or Sn from first-principles calculations, Appl. Physics Letter 93 (2008) 121902.

[2] M.M. Gasik, H. Hu, Phase equilibria and thermal behaviour of biomedical Ti-Nb-Zr alloy, 17th Plansee Seminar, Reutee, Austria, 25-30 May 2009, Vol. 1, RM 29/1-7.

[3] S.Y. Yu, J.R. Scully, Corrosion and passivity of Ti-13%Nb-13%Zr in comparison to other biomedical implant alloys, Corrosion 53 (1997) 965-976.

[4] M.A. Baker, S.L. Assis, R. Grilli, I. Costa, Investigation of the electrochemical behaviour and surface chemistry of a TI-13Nb-13Zr alloy exposed in MEM cell culture media with and without the addition of H_2O_2, Surf. Interface Anal. 40 (2008) 220-224.

[5] S.L. Assis, S. Wolynec, I. Costa, Corrosion characterization of titanium alloys by electrochemical techniques, Electrochim. Acta 51 (2006) 1815-1819.

[6] S.L. Assis, I. Costa, Electrochemical evaluation of Ti-13Nb-13Zr, Ti-6Al-4V and Ti-6Al-7Nb alloys for biomedical application by long-term immersion tests, Mater. Corros. 58 (2007) 329-333.

[7] S.L. Assis, S. Wolynec, I. Costa, The electrochemical behaviour of Ti-13Nb-13Zr alloy in various solutions, Mater. Corros. 59 (2008) 739-743.

[8] I. Cvijovic-Alagic, Z. Cvijovic, S. Mitrovic, V. Panic, M. Rakin, Wear and corrosion behaviour of Ti-13Nb-13Zr and Ti-6Al-4V alloys in simulated physiological solution, Corros. Sci. 53 (2011) 796-808.

[9] P. Majumdar, S.B. Singh, U.K. Chatterjee, M. Chakraborty, Corrosion behaviour of heat treated boron free and boron containing Ti-13Zr-13Nb (wt%) alloy in simulated body fluid, J. Mater. Sci. - Mater. Med. 22 (2011) 797-807.

[10] M.F. Lopez, L. Soriano, F.J. Palomares, M. Sanchez-Agudo, G.G. Fuentes, A. Gutierrez, J.A. Jimenez, Soft x-ray absorption spectroscopy study of passive and oxide layers of titanium alloys, Surf. Interface Anal. 33 (2002) 570-576.

[11] C. Morant, M.F. Lopez, A. Gutierrez, J.A. Jimenez, AFM and SEM characterization of non-toxic vanadium-free Ti alloys used as biomaterials, Appl. Surf. Sci. 220 (2003) 79-87.

[12] M.F. Lopez, J.A. Jimenez, A. Gutierrez, Corrosion study of surface-modified vanadium-free titanium alloys, Electrochim. Acta 48 (2003) 1395-1401.

[13] A. Robin, O.A.S. Carvalho, S.G. Schneider, S. Schneider, Corrosion behavior of Ti-xNb-13Zr alloys in Ringer's solution, Mater. Corros. 59 (2008) 929-933.

[14] Y.H. Jeong, H.C. Choe, W.A. Brantley, Electrochemical and surface behaviour of hydroxyapatite/Ti film on nanotubular Ti-35Nb-xZr alloys, Appl. Surf. Sci. 258 (2012) 2129-2136.

[15] Z. Cai, H. Nakajima, M. Woldu, A. Berglund, M. Bergman, T. Okabe, In vitro corrosion resistance of titanium made using different fabrication methods, Biomaterials 20 (1999) 183-190.

[16] R. Van Noort, The implant material of today, J. Mater. Sci. 22 (1987) 3801-3811.

[17] J.F. Moulder, W.F. Stickle, P.E. Sobol, K.D. Bomben, Handbook of X-ray photoelectron spectroscopy, Physical Electronics USA, Inc., Chamhassen, 1995.

[18] A.V. Naumkin, A. Kraut-Vass, S.W. Gaarenstroom, C.J. Powell, NIST X-ray photoelectron spectroscopy database. NIST standard reference database 20, version 4.1. US Secretary of Commerce on behalf of the United States of America, 2012..

[19] J. Black, Biological performance of materials: Fundamentals of biocompatibility, M. Decker Inc. NY, 1992.

[20] D.J. Blackwood, A.W.C. Chua, K.H.W. Seah, R. Thampuran, Corrosion behaviour of porous titanium-graphite composite designed for surgical implants, Corros. Sci. 42 (2000) 481-503.

[21] Y. Tanaka, M. Nakai, T. Akahori, M. Niinomi, Y. Tsutsumi, H. Doi, T. Hanawa, Characterization of air-formed surface oxide film on Ti-29Nb-13Ta-4.56Zr alloy surface using XPS and AES, Corros. Sci. 50 (2008) 2111-2116.

[22] I.S. Park, U.J. Choi, H.K. Yi, B.K. Park, M.H. Lee, T.S. Bae, Biomimetic apatite formation and biocompatibility on chemically treated Ti-6Al-7Nb alloy, Surf. Interface Anal. 40 (2008) 37-42.

[23] I. Milosev, T. Kosec, H.H. Strehblow, XPS and EIS study of the passive film formed on orthopaedic Ti-6Al-7Nb alloy in Hank's physiological solution, Electrochim. Acta 53 (2008) 3547-3558.

[24] W. Simka, Preliminary investigations on the anodic oxidation of Ti-13Nb-13Zr alloy in a solution containing calcium and phosphorus, Electrochim. Acta 56 (2011) 9831-9837.

[25] I. Milosev, M. Meticos-Hukovic, H.H. Strehblow, Passive film on orthopaedic TiAlV alloy formed in physiological solution investigated by X-ray photoelectron spectroscopy, Biomaterials 21 (2000) 2103-2113.

Classification of Phyto-pathogens Using Infrared Spectroscopy and Advanced Computerized Methods

Ahmad. SALMAN
Department of Physics, SCE-Shamoon College of Engineering
Beer-Sheva 84100, Israel

and

Elad. SHUFAN
Department of Physics, SCE-Shamoon College of Engineering
Beer-Sheva 84100, Israel

and

Leah. TSROR
Department of Plant Pathology, the Institute of Plant Protection
Agricultural Research Organization, Gilat Experiment Station, M.P. Negev, 85250, Israel

and

Raymond. MOREH
Department of Physics, Ben-Gurion University of the Negev
Beer-Sheva 84105, Israel

and

Mahmoud. HULEIHEL
Department of Microbiology, Immunology and Genetics, Faculty of Health Sciences
Ben-Gurion University of the Negev, Beer-Sheva 84105, Israel

and

Shaul. MORDECHAI
Department of Physics, Ben-Gurion University of the Negev
Beer-Sheva 84105, Israel

ABSTRACT

Fungi are serious pathogens for many plants and crops, potentially causing severe economic loss. Early detection and identification of these pathogens is crucial for their timely control. Currently existing methods available for identification of fungi are time consuming, expensive and not always very specific.

We used Fourier Transform InfraRed spectroscopy (FTIR) attenuated total reflectance (ATR), combined with Principal Component Analysis (PCA), and Linear Discriminant Analysis (LDA), for differentiating fungal phyto-pathogens at the isolate level. Four different fungi genera were investigated; *Colletotrichum*, *Verticillium*, *Fusarium* and *Rhizoctoniai*. Our main goal was to differentiate these fungi samples at the level of isolates, based on their infrared (IR) fingerprint absorption spectra. Based on our computerized and objective analyses, our results are in high compliance with existing biological classification methods. FTIR, combined with advanced computerized methods, provides an inexpensive and reagent-free technique that delivers accurate results on fungi classification within few minutes. FTIR may also turn out to be an important *in situ* and *in vivo* alternative diagnostic tool in agricultural.

At the generic level, the identification success rate was 97.5% using five principal components (PCs), while at the isolates level the identification success rates were 97.1%, 90%, and 89%, respectively, for *Verticillium dahliae*, *Colletotrichum coccodes*, and *Fusarium oxysporum*.

Keywords: FTIR–ATR, *Colletotrichum coccodes*, *Verticillium dahliae*, *Fusarium oxysporum*, *Rhizoctonia solani*, fungal detection, PCA, LDA.

1. INTRODUCTION

Living organisms are biologically classified into different units based on their similarity. For example, in fungi, groups of organisms that can interbreed and produce fertile offspring (with DNA similarity) are called species. A genus consists of species that are believed to have the same ancestors. Fungal isolates usually result from one or more mutations in the species.

Colletotrichum coccodes, *Verticillium dahliae*, *Fusarium oxysporum* and *Rhizoctonia solani* are soil-borne fungi pathogens that attack a variety of hosts, causing serious damage to crops and plants. These fungi are grouped into four classes at the generic level.

Colletotrichum coccodes causes anthracnose in tomatoes and black dot disease in potatoes. *Verticillium dahliae* attacks and causes a wilt disease in many species of eudicot plants. *Fusarium* is a large fungi genus with a wide variety of species

and isolates that inhabit soil and vegetation. It is distributed worldwide and associated with both warm and cold weather **[1, 2]**. *Rhizoctonia solani* attacks seeds, roots, leaves and fruits. Many economically important plants are susceptible, including cotton, tomatoes, potatoes, eggplants, and peppers.
Symptoms alone cannot determine the exact disease because in some cases different infections that are caused by different genera or species have the same symptoms. For example, a solanaceous crop may be infected by *Fusarium* wilt and *Verticillium* wilt, with both having the same symptoms.
Figures 1A–D show pictures of plants and crops infected by the investigated fungi genera. Fig. 1A shows olive trees infected with *Verticillium*. In Fig. 1B *Fusarium* wilt symptoms on tomato leaves appear as leaf wilting. Yellowing can be seen and eventually plant death can occur. Infected plants usually survive but both the yields and the fruits may diminish, depending on the severity of attack. Fig. 1C shows potato tubers infected with *Rhizoctonia*, which causes serious damage to the fruit. Fig. 1D shows tomato (1) and potato (2) crops infected with *Colletotrichum*.

A) ***Verticillium*** **on olive**

B) ***Fusarium*** **on tomato**

C) ***Rhizoctonia*** **on potato**

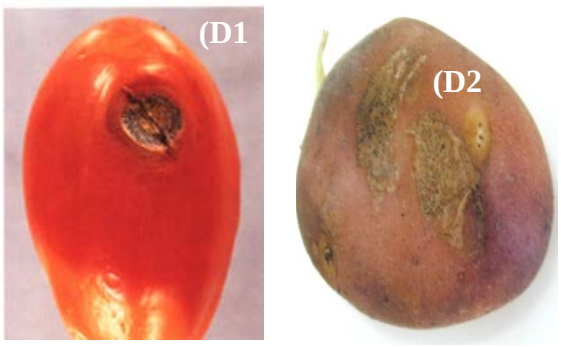

D) *Colletotrichum* on (1) tomato and (2) potato

Figure 1: Pictures of plants and fruits infected by the investigated fungi genera.

Early stage disease detection is essential for effective treatment and precise targeting **[3]** to take place, thus preventing substantial economic losses **[1, 4]** due to crop damage caused by fungi diseases. Early diagnosis is also important for detecting the origin of newly discovered isolates, in order to treat the disease in its early stages. Early detection could also prevent unnecessary soil fumigation or the use of fungicides and bactericides, thus averting considerable environmental pollution.
The techniques currently used for the detection of fungal pathogens are mainly based on the physiological characteristics of the fungi **[1, 5, 6]**. These techniques are usually time-consuming and not always specific **[7]**. In addition, immunological **[8, 9]** and molecular techniques (based on Polymerase Chain Reaction (PCR) amplifications of specific DNA fragments that depend on the availability of two specific DNA primers **[10-12]** have also been used **[13-15]**. Although these two later techniques are accurate and specific, they are still limited for small number of fungi. Applying these techniques for other fungi is very complicated and not always possible. Early diagnosis is also important for detecting the origin of newly discovered isolates, in order to treat the disease in its early stages.
FTIR spectroscopy, as used in this study, provides detailed information about the chemical composition of cells at the molecular level, allowing for the measurement of very small samples. It is a very sensitive method with high resolution and rapid performance, which makes it very economical as well.
The IR spectrum of any compound is known to provide a unique "fingerprint" **[16]**. IR spectroscopy has been used widely in applications requiring qualitative and quantitative analysis of biological samples through the molecular fingerprint of their vibrational spectrum. Recently, IR spectroscopy has demonstrated encouraging trends in detection and characterization of various types of phyto-pathogens **[17-28]**.
The main goal of the present study was to test the feasibility of the FTIR–ATR methodology in differentiating 30 isolates obtained from four different fungi genera**:** *Colletotrichum* (15 isolates), *Verticillium* (6 isolates) , *Fusarium* (8 isolates) and *Rhizctonia* (2 isolates). The classification procedure was done in two phases. In the first, the fungal samples were classified at the generic level, while in the second stage; the samples were classified at the isolate level. The classification procedures were based on IR absorption spectra of the samples, and using advanced mathematical and statistical techniques, PCA followed by LDA.
FTIR–ATR sampling technique is one step towards using mid IR fibers for *in vivo* measurements. The development of these fibers will enable us to use them for *in vivo* measurements using a compact portable IR spectrometer.
Recently, acceleration in the development of IR fiberoptics probes has increased the importance of FTIR–ATR studies in this field, because they have similar operating principles. Thus, the evolution of the FTIR–ATR system for classification of

fungal samples at the isolate level will be of great importance in future *in vivo* and *in situ* examination through the use of fiberoptic probes. These measurements will probably take only a few minutes, therefore proving to be much faster than the classical existing microbiological methods.

2. MATERIALS AND METHODS

Fungi

Several isolates from different phytofungal genera were examined in this study. The fungal isolates were provided by the Department of Plant Pathology, the Institute of Plant Protection, Agricultural Research Organization, at the Gilat Experiment Station, Israel.

The tested fungi were isolated from appropriate infected stems or tubers. The isolated fungal samples were placed on potato dextrose agar (PDA) and incubated at 27ºC in the dark for several days. Conidia were grown into medium containing 0.2% sorbose, 15% agar and 100ppm streptomycin sulphate (SA) for 24 h at 27ºC in the dark. Monoconidial cultures were obtained from each isolate (by micromanipulation) and maintained on czapek dox agar (CDA) at 6ºC.

Each isolate, in five replicates, was cultivated in different batches for 3–10 days at 27°C in continuous shaking. Samples of the grown fungi were identified by classical microbiological techniques based on microscopic observations **[2]**.

For spectroscopic examinations, the samples were separated and purified by spinning about 1.5 ml of the fungal mixture at 13200 rpm for 4 minutes, rinsing and washing the pellet 4 times with distilled water, and suspending the pellet in an appropriate volume of distilled water (about 1 ml).

Using pure samples is very important in this basic research in order to minimize the number of controlling experimental parameters such as growth conditions, amount of sample examined, and duration of growth. Verification that each absorption band in the IR spectrum is due to the specific sample is very desirable.

Table 1: Details of the isolates and measurements are listed.

	Fusa.	*Coll.*	*Rhiz.*	*Vert.*
No. of isolates	8	14	2	6
No. of measure.	169	251	51	107

Sample preparation

The fungi samples were first crushed into small pieces and then mixed into the distilled water to obtain a suspension. About 500 µl of each fungal suspension sample was spread homogenously on the surface of the ATR ZnSe crystal to cover the entire crystal surface. These samples were air dried for about 30 min until all water had evaporated and were then measured by ATR spectroscopy. The ATR crystal employed in this study has a trapezoid shape 80 mm long, 10 mm wide, and 4 mm thick, and was obtained from PIKE technologies.

FTIR measurements

A Bruker Tensor 27 spectrometer attached to a DTGS detector was used to perform the measurements in the ATR mode. The samples were dried before measurements and were scanned 128 times in the range of 600–4000 cm^{-1}, with a 4 cm^{-1} spectral resolution. Baseline correction, bisecting, ATR correction, and normalization were done using OPUS 7.

Spectral Analysis

The details of the genera and isolates investigated in this study are listed in Table 1. After spectral manipulations, the spectra were then bisected into 2 regions (800–1775 cm^{-1}) and (2800–2990 cm^{-1}) to exclude the water absorption band and the "dead" region between amide I and the lipid bands.

PCA and LDA statistical analysis

PCA is a standard approach for dimensionality reduction, widely used in pattern recognition and also for a rough differentiation of measured data into different categories. We used multivariate analysis PCA and LDA for the classification of the samples into generic and isolate levels **[18]**.

LDA was used to discriminate between the different classes (genus and isolates) by constructing a linear combination of the variables. Part of the data is used for training and the others for testing. We have tested the identification by the "leave–one–out" (LOO) procedure—one data point is chosen for testing and the rest for training, with the procedure being repeated as many times as the number of samples.

3. RESULTS AND DISCUSSION

Early detection and identification of phyto-pathogens at the isolate level is very important for controlling and reducing the pathogen's severity through fungicides **[29]**, thereby minimizing economic agriculture losses.

The currently used classical physiological methods are not effective for accurate identification between isolates at the isolate level, due to the high morphological similarity between them. Molecular and serological methods are also not available for all these isolates.

The utilizing of IR spectroscopy in agriculture has been increasing and gaining momentum **[18, 19, 24-27]**. Many studies have shown that it is possible to use FTIR-ATR spectroscopy for detection and differentiation of the phyto-ogens at the level of isolates **[18, 24]**. Using an ATR sampling technique has special importance because the working principle of this technique is similar to that of remote fiberoptic probes. Hence, developing the ATR technique may lead in the future towards *in vivo* measurements using IR fibers.

In Figure 2, two measurements from each of the four genera (*Colletotrichum*, *Verticillium*, *Fusarium* and *Rhizoctonia*) investigated in this study are presented. The spectra were plotted in the (1775–800 cm^{-1}) wavenumber region, each genus with a different color. The main absorption bands and their assignments are labeled in the figure. In the high wavenumber region 2800–2990 cm^{-1}, (not shown) the phospholipids **[30]** are the main attributers due to their CH_2 and CH_3 stretching at the bands detected at 2853 and 2922 cm^{-1}. In the wavenumber region 1775–800 cm^{-1} shown in the figure, the spectrum was divided into three ranges. The first (1800–1485 cm^{-1}), where the features are attributed by proteins due to amide I and II functional groups with centroids at 1650 cm^{-1} and 1553 cm^{-1} respectively, while the band centered at 1743 cm^{-1} is attributed from lipids **[31]**. In the second range (1485–1185 cm^{-1}), lipids, proteins, phospholipids are the main attributer due to their CH_2, CH_3 and P=O functional groups. The amide III band is observed at 1253 cm^{-1}. In the third range, (1185–900 cm^{-1}) **[24]**, the vibrations of the functional groups C–O–C, C–O–P (polysaccharides, carbohydrate and nucleic acid vibrations) are the main attributers. The chitin band which is specific to fungi is detected at 1151 cm^{-1} and 1076 cm^{-1} due to its C–O and C–C stretching vibrations and the glycogen C–O stretching vibration is detected at 1024 cm^{-1}. As can be seen from the figure, at the generic level there are clear differences in the amide I and II, chitin and glycogen peaks, which leads to good differentiation

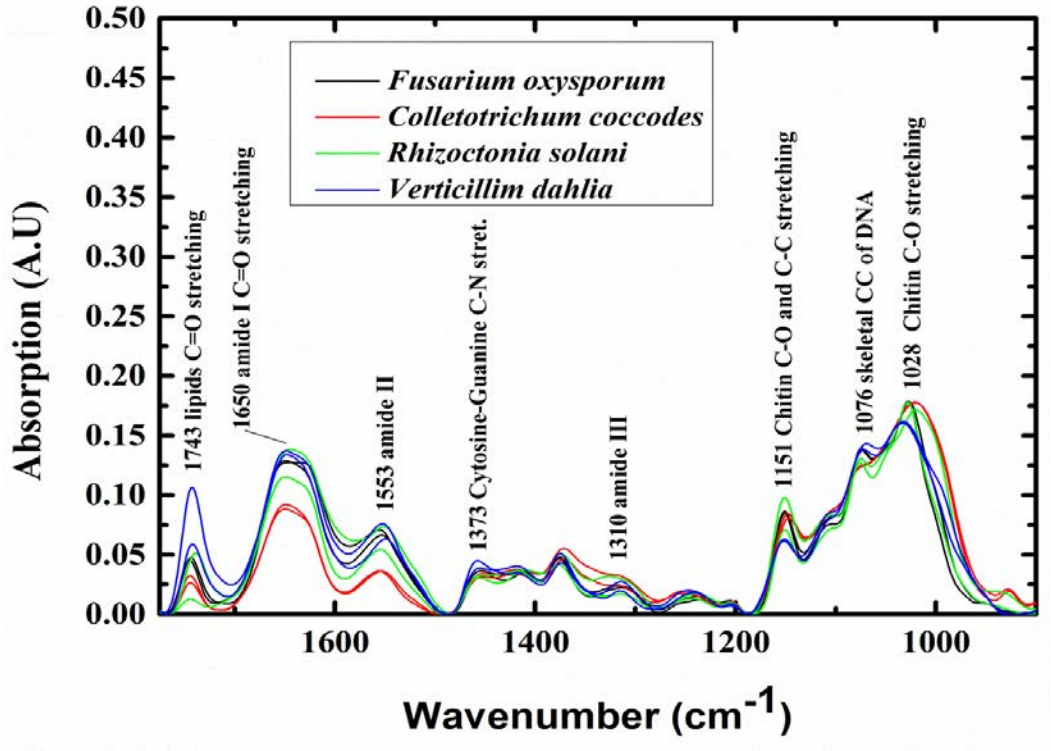

Figure 2: Mid IR absorption spectra in the fingerprint region (1775–800 cm^{-1}) for the investigated genera, *Fusarium ,Colletotrichum, Rhizoctonia and Verticillium*. From each genus (represented in different color), two measurements were plotted.

in this level. The intensities of the absorption bands in the amide I and II regions for the *Colletotrichum* fungus is lower than the others and this indicates lower protein content relative to Fusarim, *Rhizoctonia* and *Verticillium* fungi.

Our classifying procedure was performed in two stages, in the first the samples were classified into four generic classes, while in the second the samples were classified at the isolate level which is more ambitious. For this goal, we generated 3D plot (Figure 3) using PCA calculations, which enabled us to describe the variability among the spectra using the first four PCs in the first classification stage.

PCA is used for dimensionality reduction and also for a rough differentiation of the measured data into different categories. In the PCA analysis each spectrum was calculated as a superposition of the four PCs, which means that each spectrum in the new domain was identified using four numbers that are the coefficients of the PCs. In Figure 3 the measurements are presented in the reduced space in a 3D plot, defined by three PCs—PC1, PC2, and PC4. The data is divided into four groups that are colored differently to represent the four genera—*Colletotrichum*, *Verticillium*, *Fusarium* and *Rhizoctonia.* Although the separations into four groups were good, still there was overlapping between the data, so we applied LDA using the LOO algorithm to achieve better classification.

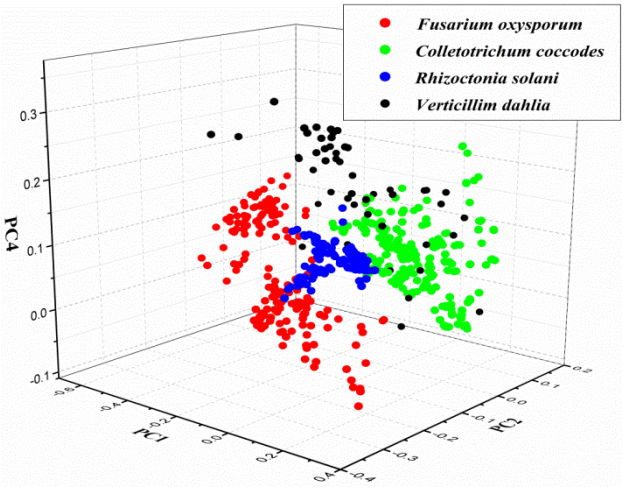

Figure 3: Complete datasets of ***the investigated genera*** presented in a 3D PCs domain. This figure summarizes the generic classification results.

Using LDA with the LOO algorithm the four genera were differentiated with 93.4% success rate using four PCs. When we used five 5 PCs the identification success rate was 97.5%. At the generic level a few PCs were enough to achieve sufficient success, while at the isolates level more PCs were required. PCA enabled us to capture the variability of the fungi using a small number of PCs. In the first stage the examined fungi genera were successfully differentiated with a high degree of accuracy using four PCs. The isolates of the same species result from one or more mutations, so the differences between their spectra were minor. Therefore, we used a higher number of PCs for good classification. Choosing the number of PCs is task-dependent, that is, the number of classes to be classified, the level of classification (genus, species or isolates), and the type of samples.

A more comprehensive method of differentiation is the LDA. The LDA calculations, were designed applying the LOO algorithm, using different sets for prediction each time, so that the test sets are statistically independent. The LOO method is a common method of cross-validation, extensively explored in machine learning, and used to estimate the error in small sized populations. Using LOO ensures the validity of results **[32]**.

The LDA calculation defines a linear combination of each category's features, which enables it to separate the data to specific categories. The LDA results based on the low region, using the LOO algorithm with four PCs, are listed in Table 2, which summarizes the classification results of the first stage classification, which is the generic classification.

The high wavenumber region was also tested to differentiate among the genera but the low region results were much superior.

Table 2: Generic classification results using LDA for the first stage classification between *Fusarium (Fusa) ,Colletotrichum (Coll.), Rhizoctonia (Rhiz.) and Verticillium (Vert.).*

	Fusa.	*Coll.*	*Vert.*	*Rhiz.*
Fusa.	156	1	0	12
Coll.	0	248	0	3
Vert.	0	0	104	0
Rhiz.	11	10	0	30

At the isolates level we tried to differentiate between the isolates of *Colletotrichum coccodes* (14 isolates), *Verticillium dahliae* (6 isolates) and *Fusarium oxysporum (8 isolates).* We had only two isolates of *Rhizoctonia solani,* so it was excluded from the analysis in the second stage of differentiation (isolate level).

As mentioned earlier and expected, the differences among the samples at the generic level are much larger than at the isolate level. Figure 4 shows four different isolates of *Verticillium dahliae*, with three measurements of each of the isolates that

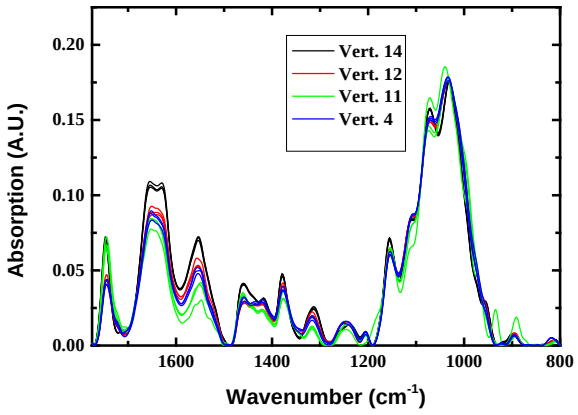

Figure 4: Mid IR absorption spectra in the fingerprint region (1775–800 cm^{-1}) for four isolates of *Verticillium*. For each isolate three measurements were plotted in different color.

have the same colors. As can be seen from the figure, the changes between the spectra are minute relative to the generic differences shown in Figure 2.

At this level of differentiation we used the LDA calculation with the LOO algorithm. 2D and 3D plots were not able to differentiate among the isolates of each species.

Due to the similarity between the isolates of each of the three genera investigated in this study—*Colletotrichum coccodes*, *Verticillium dahliae* and *Fusarium oxysporum*—more PCs had to be used than in the first (generic) stage of identification **[20]**.

In order to choose the number of PCs at the isolate level, we calculated the identification error (in percentage) versus the number of PCs (data not shown) derived using LDA with the LOO algorithm and the number of PCs was chosen to give a good differentiation results.

Similar calculations were performed for the other two genera, and for each one a different number of PCs was chosen for this stage of identification.

The LDA results using the LOO algorithm and 17 PCs showed that it was possible to differentiate between the *Colletotrichum* isolates with a 90 % success rate, while the classification success rates of the *Fusarium* (18 PCs) and *Verticillium* (6 PCs) isolates were 85.5 % and 97.1% respectively.

Based on the mid IR absorption spectra, there were no specific features that indicated the changes between the different isolates. The differences are spread over the entire spectrum and are not specific to a certain spectral band.

The applied method is objective and computerized. Enlarging the database and the number of isolates will improve the statistics and bring the method closer to reality, where large numbers of isolates exist. The method shows a great potential for the identification and study of phytofungal pathogens at the level of isolate identification.

In summary, mid IR vibrational spectroscopy in the ATR mode, in tandem with advanced mathematical and statistical methods, provides a good methodology for classification of fungi at the isolate level. The database and numbers of isolates should be enlarged in order to improve the statistics and better simulate the actual agricultural problem, where tens of isolates of each species do exist.

4. CONCLUSIONS

There is great potential for the use of FTIR-ATR spectroscopy in tandem with appropriate mathematical tools in order to obtain an easy and rapid discrimination and identification of various fungi genera and isolates—the causes of significant damage in agriculture. The simplicity of sample preparation, short measurement times (<1 min) when compared to other available methods, and low costs, make the FTIR-ATR technique suitable for large-scale screening of fungal samples, and for routine analysis. These facts also encourage the possibility of developing FTIR-ATR spectroscopy as a reliable method for rapid identification of fungal pathogens.

Combining the advantages of FTIR spectroscopy with other routinely used techniques offers the chance to improve the efficiency of fungal classification and identification.

ACKNOWLEDGMENTS

Financial support from SCE-Shamoon College of Engineering internal research funding is gratefully acknowledged.

The help of Dr. Itshak Lapidot and his fruitful discussion concerning pattern recognition issues are gratefully acknowledged.

REFERENCES

1. G.N. Agrios **Plant pathology** San Diego ; London: Academic Press 3rd Ed, 1988.
2. L. Tsror, M. Hazanovsky, S. Mordechi-Lebiush, & S. Sivan "Aggressiveness of Verticillium dahliae isolates from different vegetative compatibility groups to potato and tomato". **Plant Pathology**, Vol. 50, No. 4, 2001, pp. 477-482.
3. G.V. Doern, R. Vautour, M. Gaudet, & B. Levy "Clinical impact of rapid in vitro susceptibility testing and bacterial identification". **J Clin Microbiol**, Vol. 32, No. 7, 1994, pp. 1757-1762.
4. J. Katan Plant Diseases in Israel. Principles in Plant Pathology, ed J. Rotem JP, and Y. Ben-YephetVolcani Center, Bet-Dagan, Israel), 1998.
5. G.-H. Kim, J.-J. Kim, Y.W. Lim, & C. Breuil "Ophiostomatoid fungi isolated from Pinus radiata

logs imported from New Zealand to Korea". **Canadian Journal of Botany**, Vol. 83, No. 3, 2005, pp. 272-278.

6. U. Moreth & O. Schmidt Investigations on ribosomal DNA of indoor wood decay fungi for their characterization and identification**.** in *Holzforschung* (2005), 90.
7. G.L. Schumann & C.J. D'Arcy **Essential plant pathology** St. Paul, Minn.: APS Press 2nd Ed, 2010.
8. S.E. Maddison "Serodiagnosis of parasitic diseases". **Clin Microbiol Rev**, Vol. 4, No. 4, 1991, pp. 457-469.
9. A.F. da Silva, M.L. Rodrigues, S.E. Farias, I.C. Almeida, M.R. Pinto, & E. Barreto-Bergter "Glucosylceramides in Colletotrichum gloeosporioides are involved in the differentiation of conidia into mycelial cells". **FEBS Lett**, Vol. 561, No. 1-3, 2004, pp. 137-143.
10. A.K. Lees & A.J. Hilton "Black dot (Colletotrichum coccodes): an increasingly important disease of potato". **Plant Pathology**, Vol. 52, No. 1, 2003, pp. 3-12.
11. R.K. Saiki, S. Scharf, F. Faloona, K.B. Mullis, G.T. Horn, H.A. Erlich, & N. Arnheim "Enzymatic amplification of beta-globin genomic sequences and restriction site analysis for diagnosis of sickle cell anemia". **Science**, Vol. 230, No. 4732, 1985, pp. 1350-1354.
12. C. Torres-Calzada, R. Tapia-Tussell, A. Quijano-Ramayo, R. Martin-Mex, R. Rojas-Herrera, I. Higuera-Ciapara, & D. Perez-Brito "A species-specific polymerase chain reaction assay for rapid and sensitive detection of Colletotrichum capsici". **Mol Biotechnol**, Vol. 49, No. 1, 2011, pp. 48-55.
13. N.R. O'Neill, P. van Berkum, J.J. Lin, J. Kuo, G.N. Ude, W. Kenworthy, & J.A. Saunders "Application of amplified restriction fragment length polymorphism for genetic characterization of colletotrichum pathogens of alfalfa". **Phytopathology**, Vol. 87, No. 7, 1997, pp. 745-750.
14. S. Nikkari & D.A. Relman "Molecular approaches for identification of infectious agents in Wegener's granulomatosis and other vasculitides". **Current opinion in rheumatology**, Vol. 11, No. 1, 1999, pp. 11-16.
15. M. Vaneechoutte & J. Van Eldere "The possibilities and limitations of nucleic acid amplification technology in diagnostic microbiology". **J Med Microbiol**, Vol. 46, No. 3, 1997, pp. 188-194.
16. D. Naumann, D. Helm, & H. Labischinski "Microbiological characterizations by FT-IR spectroscopy". **Nature**, Vol. 351, No. 6321, 1991, pp. 81-82.
17. A. Salman, I. Lapidot, A. Pomerantz, L. Tsror, Z. Hammody, R. Moreh, M. Huleihel, & S. Mordechai "Detection of Fusarium oxysporum Fungal Isolates Using ATR Spectroscopy". **Spectroscopy: An International Journal**, Vol. 27, No. 5-6, 2012, pp.
18. A. Salman, I. Lapidot, A. Pomerantz, L. Tsror, E. Shufan, R. Moreh, S. Mordechai, & M. Huleihel "Identification of fungal phytopathogens using Fourier transform infrared-attenuated total reflection spectroscopy and advanced statistical methods". **J Biomed Opt**, Vol. 17, No. 1, 2012, pp. 017002.
19. A. Salman, A. Pomerantz, L. Tsror, I. Lapidot, R. Moreh, S. Mordechai, & M. Huleihel "Utilizing FTIR-ATR spectroscopy for classification and relative spectral similarity evaluation of different Colletotrichum coccodes isolates". **Analyst**, Vol. 137, No. 15, 2012, pp. 3558-3564.
20. A. Salman, A. Pomerantz, L. Tsror, I. Lapidot, A. Zwielly, R. Moreh, S. Mordechai, & M. Huleihel "Distinction of Fusarium oxysporum fungal isolates (strains) using FTIR-ATR spectroscopy and advanced statistical methods". **Analyst**, Vol. 136, No. 5, 2011, pp. 988-995.
21. A. Salman, L. Tsror, A. Pomerantz, R. Moreh, S. Mordechai, & M. Huleihel "FTIR spectroscopy for detection and identification of fungal phytopathogenes". **Spectroscopy: An International Journal**, Vol. 24, No. 3, 2010, pp. 261-267.
22. M.J. GUPTA, J.M. IRUDAYARAJ, C. DEBROY, Z. SCHMILOVITCH, & A. MIZRACH **Differentiation of food pathogens using ftir and artificial neural networks** St. Joseph, MI, ETATS-UNIS: American Society of Agricultural Engineers, 2005.
23. H. Lamprell, G. Mazerolles, A. Kodjo, J.F. Chamba, Y. Noël, & E. Beuvier "Discrimination of Staphylococcus aureus strains from different species of Staphylococcus using Fourier transform infrared (FTIR) spectroscopy". **International Journal of Food Microbiology**, Vol. 108, No. 1, 2006, pp. 125-129.
24. A. Naumann "A novel procedure for strain classification of fungal mycelium by cluster and artificial neural network analysis of Fourier transform infrared (FTIR) spectra". **Analyst**, Vol. 134, No. 6, 2009, pp. 1215-1223.
25. R. Linker & L. Tsror "Discrimination of Soil-Borne Fungi Using Fourier Transform Infrared Attenuated Total Reflection Spectroscopy". **Appl. Spectrosc.**, Vol. 62, No. 3, 2008, pp. 302-305.
26. G. Fischer, S. Braun, R. Thissen, & W. Dott "FT-IR spectroscopy as a tool for rapid identification and intra-species characterization of airborne filamentous fungi". **J Microbiol Methods**, Vol. 64, No. 1, 2006, pp. 63-77.
27. V. Shapaval, T. Moretro, H.P. Suso, A.W. Asli, J. Schmitt, D. Lillehaug, H. Martens, U. Bocker, & A. Kohler "A high-throughput microcultivation protocol for FTIR spectroscopic characterization and identification of fungi". **J Biophotonics**, Vol. 3, No. 8-9, 2010, pp. 512-521.
28. F.L. Martin, J.G. Kelly, V. Llabjani, P.L. Martin-Hirsch, Patel, II, J. Trevisan, N.J. Fullwood, & M.J. Walsh "Distinguishing cell types or populations based on the computational analysis of their infrared spectra". **Nat Protoc**, Vol. 5, No. 11, 2010, pp. 1748-1760.
29. J. Ingram, T. Cummings, & D. Johnson "Response of Colletotrichum Coccodes to Selected Fungicides Using a Plant Inoculation Assay and Efficacy of Azoxystrobin Applied by Chemigation". **American Journal of Potato Research**, Vol. 88, No. 4, 2011, pp. 309-317.
30. Z. Movasaghi, S. Rehman, & D.I. ur Rehman "Fourier Transform Infrared (FTIR) Spectroscopy of Biological Tissues". **Applied Spectroscopy Reviews**, Vol. 43, No. 2, 2008, pp. 134-179.
31. R.K. Dukor Vibrational Spectroscopy in the Detection of Cancer. Handbook of Vibrational Spectroscopy, (John Wiley & Sons, Ltd), 2006.
32. T. Evgeniou, M. Pontil, Andr\, \#233, & Elisseeff "Leave One Out Error, Stability, and Generalization of Voting Combinations of Classifiers". **Mach. Learn.**, Vol. 55, No. 1, 2004, pp. 71-97.

Anticorrosive properties of new titanium based alloy in corrosive environments

Paula DROB, Ecaterina VASILESCU, Cora VASILESCU, Silviu I. DROB, Mihai V. POPA
Romanian Academy, Institute of Physical Chemistry "Ilie Murgulescu", Bucharest, Romania

and

Steliana IVANESCU
SC R&D Consulting and Services SRL, Bucharest, Romania

ABSTRACT

A new Ti-6Al-2Nb-1Ta alloy was obtained to satisfy the mechanical and anticorrosion requirements in neutral corrosive environment. The corrosion behaviour of this new Ti-6Al-2Nb-1Ta alloy in 0.1M Na_2SO_4, 3% NaCl solutions and synthetic sea water was studied in this paper, using potentiodynamic and linear polarisation method, electrochemical impedance spectroscopy (EIS) and monitoring of the open circuit potentials. The structure of the alloy represents an $\alpha + \beta$ uniform structure with un-oriented grains. From the polarisation potentiodynamic curves it resulted that the studied alloy is self passivated in all three solutions having a very good and very easy tendency to passivation. The most favourable values of the electrochemical parameters were registered in 0.1M Na_2SO_4 solution due to its reduced corrosivity. EIS measurements proved the improvement of the passive layer resistance with the immersion time. An electric equivalent circuit with two tome constants was fitted. The values of the polarisation resistances showed very good protective capacities which improved in time. The open circuit potentials have the general tendency to ennoble in time, suggesting the thickening of the passive films and the increase of their protective capacities.

Keywords: Ti-6Al-2Nb-1Ta alloy, Microstrucutre, Corrosion rates, EIS, Neutral solutions.

1. INTRODUCTION

Sea water is a very corrosive complex environment; the corrosion of the metallic structures in the sea water is influenced by many factors as: salinity, temperature, pH, relative its velocity, bacteria and marine organisms [1-3]. Saline neutral media based on NaCl solutions of different concentration as: 240 g/L [4], 0.15M [5], 0.5M [6], and 0.9% (physiological serum) [7-9] were used as corrosive electrolytes for the study of the behaviour of the various alloys. Sodium sulphate salt is used in daily life in power detergents, wood pulp processing for Kraft paper, textile lining processes, etc. [5-10]; sulphate ions have a reduced corrosivity but the resistance of a reduced number of alloys was studied. Aggressive neutral solutions are the solutions that simulate the human physiological fluid as: Hank, Ringer, Ringer-Brown, etc. solutions. Many alloys have good resistance in these media: Ti-6Al-4V [11], Ti-6Al-7Nb [12], Ti-35Nb [13], Ti-30; 40; 50Ta [14], Ti-5Al-2Nb-1Ta [15]. In the last years, new alloys with very good mechanical and corrosion resistance properties were obtained: Ti-40Al-15Nb [16], Ti-40Al-16Nb [17], Ti-45Al-10Nb [18], Ti-46Al-2Cr-2Nb [19], Ti-48Al-2Cr-2Nb [20], Ti-47Al2Mn-2Nb [21].

A new Ti-6Al-2Nb-1Ta alloy was obtained to satisfy the mechanical and anticorrosion requirements in neutral corrosive environment. The corrosion behaviour of this new Ti-6Al-2Nb-1Ta alloy in 0.1M Na_2SO_4, 3% NaCl solutions and synthetic sea water was studied in this paper, using potentiodynamic and linear polarisation method, electrochemical impedance spectroscopy and the monitoring of the open circuit potentials.

2. EXPERIMENTAL

The new alloy was obtained (in casting state) by vacuum melting in a levitation furnace using a vacuum level 6-8 $\times$ 10^{-4} mmHg**.** Its composition comprises (%weight): 5.98% Al, 2.02% Nb, 1.1% Ta, 0.036%Fe, 0.185%O_2, 0.004%N_2, 0.001%H_2, balance Ti.

The electrodes (obtained from ingots) were grinded with metallographic paper of different granulations and alumina to a mirror surface. Then, the electrodes were ultrasonically degreased in acetone, fixed in a Stern-Makrides hold system and rinsed with bi-distilled water.
All electrochemical measurements were carried out at room temperature in:
- 0.1M Na_2SO_4 solution of pH = 7.1;
- 3% NaCl solution of pH = 7.68;
- synthetic sea water of composition (g/L); NaCl – 24.53; $MgCl_2.6H_2O$ – 11; Na_2SO_4 – 4.099; KBr – 0.101; NaF –

0.003; $CaCl_2$ – 1.16; KCl – 0.695; $NaHCO_3$ - 0.201; H_3BO_3 – 0.027; pH = 7.79.
The following experimental techniques were used: potentiodynamic and linear polarisation, electrochemical impedance spectroscopy (EIS) and monitoring of the open circuit potentials (E_{oc}) for 1200 immersion hours in the third solutions.

The cyclic potentiodynamic polarization was applied beginning from -0.5 V to +4.0 V (vs. Ag/AgCl) using a scan rate of 10 mV/sec. Voltalab 80 equipment with its VoltaMaster 4 program were used. From the voltammograms, the main electrochemical parameters were determined: E_{corr} - corrosion potential, like zero current potential, E_p – passivation potential at which the current density is constant; ΔE_p – passive potential range of the constant current; $|E_{corr} - E_p|$ difference represents the tendency to passivation (low values characterise a good, easy passivation); E_b – breakdown (pitting) potential, the first potential value on the direct curve when the current density begins to increase; E_{pp} – pitting protection potential at which the current density on the negative sweep equals the passive current density; E_b – E_{pp} difference represents the pitting corrosion resistance (low values mean that the pit repassivation takes place very easy and quickly); i_p – passive current density. If the reverse curve presents lower currents than the direct curve, it results a very stable passive state. If the reverse curve shows higher currents than the direct curve, pitting corrosion exists [22].

The linear polarization measurements (Tafel) were applied for a range of ± 200 mV around the open circuit potential, with a scan rate of 10 mV/sec. The same Voltalab 80 equipment with its VoltaMaster 4 program that delivered the values of the corrosion current densities (i_{corr}) and rates (V_{corr}), polarisation resistance R_p.

Electrochemical impedance spectroscopy (EIS) measurements were carried out using a potentiostat AUTOLAB model PGSTAT 100. A sine wave of 15 mV was applied to the working electrode at the open circuit potential of the system (measured versus Ag/AgCl electrode). The spectra were acquired in the 10^5 Hz – 10^{-2} Hz frequency range. The impedance spectra were displayed as Nyquist and Bode diagrams (impedance modulus and phase angle vs. frequency). EIS results were analyzed with the complex, non-linear, least-square fitting program ZVIEW and an equivalent circuit that fits to the experimental data was proposed.

The open circuit potentials E_{oc} were monitored with the exposure time (1200 exposure hours till present) using a performing Hullett-Pakard multimeter.

Alloy microstructure was determined by metallographic microscopy with an Olimpus Japan PME3-ADL microscope. The specimen were polished on emery paper and alumina to mirror finish, ultrasonically cleaned using deionised water and etched in Kroll's reagent containing 10 ml of 40% HF, 5 ml of 65% HNO_3 and 85 ml of H_2O for the microscopic observations.

3. RESULTS AND DISCUSSIONS

Structure of the new Ti-6Al-2Nb-1Ta alloy
The alloy contains aluminium that is α stabilizer and niobium and tantalum that are β stabilizers; so, a bi-phase α + β is expected to be obtained.
According to Figure 1, the structure of the new Ti-6Al-2Nb-1Ta alloy represents an α + β uniform structure with un-oriented grains; the grain size is about 10 μm. This uniform structure can be favourable for a good resistance of this new alloy to corrosion.

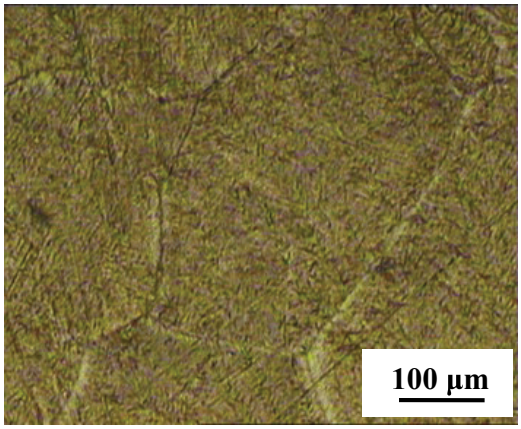

Fig. 1. Micrograph of Ti-6Al-2Nb-1Ta alloy

Corrosion behaviour resulted from cyclic potentiodynamic curves
Corrosion behaviour in 0.1M Na_2SO_4 solution
The new Ti-6Al-2Nb-1Ta alloy presented a spontaneous passivation (Fig. 2), without active-passive dissolution potential range, in 0.1M Na_2SO_4 solution. The corrosion potentials (E_{corr}) varied from about -49 mV to about +120 mV (Table 1) and are placed in the passive potential range of Ti, Al, Nb and Ta on the Pourbaix diagrams [23]. Therefore, the alloy is in the passive state with a large passive potential range (ΔE_p) and low passive current densities (i_p) (Table 1). Also, the differences $|E_{corr} - E_p|$ had very low values, showing a very good and very easy tendency to passivation (Table 1) in 0.1M Na_2SO_4 solution [24-26]. The corrosion potentials shifted to electropositive direction with the increasing time. Blackwood et al. [27] showed that the ennobling of the corrosion potential represents the increase of the passive film thickness; so, the passive film on the Ti-6Al-2Nb-1Ta alloy surface thickened in time, improved its protective capacity.

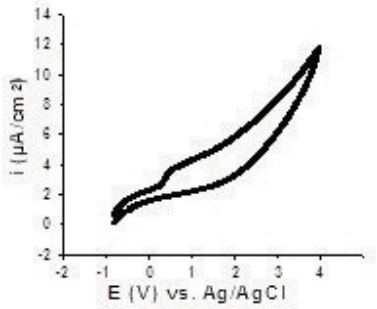

Fig.2. Cyclic potentiodynamic polarization curve for Ti-6Al-2Nb-1Ta alloy in 0.1M Na_2SO_4 solution

Corrosion behaviour in 3% NaCl solution

In 3% NaCl solution (Fig. 3) the Ti-6Al-2Nb-1Ta alloy exhibited self-passivation and its corrosion potentials (E_{corr}) had electropositive values which ennobled in time (Table 1) and were placed in the passive potential ranges of Ti, Al, Nb, Ta on the Pourbaix diagrams [23]. The alloy has a large passive potential ranges (ΔE_p), low values of the passive current densities (i_p) and tendencies to passivation ($|E_{corr} - E_p|$), showing a very good passive state that improved in time.

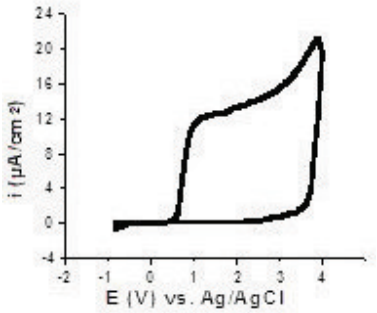

Fig. 3. Cyclic potentiodynamic polarization curve for Ti-6Al-2Nb-1Ta alloy in 3% NaCl solution

Pitting corrosion was registered at very electropositive values of the breakdown potentials (E_b). The pitting protection potentials (E_{pp}) had electropositive values and the pitting protection resistances, the differences $E_b - E_{pp}$ had low values, showing that the pit repassivation take places easily in a narrow potential range (Table 1). Because all the pitting corrosion parameters presented good values in time, that can not be reached in nature [28], it results that this kind of local corrosion can not appear on this alloy surface, even in long term using conditions.

Corrosion behaviour in synthetic sea water

In synthetic sea water (Fig. 4), also the alloy was self-passivated, presenting electropositive values of the corrosion potentials (E_{corr}), high values of the passive potential ranges (ΔE_p) and very low values of the tendency to passivation ($|E_{corr} - E_p|$) and passive current densities (i_p). These values improved in time (Table 1), showing the increase of alloy protective properties [27].

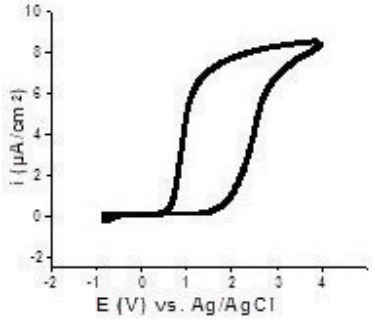

Fig. 4. Cyclic potentiodynamic polarization curve for Ti-6Al-2Nb-1Ta alloy in synthetic sea water

Table 1. Main electrochemical parameters for Ti-6Al-2Nb-1Ta alloy in studied solutions

Time (h)	E_{corr} (mV)	E_p (mV)	ΔE_p (mV)	$\|E_{corr} - E_p\|$ (mV)	E_b (mV)	E_{pp} (mV)	$E_b - E_{pp}$ (mV)	i_p ($\mu A/cm^2$)
0.1M Na_2SO_4								
0	- 49	-20	>4000	29	-	-	-	0.85
100	+25	+50	>4000	75	-	-	-	0.70
200	+59	+120	>4000	61	-	-	-	0.63
500	+122	+150	>4000	28	-	-	-	0.52
3% NaCl								
0	-490.5	-480	1280	10.5	+2100	+800	1300	0.98
100	-418.1	-390	1370	28.1	+2200	+980	1220	0.86
200	-324.7	-300	1320	24.7	+2250	+1020	1230	0.69
500	-311.9	-290	1360	21.9	+2300	+1070	1420	0.55
Synthetic sea water								
0	-511.1	-500	1300	11.1	+1500	+800	1300	1.10
100	-483.6	-470	1370	13.6	+1600	+900	1300	0.90
200	-365.4	-345	1295	20.4	+1650	+950	1300	0.75
500	-255.3	-230	1230	25.3	+1700	+1000	1300	0.62

Pitting corrosion was observed; the pit repassivation potentials (E_{pp}) had electropositive values and the pitting corrosion resistances ($E_b - E_{pp}$) had low values, revealing a reduced tendency to pitting corrosion. Moreover, all pitting parameters improved their values in time showing that the pitting corrosion can not appear in sea water even in long term working conditions [28].

Corrosion behaviour resulted from EIS measurements

Both Nyquist and Bode plots for the new Ti-6Al-2Nb-1Ta alloy are similar both in 0.1M Na_2SO_4 (Fig. 5), 3% NaCl (Fig. 6) solutions and synthetic sea water (Fig. 7).

The Nyquist plots (Fig. 5a, Fig. 6a, Fig. 7a) for the new Ti-6Al-12Nb-1Ta alloy exhibited an incomplete, large semicircle indicating a capacitive behaviour, a passive film. The diameters of these semicircles became larger in time, showing an increase of the impedance, i.e. a nobler electrochemical behaviour of the alloy [8].

The Bode impedance plots (Fig. 5b, Fig. 6b, Fig. 7b) presented in the low and middle frequency ranges high impedance values, suggesting high corrosion resistance [14]. The impedance slightly increased with the immersion time, showing the increase of the passive film resistance.

The Bode phase plots (Fig. 5c, Fig. 6c, Fig. 7c) revealed phase angles closed to -70^0 over a wide frequency range, i.e. a capacitive behaviour, a passive film as an insulator but not fully capacitive because the values (Table 2) of the independent frequency parameter, n, varied from 0.7 to 0.9 (when n = 1, the passive layer acts as a pure capacitor) [14]. Also, the phase angle presented some inflections; so, there are two relaxation time constants showing the existence of a bi-layered passive film: a compact, inner, barrier layer and a less compact, outer layer [7,8]. The phase angle increased in time from about -60^0 (after 1 immersion hour) to about -70^0 (at 500 immersion hours), proving the improvement of the passive layer resistance.

An electric equivalent circuit with two time constants (Fig. 8) was used to model the experimental spectra: the first time constant represents the dense, inner, barrier layer and it is represented by the Q_1 and R_1 (capacitance and resistance of the barrier layer); the second time constant represents the outer porous layer, illustrated by Q_2 and R_2 (capacitance and resistance of the porous layer). The resistances R_1 of the barrier layer and the resistances R_2 of the porous layer increased in time due to the slight thickening of the passive film [14]; also, the corresponding Q_1 and Q_2 capacitances decreased in time (Table 2) suggesting the same process of the increase of the passive film thickness [14]. Therefore, the corrosion resistance of the Ti-6Al-2Nb-1Ta alloy improved with the immersion time in 0.5M Na_2SO_4 and 3% NaCl solutions and synthetic sea water till present (500 hours).

From Table 2 can be observed that the values of the outer layer resistances (R_2) are lower than of the inner layer (R_1) i.e., the inner barrier layer is more protective, more resistant [29].

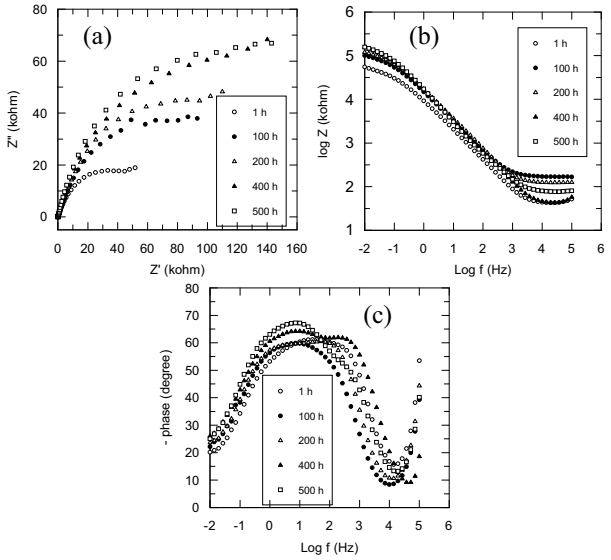

Fig. 5. Impedance spectra for Ti-6Al-2Nb-1Ta alloy in 0.1M Na_2SO_4: a) Nyquist plots; b) Bode impedance plots; c) Bode phase plots

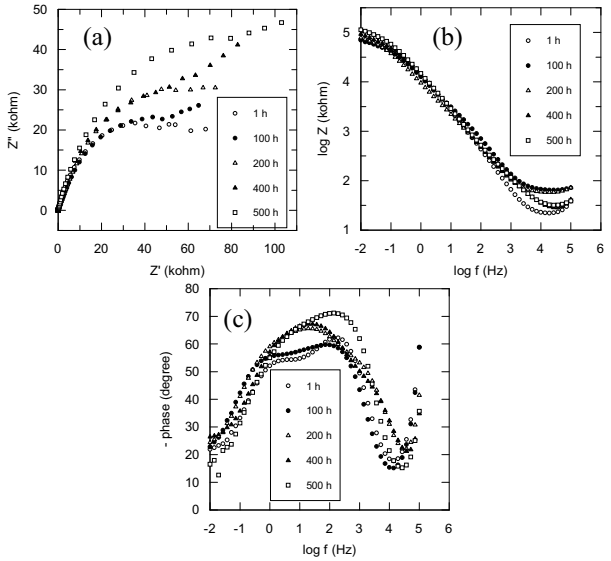

Fig. 6. Impedance spectra for Ti-6Al-2Nb-1Ta alloy in 3% NaCl: a) Nyquist plots; b) Bode impedance plots; c) Bode phase plots

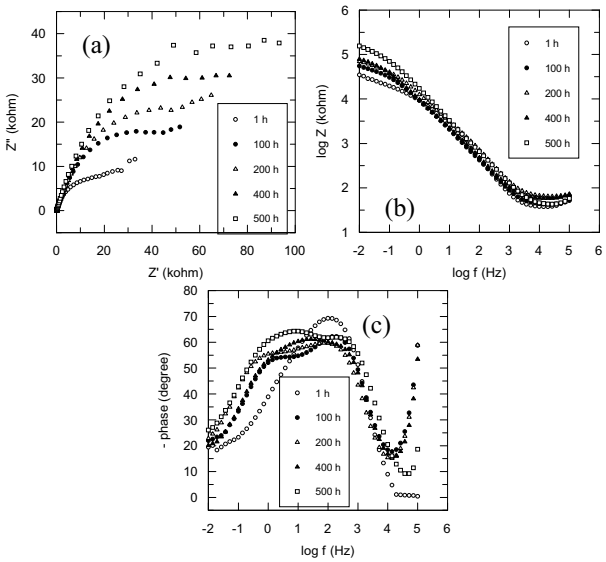

Fig. 7. Impedance spectra for Ti-6Al-2Nb-1Ta alloy in synthetic sea water: a) Nyquist plots; b) Bode impedance plots; c) Bode phase plots

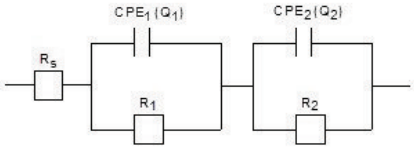

Fig. 8. Electric equivalent circuit with two time constants.

Table 2. Parameters of the equivalent circuit for Ti-6Al-2Nb-1Ta alloy

Time (h)	Q_1 (F/cm^2)	R_1 ($\Omega\ cm^2$)	n_1	Q_2 (F/cm^2)	R_2 ($\Omega\ cm^2$)	n_2
0.1M Na_2SO_4						
1	$0.39x10^{-3}$	$1.40x10^5$	0.72	$0.19x10^{-4}$	$1.07x10^4$	0.73
100	$0.29x10^{-3}$	$1.82x10^5$	0.73	$0.15x10^{-4}$	$7.57x10^4$	0.72
200	$0.20x10^{-3}$	$2.12x10^5$	0.85	$0.15x10^{-4}$	$11.10x10^4$	0.71
400	$0.17x10^{-3}$	$2.26x10^5$	0.92	$0.14x10^{-4}$	$13.74x10^4$	0.73
500	$0.13x10^{-3}$	$2.58x10^5$	0.81	$0.12x10^{-4}$	$16.00x10^4$	0.84
3% NaCl						
1	$0.41x10^{-3}$	$3.51x10^4$	0.70	$0.28x10^{-4}$	$1.32x10^3$	0.83
100	$0.32x10^{-3}$	$5.82x10^4$	0.70	$0.27x10^{-4}$	$1.40x10^3$	0.81
200	$0.52x10^{-4}$	$6.86x10^4$	0.73	$0.21x10^{-4}$	$2.33x10^4$	0.75
400	$0.32x10^{-4}$	$14.38x10^4$	0.95	$0.18x10^{-4}$	$7.44x10^4$	0.72
500	$0.29x10^{-4}$	$15.45x10^4$	0.87	$0.17x10^{-4}$	$12.67x10^4$	0.73
Synthetic sea water						
1	$0.56x10^{-4}$	$3.44x10^4$	0.76	$0.41x10^{-4}$	$1.22x10^3$	0.72
100	$0.43x10^{-4}$	$5.63x10^4$	0.71	$0.32x10^{-4}$	$1.39x10^3$	0.82
200	$0.35x10^{-4}$	$6.59x10^4$	0.73	$0.28x10^{-4}$	$1.98x10^4$	0.83
400	$0.23x10^{-4}$	$13.47x10^4$	0.88	$0.25x10^{-4}$	$5.64x10^4$	0.89
500	$0.22x10^{-4}$	$15.10x10^4$	0.95	$0.21x10^{-4}$	$10.16x10^4$	0.91

Corrosion resistance resulted from Tafel diagrams

Corrosion current densities were determined from Tafel diagrams. One example of these plots is presented in Fig. 9. In 0.1M Na_2SO_4 solution (Table 3), the new Ti-6Al-2Nb-1Ta alloy presented very low values of the corrosion current densities and rates, placed in the "Perfectly Stable" class. Polarisation resistances increased in time showing higher resistances of the passive film and better protective capacities [24-26].In 3% NaCl solution, also, low values of the corrosion current densities and rates in the "Very Stable" resistance class were obtained. R_p values increased with the immersion time, proving the same increasing protective resistances of the passive layer (Table 3). In synthetic sea water (Table 3), similar values of the corrosion current densities and rates it resulted and the new Ti-6Al-2Nb-1Ta alloy is "Very Stable". Also, the values of the polarisation resistances showed very good protective capacities which improved in time. The best corrosion rates and parameters from Table 3 were obtained in 0.1M Na_2SO_4 solution, confirming the results of the potentiodynamic cyclic curves i.e. its lowest corrosivity.

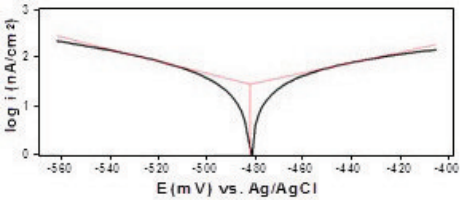

Fig. 9. Tafel curves for Ti-6Al-2Nb-1Ta alloy in synthetic sea water.

Table 3. Corrosion rates and ion release for Ti-6Al-2Nb-1Ta alloy in studied solutions

Time (h)	i_{corr} ($\mu A/cm^2$)	V_{corr} ($\mu m/y$)	Resistance class	R_p ($k\Omega.cm^2$)
0.1M Na_2SO_4				
0	0.0357	0.323	PS	3.89
100	0.0274	0.248	PS	4.46
300	0.0144	0.131	PS	6.03
500	0.0126	0.114	PS	7.25
3% NaCl				
0	0.227	2.054	VS	3.73
100	0.146	1.322	VS	3.93
300	0.138	1.446	VS	4.85
500	0.122	1.305	VS	5.56
Synthetic sea water				
0	0.285	3.31	VS	2.13
100	0.203	2.36	VS	3.75
300	0.156	1.81	VS	4.79
500	0.146	1.500	VS	5.42

PS – Perfectly Stable; VS – Very Stable.

Corrosion resistance resulted from monitoring of open circuit potentials

The open circuit potential values (Fig.10) became more electropositive in time for the Ti-6Al-2Nb-1Ta alloy both in 0.1M Na_2SO_4, 3% NaCl solutions and synthetic sea water. All open circuit potential values are placed in the passive passive potential range of Ti, Al, Nb and Ta on Pourbaix diagrams [23] showing the enobling of its behaviour.

The most electropositive values of the open circuit potentials were registered in 0.1M Na_2SO_4 solution. Though in 3% NaCl solution and synthetic sea water were obtained slightly more electronegative values of the open circuit potentials, about -300 mV, -350 mV, these values are placed in the same passive potential range of Ti, Al, Nb and Ta on Pourbaix diagrams [23] and the general tendency is to ennoble in time, suggesting [27] the thickening of the passive films and the improvement of their protective capacities.

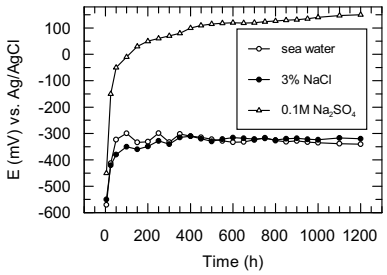

Fig. 10. In time variation of open circuit potentials for Ti-6Al-2Nb-1Ta alloy in studied solutions

4. CONCLUSIONS

1.The new Ti-6Al-2Nb-1Ta alloy presented a spontaneous passivation both in 0.1M Na_2SO_4, 3% NaCl solutions and synthetic sea water.
2.Pitting corrosion was registered in 3% NaCl solution and synthetic sea water but, the all pitting corrosion parameters had good values that can not appear in nature and the pitting corrosion can not develop even in long term working conditions.
3.The Nyquist plots for the new Ti-6Al-2Nb-1Ta alloy exhibited an incomplete, large semicircle indicating a capacitive behaviour, a passive film.
4.The Bode impedance plots presented in the low and middle frequency range high impedance values, suggesting high corrosion resistance.
5.The Bode phase plots revealed phase angles closed to -70^0 over a wide frequency range, i.e. a capacitive behaviour, a passive film as an insulator but not fully capacitive.
6.An electric equivalent circuit with two time constants was used to model the experimental spectra.
7.The new Ti-6Al-2Nb-1Ta alloy presented very low values of the corrosion current densities and rates, placed in the "Perfectly Stable" and "Very Stable" class.
8.The open circuit potential values became more electropositive in time showing that the passive film on the Ti-6Al-2Nb-1Ta alloy surface thickens in time.

5. REFERENCES

[1] K. V. S. Ramana, S. Kaliappan, N. Ramanathan, V. Kavitha, *Mater. Corros*. **2007**, *58*, 673.
[2] T. Bellezze, G. Roventi, A. Quaranta, R. Fratesi, *Mater. Corros*. **2008**, *59*, 727.
[3] R. Galvan-Martinez, R. Orozco-Cruz, R. Torres-Sanchez, E. A. Martinez, *Mater. Corros*. **2010**, *60*, 872.
[4] I. V. Riskin, V. B. Torshin, Ya. B. Skuratnik, M. A. Dembrovsky, *Corrosion* **1984**, *40*, 66.
[5] M. Pankuch, R. Bell, C. A. Melendres, *Electrochim. Acta* **1993**, *38,* 2777.
[6] W. R. Osorio, L. C. Peixoto, A. Garcia, *Mater. Corros*. **2010**, *61*, 407.
[7] S. L. Assis, S. Wolynec, I. Costa, *Mater. Corros*. **2008**, *59*, 739.
[8] B. L. Wang, Y. F. Zheng, L. C. Zhao, *Mater. Corros*. **2009**, *60*, 788.
[9] S. Tamilselvi, R. Murugaraj, N. Rajendran, *Mater. Corros*. **2007**, *58*, 113.
[10] M. A. Ameer, A. A. Ghoneim, A. M. Fekry, *Mater. Corros*. **2010**, *61*, 580.
[11] M.V. Popa, I. Demetrescu, E. Vasilescu, P. Drob, A. Santana Lopez, J. Mirza-Rosca, C. Vasilescu, D. Ionita, *Electrochim. Acta* **2004**, *49*, 2113.
[12] L. Thair, U. Kamachi Mudali, R. Asokamani, R. Baldev, *Mater. Corros*. **2004**, *55*, 358.
[13] A. Cremasco, W. R. Osorio, C. M. A. Freire, A. Garcia, R. Caram, *Electrochim. Acta* **2008**, *53*, 4867.
[14] D. Mareci, R. Chelariu, G. Ciurescu, D. Sutiman, T. Gloriant, *Mater. Corros*. **2010**, *61*, 768.
[15] S. Tamilselvi, N. Rajendran, *Mater. Corros*. **2007**, *58*, 285.
[16] C. T. Yang, Y. C. Lu, C. H. Koo, *Intermetallics* **2002**, *10*, 161.
[17] C. T. Yang, C. H. Koo, *Intermetallics* **2004**, *12*, 235.
[18] W. J. Zhang, S. C. Deevi, G. L. Chen, *Intermetallics* **2002**, *10*, 403.
[19] Q. F. Xia, J. N. Wang, J. Yang, Y. Wang, *Intermetallics* **2001**, *9*, 361.
[20] J. Chraponski, W. Szkliniarz, A. Koscielna, B. Serek, *Mater. Chem. Phys*. **2003**, *81*, 438.
[21] D. Lin, Y. Wang, J. Liu, C. C. Law, *Intermetallics* **2000**, *8*, 549.
[22] E. Vasilescu, P. Drob, D. Raducanu, I. Cinca, D. Mareci, J. M. Calderon Moreno, M. Popa, C. Vasilescu, J. C. Mirza Rosca, *Corros. Sci.* **2009**, *51*, 2885.
[23] M. Pourbaix, *Atlas of Electrochemical Equilibria in Aqueous Solutions*, NACE, Houston, **1974**.
[24] M. V. Popa, I. Demetrescu, E. Vasilescu, P. Drob, A. Santana Lopez, J. Mirza-Rosca, C. Vasilescu, D. Ionita, *Rev. Chim (Buch)* **2010**, *61*, 168.
[25] M. V. Popa, E. Vasilescu, P. Drob, D. Mareci, J.M. Calderon Moreno, S. Ivanescu, C. Vasilescu, J.C. Mirza Rosca, *Mater. Corros.* **2009**, *60,* 949.
[26] M. V. Popa, E. Vasilescu, P. Drob, C. Vasilescu, I. Demetrescu, D. Ionita, *J. Mater. Sci. Mater. Med.* **2008**, *19*, 1.
[27] D. J. Blackwood, A. W. C. Chua, K. H. W. Seah, R. Thampuran, S. H. Teoh, *Corros. Sci.* **2003**, *42*, 481.
[28] U. R. Evans, *The corrosion of the metals*, E. Arnold, London, 1969.
[29] S. I. Assis, I. Costa, *Mater. Corros.* **2007**, *58,* 329.

One-dimensional Steady-state Analysis of Bioheat Transfer Equation: Tumour Parameters Assessment for Medical Diagnosis Application

Shazzat HOSSAIN
Department of Electrical and Computer Engineering, Ryerson University
Toronto, ON, M5B 2K3, Canada

and

Farah MOHAMMADI
Department of Electrical and Computer Engineering, Ryerson University
Toronto, ON, M5B 2K3, Canada

ABSTRACT

A simplified one-dimensional bioheat transfer model of the spherical living tissues in the steady state has been set up for application in heat transfer studies based on the Pennes' bioheat transfer equation and its corresponding analytical solution by using Bessel's equation has been derived in this paper. The obtained analytical solution is applied to analyze the effects of the metabolic heat generation, the tissue thermal conductivity, the blood perfusion and the coefficient of heat transfer on the temperature distribution in living tissues. A further parametric analysis has been made to reveal the tumour size, hyperactivity rate and location based on the temperature distribution profile. The results show that the derived analytic solution is useful to easily and accurately study the thermal behaviour of the biological system, and can be extended to thermal behaviour research of biological system, thermal parameter measurements, temperature field reconstruction and clinical treatment.

Keywords: Bioheat transfer, Pennes' equation, Analytical solution, Bessel functions, Tumour.

1. INTRODUCTION

In live biological body the spatial temperature distribution in tissues plays a vital role in many physiological processes. Recent advancement in the bioheat transfer research field has paved a key foundation in hyperthermia cancer therapy, thermal diagnosis, cryogenic surgery etc. [1, 2]. The quantitative and accurate analysis of bioheat transfer is to effectively understand and model the heat transfer mechanism of the biological system.

The complexity underlying in the precise thermal analysis process of living tissues remains not only for its heterogeneity and anisotropy but also for conduction, convection, and radiation heat flow, cell's metabolism, and blood perfusion etc. Accordingly, it is very difficult to build precise and exact thermal models and most of the proposed bioheat equations are very complicated thus complex but not unattainable to solve analytically.

The analytical solutions of these equations have important significance in the study of bioheat transfer because they reflect actual physical feature of the equations and can be used as standards to verify the corresponding numerical results and as a proof to the reasonability of in-vitro mode analysis. Various techniques have been proposed to obtain analytical solutions of these equations. The estimation of temperature distribution in biological tissues at steady-state in one dimensional Cartesian coordinate was presented by Zhou et al. [3]. The same analysis in cylindrical geometry with showing the parameters effect in spatial temperature distribution was depicted in [4]. Shih et al. [5] presented and discussed the solution for the models of living tissue with applying sinusoidal heat flux on skin surface. For local magnetic hyperthermia, the time dependent analytical analysis of bioheat equation was performed by Gutierrez [6] in the spherical system to estimate the localized and concentrated heat required for the ablation of the cancerous cells. In this paper, the derivation of the general analytic solution for one-dimensional steady-state model of the spherical living tissue is conducted by adopting the Pennes' bioheat transfer equation [7-9]. The fundamental Pennes' equation and its solution are presented in the following two consecutive sections. The section 2 is devoted to present the analytic solution methodology. The application of obtained solution to the tissue's internal temperature distribution and the thermal effect of tumours are described in section 3.

2. METHODS

Pennes, in 1948, proposed a model considering cell's metabolism and blood perfusion effects on temperature distribution in live biological bodies, at steady-state condition which is written in one-dimensional spherical coordinate system as:

$$\frac{1}{r^2}\frac{d}{dr}\left(r^2\frac{dT}{dr}\right)+\frac{w_b c_b}{k}\left(T_a-T\right)+\frac{q_m}{k}=0 \quad (1)$$

where, w_b, c_b are the perfusion rate per unit volume and specific heat of blood, respectively; k is the thermal conductivity of tissue; q_m is the metabolic heat generation per unit volume; T_a and T represent the artier blood and tissue temperature, respectively.

For axially symmetrical model the boundary conditions are described as:

$$r=0,\ \frac{dT}{dr}=0 \qquad (2a)$$

and

$$r=R,\ -k\frac{dT}{dr}=h_a\left(T-T_e\right) \qquad (2b)$$

where, R is the radius of the concerned tissue; h_a is the heat exchange coefficient which accounts for both the convection and radiation heat loss on the tissue surface; T_e is the ambient temperature.

To obtain dimensionless heat equation and boundary conditions the following characteristics quantities are proposed:

$$r^* = \frac{r}{R}, \quad T^* = \frac{T - T_e}{T_a - T_e} \qquad (3)$$

Substituting (3) into (1) lead to:

$$\frac{1}{r^{*2}}\frac{d}{dr^*}\left(r^{*2}\frac{dT^*}{dr^*}\right) + \frac{w_b c_b R^2}{k}\left(1 - T^*\right) + \frac{q_m R^2}{k\left(T_a - T_e\right)} = 0 \qquad (4)$$

and the dimensionless boundary conditions are:

$$r^* = 0, \ \frac{dT^*}{dr^*} = 0 \qquad (5a)$$

and

$$r^* = 1, \ \frac{dT^*}{dr^*} = -\frac{h_a R}{k} T^* \qquad (5b)$$

Here, the dimensionless parameters and variables are defined as:

$\frac{w_b c_b R^2}{k} = w^*$, $\frac{q_m R^2}{k\left(T_a - T_e\right)} = q_m{}^*$ and $\frac{h_a R}{k} = h_a{}^*$

Therefore, the dimensionless governing equation is:

$$\frac{1}{r^{*2}}\frac{d}{dr^*}\left(r^{*2}\frac{dT^*}{dr^*}\right) - w_b{}^* T^* + w_b{}^* + q_m{}^* = 0 \qquad (6)$$

and the boundary conditions are:

$$r^* = 0, \ \frac{dT^*}{dr^*} = 0 \qquad (7a)$$

and

$$r^* = 1, \ \frac{dT^*}{dr^*} = -h_a{}^* T^* \qquad (7b)$$

By dropping the superscripts * and letting $w_b{}^* = \alpha$ and $w_b{}^* + q_m{}^* = \beta$, the equation (4) becomes:

$$\frac{1}{r^2}\frac{d}{dr}\left(r^2\frac{dT}{dr}\right) - \alpha T + \beta = 0 \qquad (8)$$

To solve the equation (8), let's assume $T = \frac{H_{(r)}}{\sqrt{r}}$ and by differentiating we obtain,

$$\frac{dT}{dr} = r^{-1/2}H' - \frac{1}{2}r^{-3/2}H \qquad (9)$$

Substituting (9) in (8) we get,

$$\frac{1}{r^2}\frac{d}{dr}\left(r^{3/2}H' - \frac{1}{2}r^{1/2}H\right) - \alpha r^{-1/2}H = -\beta \qquad (10)$$

The homogeneous equation is:

$$\frac{1}{r^2}\frac{d}{dr}\left(r^{3/2}H' - \frac{1}{2}r^{1/2}H\right) - \alpha r^{-1/2}H = 0 \qquad (11)$$

After simplifying and multiplying by $r^{1/2}$ we get

$$r^2H'' + rH' - \left(\alpha r^2 + \left(\frac{1}{2}\right)^2\right)H = 0 \qquad (12)$$

The equation (12) is modified Bessel equation of half kind and therefore the solution is:

$$H = C_1 I_{1/2}\left(\sqrt{\alpha}r\right) + C_2 K_{1/2}\left(\sqrt{\alpha}r\right) \qquad (13)$$

According to the characteristics of Bessel's equation, we have, $C_2 = 0$. Therefore, the solution to (13) is:

$$H = C_1 I_{1/2}\left(\sqrt{\alpha}r\right) \qquad (14)$$

The exact solution in terms of $T(r)$ is:

$$T = C_1\frac{I_{1/2}\left(\sqrt{\alpha}r\right)}{\sqrt{r}} + T_p \qquad (15)$$

where, T_p is the particular solution and $T_p = \frac{\beta}{\alpha}$.

Therefore, the temperature expression considering the superscript * again:

$$T^*\left(r^*\right) = C_1\frac{I_{1/2}\left(\sqrt{\alpha}r^*\right)}{\sqrt{r^*}} + \frac{\beta}{\alpha} \qquad (16)$$

Considering the boundary condition of (7b), some simple derivations lead to:

$$\frac{dT^*}{dr^*} = C_1\left(-\frac{I_{1/2}\left(\sqrt{\alpha}r^*\right)}{2r^*\sqrt{r^*}} + \frac{\sqrt{\alpha}I_{3/2}\left(\sqrt{\alpha}r^*\right) + \frac{1}{2r^*}I_{1/2}\left(\sqrt{\alpha}r^*\right)}{\sqrt{r^*}}\right) \qquad (17)$$

$$C_1 = -\frac{h_a{}^* T^*}{\left(-0.5\ I_{1/2}\left(\sqrt{\alpha}\right) + \sqrt{\alpha}I_{3/2}\left(\sqrt{\alpha}\right) + 0.5\ I_{1/2}\left(\sqrt{\alpha}\right)\right)} \qquad (18)$$

$$T^* = -\frac{h_a{}^* T^*}{\sqrt{\alpha}I_{3/2}\left(\sqrt{\alpha}\right)}\frac{I_{1/2}\left(\sqrt{\alpha}r^*\right)}{\sqrt{r^*}} + \frac{\beta}{\alpha} \qquad (19)$$

$$T = T_e + \frac{\beta}{\alpha}\left(\frac{1}{1 + \frac{h_a{}^* I_{1/2}\left(\sqrt{\alpha}r^*\right)}{\sqrt{\alpha}r^* I_{3/2}\left(\sqrt{\alpha}r^*\right)}}\right)\left(T_a - T_e\right) \qquad (20)$$

3. RESULTS

By applying the obtained analytic solution in (20), the interior steady-state temperature of living tissues in a body organ, which could be approximated as spherical in shape (for example- female breast, buttock), in the resting person can be easily and accurately obtained, which can facilitate the further analysis of the heat transfer characteristics of living tissues embedding hyperactive nodule.

The effect of major thermal parameters on the temperature distribution of spherical living tissues are discussed, wherein, the typical parameter values, chosen for theoretical analysis are presented in Table 1.

Table 1: Parameter values used in theoretical analysis

Parameter	Value and Unit
w_b	3 $kg/(s.m^3)$
c_b	3850 $J/(kg.{}^oC)$
k	0.48 $W/(m.{}^oC)$
h_A	8.77 $W/(m^2.{}^oC)$
q_m	1085 W/m^3
T_a	37 ^oC
T_e	25 ^oC

The upshot of the metabolic heat generation, the heat exchange coefficient, the blood perfusion, and the tissue thermal conductivity on temperature profile are shown in Figs. 1 to 4, respectively.

In Fig. 1, the family of graphs shows that changes in metabolic heat generation elevates the inner tissue temperature magnitudes but maintains an almost constant slope in the temperature flow path to the boundary regardless the metabolic rate.

The Fig. 2 asserts that the higher the coefficient of heat transfer, the lower the temperature near the boundary of the body. This ambient dependence phenomenon in thermal distribution of biological body produces a distinguishable elevation in skin temperature and is a tool for analyzing benign stage tumour.

The effect of blood perfusion rates on the temperature distribution is illustrated in Fig. 3. The curves indicate that the gradient of the temperature variation in redial direction decreases with increasing blood perfusion, which is a result of higher rate of heat distribution caused by the blood perfusion. Moreover, the differences between the effects of the higher blood perfusion rates on temperature distribution become smaller.

The simulation results presented in Fig. 4 shows the changes in the values of the tissue thermal conductivity has effect on body heat transfer capacity.

The effect of tumour, located at the center of the spherical model (see Fig 5) surrounded by sound tissues, on the thermal distribution of body is presented in the Fig.6. The incremental temperature distribution of a tumour of radius 5mm at depth 4 cm which has 2- 5 times higher hyperactivity than average sound tissue is presented.

A center tumour of different size with a constant metabolism of 5 times higher than healthy tissues is presented in Fig. 7. This figure shows that radius has no effect on the temperature established at the centre of the nodule.

The resultant thermal profile of a tumour at centered origin embedded in healthy tissues is presented in Figs. 8 and 9 for different tumour sizes and metabolism rates, respectively.

The Fig. 8 concludes that the maximum raise in the temperature at the model origin does not depend on the size of the tumour. The size has effect on the temperature magnitude at the boundary only. While the intensity influences both the temperature grow at origin and amount of temperature that reach to the boundary, it is evident from Fig 9.

If the tumour is not located at a depth of 2 cm rather than being at the model origin, as shown in Fig. 10, the temperature flow in the outward direction for different tumour sizes and metabolism rates are presented in Figs. 11 and 12, respectively.

It can be seen from Fig. 11 that an abrupt change in temperature profile at the tumour position makes a constant vertex at 46^{o}C for all the values of radius. The analysis also shows that the increasing hyperactivity rate of tumour tissues increases both the temperature magnitude at the tumour location and at boundary which is conveyed by Fig. 12.

4. Discussion

In this paper, the steady-state bioheat transfer model of the spherical living tissues has been analyzed based on Pennes' equation, and the corresponding equation has been solved in one-dimensional domain. The Bessel's equation involving analytical solution is obtained in this study is useful for describing the tissue temperature distribution in radial direction.

Taking account of the parametric studies, the thermal conductivity and blood perfusion effects are neglected for further analysis in case of tumours, though the thermal conductivity of the tumour cells is somewhat increase from that of sound tissue but it plays an insignificant effect on temperature profile and likewise the blood perfusion rate in a particular organ is assumed to be undisturbed by the cancerous cells.

Observing the linearity in thermal profile with the variations in tissue metabolism, the superposition theorem is employed to compute the temperature distribution of spherical shaped organ embedding tumour within. Analysis with varying tumour location is performed using the concept of coordinate origin shifting.

The temperature reach to the skin boundary bear the signature of availability of tumour in a particular organ of biological body and analyzing and mapping the temperature reveal some idea about the clinical features of tumour. This aspect needs further analysis to pinpoint the correlation among the tumour parameters with temperature at skin surface so that an invasive, non-contact, radiation free diagnostic tool can be invoked employing infrared (IR) thermogram.

5. REFERENCES

[1] Chato J: Measurement of thermal properties of biological materials. A Shitzer, RC. Eberhart (Eds.), Heat transfer in Medicine and biology, Plenum Press, NY, pp. 1:167-173, 1985.

[2] Bowman HF: Estimation of tissue blood flow. A Shitzer, RC. Eberhart (Eds.), Heat transfer in Medicine and biology, Plenum Press, NY, pp. 1: 193-230, 1985.

[3] Zhou Minhua and Chen Qian,. Estimation of Temperature Distribution in Biological Tissue by Analytic Solutions to Pennes' Equation. 2nd International Conference on Biomedical Engineering and Informatics, BMEI, IEEE, Nanjing, China. 2009.

[4] Zhou Minhua, Chen Qian, Study of the surface temperature distribution of the tissue affected by the point heat source. IEEE, 2007.

[5] Tzu-Ching Shih, Ping Yuan, Win-Li Lin, and Hong-Sen Kou, 2007. Analytical Analysis of the Pennes' Bioheat Transfer Equation with Sinusoidal Heat Flux Condition on Skin Surface. IPEM, Medical Engineering & Physics, vol. 29, issue 9, pp. 946-953.

[6] Gustavo Gutierrez, 2007. Study of the Bioheat Equation with a Spherical Heat Source for Local Magnetic Hyperthermia. XVI Congress on Numerical Methods and their Applications, Cordoba, Argentina, October 2-7.

[7] Kai YUE, Xinxin ZHANG, and Fan YU, An Analytic Solution of One-dimensional Steady-state Pennes' Bioheat Transfer Equation in Cylindrical Coordinates. Journal of Thermal Science, Vol. 13, Issue 3, pp. 255-258, 2004.

[8] Tzu-Ching Shih, Ping Yuan, Win-Li Lin, and Hong-Sen Kou, Analytical Analysis of the Pennes' Bioheat Transfer Equation with Sinusoidal Heat Flux Condition on Skin Surface. IPEM, Medical Engineering & Physics, vol. 29, issue 9, pp. 946-953, 2007.

[9] Ricardo Romero, Joel N. Jimenez-Lozano, Mihir Shen and F. Javier Gonzalez, Analytical Solution of the Pennes Equation for Burn-Depth Determination from Infrared Thermographs. Mathematical Medicine and Biology, vol. 27, pp. 21-38, doi: 10.1093/imammb/dqp010, Advance Access publications, 2009.

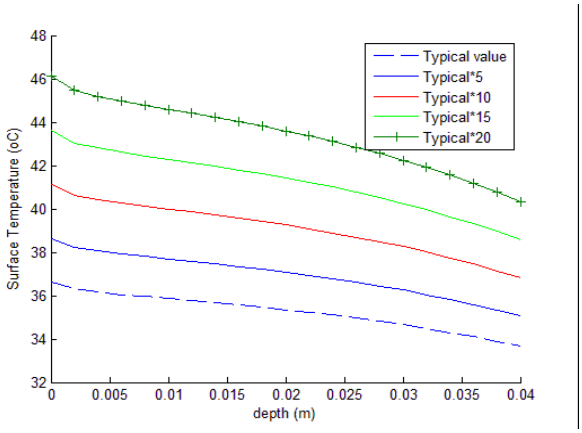

Fig. 1 Temperature Distribution for different metabolic rate

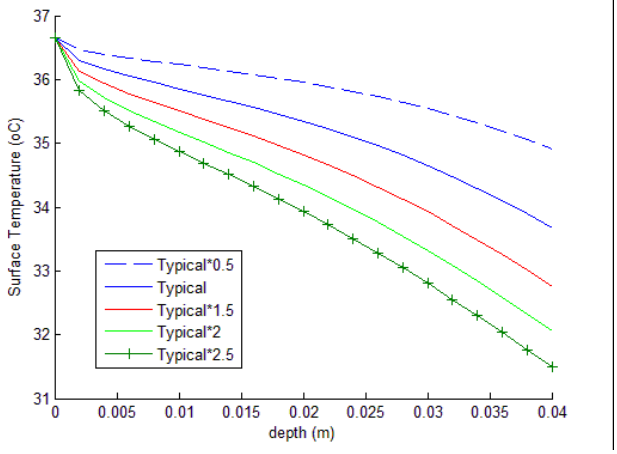

Fig. 2 Temperature Distribution for heat exchange coefficient

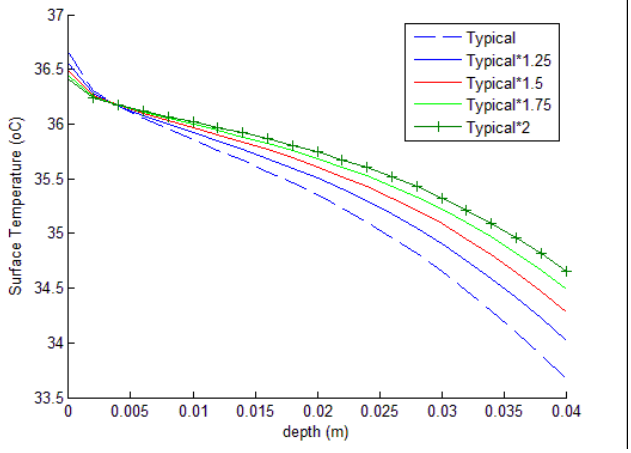

Fig. 3 Temperature Distribution for different perfusion rate

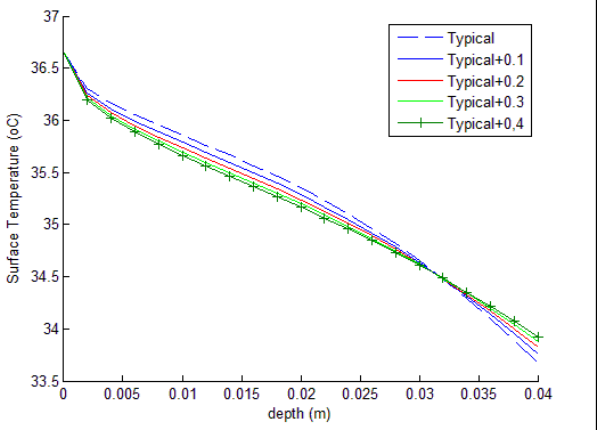

Fig. 4 Temperature Distribution for different tissue thermal conductivities

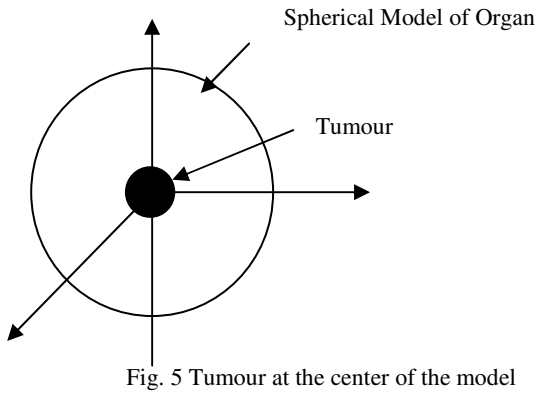

Fig. 5 Tumour at the center of the model

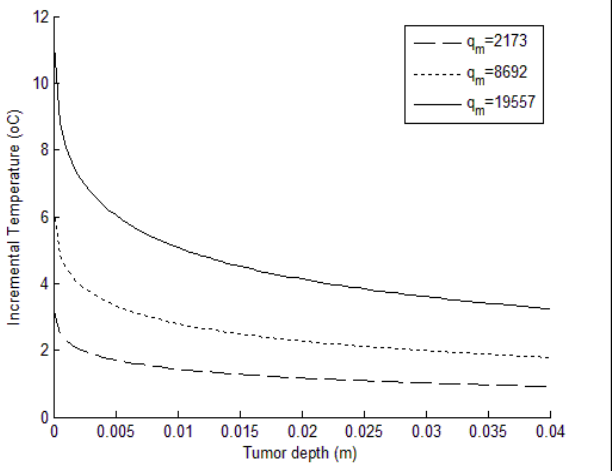

Fig. 6 Temperature Distribution for Tumour

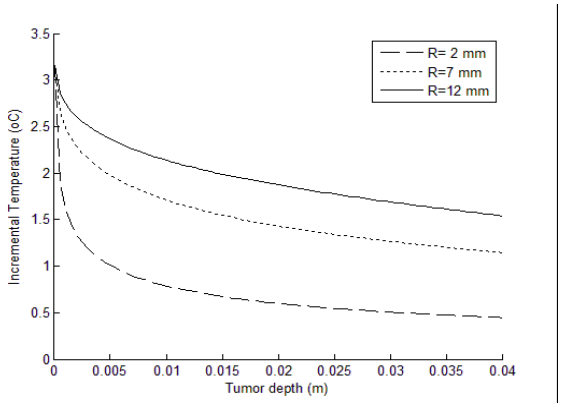

Fig. 7 Temperature Distribution of Tumour

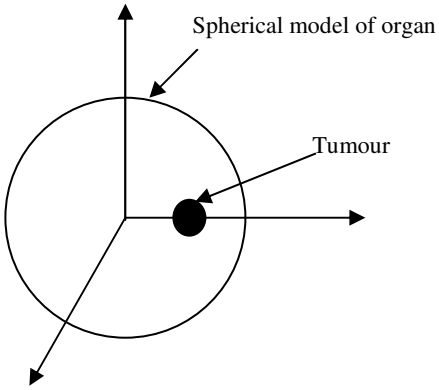

Fig. 10 Tumour not at the center of the Model

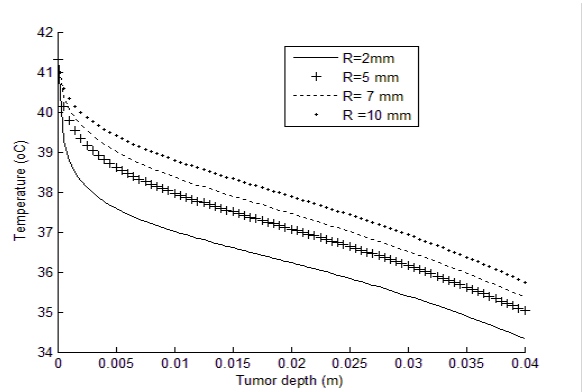

Fig. 8 Tumour in Sound Tissue

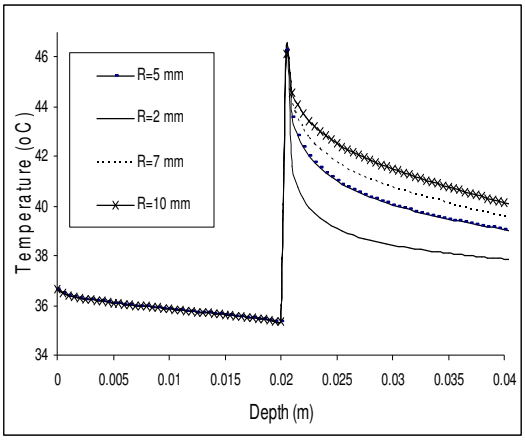

Fig. 11 Tumour in Sound Tissue

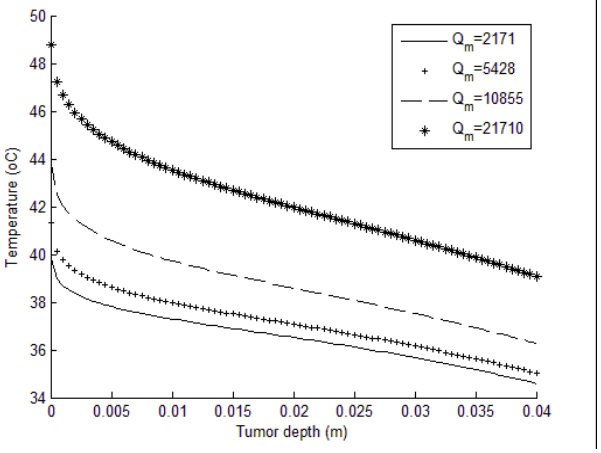

Fig. 9 Tumour in Sound Tissue

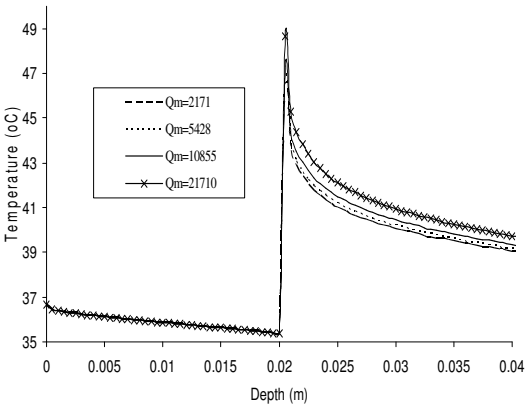

Fig. 12 Tumour in Sound Tissue

Sustainable Energy Generation in Microbial Fuel Cell Catalyzed with *Bacillus Subtilis* Species

Zainab Z. Ismail*
Department of Environmental Engineering, Baghdad University
Baghdad, Iraq

and

Ali J. Jaeel
Department of Civil Engineering, Wasit University
Wasit, Iraq

* Corresponding author (Z.Z. Ismail), Email: zismail9@gmail.com

ABSTRACT

Microbial fuel cell (MFC) attracts growing efforts as a kind of environmentally friendly biotechnology. In this study, the aerobic bacterium *Bacillus subtilis* has been utilized in a dual-chambered upflow microbial fuel cell fueled with actual domestic wastewater. The MFC system was continuously operated for 75 days. The performance of the UMFC was mainly evaluated in accordance with the COD removal and maximum power generation as well as BOD reduction. The results revealed that the microorganism ***Bacillus subtilis*** is electrochemically active culture. The maximum observed effeciency of COD removal and power generation were 90% and 270 mW/ m^2, respectively.

Keywords: MFC, Anaerobic treatment, Power generation, Wastewater, and ***Bacillus subtilis***

1. INTRODUCTION

Microbial fuel cell (MFC) can be considered as a novel bioreactor utilize microorganisms as catalysts to convert chemical energy stored in organic substrates to electricity by the electrochemical technology [1]. Many researchers have reported the generation of electricity using activated sludge as the source of microorganisms. However, when using a mixed community, the electrochemical activity of a few bacterial species enhances the power output of the whole system. However, fewer studies using single type of microorganisms have been previously reported. Nimje et al. [2] studied the energy generation by a strain of *Bacillus subtilis* in a MFC fed with synthetic glucose-based wastewater. The maximum observed power density was 1050 mW/m^2. Rahimnejad et al. [3] used a dual chambered air–cathode MFC fed with glucose solution as a substrate having an initial concentration of 30 g/L. The system was inoculated with anaerobic pure culture of *Saccharomyces cerevisiae*. Maximum produced power density was 283 mW/ m^2. Fatemi et al. [4] evaluated electricity generation in a dual chambered MFC inoculated with *Saccharomyces cerevisiae*. Glucose with initial concentration of 4 g/l was used as an electron donor. The power density and maximum COD removal efficiency were 10.1 mW/ m^2 and 54%, respectively. In this study the performance of a two-chambered MFC fueled with ***actual domestic wastewater*** and bio-catalyzed with an anaerobically grown bacterium ***Bacillus subtilis*** has been evaluated.

2. MATERIALS AND METHODS

An upflow MFC consisted of a dual rectangular chambers made of transparent acrylic parallelepiped having dimensions of 52 x 9.4 x 9.4 cm was used in this study. The anode and cathode chambers contained graphite plain electrodes; each had a surface area of 60 cm^2. The two chambers were separated by a cation exchange membrane (CEM) type CMI-7000, supplied by membrane international INC., NJ. The CEM sheet of dimensions 10X10 cm was placed between two perforated glass sheets. The MFC was inoculated with ***Bacillus subtilis*** and continuously fed with ***actual domestic wastewater*** at a rate 0.1 mL/min and average initial COD concentration of 380 mg/L. The ***Bacillus subtilis*** was isolated from a mixed culture of activated sludge freshly collected from a local sewage treatment plant. The schematic diagram of the microbial fuel cell as well as the ports details are given in Figs. 1 and 2, respectively. The UMFC was operated at temperature 28 ± 2°C. The freshly collected wastewater was primarily clarified and settled before entering the upflow MFC. The composition of the primarily clarified actual wastewater performed in this study with its constituents average concentration expressed in (mg /L) was as follows: BOD (200), COD (400), total phosphorus (12.8), nitrate nitrogen (9), ammonium nitrogen (24), chloride (30), sulfate (200), and pH (7.0). To start up the MFC operation, the anodic chamber was flushed with nitrogen, and then bacterium ***Bacillus subtilis*** was placed in the anodic compartment of the UMFC without aeration for 7 days in order to favor the enrichment of the cultures. The ***Bacillus subtilis*** was previously isolated from an activated sludge collected from the deep bottom of an aeration tank in a local sewage treatment plant. The wastewater was not pumped into the MFC during this conditioning period, thus the only substrate available for the microorganisms was obtained from the endogenous metabolism. After 7 days, the UMFC was fed with actual wastewater, at the same time the air was injected through the cathode chamber. Dissolved oxygen concentrations were measured in the anodic and cathodic compartments. The measured values of dissolved oxygen in the cathodic chamber indicated saturated concentrations. On the contrary, in the anodic chamber the oxygen concentration was observed to be very low indicating anaerobic conditions in this compartment. An external resistance of 300 Ω was placed between the anode and cathode.

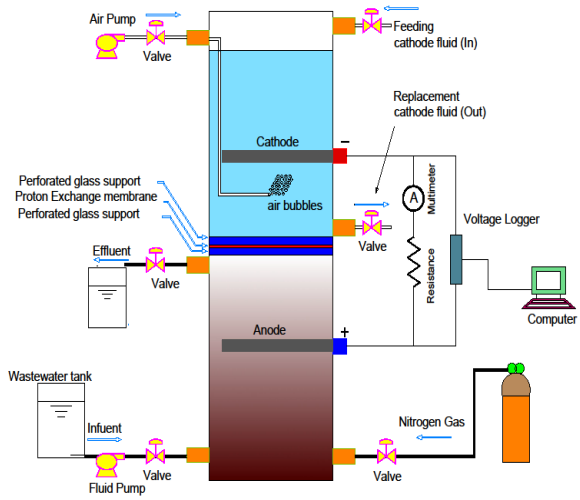

Fig. 1 Schematic diagram of the MFC

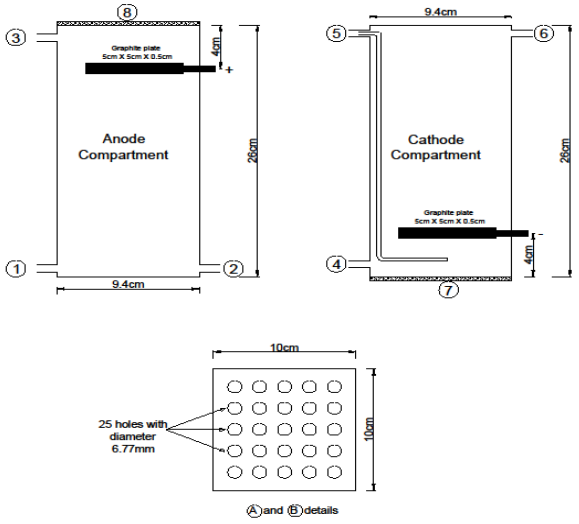

Fig. 2 Microbial fuel cell with membrane, Port 1: wastewater inlet, port 2: nitrogen flushing, port 3: outlet of wastewater, port 4: replacement of catholyte, port 5: aeration, port 6: catholyte feeding, 7 and 8 are the perforated glass sheets.

3. RESULTS AND DISCUSSION

COD Removal

MFC was continuously operated for 15 days before achieving the steady state condition. COD reduction was up to 90% upon achieving steady conditions as shown in the Fig. 3. Average initial COD concentration was 400 mg/l and volumetric COD loading rate to this MFC was 0.847 kg COD/m^3 d. After achieving steady state, the average effluent concentration of COD was 40 mg/l. The observed COD removal efficiency was more than the reported efficiency of 54% [4], using (Saccharomyces cerevisiae) as a pure microorganism for anodic inoculation, and 83% COD removal reported by Chaudhuri and Lovley, [5] using Rhodoferax ferrireducens.

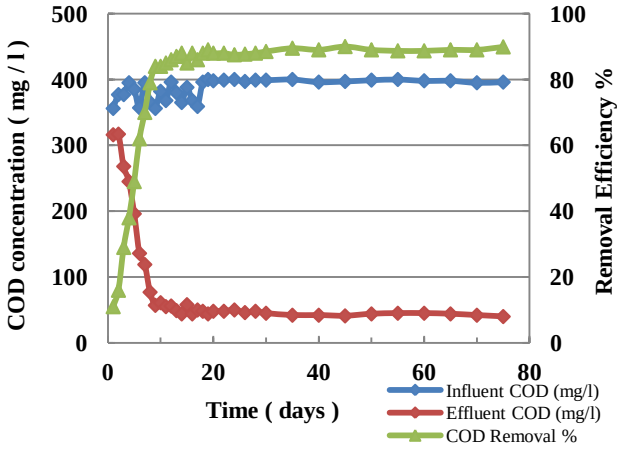

Fig. 3 COD removal efficiency

Current Generation

In this study, the MFC system generated maximum stable power outputs of 270 mW/ m^2 and maximum obtained Coulombic efficiency was 49.6%. The results proved that the pure microorganism ***Bacillus subtilis*** is electrochemically active and the performance of MFC inoculated with this pure culture is comparable, even higher to those inoculated with mixed cultures. For electricity generation, the current increased rapidly for the first 5 days, then increased slowly for the next 7 days to a maximum constant value of 3.60 mA as shown in Fig. 4. The current was maintained stable for more than 60 days under the given conditions. The open circuit potential was 0.81volt and the maximum closed circuit voltage drop a cross continuous external resistance 125 Ω was 0.45 volt Fig. 5. The electrochemical activity of the applied species ***Bacillus subtilis*** type of species is one of the most commonly used hosts in fermentation production, because it is simple to cultivate. Also, its products, the protein and metabolites are often secreted in the growth medium, M9 [2]. Additionally, the composition of M9 medium supplemented with glucose was employed to culture bacteria in the anode with biofilm might cause maximum productivity.

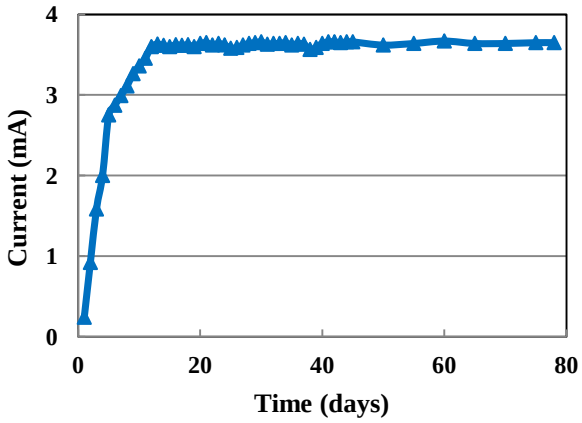

Fig. 4 Variation of the current with time

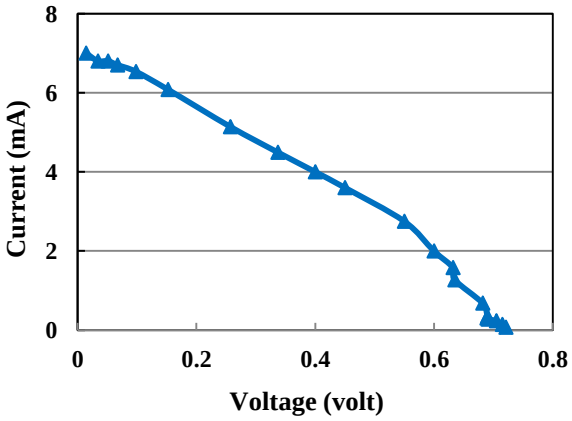

Fig. 5 Voltage-current relationship at different external resistances

Polarization Curve

The UMFC inoculated with pure culture ***Bacillus subtilis*** produced a power density due to the existing of electrogenic bacteria which transfer electrons to the electrode without interfering mediator in the anode chamber (Fig.6). The electrogenic bacteria existing in pure cultures have higher electrochemical activity than mixed culture leading to more power generation in MFC inoculated with pure culture.

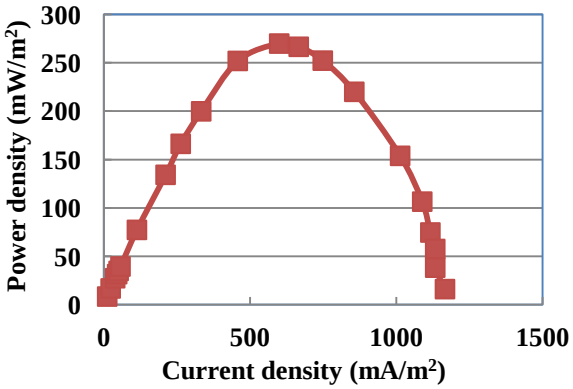

Fig. 6 Polarization curve

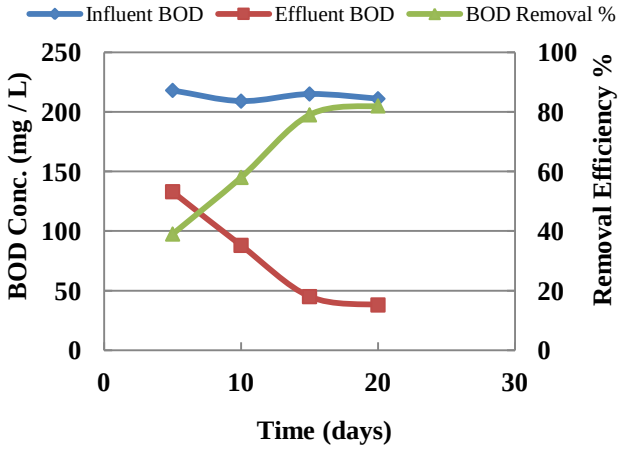

Fig. 7 BOD removal efficiency

BOD removal

Although the performance of microbial fuel cells were mainly evaluated in term of chemical oxygen demand (COD), measurements of biological oxygen demand (BOD) was also performed. Results revealed that the reduction in BOD concentration was up to 82% after 20 days operation as given in Fig. 7.

Granulation of biomass in UMFC

Upon reaching steady state conditions in the MFC, the electrode in the anodic chamber was almost fully covered with a thick layer of bio-film and the biomass granules formation was visible in the anode chamber. After 75 days of continuous operation, the MFC was emptied and small portions of the biofilm were scratched from the electrode surfaces and collected for microscopic examination from anode chamber. The anodic biofilm was partially granulated having 1-2 mm size of granules. The Scanning Electron Microscopy (SEM) images of the biofilm (Figs. 8 and 9) revealed the porous and spongy structure with some cracks on the surface. Similar observations were previously reported by Fang et al. [6] and Ghangrekar & Shinde [7]. They suggested that the porous structure of granules with multiple cracks on the surface is likely to facilitate the passage of nutrients and substrates as well as the release of hydrogen, which had a very limited solubility of 1.58 mg/l in water, thus these granules did not exhibit a layered structure because of the simplicity of the acidification process.

4. CONCLUSION

This study demonstrated and evaluated the performance of an upflow dual-chambered mediator-less microbial fuel cell (UMFC) catalyzed with ***Bacillus subtilis*** consortium for simultaneous wastewater treatment and power generation. The biofilms which grow under anaerobic environment and attached to the surfaces of the anode were the main contributors to the electricity generation. The results demonstrated that the aerobic Gram-positive species ***Bacillus subtilis*** was able to grow anaerobically and produce a biofilm in

microbial fuel fell, which generated a long-term power output.

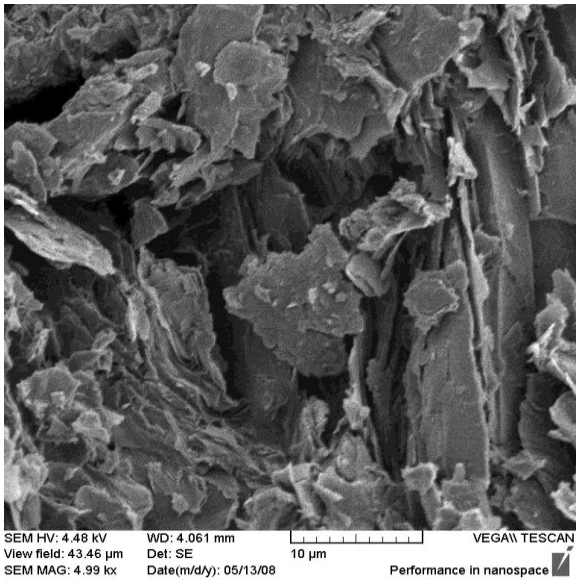

Fig. 8 SEM image for anode surface before granulation of biomass

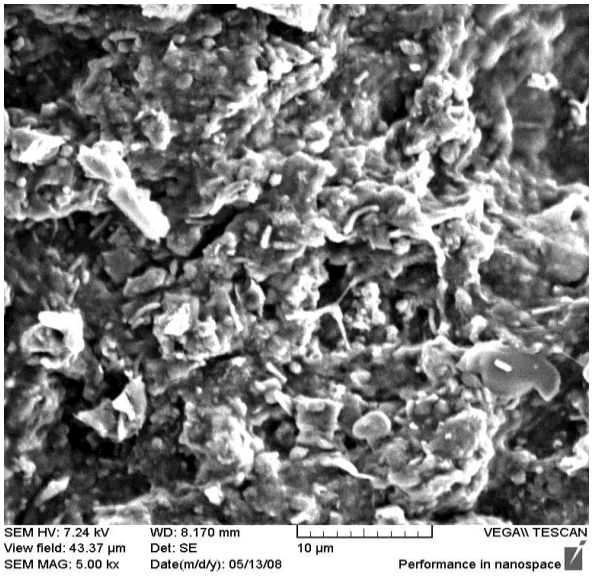

Fig. 9 SEM image for anode surface after granulation of biomass

5. REFERENCES

[1] Z-D. Liu, H-R. Li, "Effects of bio-and abio-factors on electricity production in a mediatorless microbial fuel cell", **Biochemical Engineering Journal**, Vol. 36, 2007, pp. 209-214.

[2] V.R. Nimje, C.Y. Chen, C.C. Chen, J.S. Jean, A.S. Reddy, C.W. Fan, K.Y. Pan, H.T. Liu, J.T. Chen, "Stable and high energy generation by a strain of Bacillus subtilis in a microbial fuel cell", **Journal of Power Sources,** Vol. 190, 2009, pp. 258-263.

[3] M. Rahimnejad, A.A. Ghoreyshi, G. Najafpour, T. Jafary, "Power generation from organic substrate in batch and continuous flow microbial fuel cell operations" **Applied Energy,** Vol. 88, 2011, pp. 3999–4004.

[4] S. Fatemi, A.A. Ghoreyshi, G. Najafpour, M. Rahimnejad, "Bioelectricity generation in mediator-Less microbial fuel cell: Application of pure and mixed Cultures", **Iranica Journal of Energy & Environment**, Vol. 3, 2012, pp. 104-108.

[5] S.K. Chaudhuri, D.R. Lovley, "Electricity generation by direct oxidation of glucose in mediator-less microbial fuel cells", **Nature Biotechnology,** Vol. 21, 2003, pp. 1229 - 1232.

[6] H.H. Fang, H. Liu, T. Zhang, "Characterization of a Hydrogen Producing granular sludge", **Biotechnology and bioengineering,** Vol. 78, 2002, pp. 44-52.

[7] M.M. Ghangrekar, V.B. Shinde, "Performance of membrane-less microbial fuel cell treating wastewater and effect of electrode distance and area on electricity production" **Bioresource Technology,** Vol. 98, 2007, pp. 2879-2885.

Managerial Innovations in the ICT Sector: Thinking Lean and Acting Agile

Carine Khalil
Laboratoire Génie Industriel - Ecole Centrale Paris
carine.khalil@ecp.fr

ABSTRACT

Management innovation is becoming essential for addressing the challenges faced in software industries. New managerial approaches have been progressively developed over the last two decades in order to cope with the inevitable market changing demands. These managerial innovations known as agile methods enhance team's ability to adapt to unpredictable environments. Many agile methods exist, each, emphasizing a set of managerial practices and tools. This research paper aims at exploring three famous agile methods and suggesting a sustainable agile methodology where practices and tools are guided by a key principle: "knowledge creation".

Keywords: Managerial Innovation, Lean Development, Scrum, Extreme Programming, Innovative Management Philosophy.

1. INTRODUCTION

In today's competitive and fast changing environment, an increasing attention is being paid to the role of managerial innovations in organizations. Different types of innovations have been investigated: new products, new methods of production, new markets, new technologies, and new ways to organize business [1]. Over the last two decades, research works have mainly focused on product innovations, technology and business models innovations. In fact, these types of innovation do not constitute a sustainable advantage for enterprises. They can be easily imitated by competitors. In response, a number of researchers [2, 3, 4] have shown a keen interest in managerial innovations. Management innovation seems to help organizations in building long-term competitiveness [2]. Given this focus, this research work aims at exploring managerial innovations in the ICT industry where the market is highly competitive.

With the technological surge, traditional management practices such as sequential development, complete definition of the product, extensive planning and documentation have been questioned by a number of practitioners. They are considered as unable to cope with changes. Thus, they were progressively replaced by new management and development methods known as agile methods. These methods enhance collaboration, frequent feedback, and adaptation to changes. They also empower team members and encourage self-management and organization. In this respect, agile methods, as innovation management, alter the way software projects are organized and managed.

Different agile methods exist (scrum, extreme programming, lean development; crystal, feature driven development, dynamic systems development, adaptive software development). Although these methods are based on common values and principles (Agile Manifesto[1]), each method emphasizes different managerial practices and tools. It is beyond the scope of this work to review the various agile methods. Hence, we will be focusing on the three most popular agile methods: scrum, extreme programming and lean development. We assume that each method represents a type of agility[2], yet, complementary in guiding and managing software projects. Although the three methods have been largely explored by academics and practitioners, they were rarely investigated as complementary software development methods. This research work aims at filling this gap by proposing a methodology[3] based on scrum, XP and lean development practices and principles. We suppose that the combination of these methods can improve managerial innovations within software industries.

The following paper is structured as follows: section (I) introduces agile methods as managerial innovations in software industries. Section (II) presents scrum, extreme programming and lean development approaches. Section (III) suggests a methodology that integrates and combines the various agile practices and tools. Lean principles are viewed as the guide for deploying scrum and extreme programming practices.

2. AGILE METHODS AS MANAGERIAL INNOVATIONS

Management innovation is defined as a "marked departure from traditional management principles, processes, and practices -- a departure from customary organizational forms that significantly alters the way the work of management is performed" [2]. In ICT sector, management innovation is essential for addressing the challenges faced by enterprises working in unpredictable and changing environments. Until the late 90's, the most widely used software development methods were based on sequential approaches. Each phase consists on a set of activities and deliverables that must be accomplished before the following phase. The project proceeds according to clearly defined phases and the deliverable is

[1] http://agilemanifesto.org/

[2] The ability of a team to rapidly respond to change by reconfiguring its resources.

[3] Methodology is defined as a guideline system based on principles, methods, techniques and tools.

produced at the end of the process. However, traditional management principles and processes were perceived as unable to adapt to inevitable changing demands and requirements [5, 6, 7]. In response, new "lightweight" project management methods, called agile methods, have blossomed and gained popularity. These emergent methods recommend short iterations during which changes are progressively integrated in the software product. They also advocate constant interactions and exchanges between team members. It is an attempt to bring people together and enhance collective practices and achievements.

3. SCRUM, EXTREME PROGRAMING AND LEAN DEVELOPMENT: PRINCIPLES AND PRACTICES

Scrum employs an iterative and incremental approach for managing projects. Three pillars uphold the scrum development process: transparency, inspection and adaptation [8]. The main purpose of scrum is to foster team productivity by providing "light" management practices (pre-sprint, daily sprint, retrospective meetings, sprint planning meeting, product backlog, burndown charts, etc.) and creating an environment where teams can easily communicate and adapt to changes. Table 1 summarizes the characteristics of scrum method.

Table 1: Characteristics [4] of scrum method

Scrum [8]	
Principles	Transparency, inspection and adaptation.
Roles	Scrum master, product-owner, scrum team
Management Practices	Pre-sprint, sprint planning meeting, daily sprint, post-sprint meeting and retrospective meeting.
Management Tools	Product backlog, sprint backlog, burndown charts

The extreme programming method relies on a set of engineering practices and collaborative tools that consist in lowering the cost of changes and ensuring knowledge capitalization [9]. Table 2 summarizes the characteristics of extreme programming.

Table 2: Characteristics[5] of XP method

XP [9]	
Principles	Communication, simplicity, feedback, respect and courage.
Engineering Practices	Continuous integration, unit-testing, acceptance tests, refactoring and simple design.
Management and collaboration practices	Planning game, stand-up meeting, pair programming, collective code ownership, on-site customer and metaphor.
Management tools	User-stories, story-cards and story-boards.

Lean development is a way of thinking, a philosophy that encompasses a system-level perspective and therefore extends beyond development practices. It is a set of principles that organizations use in order to adapt tools and methods to their own specific contexts and capabilities. It goes beyond scrum and extreme programming methods, by providing a broader perspective that enables these methods to thrive [6].

Table 3: Characteristics[6] of lean development

Lean [10]	
Principles	Eliminate wastes, build quality, create knowledge, defer commitment, deliver fast, respect people, optimize the whole
Management practices and tools	Pull system, kaizen sessions, pareto cause analysis, 5 whys, A3 problem solving.

Each one of these methods represents a particular type of "agility", however, complementary in developing and managing software projects. Scrum advocates "light" management practices based on frequent collaboration between team members. Constant exchanges add agility to the development process by providing rapid feedback on the implemented functionalities [11]. It facilitates the monitoring of the project progress [12] and improves organizational learning [13]. Unlike extreme programming, scrum doesn't focus on engineering practices. XP engineering practices reduce cost changes and improve code quality. They also provide permanent feedback on the developed codes [14, 15]. They enable developers to quickly resolve bugs and defects and decrease the number of problems related to late code integration. However, concerning lean development, its principles guide and govern the implementation of scrum and extreme programming practices and tools. Unlike scrum and XP practices, lean principles are invariable regardless the implementation context. Accordingly, lean development goes beyond scrum and extreme programming methods. It overpasses development activities and concerns the different levels of the organization. In this respect, building a methodology where lean principles guide scrum and extreme programming practices can create value for software organizations.

4. TOWARDS A SUSTAINABLE INNOVATIVE AGILE METHODOLOGY

The literature review of lean manufacturing [16] shows that lean manufacturing principles have clearly inspired agile practitioners. Mainly, principles written in the agile manifesto are based on lean management pillars:

[4] Scrum practices, tools and roles are defined in Annex I.
[5] XP practices and tools are defined in Annex I.
[6] Lean principles and practices are defined in Annex I.

eliminating wastes and delivering on time a product that meets customers' needs. However, unlike lean development that encompasses the different levels of an organization, agile methods have mostly focused on the development activities. This can possibly explain why the implementation of scrum and extreme programming, in large and complex organizations, is challenging [17, 18]. Agile practices seem more suitable for small teams because actors can easily communicate and collaborate. Thus, by considering lean principles as the basis of agile methods, it may be easier to scale agile practices and implement them in large organizations. Given this focus, we suggest a methodology where lean principles govern the implementation of scrum management practices and XP engineering and collaboration practices. This methodology is identified as "EXSL" methodology. Table 4 describes the management philosophy of EXSL methodology.

Table 4: Components of EXSL methodology

Values	RESPECT PEOPLE
	OPTIMIZING THE WHOLE
Key principle	**Practices and tools**
Create Knowledge	Engineering practices: continuous integration, refactoring, unit-testing. Collaboration and management practices: short development cycles, daily meetings, functionalities prioritization, pull system, pair programming, retrospective meetings, kaizen sessions, frequent feedback with the client, and informative workspace (story-boards, virtual whiteboard). Problem solving tools: A3 problem solving, pareto analysis, 5 why's.
⇩	
Strategic objectives	
Eliminate Wastes (extra features, delays, handoffs, relearning, partially done work, tasks switching, and defects) [10]	
Building quality	
Delivering fast	

EXSL methodology is an iterative and incremental framework for developing and managing software projects and solutions. This methodology relies on existing software development practices and tools. It advocates people respect (people as drivers for organizational success) and focuses on optimizing the entire system in an organization. These two values serve as a guiding force in the EXSL environment. Besides, this methodology is based on a key lean principle: "create knowledge". This principle guides the creation of an environment where actors can quickly respond to changes and continuously improve their development process. Throughout constant feedback, agile practices help teams in identifying and fixing defect as early in the development process as possible. Therefore, agile engineering and management practices foster individual and collective knowledge. They help organizations in decreasing wastes, building quality and delivering fast a product that meets customers' requirements.

Agile practices should be viewed as governed by "create knowledge" principle. By integrating this management philosophy, team members would be properly adapting the agile toolkit to their organization. Thus, agile practices are not seen as an end in themselves. They facilitate means though which lean values and principles are materialized.

5. CONCLUSION

EXSL methodology underlines an innovative management philosophy for developing software projects. This methodology is obviously inspired by lean development approach. However, it focuses on one key lean principle: "create knowledge". It combines scrum, extreme programming and lean manufacturing practices and tools in order to serve this principle. Thus, agile engineering and management practices are viewed as a toolkit for enhancing individual and collective learning processes within software organization. By doing so, software organizations decreases wastes and meet their strategic objectives.

Nevertheless, this methodology requires further theoretical and empirical investigation. In addition to that, the development framework should be described more precisely and necessitates empirical validation. Hence, this research study offers a first vision of an innovative management philosophy that stresses on knowledge creation in software industries. This is achieved by combining principles, practices and tools from the three most famous agile approaches.

6. REFERENCES

[1] J. A. Schumpeter, **The theory of economic development**, New Brunswick, NJ: Transaction Publishers, 1983.

[2] F. Damanpour and D. Aravid, "Managerial innovation: conceptions, processes, and antecedents", **Management and Organization Review**, Vol. 8, N°2, 2011, pp. 1-47.

[3] J. Birkinshaw, G. Hamel and M. Mol "Management innovation", **Academy of Management Review**, Vol. 33, 2008, pp. 825-845.

[4] G. Hamel "The Why, What and How of Management Innovation", **Harvard Business Review**, 2006, pp.74-84.

[5] J Highsmith, and A. Cockburn, "agile software development: the business of innovation", **Computer**, vol. 34, N°9, 2001, pp. 120–122.
[6] M. Poppendieck, and T. Poppendieck, **Implementing lean software development: from concept to cash**, Addison-Wesley, 2006.
[7] K. Petersen, and C. Wohlin, "A comparison of issues and advantages in agile and incremental development between state of the art and an industrial case", **Journal of systems and software**, vol. 82, N°9, 2009, pp. 1479-1490.
[8] K. Schwaber, **Agile project management with Scrum**, Microsoft Press, 2004.
[9] K. Beck and C. Andres, **Extreme Programming Explained: Embrace Change**, Addison-Wesley Professional, 2nd edition, 2004.
[10] M. Poppendieck, and T. Poppendieck, **Lean software development: an agile toolkit**, Addison-Wesley, 2003.
[11] D. Karlström and P. Runeson, "Combining agile methods with stage-gate project management", **IEEE Computer Society**, Vol. 22, N°3, 2005, pp. 43-49.
[12] Begel and N. Nagappan, "Usage and Perceptions of Agile Software Development in an Industrial Context: An Exploratory Study", **IEEE Computer Society**, Madrid, 2007, pp. 255-264.
[13] P. Middleton, A. Flaxel and A. Cookson, "Lean software management case study: Timberline Inc.", **Lecture notes in computer science**, N°3556, 2005, pp. 1-9.
[14] M. Paasivaara, and C Lassenius, "Using Iterative and Incremental Processes in Global Software Development", **Proceedings of the ICSE Workshop on Global Software Development**, 2004, pp. 42-47.
[15] S. Berczuk, "Back to Basics: The role of agile principles in success with an distributed Scrum team", **Proceedings of Agile Conference, Washington,** DC, 2007, pp. 382-388.
[16] P.J. Womack and T.J Daniel, **Lean thinking, s**econd edition, Simon & Schuster, Inc. 2003.
[17] M. Paasivaara, S. Durasiewicz and, C. Lassenius. Distributed agile development: using Scrum in a Large Project, **Global Software Engineering**, 2008, pp. 87- 95.
[18] Khalil and, V. Fernandez, "Implementation of agile practices in a distributed and large organization: a contextual factors analysis", The 10th IASTED **International Conference on Software Engineering, Innsbruck**, Austria, 2011.

ANNEX

A3 problem solving: A3 problem solving is a structured approach to resolve problems. Toyota engineers learn the discipline of condensing complex thinking to a single A3 sheet of paper. Different A3 reports have different purposes, but all of them capture critical knowledge in a way that is easy to store in a database, easy to post in a work area, etc.

Burndown Chart: It **s**hows work remaining over time. Work remaining is the Y axis and time is the X axis. The work remaining should jig up and down and eventually trend downward.

On-site customer: It consists on having a real, live user that constantly collaborates with the development team. The on-site customer is available full-time to answer questions.

Collective code ownership: It's an extreme programming practice where anyone can change the code, anywhere in the system, at any time.

Continuous integration: It consists on integrating and building the system many times a day, every time a task is completed.

Daily scrum: It's a fifteen-minute daily meeting for each team member to answer three questions: what have i done since the last scrum meeting? What will i do before the next scrum meeting? And what prevents me from performing my work as efficiently as possible?

Iterative development: The main idea of an iterative approach is to divide the development cycle into simpler and more manageable units. Each unit is analyzed, designed and implemented in order to produce an executable deliverable with a limited set of functionalities. The final executable deliverable encompasses all the functionalities expected from the system.

Kaizen: it's a Japanese term that means continuous improvement. Kaizen events consist on gathering operators, managers, owner of a process in one place, mapping the existing process in order to improve it.

Pareto cause analysis: It is an application of the "vital few trivial many" rule, also called 80/20 rule. The analysis proceeds thus: Divide a problem into categories, find the biggest category, look for the root cause of the problem creating that category and fix it.

Planning-Game: It's a meeting attended by both development and business teams (client representative) in order to identify and prioritize stories of the next release or iteration. It combines business priorities and technical estimates.

Post-sprint meeting: At the end of the sprint iteration, a post-sprint meeting is held to review progress, demonstrate features to the customers and review the project from a technical perspective.

Product-backlog: The product backlog is the requirements for a system, expressed as a prioritized list of product backlog items. These included both functional and non-functional customer requirements, as well as technical team-generated requirements. While there are multiple inputs to the product backlog, it is the sole responsibility of the product owner to prioritize the product backlog.

Product backlog item: In Scrum, a product backlog item ("PBI", "backlog item", or "item") is a unit of work small enough to be completed by a team in one sprint iteration. Backlog items are decomposed into one or more tasks listed in a sprint backlog.

Product-owner: In scrum, a single person must have final authority representing the customer's interest in backlog prioritization and requirements questions. This person must be available at any time especially during the sprint planning meeting and the sprint review meeting.

Pair programming: It consists on having two people working side-by-side on the same task. It provides continuous code review in a flow rather than a batch.

Pull system: To reduce inventory holding costs and lead times, Toyota developed the pull production method wherein the quantity of work performed at each stage of the process is dictated solely by demand for materials from the immediate next stage.

Retrospective meeting: The sprint retrospective meeting is held at the end of every sprint after the sprint review meeting. The team and scrum-master meet to discuss what went well and what to improve in the next sprint.
Scrum-Master: The scrum-master is a facilitator for the team and product owner. Rather than managing the team, the Scrum-Master works to assist both the team and product owner.
Scrum team: It consists of seven plus or minus two people. For software development projects, the team members are usually a mix of software engineers, architects, programmers, analysts, testers, designers, etc.
Sprint: It defines the work for a sprint, represented by the set of tasks that must be completed to realize the sprint's goals, and the selected set of product backlog item.
Sprint Planning Meeting: The Sprint planning meeting is a negotiation between the team and the product owner about what the team will do during the next sprint. The product owner and all team members agree on a set of sprint goals, which is used to determine which product backlog items will be implemented in the next sprint. Then, the scrum-master and his team focus on how the selected product items will be implemented. .
Stand-up meeting: It's a fifteen daily meeting for XP teams. During this meeting, developers share their experiences of the day before, talk about their progress since the last stand-up and the anticipated work until the next stand-up.
Story-cards: They represent brief details of the tasks being actively worked upon.
The 5 why's: It refers to the practice of asking, five times, why the failure has occurred in order to go to the root cause/causes of the problem. There can be one or more cause to a problem as well.
Test driven development: It consists on writing the tests before writing codes in order to prevent defects. The goal of lean software development is to prevent defect from getting into the code base in the first place and the tool to do this is the test-driven development.
Unit-tests: They are written by developers to test their design intent. Unit-tests help a developer to really consider what needs to be done.

Experimental Investigation and CFD Simulation of Active Damping Mechanisms for Propellant Slosh in Spacecraft and Launch Vehicles

Dhawal Leuva
Graduate Student, Aerospace Engineering, Embry Riddle Aeronautical University
Daytona Beach, Florida 32114

Priya Sathyanarayan
Student Research Assistant, Mechanical Engineering, Embry Riddle Aeronautical University
International Baccalaureate Program, Spruce Creek High School, Daytona Beach, Florida 32114

Deepak Sathyanarayan
Student Research Assistant, Bio-Medical Engineering, Duke University
Durham, North Carolina 27708

and

Sathya Gangadharan
Professor, Mechanical Engineering, Embry Riddle Aeronautical University
Daytona Beach, Florida 32114

ABSTRACT

Violent motion of propellant in the tank due to inertial forces transferred from actions like stage separation and trajectory correction is termed as propellant slosh. If unchecked, propellant slosh can reach resonance and lead to complete loss of the stability of spacecraft, change the trajectory or increase consumption of propellant from the calculated requirements, thereby causing starvation of the latter stages. A spherical tank modeled for CFD simulation in ANSYS CFX software package considers free surface of the propellant exposed to atmospheric pressure. The propellant is hydrazine. Hydrazine being toxic and its properties being close to that of water, water is used as propellant for experimental study. For close comparison of the data, water is chosen as propellant in CFD simulation. The research is done in three phases. First phase is modeling of CFD simulation and validation of model by comparison to previous experimental results. Second phase is developing a damping mechanism and simulating the behavior by FSI model. Third phase is experimental development of damping mechanism and comparing the FSI simulation and experimental results. Various passive damping devices (diaphragm and baffles) and active damping device (frequency control) are compared in terms of their effectiveness in damping of fuel slosh.

I. INTRODUCTION

For spin stabilized spacecraft, unwanted vibrations lead to propellant slosh [1]. Energy dissipation of this propellant slosh is difficult. This energy causes nutation of spacecraft about its spin axis [2, 3]. For non-spinning spacecraft, actions like trajectory control and stage separation induced propellant slosh.

Sloshing is of two types. First type is small amplitude sloshing caused by transient excitation so the amplitude is small with well-defined oscillation frequency. It is the function of gravity, tank shape and propellant fill level in the tank [4]. Second type of sloshing is large amplitude sloshing caused during main engine ignition and burnout, the waves begin to break and oscillations become erratic in large amplitude sloshing.

When slosh waves are allowed to freely oscillate, they have a tendency to reach resonance. At resonance, slosh waves have maximum amplitude. The forces of sloshing propellant cause the spacecraft to nutate about its spin axis. Traditional vector correction methods are used to correct the nutation, but high frequency of direction change and high magnitude of sloshing propellant forces quickly overpower the corrections being made and sometimes results in more nutation and complete loss of spacecraft.

To prevent sloshing, presently many passive damping devices are being used. These passive damping devices (diaphragms and baffles) provide excellent propellant slosh damping for a small range of frequency and small amplitude of sloshing, but they are not effective when propellant fill level changes and sloshing frequency is outside their design range. These devices are bulky, consume space, add significant weight, have small operation range and requires extensive testing [5]. Active damping devices are developed to overcome the disadvantages of passive damping devices. Active damping devices work for a wide range of amplitude and frequencies and for all the propellant fill level in the tanks.

An active damping device consist a device that can generate high frequency small amplitude waves with opposite phase to that of sloshing waves. The ultimate goal for active damping device development research is to make an automated device with a feedback loop that can measure tank fill level, amplitude and frequency of propellant slosh in real time and apply required input of amplitude and frequency of damping waves to quickly stop propellant sloshing [6].

II. APPROACH

CFD Theory

Computational Fluid Dynamics (CFD) is used to model the propellant slosh behavior. The CFD method solves Navier Stokes equations at required points in the fluid domain to get the properties of the fluid flow at those points. Simple CFD problems were solved analytically, but with increase in fluid flow complexity, mathematical complexity increases exponentially. With the advancement of computers since 1950s, with powerful graphics and 3D interactive capability, use of CFD has gone beyond research and into industry as a design tool. Experiments can give macro data at certain points in the flow field, but with CFD, flow field can be resolved to details like turbulence, viscous forces and velocity. All this makes CFD an essential and useful tool for complex flows like propellant slosh.

CFD is solution of Navier Stokes equations. Navier Stokes equations are set of partial differential equations describing processes of momentum and heat and mass transfer. These equations have no known general analytical solution, but can be solved numerically by discretization. The four Navier Stokes equations are: x-momentum, y-momentum, z-momentum and continuity equation respectively shown below in their conservation cartesian coordinate form.

$$\frac{\partial(\rho u)}{\partial t} + \nabla.(\rho u V) = -\frac{\partial p}{\partial x} + \frac{\partial \tau_{xx}}{\partial x} + \frac{\partial \tau_{xy}}{\partial y} + \frac{\partial \tau_{xz}}{\partial z} + \rho f_x \ldots\ldots\ldots\ldots\ldots (1)$$

$$\frac{\partial(\rho v)}{\partial t} + \nabla.(\rho v V) = -\frac{\partial p}{\partial y} + \frac{\partial \tau_{xx}}{\partial x} + \frac{\partial \tau_{xy}}{\partial y} + \frac{\partial \tau_{xz}}{\partial z} + \rho f_y \ldots\ldots\ldots\ldots\ldots (2)$$

$$\frac{\partial(\rho w)}{\partial t} + \nabla.(\rho w V) = -\frac{\partial p}{\partial z} + \frac{\partial \tau_{xx}}{\partial x} + \frac{\partial \tau_{xy}}{\partial y} + \frac{\partial \tau_{xz}}{\partial z} + \rho f_z \ldots\ldots\ldots\ldots\ldots (3)$$

$$\frac{\partial \rho}{\partial t} + \nabla.(\rho V) = 0 \ldots\ldots\ldots\ldots\ldots (4)$$

CFD applies these equations across a discretized domain. This process is called discretization. These equations are solved numerically using finite volume technique (explained in ANSYS CFX Theory) and further discretization makes CFD method at best an approximation to the exact solution. Though being an approximation, CFD gives an accurate understanding of the flow process and is known to give exceptional results.

Apart from using Navier Stokes equations, free surface problems like propellant slosh pose an additional difficulty of tracking free surface, clearly defining the boundary of the different phase fluids. All the CFD software use Volume of Fluid (VOF) model to track velocity, location and shape of the free surface between different phases of fluids.

Finite volume technique used to solve Navier Stokes equation stores the values of all the properties like velocity, pressure, density, temperature and volume fraction of the fluid at center of each control volume. VOF model extracts the volume fraction data at each control volume to determine the shape and location of the free surface.

Volume fraction, as the name suggests is the ratio between the volumes of the two fluids at each control volume. For the case of water and air, if the volume fraction of water is 1 at the control volume, means control volume is completely filled with water. If the volume fraction of water at a control volume is 0.5, means 50 percent of the control volume is filled with water and the other 50 percent is filled with air (Figure 1). If the volume fraction of water at a control volume is 0, means that control volume does not contain water but at the same time the volume fraction of air at that control volume will be one. In short, for any fluid system such as air-water fluid system, the summation of individual volume fractions of air and water at each control volume should equal to 1.

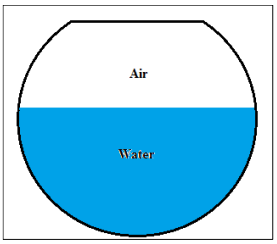

Figure 1. Volume fraction distribution, volume fraction of air is 0.5 and volume fraction of water is 0.5.

Solution of volume fraction conservation equation defined by Hirt and Nichols [6] is used in tracking of the free surface throughout the volume

$$\frac{\partial F}{\partial t} + u\frac{\partial F}{\partial x} + v\frac{\partial F}{\partial y} + w\frac{\partial F}{\partial z} = 0 \ldots\ldots\ldots\ldots\ldots (5)$$

The function F in the above equation represents volume fraction at each control volume. The range of function F is $0 \leq F \leq 1$ as discussed above. Finding the location of free surface does not solve the problem completely since still the orientation of the free surface is unknown (Figure 2). The three diagrams (Figure 2) show the simplest possibility of the orientation of the free surface. VOF technique uses the gradient of volume fraction at each control volume across the free surface to determine the slope of the free surface and there by the orientation of the free surface over the entire control volume can be known and plotted.

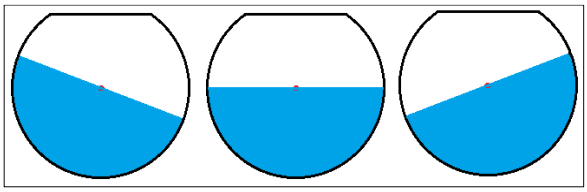

Figure 2. Free surface orientation for 0.5 volume fraction

Propellant slosh is a transient process. The slosh waves changes with time, with the change in slosh waves, the forces acting on the wall of the tank changes. Simulation of such problems is done by breaking the duration of entire simulation run into small time segments known as time steps in CFD software. The size of the time step is chosen depending on the velocity of the propellant slosh. For this research, usually the entire time for the simulation including time for tank excitation and time for natural damping of slosh waves took 10 seconds. If the time step of 0.1 second is selected, the simulation fails since for this time step the velocity of the slosh wave is very high and the

solution diverges. After careful analysis, time step of 0.01 second is chosen which gives sufficient convergence of the solution and accuracy. Size of the time step depends on the mesh size and the change in the velocity between the time step. Finer the mesh, bigger the time step. Meaning, 0.1 second time step can work for propellant slosh if the mesh used is fine. But on the other hand finer mesh means more calculation time without improving quality of the result. Also for the educational versions of CFD software, there is a limitation of number of nodes that can be used for simulation, hence for this research time step size is reduced instead of having finer mesh.

Forces acting on the tank wall are plotted against time. These results require further analysis to extract natural frequency.

ANSYS CFX Theory

Navier Stokes equations can be solved numerically using various techniques. Finite volume technique is one of the most commonly used methods for the solution of these equations and ANSYS CFX also uses this technique. In finite volume technique, the flow field is divided into sub-regions called control volume. The above mentioned discretized Navier Stokes equations are solved numerically over the control volume. Thus approximate values of the variables are calculated throughout the domain at specific points to form full flow characteristic.

ANSYS CFX converts Navier Stokes equations into integral form over each control volume. Gauss's Divergence Theorem is used to convert these integrals with divergent and gradient operators into surface and volume integrals which are further discretized and converted to linearized equations and assembled into a solution matrix and solved using First or Second order Backward Euler Schemes [6].

CFD Simulation

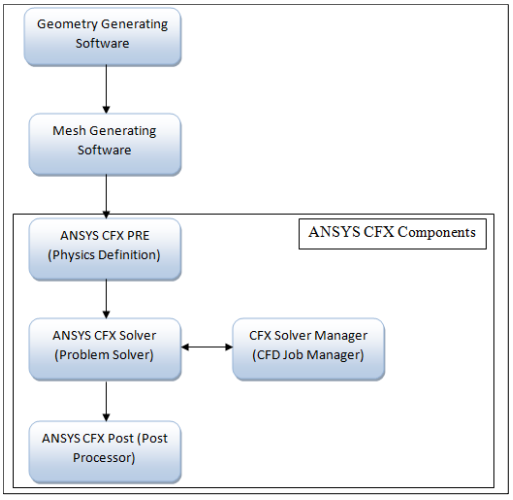

Figure 3. Flowchart showing CFD simulation process

In ANSYS CFX, the simulation process is split into four steps:

1. Creating geometry and mesh
2. Defining the physics of the problem
3. Solving the CFD problem
4. Analyzing the result in post processor

An axisymmetric model of a spherical tank with a cut opening at the top of the tank is generated in CATIA. Pointwise software is used to generate mesh. ANSYS CFX and ANSYS Workbench software package are used for CFD simulations, FSI simulations and for result interpretation respectively.

The spherical tank is 12.9 inches in diameter. The diameter is chosen to confirm with the tank diameter used for experiment to validate the preliminary free surface sloshing model simulated in ANSYS CFX. These experiments were performed in a spherical tank which had opening at the top, exposed to atmospheric pressure and temperature. The preliminary CFD model is generated to closely match those conditions. The tank is excited laterally for amplitudes ranging from 3 millimeter to 3 centimeter. Lateral excitation amplitude is chosen to prevent spillage of propellant form the tank top. Usually hydrazine is used as propellant in rockets. Since hydrazine is toxic and has physical properties similar to water, water was used as propellant in experimental analysis. To confirm CFD simulation results closely to experimental data, CFD model is developed using water as propellant. Also, it has been proven by experiments that at 60 percent tank fill level, amplitude of the sloshing waves are maximum. So all CFD models and subsequent experiments are performed with 60 percent tank fill level. The simulation is done for 10 second with 0.01 time step size.

The active damping device being simulated presently consist a thin flexible membrane at the bottom of the tank. The membrane is moved by plunger mechanism. The frequency of the membrane can be controlled manually. This model is for FSI simulation. For FSI simulation, ANSYS mechanical is coupled with ANSYS CFX. The tank is first simulated to oscillate laterally for 3 second and generate sloshing waves at natural frequency, the oscillation of the tank stops at 3 second and the vertical oscillation of the flexible membrane will being at very high frequency of 13.5 hertz. This FSI simulation is being done for 10 second with time step size of 0.01s.

Experimental Testing

The Embry-Riddle Aeronautical University Fuel Slosh Test Facility has a pre-existing experimental set-up to test lateral fuel slosh. The experimental rig, seen in Figure 4, is an adjustable force-balance fixture which rests atop a single-axis linear actuator. An adjustable rotary scroll allows for the experimental set-up to accommodate a variety of different tank shapes and sizes. However, in keeping with the purpose of the experiment, the experimental set-up used in this research will be exactly the same as in past tests.

The fuel tank will be made of standard polycarbonate and will measure 12 inches in diameter. All test cases will use this fuel tank. The research will also include four standard diaphragm shapes used in current spacecraft fuel tanks, the crater-shape, the mountain-shape, the yin-yang-shape and the high-ridge-shape. Instead of a flexible, rubber-like diaphragm, the new diaphragm will be a rigid, metallic diaphragm. In order to eliminate the costly manufacturing of the metallic diaphragm, an alternative diaphragm will be used to simulate a metallic diaphragm. All four metallic diaphragm geometries will be manufactured using machine-molded foam profiles cut from a

three axis CNC surface router. The molds will then be coated in fiberglass to give the geometries rigid, metallic-like properties.

Continuing to follow past research methods, a liquid propellant fill level of 60% will be used as this is the fill level of greatest interest to researchers. It is at this fill level that the fluid slosh imparts the highest forces on the sidewalls of the tank and the diaphragm.[5] Liquid Hydrazine is a common spacecraft propellant which is highly flammable and toxic and not suitable to store in the lab or use in the experiment. Therefore, a non-hazardous substitute, water, will be used. Water has similar density and viscous properties to liquid Hydrazine which make this an acceptable substitution.

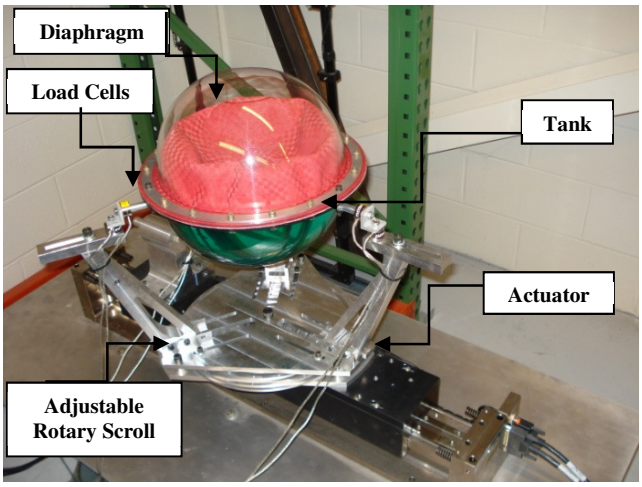

Figure 4. Fuel slosh experimental test facility at Embry-Riddle Aeronautical University.

Data from experimental tests will be acquired via six dynamic load cells mounted in equal intervals around the center-line of the fuel tank. These six load cells will resolve the forces and moments in the radial, tangential and vertical directions. The load cells will transmit the data through a six channel signal amplifier and conditioner where they are filtered, amplified and transmitted to the data acquisition system, LabVIEW. LabVIEW outputs the data into six frequency vs. time graphs to represent the 3 forces and moments from the load cells.

III. RESULTS AND DISCUSSION

Resonant Frequency

The resonant frequency of the slosh is found by performing a frequency sweep from 3.75 Hz to 6.75 Hz. The Figure 5 illustrates the experimental frequency sweep performed to determine the resonant frequency.

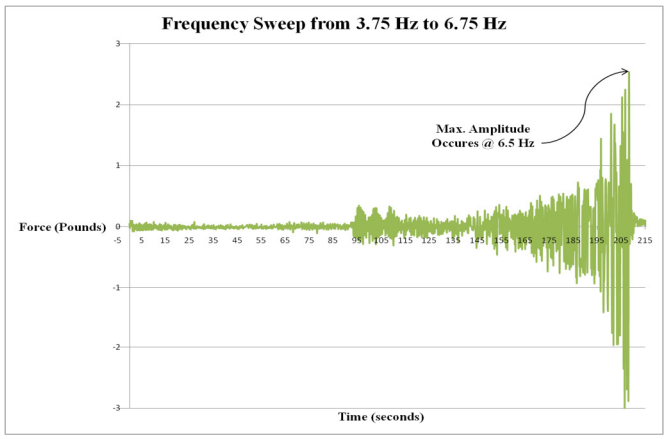

Figure 5. Frequency sweep performed to determine resonant frequency of sloshing liquid.

Figure 6 shows the CFD results obtained by simulation of free surface slosh. Tank is excited for 8 seconds to determine natural frequency trend. The model for free surface slosh is shown in Figure 7.

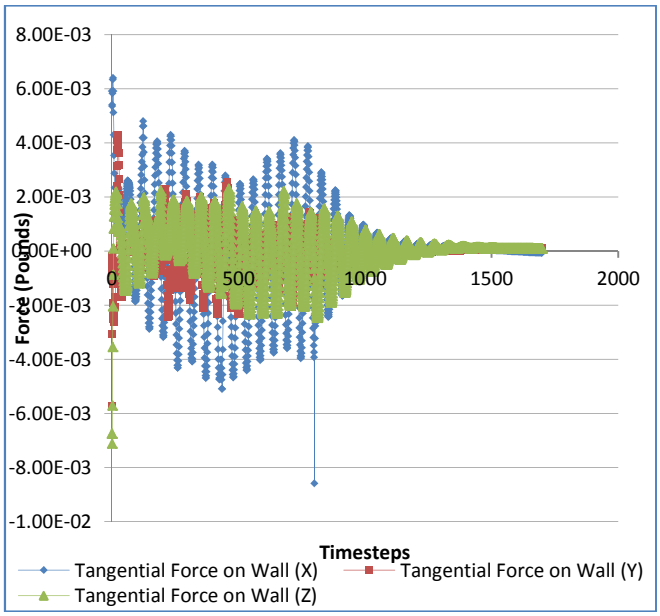

Figure 6. CFD results showing the force response characteristics.

To experimentally determine the physical effects the active damping mechanism posed on the dynamic behavior of the propellant tank, a model tank was mounted on a linear actuator and excited at various frequencies' to excite the liquid inside and cause the fuel to slosh. To conclude on the damping effectiveness of the active damping mechanism and understand how this mechanism compares to passive types of Propellant Management Devices (PMD's) that are currently in use, four different tests were run. The first test acted as a control, this test consisted of the model propellant tank being excited with no PMD implemented, this type of tank is known as a bare tank. The test provided the settling time of the liquid within the tank when no internal force or structure was present. For validation purposes, the model propellant tank was filled to approximately

60% maximum capacity. This fill level was maintained throughout all of the testing (Figure 8).

The second and third tests were performed exactly like the control test except a certain type of passive PMD was installed within the tank. The two types of PMD's used were an elastomeric diaphragm (Figure 9) and a rigid baffle (Figure 10). These structures remain stationary within the tank and provide a barrier to the liquid to minimize the sloshing distance the liquid can travel; thus minimizing the total amount of force the liquid can pose within the system.

The fourth and final test was performed the same as the first three, however, in this instance the active damping mechanism was placed within the tank. The active damping mechanism proved to significantly dampen the liquid (Figure 11). The results of all four tests illustrate the settling time for each test.

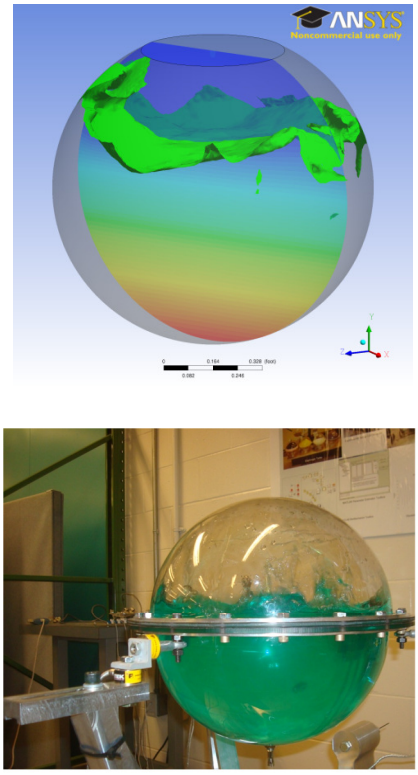

Figure 7. CFD simulation model and experimental setup representing the free surface slosh in the tank.

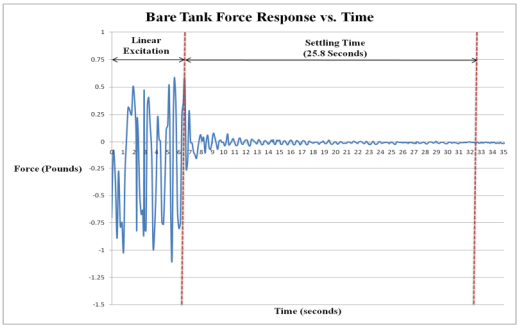

Figure 8. Experimental results of control test performed on bare propellant tank configuration.

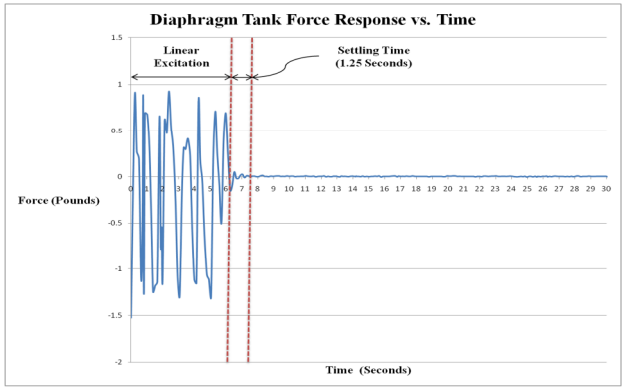

Figure 9. Experimental results depicting settling time of diaphragm implemented experimental setup.

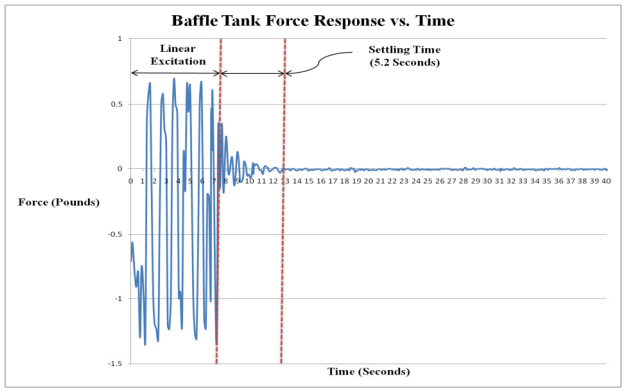

Figure 10. Experimental results of tests performed on propellant tank with baffle implemented.

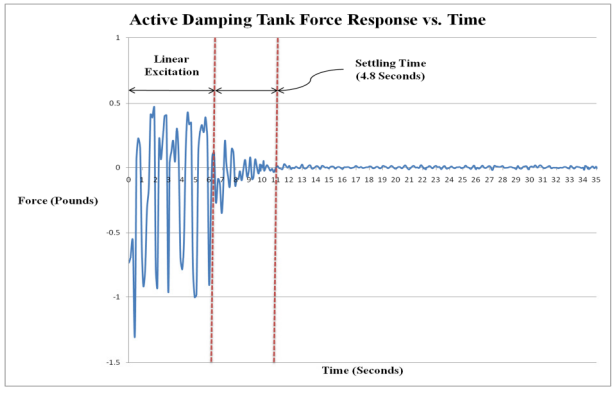

Figure 11. Experimental results gathered from active damping experimental procedures.

IV. CONCLUSION

Based on the experimental data, the active damping mechanism provided a settling time that fell closely between that of the two commonly used PMD's. As expected the diaphragm was the most effective, with a settling time of approximately 1.25 seconds, it dampened the liquid slosh quicker than any of the other PMD's. However, the active damping mechanism provided a settling time of approximately 4.8 seconds that is 0.4

seconds quicker than the baffle. While the active damping mechanism proved to provide less damping than the diaphragm, it did prove to provide more damping than the baffle. These results show that the theory of active damping is, indeed, valid. It is important to note that the active damping mechanism was not optimized. Future testing needs to be done that will provide an optimized mechanism to determine the full potential of the damping method. Furthermore, all experimental results will be compared to a model made using Computational Fluid Dynamics (CFD) to validate the test results as well as further advance the ability to model active damping techniques.

V. REFERENCES

[1] Hubert, C., "Behavior of Spinning Space Vehicles with Onboard Liquids," **NASA/Kennedy Space Center NAS10-02016,** 2003.

[2] Chapman, Y., "Modeling and Parameter Estimation of Spacecraft Lateral Fuel Slosh," **Embry-Riddle Aeronautical University**, 2008.

[3] Abramson, H., "The Dynamic Behavior of Liquids in Moving Containers," **NASA SP-106**, 1966.

[4] Marsell, B., "A Computational Fluid Dynamics Model for Spacecraft Liquid Propellant Slosh", **M.S. Thesis, Embry-Riddle Aeronautical University**, Daytona Beach, Florida, 2009.

[5] Schlee, K., "Modeling and Parameter Estimation of Spacecraft Fuel Slosh Using Pendulum Analogs**", M.S. Thesis, Embry-Riddle Aeronautical University**, Daytona Beach, Florida, 2006.

[6] Leuva, D., "Experimental Investigation and CFD Simulation of Active Damping Mechanism for Propellant Slosh in Spacecraft Launch systems", **M.S. Thesis, Embry-Riddle Aeronautical University**, Daytona Beach, Florida, 2012.

Software Development Productivity Prediction of Individual Projects Applying a Neural Network

Cuauhtémoc LÓPEZ-MARTÍN
Information Systems Department, Universidad de Guadalajara
Jalisco, México
cuauhtemoc@cucea.udg.mx

Arturo CHAVOYA
Information Systems Department, Universidad de Guadalajara
Jalisco, México
achavoya@cucea.udg.mx

Maria Elena MEDA-CAMPAÑA
Information Systems Department, Universidad de Guadalajara
Jalisco, México
emeda@cucea.udg.mx

ABSTRACT

Machine learning techniques have been applied in the software engineering field and their models could be applied for predicting the development productivity of software developers. In this paper, a neural network model was trained from a data set of 140 individual projects developed from between years 2005 and 2008 with practices based on a process specificaly designed to laboratory learning environments: Personal Software Process (PSP). Then, this model was applied for predicting the productivity of a new projects consisting of 156 projects developed from between years 2009 and 2010. The code in all projects was developed by 74 graduated students, using object oriented programming languages C++ and Java. Prediction accuracy obtained from neural network was compared to those obtained from a fuzzy logic model as well as from a statistical regression model. Results suggest that a neural network model could be used for predicting development productivity of individual projects, when they are developed in a disciplined way in a laboratory learning environment.

Keywords: Software development productivity prediction, feedforward neural network, fuzzy logic, statistical regression.

1. INTRODUCTION

There are at least the following four options to collect as well as to report software production data [20]: programmer self report, project or team manager, outside analysts or observers, and automated performance monitors. This study was related to the first option. In order to reduce bias, each developer used the same individual practices based upon Personal Software Process (PSP). The PSP was selected because their practices and methods have been used for delivering quality products on predictable schedules [19].

There are diverse measures of productivity ([5] [20] [24]). The measure of productivity most commonly used is the one of size over effort productivity = size / effort. That is the one used in this study; the size is measured using number of lines of code developed by unit of effort. There have been two main directions on the study of productivity in software engineering literature [24]: (1) researches have been focused on the measure or estimation of productivity, and (2) emphasis has been laid on the discovery of methods or significant factors for productivity improvement. The approach of this study is related to first direction.

The prediction activity of software development productivity could be applied from an individual level. This activity has been accomplished by means of techniques such as expert judgment and linear or non-linear statistical regression [10]. This study proposes the application of a machine learning technique: a neural network.

There are two main stages when applying an estimation and prediction model [15]:

1) Model verification: The model is generated and then applied to original data set and their accuracy is evaluated.

2) Model validation (or model prediction): Once the adequacy of the model has been checked, it is applied to a new data set for predicting productivity and its accuracy is evaluated

The main contribution of this paper is the use of a neural network model for estimating and predicting development productivity in individual software projects, since we have not found any research of this kind. The hypothesis is the following:

Prediction accuracy of a neural network model is better than the accuracy of a fuzzy logic model and of a statistical regression model when these three models are applied for predicting software development productivity of individual projects that have been developed with personal practices in laboratory learning environments.

Fuzzy logic

A fuzzy model has two main properties [18]: (1) It operates at a level of linguistic terms (fuzzy sets), and (2) it represents and processes uncertainty.

Software projects are usually described using categorical data (nominal or ordinal scale) such as *small*, *medium*, *average*, or *high* (linguistic terms or values). A more comprehensive approach to deal with linguistic values is using the fuzzy set theory. Specifically, fuzzy logic offers a particularly convenient way to generate a keen mapping between input and output spaces thanks to the natural expression of fuzzy rules [23]. In this study, data defuzzification is constructed based on a rule induction system, replacing the crisp facts with fuzzy inputs. Then an inference engine uses a base of rules to map inputs to a fuzzy output which can either be translated back to a crisp value, or left as a fuzzy value.

Neural network

An artificial neural network, or simply a neural network (NN), is a technique of computing and signal processing that is inspired in processing done by a network of biological neurons [8]. A basis for construction of a neural network is an artificial neuron.

An artificial neuron implements a mathematical model of a biological neuron. The input into an artificial neuron is a vector of numeric values $\vec{x} = \{x_1, x_2, ..., x_j, ..., x_m\}$. The neuron receives the vector and perceives each value, or component of the vector, with a particular independent sensitivity called weight $\vec{w} = \{w_1, w_2, ..., w_j, ..., w_m\}$. Upon receiving the input vector, the neuron first calculates its internal state *v*, and then its output value *y*. The internal state v of the neuron is a sum of the inner product of the input vector and the weight vector and a numerical value called bias b: $v = \vec{x} \cdot \vec{w} + b = \sum_{j=1}^{m} y_j w_j + b$. This function is also known as "transfer function". The output of the neuron is a function of its internal state $y = \Phi(v)$. This function is also known as "activation function". The principal task of the activation function is to scale all possible values of the internal state into a desired interval of output values. The intervals of output values are for example [0, 1] or (-1, 1). The most used activation functions are of three types:

1. Threshold function, $\Phi(v) = \begin{cases} 1, v > 0 \\ -1, v \le 0 \end{cases}$
2. Piecewise-linear $\Phi(v) = \begin{cases} -1 & v \le v_1 \\ a_1 v + a_0 & v_1 < v \le v_2 \\ 1 & v_2 < v \end{cases}$
3. Non-linear. $\Phi(v) = \frac{1}{1 + e^{-av}}$ for (0,1), $\Phi(v) = \tanh(v)$ for (-1,1).

The learning in an artificial neuron is produced by adjusting values of the bias b and weights w_j. A single neuron can be applied only to simple tasks. For more complex tasks, multiple neurons are connected into a network.

There are two types of network architectures: feedforward and recurrent networks. A feedforward network consists of layers of neurons. There is an input layer, an output layer and optionally one, or more hidden layers in-between the input and the output layers. After a network receives its input vector, layer by layer of neurons processes the signal, until the output layer emits an output vector as response. The neurons in the same layer are processing the signal in parallel. In the feedforward network the signals between neurons always flow from the input layer toward the output layer. In recurrent networks some signals flow backwards and may be delayed certain number of processing steps. In other words, recurrent networks contain loops of signal flow, while feedforward networks do not.

Neural network learns by adjusting its parameters. The parameters are the values of bias and weights in its neurons. Some neural networks learn constantly during their application, while most of them have two distinct periods: training period and application period. During the training period a network is processing prepared inputs and adjusting its parameters. It is guided by some learning algorithm, in order to improve its performance. Once the performance is acceptably accurate, or precise, the training period is completed. The parameters of the network are then fixed to the learned values, and the network starts its period of application for the intended task.

There is a variety of tasks that neural network can be trained to perform. The most common tasks are: pattern association, pattern recognition, function approximation, automatic control, filtering and beam-forming. In the present work a feedforward neural network with one hidden layer is applied for function approximation.

Software measurement

Measures of source code size can be classified in physical source lines and in logical source lines [16]. The count of physical lines gives the size in terms of the physical length of the code as it appears when printed. Lines of code have been used by previous researches focused on productivity analysis of projects developed by teams [3] [4] [13] [20] [21] or by individuals [19].

In this study, the independent variable in the prediction models is New and Changed (N&C) code and it is considered as physical lines of code (LOC). N&C is composed of added and modified code [9]. The added code is the LOC written during the current programming process, while the modified code is the LOC changed in the base program when modifying a previously developed program. The base program is the total LOC of the previous program while the reused code is the LOC of previously developed programs that are used without any modification.

A coding standard should establish a consistent set of coding practices that is used as a criterion when judging the quality of the produced code [9]. Hence, it is necessary to always use the same coding and counting standards. The projects developed in this study followed such guidelines.

Accuracy criterion

Magnitude of Error Relative to the estimate or MER [12] is used as criterion for prediction accuracy because it had better results over other common accuracy criteria [7]. The MER is defined as follows:

$$MER_i = \frac{|\text{Actual Productivity}_i - \text{Predicted Productivity}_i|}{\text{Predicted Productivity}_i}$$

The MER value is calculated for each observation *i* whose productivity is predicted. The aggregation of MER over multiple observations (N) can be achieved through the mean (MMER) as follows:

$$\text{MMER} = (1/N)\sum_{i=1}^{N} MER_i$$

The accuracy of an estimation technique is inversely proportional to the MMER.

Related work

Two studies were found oriented toward predicting software development productivity of individual projects using practices of Personal Software Process: the first one [10] only used a statistical model, whereas the second one [14] used a fuzzy logic model. This research proposes a neural network for the same goal.

On the other hand, efficiency of algorithms in neural network training has been evaluated when they have been used in software engineering [1]. The feed-forward multi-layer perceptron with back propagation learning algorithm are the most commonly used in the effort estimation field [17]. However, a study has not been found in which a feed-forward neural network using the Levenberg-Marquardt algorithm has been applied for predicting the software development productivity of individual projects. Among the training algorithms, the Levenberg-Marquardt algorithm is frequently used because of its efficiency [8].

2. EXPERIMENTAL DESIGN

In this study, the data collected were related to the same instruments (logs), phases, and standards suggested by PSP. The experiment was done inside a controlled environment having the following characteristics:

1. All of the developers were experienced, working on software development inside their enterprises at which they were working; however, no one of them had received a course related to personal practices for developing software at individual level.
2. All developers were studying a postgraduate program related to computer science.
3. Each developer wrote seven project assignments. However, only four of them were selected from each developer. The first three programs were not considered because they had differences in their process phases and logs, whereas in latest four programs phases are the same: plan, design, design review, code, code review, compile, testing and post-mortem, and they are based upon the same logs.
4. Each developer selected his/her own imperative programming language whose code standard had the following characteristics: each compiler directive, variable declaration, constant definition, delimiter, assign sentence, as well as flow control statement was written in a line of code.
5. Developers had already received at least one formal course about the object oriented programming language of their choice and they had good programming experience in that language. Because of the type of programming language is one of the two main factors found having significantly influence on the productivity [11], the sample of this study reduced the bias because it only involved developers whose programs were coded in C++ or Java. One reason for selecting these kinds of languages is because object-oriented languages facilitate high productivity [20].
6. As this study was an experiment with the aim to reduce bias, we did not inform developers about our experimental goal.
7. Developers filled out an Excel sheet for each task and submitted it electronically for examination.
8. Each PSP course had a group of fifteen developers or less.
9. All of developers coincided with the counting standard depicted in Table 1.
10. Developers were constantly supervised and advised about the process.
11. The code written in each program was designed so to be reused in subsequent programs.
12. The developed projects were selected from those suggested in the original PSP [9]. From a set of 18 projects, a subset of seven of them was randomly assigned to each of the 74 developers.
13. Data used in this study belong from those developers, whose data for all seven exercises were correct, complete, and consistent.

Table 1. Counting standard

Count type	**Type**
Physical/logical	Physical
Statement type	**Included**
Executable	Yes
Nonexecutable	
Declarations and Compiler directives	Yes (one by text line)
Comments and Blank lines	No
Clarifications	
{ and *}* *or begin* and *end*	Yes

3. VERIFICATION OF THE MODELS

Data analysis

Data from 140 individual projects developed by 35 practitioners between the years 2005 to 2008 were used for generating as well as for verifying the statistical, fuzzy logic and neural network models. These projects corresponded to fourth to seventh project of the course because the same process was followed in them. Because of the sample of 140 projects was coded with C++ and Java, we first had to analyze if there was any statistical difference in their productivity values. An ANOVA showed that since the p-value of the F-test was greater than 0.05, there was not a statistically significant difference between the productivity of the two languages at the 95.0% confidence level.

The validity of an ANOVA was based on the analysis of the following three assumptions of residuals [15]: 1) Independent samples: Each project was independently developed and by a single practitioner; hence, the data were independent. 2) Equal standard deviations: In a plot of this kind the residuals was roughly in a horizontal band centered and symmetric about the horizontal axis, and 3) Normal populations: A normal probability plot of the residuals was roughly linear. Hence, the three assumptions for residuals in the productivity data set were considered as met.

Correlation analysis

A scatter plot depicting the correlation between independent variable New and Changed code (N&C) and productivity (N&C/hour), showed the following: the higher program size (N&C code), the higher productivity (N&C /hour). Its value was r = 0.77. This behavior contrasts with studies of large-scale software productivity [21], whose productivity decreases as the number of lines of code increases (previous studies have concluded that irregular variations of software development productivity are primarily caused by the variations of average team size for the development [11] [24]).

Statistical model

Based on correlation analysis, the following simple linear regression equation was generated:

$$\text{Productivity} = 10.3 + 0.31701*\text{N\&C} \qquad \text{Eq.(1)}$$

The value of the coefficient of determination was r^2= 0.61 (a $r^2 > 0.5$ is acceptable value to do predictions [13]).

Fuzzy logic model

There are two main approaches for obtaining a fuzzy model from data [22]:

1. The expert knowledge is translated in a verbal form into a set of if–then rules. A certain model structure can be created, and parameters of this structure, such as membership functions and weights of rules, can be tuned using input and output data.
2. No prior knowledge about the system under study is initially used to formulate the rules, and a fuzzy model is constructed from data based on a certain algorithm. It is expected that extracted rules and membership functions can explain the system behavior. An expert can modify the rules or supply new ones based upon his or her own experience. The expert tuning is optional in this approach.

This study was based upon the first approach. The fuzzy rules were formulated based on the correlation (*r*) between independent and dependent variables. Then the fuzzy rules were derived:

1) If (*New &Changed* is *Small*) then *Productivity* is *Low*
2) If (*New &Changed* is *Big*) then *Productivity* is *High*

A fuzzy system requires that the different categories of the different inputs be represented by fuzzy sets, which in turn are represented by membership functions (MF) [2]. The MF type considered in this experiment is triangular. A triangular MF is a three-point (parameters) function, defined by minimum (a), maximum (c) and modal (b) values, that is, MF(a,b,c) where $a \leq b \leq c$. Their scalar parameters (a, b, c) are defined as follows:

$$MF(x) = 0 \text{ if } x < a$$
$$MF(x) = 1 \text{ if } x = b$$
$$MF(x) = 0 \text{ if } x > c$$

Values of MF parameters were iteratively adjusted until obtain the smallest MMER possible. These intervals were divided by next segments: *small* and *big* (N&C Code), and *low* and *high* (productivity). Table 2 depicts the values of parameters of the input and output of each of the triangular membership functions.

Table 2. Values by membership function

Parameter	N&C		Productivity	
	Small	Big	Low	High
a	1	21	1	15
b	40	102	25	40
c	70	125	30	50

Feedforward Neural Network

The network was trained to approximate a function. The productivity is considered as a function of one variable related to project size: N&C, number of new and changed lines of code.

A feedforward network with one layer of hidden neurons is sufficient to approximate any function with finite number of discontinuities on any given interval [12], hence, in this work a fully-connected feedforward neural network with one hidden layer of neurons was used. The fully-connected means that each neuron in a layer receives a signal from the neuron in it preceding layer. There is one neuron in the input layer of the network that receives a number of N&C lines of code. The output layer consists of only one neuron indicating an estimated productivity. The number of neurons in a hidden layer was empirically optimized. The range of 2 to 40 neurons was explored and the best results were obtained with four neurons in the hidden layer. The optimized Levenberg-Marquardt algorithm [6] was used to train the network.

The network passed through two phases, training and application. The first group of 140 software projects was used to train the network. This group of projects was randomly separated in three subgroups: training, validation and testing. The training group contained 70% of the projects. The input-output pairs of data for these projects were used by the network to adjust its parameters. The next 20% of data were used to validate the results and identify the point at which the training should stop. The remaining 10% of data were randomly chosen to be used as testing data, to make sure that the network performs well with the data that was not presented during parameter adjustment

Comparison of models

Linear regression model (LRM, Eq.1), fuzzy logic model (FLM) and neural network (NN) were applied to original data set for estimating productivity. The accuracy of each program (MER) as well as the accuracy by each model (MMER) was calculated:

- LRM = 0.25
- FLM = 0.26
- NN = 0.24

The ANOVA for MER of the projects as well as a Means Plot showed that there was not a statistically significant difference between the accuracy of prediction of the three models at the 95.0% confidence level (p-value was greater than 0.05). The three ANOVA residuals assumptions were met.

4. VALIDATION OF MODELS

A new group integrated by 39 practitioners developed 273 projects through the years 2009 and 2010; 117 of them, corresponding to the first, second or third project were not considered because of the reasons explained in the section 2 of this study. Hence, the sample size for validating the three models was 156. Once the three models for predicting productivity were applied to these data, the MER by project as well as the MMER for each model were calculated:

- LRM = 0.25
- FLM = 0.25
- NN = 0.20

In accordance with the ANOVA for MER of projects as well as with a Means plot, there was a statistically significant difference amongst the accuracy of prediction for the three models (p-value was less than 0.05) at 95% of confidence.

5. CONCLUSIONS AND FUTURE RESEARCH

This study was motivated from the following assumptions: (1) the performance of a development organization is determined by the performance of its engineering teams; and the performance of an engineering team is determined by the performance of the team members; and the performance of their members (engineers) is, at least in part, determined by the practices of each engineer [19], and (2) unless software developers have the capabilities provided by personal training, they cannot properly support their teams [9]. One of those practices of the organizations is the software development productivity prediction which is one of the main practices used for training developers at personal level [19].

This research proposed a feedforward neural network that was trained for predicting software development productivity related to individual projects developed inside training environments. The accuracy of the neural network model was compared with the accuracy of a fuzzy logic model as well as with a statistical model. Samples of 140 and 156 projects developed by 74 practitioners were used for estimating and predicting respectively. All projects were developed in a disciplined way based on a process done for laboratory learning environments: Personal Software Process. Results allowed accepting the following hypothesis: prediction accuracy of a feedforward neural network is statistically better than the accuracies of a fuzzy logic model as well as of a statistical regression model when these three models are applied for predicting software development productivity of individual software projects that have been developed with personal practices inside training environments. This result could be useful for trainers interested in applying an alternative model based on machine learning model such as a neural network for the productivity prediction at personal level.

Future work is related to apply other kinds of machine learning techniques for predicting productivity such as evolutionary algorithms.

ACKNOWLEDGEMENTS

Authors of this paper would like to thank CUCEA of Universidad de Guadalajara, Jalisco, México, Consejo Nacional de Ciencia y Tecnología (Conacyt), as well as to Programa de Mejoramiento del Profesorado (PROMEP).

REFERENCES

[1] Aggarwal K.K., Y. Singh, Y., Chandra, P. and Puri, M. “Evaluation of various training algorithms in a neural network model for software engineering applications”. **ACM SIGSOFT Software Engineering Notes,** Volume 30, Issue 4, 2005, pp. 1-5.

[2] Ahmed M. A., Saliu M.O. and AlGhamdi J. “Adaptive fuzzy logic-based framework for software development effort prediction”. **Journal of Information and Software Technology**. Elsevier, 2005, pp. 31-48.

[3] Boehm B., Abts Ch., Brown A.W., Chulani S., Clarck B. K., Horowitz E., Madachy R., Reifer D. and Steece B. **COCOMO II**, Prentice Hall. 2000.

[4] Cusumano M. and Kemerer, C.F. A Quantitative Analysis of U.S. and Japanese Practice and Performance in Software Development, **Management Science**, pp. 1384-1406. 1990.

[5] Fenton N.E. and Pfleeger S. L. **Software Metrics: A Rigorous and Practical Approach**, PWS Publishing Company. 1997.

[6] Finschi, l. “An Implementation of The Levenberg-Marquardt Algorithm”. **Eidgenössische Technische Hochschule Zürich**. 1996.

[7] Foss, T., Stensrud, E., Kitchenham, B., and Myrtveit, I. “A Simulation Study of the Model Evaluation Criterion MMRE”. **IEEE Transactions on Software Engineering**. Vol. 29, No. 11, pp. 985 – 995. 2003.

[8] Haykin, S. **Neural Networks: A Comprehensive Foundation**. Second edition, Prentice Hall. 1998.

[9] Humphrey W. **A Discipline for Software Engineering**. Addison Wesley. 1995.

[10] Humphrey W.S. and Singpurwalla, N.D. “Predicting (individual) software productivity”. **IEEE Transactions on Software Engineering**, vol. 17, pp. 196-207. 1991.

[11] Jiang, Z. and Comstock C. “The Factors Significant to Software Development Productivity”. **World Academy of Science, Engineering and Technology**, pp. 160 – 164. 2007.

[12] Kitchenham, B. A., MacDonell, S.G. and Pickard, L.M. “What Accuracy Statistics Really Measure”. **IEE Proceedings Software**, Vol. 148, pp. 81-85. 2001.

[13] Lawrence, M.J. “Programming Methodology, Organizational Environment, and Programming Productivity”, **Journal of Systems and Software**, Elsevier. Vol. 2, pp. 257-269. 1981.

[14] López-Martín C., Kalichanin-Balich I., Meda-Campaña M.E., Chavoya A. "Software Development Productivity Prediction of Small Programs Using Fuzzy Logic". **International Conference on Information Technology - New Generations (ITNG),** IEEE Computer Society Press, pp. 1295-1297, 2010.

[15] Montgomery D., Peck E. and Vining G. **Introduction to linear regression analysis**, John Wiley. 2001.

[16] Park, R.E. **Software Size Measurement: Framework for Counting Source Statements**. Software Engineering Institute, Carnegie Mellon University. CMU/SEI-92-TR-020. 1992

[17] Park. S. "An empirical validation of a neural network model for software effort estimation". **Journal of Expert Systems with Applications**, Elsevier, Vol. 35, pp. 929-937. 2008.

[18] Pedrycz W. and Gomide F. **An Introduction to Fuzzy Sets**. The MIT Press. 1998.

[19] Rombach D., Münch J., Ocampo A., Humphrey W.S., and Burton D. "Teaching disciplined software development". **Journal Systems and Software**, Elsevier, pp. 747- 763. 2008.

[20] Scacchi, W. "Understanding Software Productivity". **International Journal of Software Engineering and Knowledge Engineering**. Revised and reprinted in Advances in Software Engineering and Knowledge Engineering, D. Hurley (ed.), pp. 37-70. 1995.

[21] Vosburg, J., Curtis, B., Wolverton, R., Albert, B., Malec, H., Hoben S. and Liu, Y. "Productivity Factors and Programming Environments", **7th. International Conference Software Engineering**, IEEE Computer Society, pp. 143-152. 1984.

[22] Xu Z. and Khoshgoftaar T. M. "Identification of fuzzy models of software cost estimation". Elsevier. **Fuzzy Sets and Systems**. Volume 145, pp. 141-163. 2004.

[23] Zadeh L. A. "From Computing with Numbers to Computing with Words – From Manipulation of Measurements to Manipulation of Perceptions". **IEEE Transactions on Circuits and Systems** – I: Fundamental Theory and Applications, vol. 45, pp. 105-119. 1999.

[24] Zhizhong, J., Naudé, P. and Comstock, C. "An Investigation on the Variation of Software Development Productivity", **International Journal of Computer and Information Science and Engineering**, pp. 72-81. 2007.

Testbed implementation of cloud based energy management system with ZigBee sensor networks

Katsuhiro Naito, Kazuo Mori, and Hideo Kobayashi
Department of Electrical and Electronic Engineering, Mie University,
1577 Kurimamachiya, Tsu, 514-8507, Japan
Email: {naito, kmori, koba}@elec.mie-u.ac.jp

***Abstract*— Energy management systems are focused to achieve efficient electricity control in smart grid systems. In order to achieve the effective systems, various functions such as sensing mechanisms, control mechanisms, management mechanisms and user interface mechanisms are required. In this paper, we employ Arduino micro-computer as basic field devices and use virtual private server services for cloud server in order to construct a testbed system. Our testbed can provide an environment measurement function, a JEM-A equipments control function, an online monitoring function and an online control function. As the results, we show that it is a good fundamental platform to consider effective energy control mechanisms in real fields.**

***Keywords*— Energy management systems, Wireless sensor networks, Online control, JEM-A**

I. Introduction

EMS (Energy management systems) are an important function to achieve efficient control of electricity in smart grid systems. Therefore, BEMS (Building Energy Management System) for buildings and HEMS (Home Energy Management System) for homes have drawn attention as application technologies [1], [2]. Generally, they consist of various functions such as sensing mechanisms, control mechanisms, management mechanisms and user interface mechanisms. As the results, collaboration of these technologies are key issues to achieve useful systems [3], [4].

In EMS, sensing mechanisms measure environment information such as consumed energy, air temperature, air humidity etc. For these purposes, sensor network systems are a good candidate technique [5]. Especially, wireless sensor networks are well suited to these purposes because it's easy to install sensor devices in real fields [6]. Control mechanisms monitor a status of each equipment such lighting, HVAC (heating, ventilation and air conditioning), and other systems, to provide improved convenience, comfort, energy efficiency and security. etc. , and control their operation status [7], [8]. In Japan, commercial equipments usually implement JEM-A terminals [9] for monitoring and controlling. Additionally, ECHONET Lite [10] is decided as a new standard for these purposes due to the shortage of electrical power. However, equipments with ECHONET Lite functions are quite few in the present circumstances. Therefore, JEM-A is a good candidate standard for control mechanisms at this time. Management mechanisms gather the sensing information and make a decision for equipment control. User interface mechanisms provide a control method for users. Especially, remote control mechanisms are useful function to provide improved convenience according to the installation of EMS. In each mechanism, various studies have been considered recently. However, implementations including whole mechanisms are quite few.

In this paper, we develop a cloud based energy management system with wireless sensor networks and JEM-A equipments. The system consists of wireless sensor devices, a management gateway, a cloud management server and user interface terminals. Each wireless sensor device can measure environment information by using equipped sensors and transmits the measured information to the management gateway. The management gateway can make a decision for operations of each equipment by using JEM-A terminals, and forwards the measured information to the cloud management server. Therefore, the cloud management server also controls each equipment through Internet. Additionally, it provides web services for user interface terminals. Therefore, users can monitor the measured information and operation status of each equipment, and control them online.

II. Cloud based energy management system

A. System Model

Fig. 1 shows the overview of the proposed cloud based energy management system. We employ Arduino [11], which is a micro computer device, as wireless sensor network devices and a management gateway device because power consumption of Arduino is quite low and hardware cost is also inexpensive. As wireless communication devices, Xbee, which supports ZigBee protocol, is used for these devices. The cloud management server is constructed on virtual private server services. Therefore, the user interface terminal can access to the cloud management server through Internet. The explanation about each device is described as the followings.

- Wireless sensor device
  The wireless sensor device consists of an Arduino Fio, a Li-ion battery, an Xbee Pro and some sensors for air

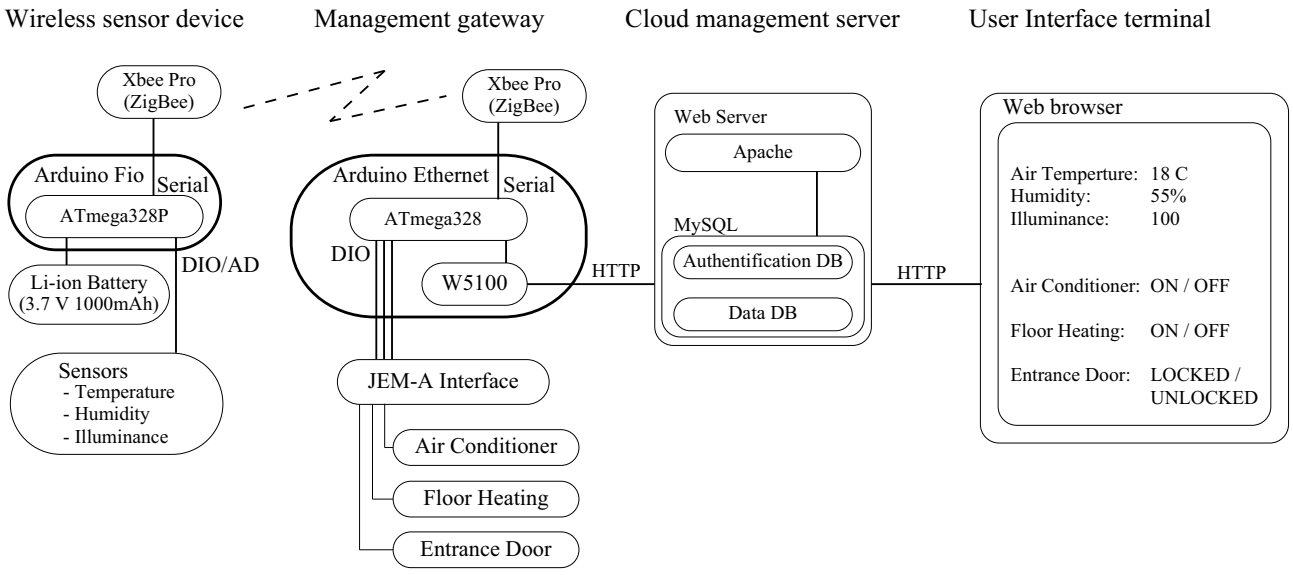

Fig. 1. System model.

temperature, humidity and illuminance. By employing deep sleep operations, it operates for more than one month even if it transmits the measured information with one minute interval. Since frequent measurement is not required in the practical usage, the wireless sensor device can operate for a few months by one time charge. Additionally, Arduino Fio supports solar panel charging. Therefore, it is possible to extend the operation period by using a solar panel.

- Management gateway
  The management gateway consists of an Arduino Ethernet, an Xbee Pro and the original JEM-A interface. The Arduino Ethernet has an ethernet interface, and suports the TCP/IP protocol stack. The management gateway also has a Hypertext Transfer Protocol (HTTP) client function and a HTTP server function. The HTTP client function is used to forward measured information to the cloud management server. The HTTP server function is used to response requests from the cloud management server. In the testbed, air conditioner, floor heating system, and electronic key system are connected via JEM-A interfaces. Therefore, the Arduino Ethernet has the original interface board between JEM-A and Digital Input/Output ports.
- Cloud management server
  The cloud management server consists of a web server function and a database server function. The web server receives the forwarded measured information from the management gateway and registers the IP address of the management gateway. It also provides a web service for user interface terminal to monitor the measured information and control the equipments under the management gateway.
- User interface terminal
  Users can access to the cloud management server by using web browser. So, almost all terminal can support these functions because the user interface is provided based on HTML5.

B. Flowchart

Fig. 2 shows the flow charts of the wireless sensor device and the management gateway. The following is the process of each device.

Wireless sensor device: The wireless sensor device performs the following operations.

- Initialization of device
  The wireless sensor device initializes I/O ports of Arduino and Xbee device after bootup. Finally, it starts the watchdog timer of Arduino to monitor the operation status of own device. The watchdog timer is refreshed when each wakeup process occurs. Therefore, the device will restart when the watchdog timer is not refreshed due to software issues.
- Periodic monitoring
  The wireless sensor device measures values such as temperature, humidity, illuminance etc. by using some sensors. The measurement is performed periodically according to predefined parameters.
- Periodic reporting
  The wireless sensor devices calculates the average value of measured value, and report the averaged value to the management gateway. The interval of reporting is set according to the predefined parameters.

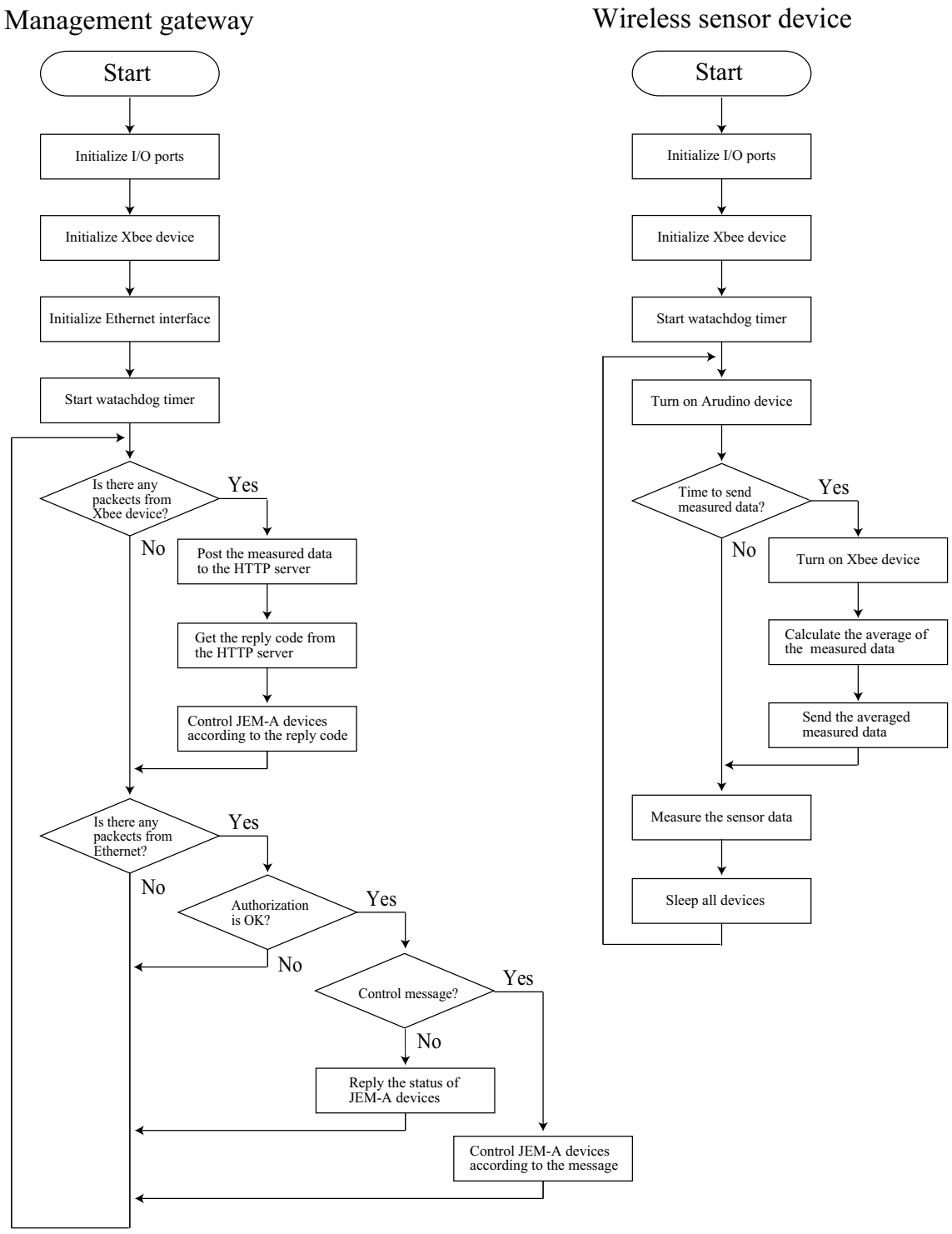

Fig. 2. Flow charts of wireless sensor device and management gateway.

- Sleep operation
  The wireless sensor device turn off all devices to change the device status to sleep status after monitoring or reporting operations.

Management gateway: The management gateway performs the following operations.

- Initialization of device
  The wireless sensor device initializes I/O ports of Arduino, Xbee device and Ethernet interface after bootup.

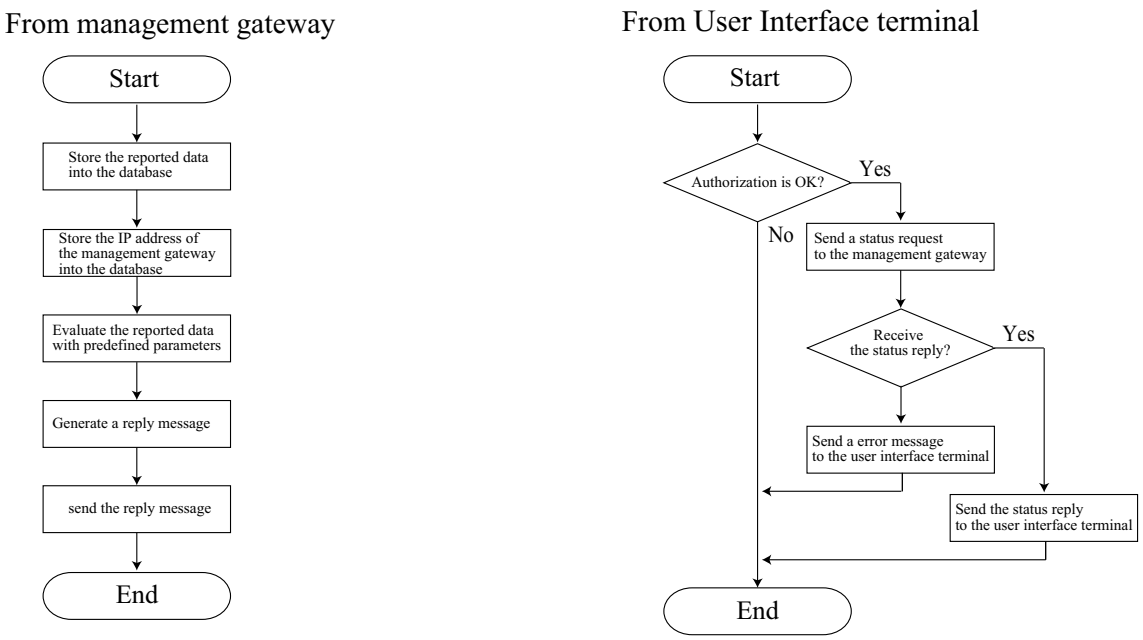

Fig. 3. Flow charts of cloud management server.

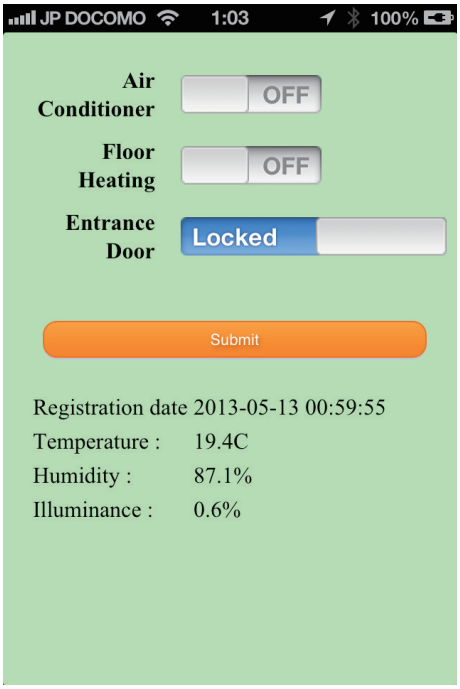

Fig. 4. User interface.

Finally, it starts the watchdog timer of Arduino to monitor the operation status of own device.

- Packet reception from the wireless sensor device
  The management gateway checks the buffer of Xbee. It receives packets from Xbee when Xbee has some data packets from the wireless sensor device. Then, it generates HTTP message including the average measured data according to the received packets, and sends to the cloud management server. The cloud management server replies the reply message including control direction for JEM-A devices. The management gateway controls JEM-A devices according to the reply message. As the results, the cloud management server can control some JEM-A devices according to the monitored data.
- Packet reception from the cloud management server
  The management gateway authorizes the message when it receives packets from the cloud management server. It replies the status of JEM-A devices when the message requests the status. It controls the JEM-A devices when the message requests to control the devices.

Cloud management server: Fig. 3 shows the flow charts of the cloud management server.

- Packet reception from the management gateway
  The cloud management server stored the reported data into the database when it receives the packets from the management gateway. Then, it stores the IP address of the management gateway into the database according to the source address in the packets. The IP address is required to communicate with the management gateway when it receives packets from the user interface terminal. It also evaluates the reported data with the predefined parameters such as threshold and operations. For examples, users can set that the air conditioner should be turned on when the temperature is more than 28 degrees Celsius. It generates the reply message according to the predefined parameters,

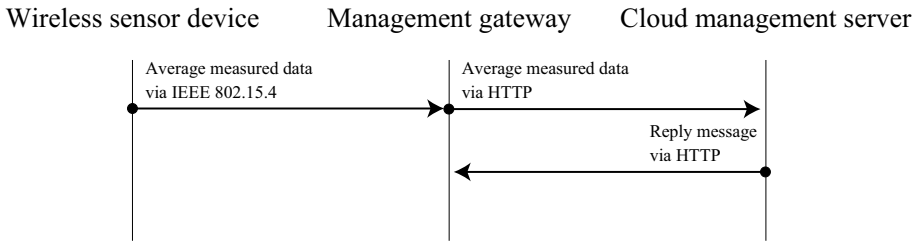

Fig. 5. Signaling for reporting measured data.

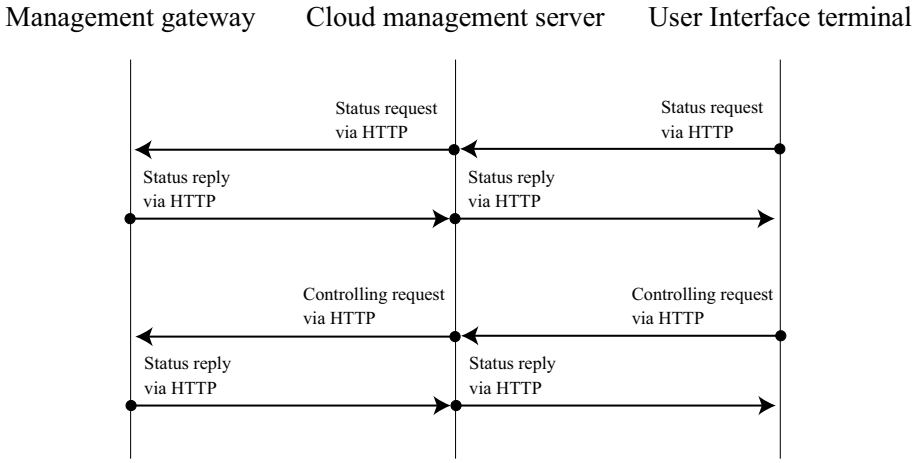

Fig. 6. Signaling for controlling devices.

and replies to the management gateway.

- Packet reception from the user Interface terminal
  The cloud management server requests the authorization to the user interface terminal when it receives the packets from the user Interface terminal. It requests the management gateway to report the status when it confirms the authorization. Then, it replies the message including the status of each JEM-A devices such as Fig. 4. It also sends the message including the control request of JEM-A devices when the user interface terminal submits the request to change the status of JEM-A devices.

C. Communication process

Periodic reporting: Fig. 5 shows the signaling for reporting measured data. The wireless sensor devices report the measured data periodically. Each signaling for reporting the data is performed individually. Therefore, it sends the measured data via Xbee devices. The unicast mode in Xbee devices supports an acknowledgement operation. Hence, it recognizes the transmission errors between the management gateway and own device. The management gateway converts the measured data from IEEE 802.15.4 protocol to HTTP. The cloud management sever replies the message when it receives the HTTP message from the management gateway. Finally, the management gateway can receive the reply message including

controlling request for JEM-A devices.

Controlling devices: Fig. 6 shows the signaling for controlling devices. The user interface terminal accesses the cloud management server via HTTP. The cloud management server requests the authorization of users. The user interface terminal posts the authorization data to the server. The server accesses the management gateway to check the status of JEM-A devices when the user is authorized. Then, it replies the status of JEM-A device to the user interface terminal. The user interface terminal also sends the controlling request when the user requests to control JEM-A devices. The server also sends the controlling request to the management gateway to control the JEM-A devices. The management gateway replies the status of JEM-A devices when it has controlled them according to the controlling request.

III. EXPERIMENTAL EVALUATION

In order to evaluate the proposed mechanisms, we have developed the testbed implementation.

Wireless sensor device

We employ Arduino Fio which is a small energy consumption microboard. It operates by Li-ion battery, and supports sleep operation to reduce consumed power. It also employs a Grove Temperature and Humidity Sensor Pro which are a 1-wired digital sensor, and Grove Light Sensor which is a analog sensor. Therefore, it can monitor temperature, humidity and illuminance periodically. As the wireless communication device, we employ Xbee Pro Series 2 which is ZigBee based long-range communication device. The Xbee operates as end device mode of ZigBee to achieve sleep operation. The sleep operation of Xbee is controlled through the digital input pin for sleep operation by Arduino Fio.

Management gateway

We employ Arduino ethernet with the wireless shield connecting to Xbee Pro Series 2. It operates by AC adapter because it waits for an access from the cloud management server and Xbee operates as coordinator mode. The IP address of ethernet interface is fixed according to the predefined address. Therefore, a global IP address or a port forwarding mechanism is required to access the management gateway from the cloud management server. In the experiment, we set a private IP address and port forwarding setting at a gateway router.

Cloud management server

We employ Cent OS on a virtual private server service. The apache web server and postgreSQL database server are used to create web applications. The application is written in PHP.

User interface terminal

Our user interface is provided as the web application using HTML5. Therefore, almost all browsers can use the web application on the Cent OS. In the experiment, we use iPhone 4s as the client device to access the could management server.

IV. CONCLUSION

In this paper, we have implemented the cloud based energy management system based on Arduino which is an open-source electronics prototyping platform and virtual private server services. The system supports measurement of environment information, data collection, operation control based on the measured information, remote monitoring and remote control. From the testbed, our developed system can achieve remote monitoring and remote controlling of JEM-A devices from various kind of browsers. As the results, we can confirm that the proposed system can work well as EMS and can be the fundamental platform for the intelligence energy management.

ACKNOWLEDGMENT

This work was supported by Grant-in-Aid for Young Scientists (B)(23700075), Japan Society for the Promotion of Science (JSPS).

REFERENCES

[1] M. Erol-Kantarci, H. T. Mouftah, “Wireless Sensor Networks for domestic energy management in smart grids,” QBSC 2010, pp. 63 - 66, 2010.

[2] Fernando Genova, Fabio Bellifemine, Marco Gaspardone, Maurizio Beoni, Cuda Maurizio, Fici Alberto, Piero Gian, “Thermal and energy management system based on low cost WirelessSensor Network Technology, to monitor, control and optimize energy consumption in Telecom Switch Plants and Data Centres,” Telecommunication - Energy Special Conference (TELESCON)2009 pp. 1-8, 2009.

[3] Nhat-Hai Nguyen, Quoc-Tuan Tran, J.-M. Leger, Tan-Phu Vuong, “A real-time control using wireless sensor network for intelligent energy management system in buildings,” Environmental Energy and Structural Monitoring Systems (EESMS) 2010, pp. 87 - 92, 2010.

[4] L.V. Thanayankizil, S.K. Ghai, D. Chakraborty, D. P. Seetharam, “Soft-green: Towards energy management of green office buildings with soft sensors,” Communication Systems and Networks (COMSNETS) 2012, pp. 1- 6, 2012.

[5] Jinsung Byun, Insung Hong, Byeongkwan Kang, Sehyun Park, “Implementation of an Adaptive Intelligent Home Energy Management System Using a Wireless Ad-Hoc and Sensor Network in Pervasive Environments,” Computer Communications and Networks (ICCCN) 2011, pp. 1 - 6, 2011.

[6] Insung Hong, Jisung Byun, Sehyun Park, “Cloud Computing-Based Building Energy Management System with ZigBee Sensor Network,” Innovative Mobile and Internet Services in Ubiquitous Computing (IMIS) 2012, pp. 547 - 551, 2012.

[7] Dae-Man Han and Jae-Hyun Lim “Design and implementation of smart home energy management systems based on zigbee,” IEEE Transactions on Consumer Electronics, Volume: 56 , Issue: 3, pp. 1417 - 1425, 2010.

[8] Dae-Man Han and Jae-Hyun Lim “Smart home energy management system using IEEE 802.15.4 and zigbee,” IEEE Transactions on Consumer Electronics, Volume: 56 , Issue: 3, pp. 1403 - 1410, 2010.

[9] JEM1427 HA terminal(JEM-A), http://www.jema-net.or.jp/English/about/index.html

[10] ECHONET Consortium, http://www.echonet.gr.jp/english/index.htm

[11] Arduino website, http://www.arduino.cc

Road side unit coverage extension with OFDM Cooperative Transmission

Katsuhiro Naito, Atsushi Ono, Kazuo Mori, and Hideo Kobayashi
Department of Electrical and Electronic Engineering, Mie University,
1577 Kurimamachiya, Tsu, 514-8507, Japan
Email: {naito, kmori, koba}@elec.mie-u.ac.jp, atsuono@com.elec.mie-u.ac.jp

Abstract— **Intelligent Transport System (ITS) has drawn attention as new important technologies for vehicular safety. Additionally, roadside to vehicle communication is also focused because it provides network services such as an Internet access from vehicles. It is well known that communication environment in ITS is severe due to fading, blocking etc. Therefore, service quality of the Internet access from vehicles deteriorates due to transmission errors. Additionally, transmission range extension mechanisms of roadside unit is important for reducing implementation costs. In this paper, we focus on an Orthogonal Frequency Division Multiplexing (OFDM) transmission technology, which is employed in IEEE 802.11p for ITS networks. In OFDM communication, vehicles can demodulate multiple OFDM signals within Guard Interval (GI) period without inter-symbol interference. In the proposed system, vehicles forward packets from roadside units at a same allocated slot. Therefore, a destination vehicle can receive multiple OFDM signals from neighbor forwarder vehicles within GI period. From the numerical results, we show that the proposed scheme can extend the transmission range of roadside units.**

Keywords— **Intelligent Transport System, Roadside to vehicle communication, Orthogonal Frequency Division Multiplexing, Multi-hop communication**

I. Introduction

Intelligent Transport Systems (ITS) have drawn attention as important mechanisms to achieve a safety driving and useful applications in vehicles [1], [2]. Communication types in ITS are classified into roadside to vehicle communication and inter-vehicle communication. The roadside to vehicle communication is an infrastructure system. Therefore, some roadside units are installed along a road. The inter-vehicle communication is an autonomous system. As the results, each vehicle communicates with neighbor vehicles autonomously [3], [4]. Additionally, the inter-vehicle communication is suitable mechanisms to extend transmission range of roadside unit to reduce installation costs [5] .

In the roadside to vehicle communication, Internet access services will be considered as useful application services in vehicles [6], [7]. It is well known that communication environment in ITS is quite severe due to fast movement of vehicles, fading, blocking etc. Especially, distance between a roadside unit and a vehicle changes due to a location of vehicles. Therefore, a signal intensity changes dynamically due to these reasons. As the results, vehicles suffer from transmission errors due to a weak signal intensity. Additionally, almost all Internet applications employ Transmission Control Protocol (TCP) to achieve reliable communication. However, TCP performance deteriorates when a segment error ratio is increased [8].

To reduce transmission errors, we have considered diversity mechanisms at roadside units [9]. Therefore, our system employs multiple transmission mechanisms from some roadside units. Additionally, we focus on Orthogonal Frequency Division Multiplexing(OFDM) which is used in IEEE 802.11p for ITS networks. In OFDM, vehicles can demodulate multiple OFDM signals within Guard Interval (GI) period without inter-symbol interference (ISI). As the results, multiple OFDM signals can be transmitted simultaneously at roadside units [10]. Additionally, we have confirmed that the multiple OFDM signal transmission is effective in multi-hop communication [11], [12]. In this paper, we employ multi-hop mechanisms to extend transmission range of roadside units. Therefore, forwarder vehicles transmit a same OFDM signal simultaneously to forward data from roadside units. From numerical results, we can find that the proposed technique can extend the transmission range of roadside units with high TCP throughput performance.

II. Range extension with OFDM cooperative communication

A. OFDM cooperative communication

In this paper, we focus on the characteristics of OFDM scheme. A transmitter of OFDM generally adds a guard interval (GI), which is a part of an OFDM symbol, to the OFDM symbol. The general purpose of GI is to mitigate the multi-path effect due to fading. Therefore, GI period is set according to maximum propagation delay in assumed

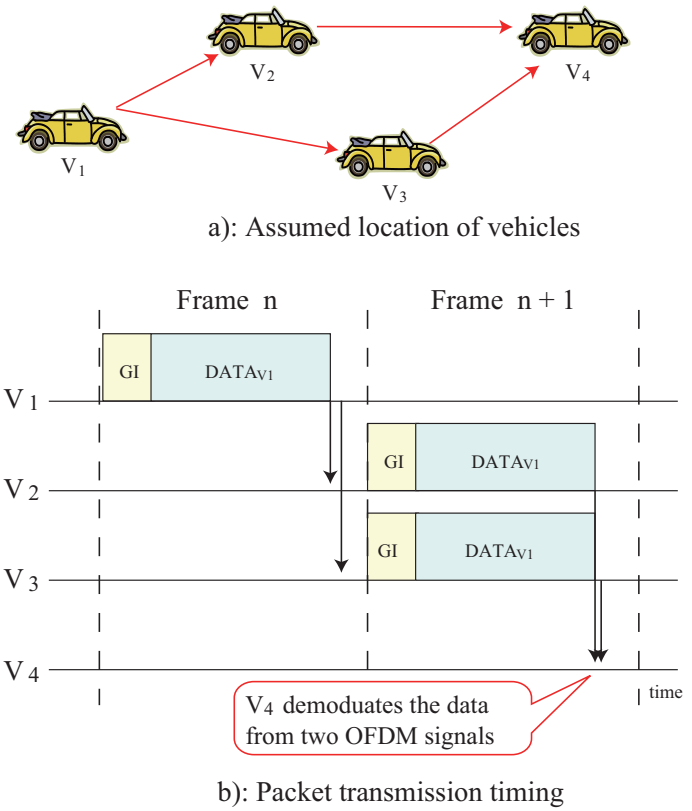

Fig. 1. Overview of the OFDM cooperative communication.

TABLE I

SIMULATION PARAMETERS IN PHYSICAL LAYER SIMULATION

Simulator	Matlab 6.5
Number of FFT points	64
Number of Subcarriers	52
Number of pilot subcarriers	14
Bandwidth	20 [Mhz]
Modulation scheme	16QAM
Symbol period	2.6 [μs]
GI period	0.52 [μs]
Channel model	Rayleigh fading
Number of multi-path	5

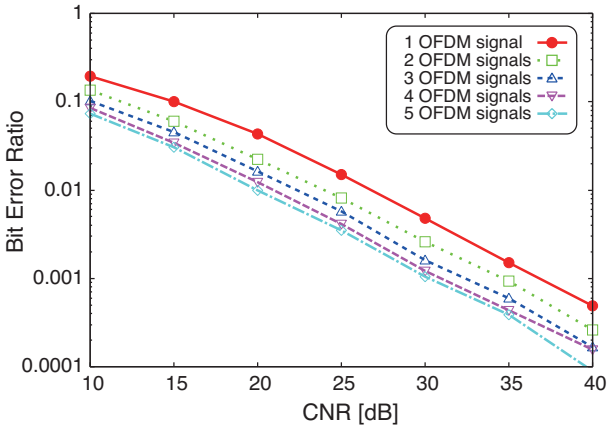

Fig. 2. BER performance in OFDM cooperative communication.

wireless communication environment. An OFDM receiver can demodulate received signals accurately when the signals arrive within GI period.

Fig. 1 shows the overview of the OFDM cooperative communication. Fig. 1 a) shows the assumed vehicle location , and Fig. 1 b) shows the overview of transmission timing at each vehicle. In the assumed system, we employ Time Division Multiple Access (TDMA) to synchronize transmission timing because arrival difference timing between signals should be within GI period. The cooperative communication processes are the followings.

- The vehicle V1 transmits the OFDM packet including the OFDM symbol and GI in the frame n. This process is typical operation in OFDM with TDMA.
- The vehicle V2 and V3 receive the OFDM packet normally. Then they transmit the received OFDM packet simultaneously in the frame $n+1$. Generally, duplicated transmissions are avoided in wireless communication systems because they cause packet reception error. However, the vehicle V4 can demodulate the duplicated OFDM packets when the arrival difference timing between the OFDM packet from V2 and that from V3 is less than the GI period in OFDM systems because OFDM is high tolerant of multiple signals within GI period.
- The vehicle V4 can receive the two OFDM packets from V2 and V3, and can demodulate the signals more reliably because it obtains the diversity effect according to multiple transmission at different points. From the previous evaluation in our research, we could find that the total signal power is the summation of signal power of each OFDM packet. Fig. 2 is the reference bit error ratio performance with the Tab. I [11].

The features of the proposed cooperative communication scheme are to obtain the diversity effect according to multiple routes and to achieve effective wireless resource usage by transmitting a same OFDM signal simultaneously. As the results, our scheme can obtain the benefit of cooperative communication without the demerit.

B. Road side unit coverage extension

In the proposed system, we employ the proposed OFDM cooperative communication to extend the transmission range of roadside units. Therefore, we employ hybrid transmission

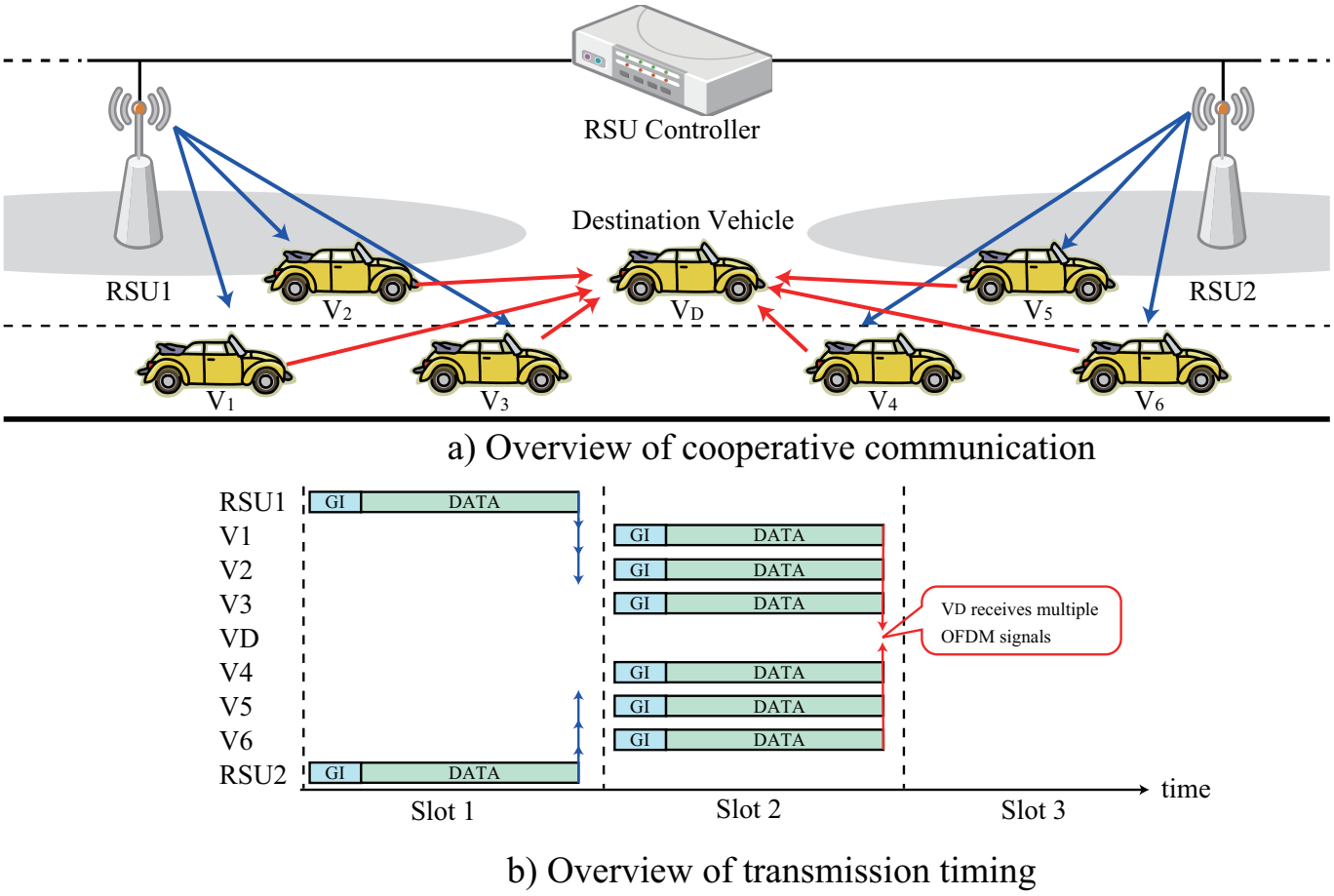

Fig. 3. Overview of the proposed communication.

of roadside to vehicle communication and inter-vehicle communication. A roadside unit has an Omni directional antenna. Vehicles near the roadside unit can receive the packet directly when it exists within the transmission range of the roadside unit. On the contrary, vehicles near a roadside unit forward a packet to a vehicle at an outer area of roadside unit transmission range when the destination vehicle exists in out of the transmission range of the roadside unit. The hybrid concepts have been proposed in the conventional researches. Then, it is well known that the concepts can improve the communication performance. However, traffic increasing due to multiple forwarding of packets is a big issue. The proposed system solves this issue to employ OFDM cooperative communication techniques because vehicles can transmit a same packet simultaneously in our techniques.

Fig. 3 shows the overview of the proposed communication. Fig. 3 a) shows the overview of the cooperative communication, and Fig. 3 b) shows the overview of transmission timing at each vehicle. In the figures, the roadside unit RSU1 and RSU2 transmit a packet to the vehicle VD. However, the vehicle VD exists in the outer area of transmission range of roadside unit RSU1 and RSU2. Therefore, multi-hop communication is required to deliver the packet to the vehicle VD.

The proposed system employs Time Division Multiple Access (TDMA) mechanisms for the access control. Therefore, the roadside unit controller assigns slots based on traffic and a vehicle location. In assignment rules, it tries to find one slot for roadside units and some slots for forwarder vehicles according to the required hop counts. The important rule is that forwarder vehicles should transmit a same OFDM signal at same slot. Fig. 3 assumes multi hop communication with one hop. In Fig. 3, the roadside units RSU1 and RSU2 transmit the OFDM signal at the slot 1 The vehicles V1, V2 and V3 receive the OFDM signal from the roadside unit RSU1 and the vehicles V4, V5 and V6 receive it from the roadside unit RSU2 . Then, these vehicles transmit the OFDM signal at the slot 2. As the results, the destination vehicle can receive six OFDM signals from neighbor vehicles. Finally, it can obtain the diversity effect and can improve packet reception performance without redundant wireless resource consumption.

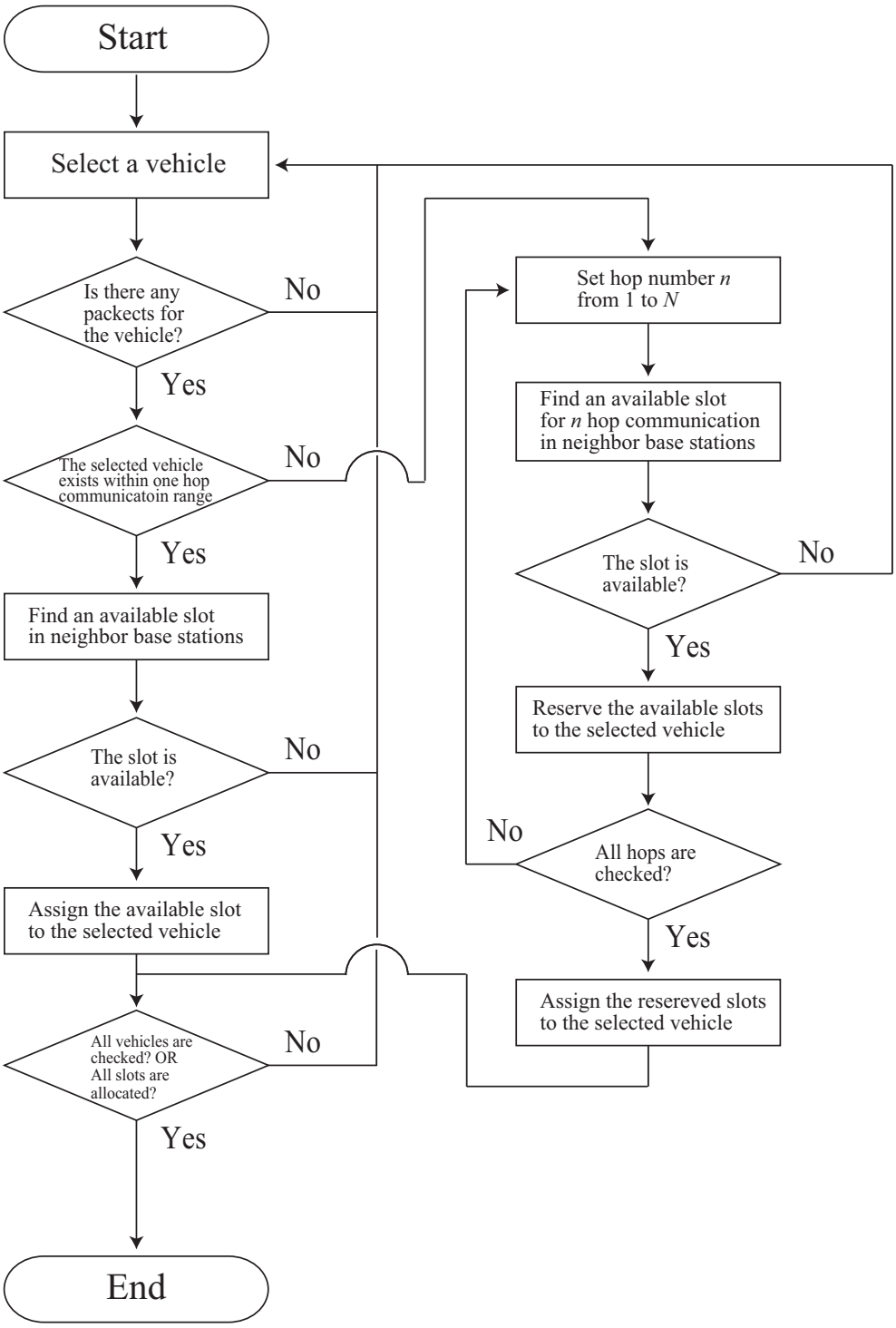

Fig. 4. Flowchart of slot allocation.

C. Slot allocation algorithm

Fig. 4 shows the flowchart of the slot allocation algorithm for the proposed scheme. The slot allocation algorithm is performed for each frame. Therefore, all slots in the frame will be assigned according to the following processes.

- The road side unit controller (RSUC) starts the allocation process when a new frame is started.
- The RSUC checks a number of vehicles in a service area. Then, it selects one vehicle.
- The RSUC checks a packet buffer to find packets for the

selected vehicle. It starts the slot allocation process for the selected vehicle when packets arrive in the packet buffer.

- The RSUC checks the location of the selected vehicle. It finds the nearest base station when the selected vehicle exists within the transmission range of RSU or it starts the allocation process for multi-hop communication when the selected vehicle exists in out of the transmission range of RSU.
- The RSUC checks the slot allocation status and allocates the free slot for the selected vehicle when the direct transmission from RSU is available. Then, it will select a next vehicle.
- The RSUC initializes the hop number n to find the free slots for the selected vehicle when the multi hop communication is required. Generally, we assume the maximum hop count N according to the distance between RSU.
- The RSUC checks the slot allocation status and reserve the free slot for nth hop communication. The 1st hop communication is used for transmission from RSUs. The later than the 2nd hop communication is used for forwarding packets from vehicles to vehicles.
- The RSUC checks the reservation status of the slots for the selected vehicle. It allocates the all slots when all of required slots are reserved.
- The RSUC ends the process when slots for all vehicles are checked or all slots are allocated.

III. Numerical results

To evaluate the proposed system, we perform the computer simulations. In the simulations, we assume that 2,000 [m] straight highway with two lanes. Road side units are installed with 100 [m] interval for only RSU transmissions, and are installed with 120, 140, and 160 [m] intervals for RSU transmission and multi-hop transmission. Each RSU has an omni directional antenna whose height is 8 [m]. The transmission power is set to 50 [dB] at 1 [m] from RSU. Each vehicle is located randomly on the road, and selects the velocity from 80, 90, 100, 110, 120 [km/h] randomly. The average speed is set to 100 [km/h] The vehicle runs on the cruising lane principally. If there is no vehicle on the passing lane, the vehicle moves to the passing lane from the cruising lane to overtake a forward vehicle. After overtaking, the vehicle moves to the cruising lane when there is no vehicle on the cruising lane. As the wireless device, we employ the IEEE 802.11p device. The transmission speed is set to 3M [bps] and GI period is 1.6 [μ s]. In the simulations, we assume Rayleigh fading as the wireless channel model, and the assumed application is a file transfer application such as FTP.

TABLE II
Simulation parameters.

Simulation time	500 [s]
Simulation trial	100 [times]
Number of vehicles	100 [vehicles]
Number of communication vehicles	10 - 40 [vehicles]
Vehicle movement	Autonomous running model [13] Object speed : Random from 80, 90, 100, 110, 120[km/h] Average speed : 100 [km/h] Acceleration velocity : 0.3 [G] Breaking velocity(1st) : - 0.3 [G] Breaking velocity(2nd) : - 0.6 [G]
Initial vehicle position	Random
Number of lanes	2 [lanes]
Width of lane	3.5 [m]
Length of lanes	2000 [m]
Interval distance between RSU	100, 120, 140, 160 [m]
Communication device	IEEE 802.11p
Transmission rates	3 [Mbps]
Transmission power	50 [dB] at 1[m] from RSU
Channel frequency	5.9 [GHz]
Antenna gain	0 [dB]
Antenna type	Omni directional
Antenna height	8[m]
Propagation path loss model	Free Space
Wireless environment	Rayleigh fading
Guard interval	1.6 [μ s]
Access control	TDMA
Number of slots	24 [slots]
Packet length	1.5 [kbytes]
Maximum hops	2 [hops]
Application	FTP

Fig. 5 shows the throughput performance. From the results, we can find that the cooperative communication scheme with only RSU can achieve good throughput according to the increasing of vehicles. In the proposed scheme, neighbor RSUs of a vehicle transmit a same OFDM symbol simultaneously in a same slot. Therefore, the vehicle can receive the two OFDM signals through different routes, and obtain the diversity effect. As the results, the vehicle can continue to communicate with neighbor RSUs, and can achieve high throughput performance.

Additionally, The proposed range extension method can extend transmission range with almost similar throughput performance within 140m. The destination vehicle can receive many same OFDM signals from neighbor forwarder vehicles because RSUC reserves two slots for roadside-to-vehicle communication and vehicle-to-vehicle communication respec-

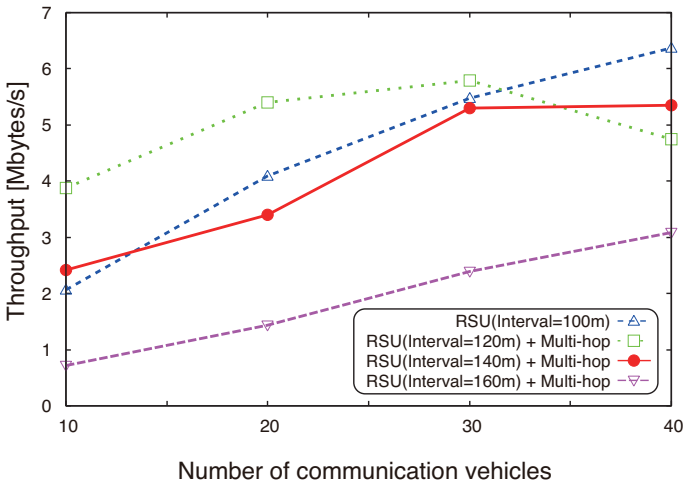

Fig. 5. Throughput performance.

tively. As the results, the vehicle can continue to communicate with RSUs even if it exists in the out of transmission range of the RSUs. Generally, the multi-hop transmission consumes a wireless resource due to multiple forwarding of packets. On the contrary, forwarder vehicles can transmit a same OFDM signal simultaneously in the proposed system. As the results, the proposed system can improve transmission error ratio without redundant wireless resource consumption.

IV. Conclusion

In this paper, we have proposed range extension mechanisms for roadside units in ITS networks. The feature of the proposed system is to employ cooperative OFDM transmission mechanisms. In the proposed scheme, neighbor RSUs of a vehicle transmit a same OFDM symbol simultaneously in a same slot. Additionally, neighbor vehicles also transmit the same OFDM symbol simultaneously in the same slot. Therefore, the vehicle can receive the some OFDM signals through different routes, and obtain the diversity effect. As the results, the vehicle can continue to communicate with neighbor RSUs, and can achieve high throughput performance. Additionally, The proposed range extension method can extend transmission range with high throughput performance. As the results, our scheme can extend transmission range without throughput degradation and redundant consumed wireless resource.

Acknowledgment

This work was supported by Grant-in-Aid for Young Scientists (B)(23700075), Japan Society for the Promotion of Science (JSPS).

References

[1] M. Koubek,S. Rea and D. Pesch, “Reliable Broadcasting for Active Safety Applications in Vehicular Highway Networks,” IEEE Vehicular Technology Conference (VTC 2010-Spring), pp. 1 - 5, 2010.

[2] Fan Yu and S. Biswas, “Self-Configuring TDMA Protocols for Enhancing Vehicle Safety With DSRC Based Vehicle-to-Vehicle Communications,” IEEE Journal on Selected Areas in Communications, Vol. 25 , Issue. 8, pp. 1526 - 1537, 2007.

[3] N. Brahmi, M. Boussedjra, J. Mouzna and M. Bayart, “Dynamic routing based on road connectivity for urban vehicular environments,” IEEE Vehicular Networking Conference (VNC 2009), pp. 1 - 6, 2009.

[4] H. Omar, W. Zhuang and L. Li, “VeMAC: A TDMA-based MAC Protocol for Reliable Broadcast in VANETs,” IEEE Transactions on Mobile Computing, Issue. 99, pp. 1 - 14, 2012.

[5] P. Salvo, F. Cuomo, A. Baiocchi and A. Bragagnini, “Road Side Unit coverage extension for data dissemination in VANETs,” Wireless On-demand Network Systems and Services (WONS 2012), pp. 47 - 50, 2012.

[6] S. Cespedes, N. Lu and X. Shen, “VIP-WAVE: On the Feasibility of IP Communications in 802.11p Vehicular Networks,” IEEE Transactions on Intelligent Transportation Systems, Issue. 99, pp. 1 - 16, 2012.

[7] M. Xing and L. Cai, “Adaptive video streaming with inter-vehicle relay for highway VANET scenario,” IEEE International Conference on Communications (ICC 2012), pp. 5168 - 5172, 2012.

[8] A. Chen, B. Khorashadi, D. Ghosal and C.-N. Chuah, “Impact of transmission power on TCP performance in vehicular ad hoc networks,” Wireless on Demand Network Systems and Services (WONS ’07), pp. 65 - 71, 2007.

[9] K. Terada, K. Naito, K. Mori and H. Kobayashi, “Study of Roadside to Vehicle Communication System with directional antenna and base station diversity technique, ” IEEE VTS Asia Pacific Wireless Communication Symposium (APWCS 2006), Aug. 2006.

[10] A. Ono, K. Naito, K. Mori and H. Kobayashi “Roadside to Vehicle Communication System with OFDM Cooperative Transmission,” IEEE VTS Asia Pacific Wireless Communication Symposium (APWCS 2011), Aug. 2011.

[11] K. Naito, K. Mori, H. Kobayashi, “Cooperative Vehicle Information Delivery Scheme for ITS Networks with OFDM Modulation Techniques,” in Proc. of the Tenth International Conference on Networks (ICN 2011), Jan. 2011.

[12] K. Naito, K. Mori, and H. Kobayashi, “OFDM cooperative flooding mechanisms for Multi-hop networks,” in Proc. of the 9th International Conference on Cybernetics and Information Technologies, Systems and Applications (CITSA 2012), July 2012.

[13] M. Adachi, Y. Morita, K. Hujimura, T. Hasegawa “A Steady of An Autonomous Cruising Traffic Flow Simulator Including Communication Network,” IPSJ SIG Technical Reports ITS, pp. 27–32, Mar. 2002.

A Method for Greening University Campus Buildings While Fostering Hands-on Inquiry-Based Students' Learning

Nader CHALFOUN, Ph.D., LEED© AP, CEA
Professor of Architecture and Environmental Sciences (chalfoun@u.arizona.edu)
The University of Arizona, College of Architecture, Planning, and Landscape Architecture, Tucson, AZ 85721

ABSTRACT

The University of Arizona is engaged in the American College and University Presidents Climate Commitment agreement that encourages U.S. universities to exercise leadership in their communities and throughout society by modeling ways to minimize global warming emissions, and provide the knowledge and educated graduates to achieve climate neutrality. Greening campus buildings is one of the major visions for this mission. This paper focuses on a methodology that was developed by the author and supported by Vice President for Student Affairs and University Housing and Residence Life, and Director of Sustainability, to educate students to conduct advanced Level III energy audit and computer analysis to identify energy efficiency improvement opportunities for three residence life campus buildings. An engineered set of site forms and specific tools and instrumentations and advanced computer simulation techniques were used during the 2011 Fall semester to facilitate the energy audits. Research team presented their findings to building directors and demonstrated that the three buildings total area of 283,174 ft² consumed on average an annual 44.2 KBtu/ft² at the cost of $401,610 per year. The energy saving strategies indicated a 17.3% or $69,410 annual operating cost savings. In addition, two of three buildings have benefitted from the project by being successfully certified for Energy Star Designation.

Keywords: Green Buildings, Energy Audit, Energy Conservation, Computer Modeling.

1. INTRODUCTION

University campus buildings contribute to a large amount of consumption, air pollution, and resource depletions. This is due, in large, to their high occupancy and heavy daily use. The University of Arizona is engaged in the American College and University Presidents Climate Commitment. This agreement emphasizes that university campuses must exercise leadership in their communities and throughout society by modeling ways to minimize global warming emissions, and by providing the knowledge and educate graduates to achieve climate neutrality. Campuses that address the climate challenge by reducing global warming emissions and by integrating sustainability into their curriculum will better serve their students and meet their social mandate to help create a thriving, ethical and civil society. These colleges and universities will be providing students with the knowledge and skills needed to address the critical, systemic challenges faced by the world in this new century and enable them to benefit from the economic opportunities that will arise as a result of solutions they develop. Described in this research, a methodology to achieve energy savings for the University of Arizona campus buildings. During the 2011 fall semester, Vice President for Student Affairs and University Housing and Residence Life Director of Sustainability initiated a project to the "House Energy Doctor[1]" (HED) program to conduct advanced energy audit and analysis to identify energy efficiency improvement opportunities for three residence life campus buildings. HED is an education, research, and community outreach program developed by Dr. Chalfoun at the University of Arizona's School of Architecture since 1986. The program promotes students learning of energy conservation and passive solar design through field investigation of existing buildings and simulation of new and innovative sustainable projects. Through an engineering approach, the project was incorporated into the class of spring 2011 Arc461K-561K, "Sustainable Design and the LEED© Initiative" taught by Dr. Chalfoun.

2. PROJECT DESCRIPTION

To achieve the goals required by this project a three-phase methodology was developed: pre-audit, audit, and post audit.

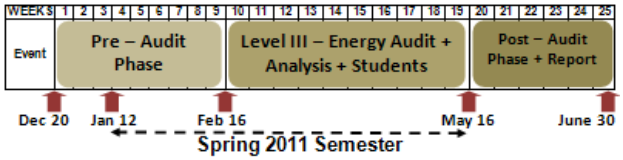

Figure1: Project Timeline

Phase one is designated for the "Pre-Audit" where all three buildings must be visited for a walk through "Level I" energy audit. This includes building envelop system,

interior loads and lighting systems, and mechanical heating, cooling, and water heating systems. During Phase two "Energy Audit" the Level III energy audit is conducted after special training is given to the students which includes teaching advanced computer energy simulation for large buildings and the use of state-of-the-art tools and site instrumentations such as light intensities measurement, solar reflectance/absorptance, blower door testing, etc. Phase three "Post Audit" was devoted for performance enhancement and parametric analysis and the development of the final report including potential LEED© and Energy Star certifications.

There is a total of 22 residence halls buildings on the University of Arizona's main campus. Three buildings were selected based on the criteria that they represents an older building (the Arizona Sonora building), a national historic registry building (the Maricopa Hall), and a newer building (La Aldea).

Figure 2: The 3 selected University of Arizona Buildings

3. PRE-AUDIT DATA COLLECTION

In order to assure successful energy audits, important information on the three selected buildings was obtained and processed in advanced. The information was then made available, in a Pre-Audit report, to the House Energy Doctor students to follow during the actual audit and measurements. The report included the following:

- Construction documents of each building.
- Equipment and mechanical system specifications.
- Mechanical system energy diagrams.
- Utilities information (electric/gas/water)
- Users and occupants information.
- Pre-visit to each building
- Development of site forms specific to Residence Life building take-offs.

Documenting the buildings' mechanical system is vital to the process. As all three buildings used District Heating and Cooling Plant (DHCP), specifications were documented with input from facilities management personal and each building director.

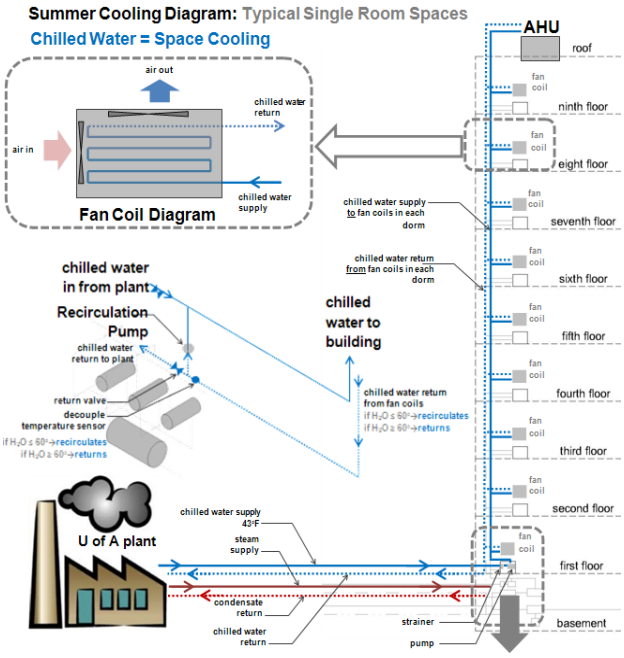

Figure 3: DHCP Diagram

4. ENERGY AUDIT

Prior to the energy audits, students in the Arc 461e-561e: Sustainable Design and the LEED© Initiative were taught principles of computer energy simulation using programs such as COMcheck, Autodesk Revit, Google Sketchup, and eQUEST. Different energy conservation strategies were examined on sample buildings. Students also were trained in the House Energy Laboratory on using different site instruments such as light meters,

pyronometers, inclinometers, blower door, duct blasters, azimuth protractor, etc. In addition, a specialized set of site forms were developed and used during the audit.

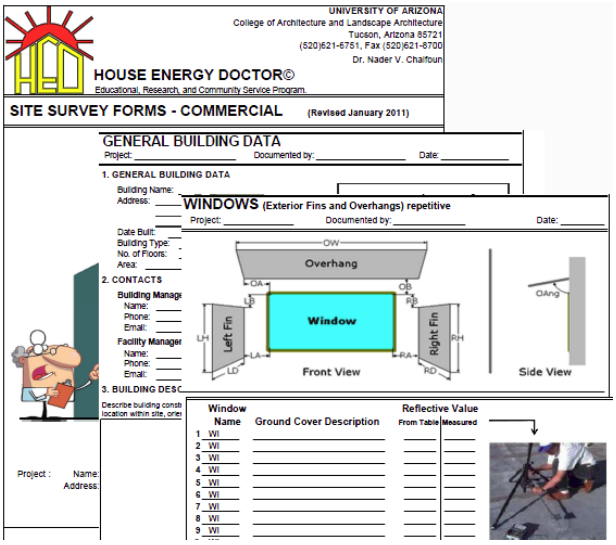

Figure 4: House Energy Doctor Site Survey Forms

During the audit day, students were divided into teams and for each building they collected the following information:

1. Building orientation and geometry in relation to sun angles (an important variable in desert architecture)
2. Size and placement of openings throughout the building facades.
3. Envelop materials information such as R-value, heat capacity, and compositions
4. Exterior and interior materials shortwave reflectance, textures, absorptance, and translucencies
5. Light intensities and distribution in all indoor spaces and daylight use potential
6. Shading devices and their locations and geometry.
7. Building use and occupancy schedules
8. Mechanical heating and cooling systems and air-handlers capacities and efficiencies
9. Building thermostat settings and scheduling, including setbacks if applicable
10. Location of ducts and duct insulation
11. Water heating equipment

Figure 5: Students Conducting the Energy Audit

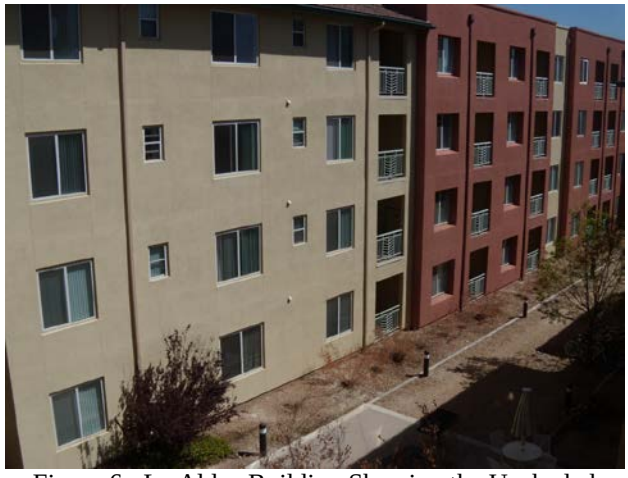

Figure 6: La Aldea Building Showing the Unshaded South Facade

5. POST ENERGY AUDIT

After all information was gathered from the three buildings, building schedules were developed, and energy performance were predicted using advanced computer simulation techniques. Energy compliance was first checked and revealed that the three buildings failed minimum commercial code requirements by ASHRAE 90.1, 2007 for Pima County and City of Tucson. Arizona/Sonora was 3% worse than code, Maricopa Hall was 45%, and La Aldea was 1%. The first two buildings are older buildings that were built prior to energy code in Arizona.

For building performance prediction and optimization, the research team used the DOE eQUEST energy simulation program to first identify basecase performance of each building. They also investigate different design aspects of the envelop, building scheduling, and the mechanical system that contribute the most to energy waste. Parametric analysis then follows to prescribe means to improve them. Computer simulation values for each building's basecase must first be validated with actual utility bills that were previously collected from facility managements. Each results must demonstrate a minimum of ± 20% in heating and cooling consumption compared to the actual onsite meters.

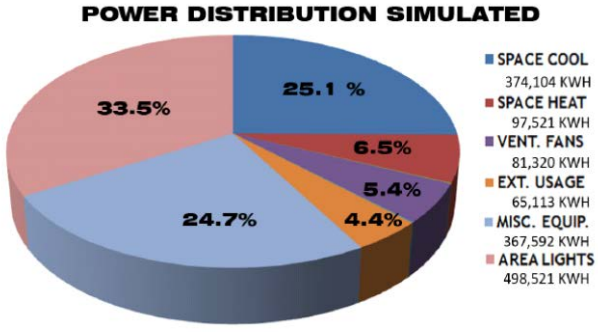

Figure 7: La Aldea Space Consumption Distribution

ELECTRIC AND GAS UTILITY BILLS						
	Electricity (KWH)			Gas (Therms)		
Month	Actual	Adjusted	Simulated	Actual	Adjusted	Simulated
Janurary	105,786.50	100,729.50	124,112.56	1,790.00	1,975.00	2,131.98
February	100,952.00	101,728.00	101,810.78	2,089.00	2,289.00	2,015.28
March	72,598.00	77,287.00	110,878.12	1,862.00	2,033.00	2,225.37
April	86,755.00	90,749.00	107,863.14	1,693.00	1,849.00	2,104.22
May	125,748.00	137,806.00	128,231.70	1,271.00	1,388.00	1,961.16
June	72,651.00	167,344.00	139,332.79	891.00	2,679.00	1,681.55
July	123,579.00	231,873.00	152,047.45	868.00	2,299.00	1,567.45
August	111,237.00	234,531.00	152,039.14	934.00	2,342.00	1,439.24
Septembe	124,043.00	129,436.00	128,445.66	1,260.00	1,009.00	1,392.56
October	120,383.00	125,838.00	113,995.64	1,375.00	1,375.00	1,545.50
Novembe	90,499.00	88,532.00	108,065.57	1,787.00	1,906.00	1,674.25
Decembe	90,234.00	90,612.00	120,275.35	2,082.00	2,206.00	1,937.62
TOTAL	1,224,465.50	1,576,465.50	1,487,098.87	17,902.00	23,350.00	21,676.17
		5.6% DIFF.			7.2% DIFF.	

Figure 8: La Aldea Basecase Simulated vs Actual Energy Consumption, Showing 5.6% Difference in Electric Bills and 7.2% Difference in Gas bills.

Some of the common major design deficiencies that were revealed by the energy analysis are:

Arizona/Sonora Residence Hall

- Inefficient windows and glazing systems
- Lack of insulation in roof and exterior walls
- Increased air leaks and infiltration due to penetration for wall fan-coil units fresh-air intakes
- Lack of daylight use caused high electric load

Maricopa Residence Hall

- Lack of insulation in exterior walls and roof
- All windows are single pane
- Lack of windows shading
- Thermostat has no setbacks

La Aldea Apartments

- Exposed roof top package units efficiency
- Lack of shading devices on exterior windows
- Envelope surface to volume area ratio
- Exterior lighting running throughout the day
- Dark heat absorbing exterior colors

These design deficiencies were then optimized each separately before making final recommendation. Results for each strategy were examined by the eQUEST software in terms of its contribution to the major heating and cooling energy consumption.

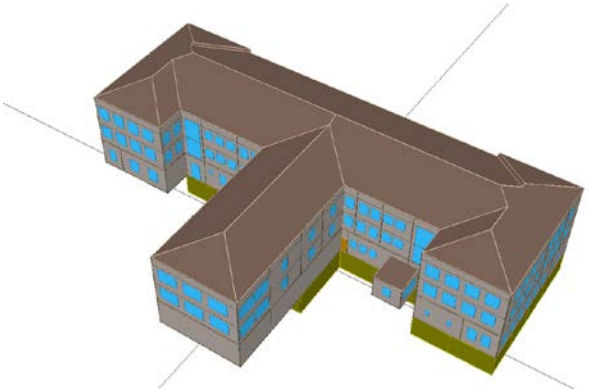

Figure 9: 3-D Model of Maricopa Residence Hall Rendered by the eQUEST software

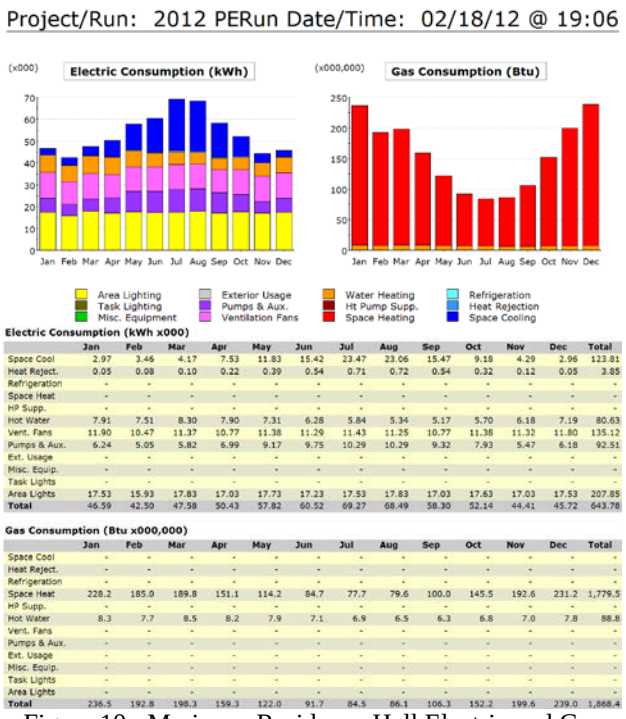

Figure 10: Maricopa Residence Hall Electric and Gas Consumption as Predicted by eQUEST

To demonstrate the optimization process, one of the strategies was to replace some of the old HVAC DX split heat pump systems at La Aldea with higher efficiency units. This strategy resulted in a annual 206,899 KWh electric savings and $15,724 cost saving.

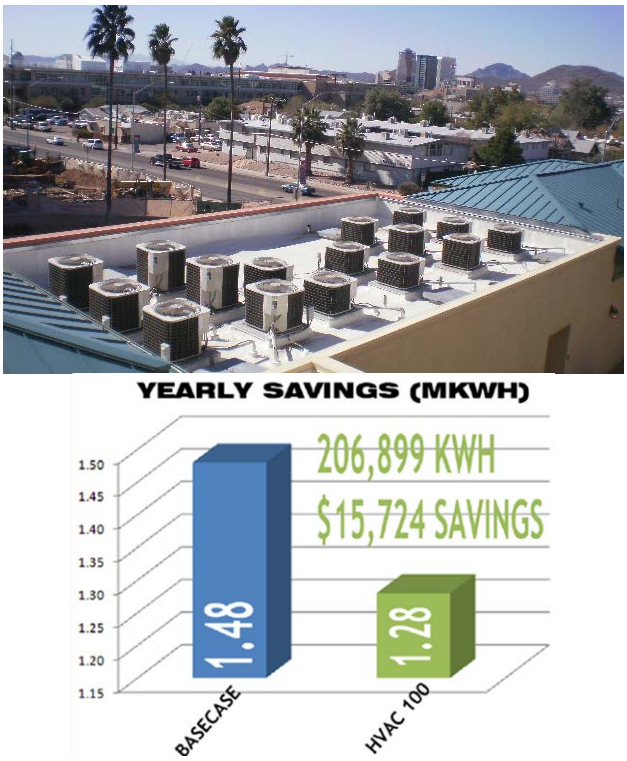

Figure 11: Energy and Cost Savings from Replacing Some Inefficient DX Split Units at La Aldea

Another important strategy was to promote the use of daylight by upgrade all light fixtures with high efficiency light bulbs and install photo sensors so that light will not turn on during the day as shown in Figure 12 below. This strategy resulted in a annual 43,417 KWh electric savings and $3,299 cost saving.

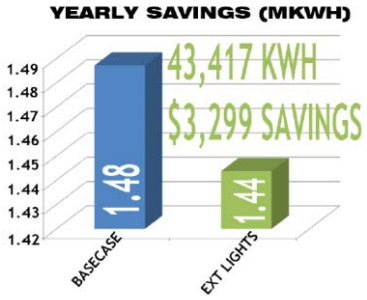

Figure 12: Energy and Cost Savings Efficient Light Bulbs and the Use of Photo Sensors at La Aldea

In the hot and dry climate of Tucson, shading becomes one of the most important strategies in energy savings as well as human thermal comfort. One proposed strategy by the investigating team is to provide a shading structure that crosses over the space between the southern and northern blocks of buildings to create a shaded courtyard. That same shading device will also block the sun from directly reaching the unshaded windows on the south.

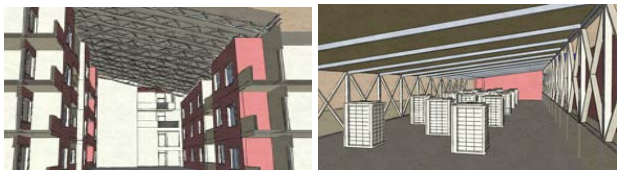

Figure 13: Proposed Different Shading Strategies

In addition a shading structure was also proposed on the west facade that will block the harsh summer afternoon sun while provides views to the Tucson mountains.

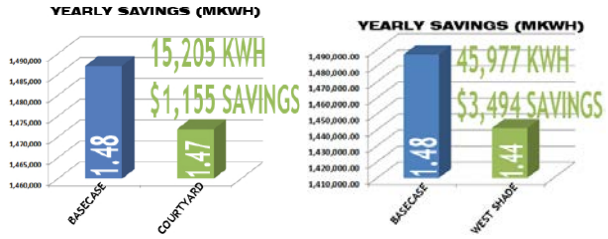

Figure 14: Combined Shading Strategies Saved an Annual Total of $4,649

Additional strategies focused on the replacement of windows to double Pane Low-e, adding external insulation, shading for most of critical building elements, replacement of more energy-saving light fixtures, and proposing change of envelope colors to increase solar reflectance in summer. As for the mechanical systems, proposed adjustments included a proposed shading device for the HVAC units on the roof top of the different buildings, changes to the thermostat and run periods on the system(s), replacement of old components with higher efficiency units, and water harvesting of condensates for landscape use. The proposed shading structure will provide thermal comfort in the courtyard spaces. Due to space limitations these strategies were not explained in this paper but will be presented at the conference venue.

6. CONCLUSION

The project demonstrates that the three buildings total area of 283,174 ft² consumed on average an annual 44.2 KBtu/ft² at the cost of $401,610 per year. If the three buildings can implement recommendations from the House Energy Doctor team, they will benefit from a 17.3% or $69,410 annual operating cost savings. In addition, two of three buildings "Arizona-Sonora" and "La Aldea" have benefitted from the project by being successfully certified for Energy Star Designation.

Building	Area ft²	Consumption KBTU/ft².yr		Energy Saving KBTU/ft².yr	
		As is	Retrofit		%
Arizona/Sonora	127,903	48.33	43.4	4.93	10.2
Maricopa	32,070	37.7	24.6	13.1	34.7
La Aldea	123,201	41.22	32.2	9.02	21.9
TOTAL/Average	283,174	44.2			

Figure 13: Annual Energy Consumption Savings

Building	Area ft²	Operating Cost S/yr		Savings
		As is	Retrofit	%
Arizona/Sonora	127,903	199,100	178,750	10.22
Maricopa	32,070	38,940	25,410	34.75
La Aldea	123,201	163,570	128,040	21.72
TOTAL	283,174	401,610	332,200	17.3

Figure 14: Annual Operating Cost Savings

Students and faculty, at the end of the semester, presented their findings to Residence Life Assistant Vice President for Student Affairs and University Housing Dr. James Van Arsdel.

Figure 15: Dr. Arsdel receiving the La Aldea Final Report from the HED students after their presentation.

Most importantly, the project demonstrated a engineering method that based on its success will now be replicated by implementing it in different other buildings as a model for greening the entire campus, and hopefully as a model to be replicated in other campuses around the nation.

7. AKNOWLEDGEMENT

The author would like to acknowledge the efforts of Dr. James Van Arsdel, Assistant Vice President for Student Affairs and University Housing and his assistants particularly those who facilitate all the pre-audit and during the audit activities. They also supplied the students with utility bills and facilitate accessibility to all three buildings. Special thanks to Dr. Abraham, director of the Office of Sustainability on Campus for his collaboration and encouragements. And last, I would like to acknowledge all the hard work and efforts that was giving by my graduate and undergraduate students in the Masters of Science program. Without them the work would have never been completed.

8. REFRENCES

[1] N. Chalfoun, **The "House Energy Doctor©; an Educational, Research and Community Service Program at the College of Architecture, The University of Arizona**, Proceedings of the Design for Desert Living Symposium, Jul. 21-26, Tucson, AZ, U.S.A. 1991

[2] N. Chalfoun and R. Michal, **Thermal Performance Comparison of Alternative Building Envelope Systems: Analysis of five Residences in the Community of Civano**, Architectural Research Centers Consortium (ARCC), College of Architecture and Environmental Design, ASU, Phoenix, Arizona, April 10-12, 2003.

[3] DOE-eQUEST **User's Manual**, 2003, James J. Hirch

Self-Adapting Parallel Kinematic Machines

Karl-Erik Neumann
Exechon AB

ABSTRACT

Historically, assembly of large aerospace structures has always required large, heavy duty, expensive machines designed and built with (and for) high accuracy over the entire work envelope. Such large machines are also generally very complex and it is normally financially and physically impossible to build these machines with more than one spindle/assembly tool.

The presentation will present “use cases” utilizing a platformless design, to deliver high dynamics and accuracy while dramatically reducing cost and eliminating the restrictions of one spindle/assembly tool. Case studies will show the application of extreme mobility in combination with adapting technologies such as cross lasers, which can perform accurate agile assembly over very large areas without the use of accurate large expensive heavy duty structures. Additional discussions will address case-studies on the ability to use small agile modules that can perform

The Parallel Kinematic Machines (PKM) developed since 1985 by Karl-Erik Neumann, starting with the Tricept 600, continuing with the Tricept 605, 805, and 9000, and the new “balljointless” Exechon X300, X700, and X1100, ending up in the latest “platformless” XT300S, XT700S, and XT1100S, has always been striving to give aerospace manufacturer a solution that utilize the flexibility and cost benefits of articulated arm robots, the performance of CNC machines, as well as the efficiency of special machines.

Exechon was founded around this dream in 2004, and the first “balljointless” X700 machine saw daylight summer 2006, and since then the technology has been licensed out to twenty one (21) Manufacturer and Integrators worldwide.

PLATFORMLESS PKM MACHINES

In 2006 the Exechon technology revolutionized the PKM technology by eliminating the ball joints that were mandatory in all previous PKM machines, and it was now time to take the technology one huge step further to prove it to be a general worldwide used technology within Aerospace and Automotive.

The way to achieve this goal was to eliminate the last remaining obstacle; the always present heavy platforms or structures holding and supporting the legs and/or actuators of all existing PKM machines.

Going from the first X700 to the X700S machine, the moving mass was reduced by 40% (300kg) by simply moving the motors for axis one to three from the moving lower platform to the neutral inner gimbals, and to further improve the dynamics and temperature stability, the motors for axis four and five was put on the outside instead of being build in.

However, to accomplish true “Self Adapting Parallel Kinematic Machines for Large Wing and Fuselage Assembly”, reducing the moving mass was not the only solution.

To reduce the cost, simplify the design, and make it possible to utilize multiple hole drilling, it was also necessary to substantially reduce the weight of the PKM module to allow it to be mobile within a low cost system.

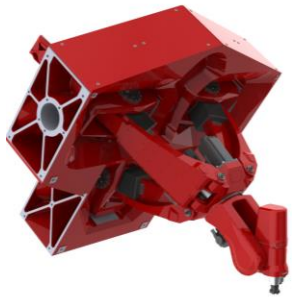

A big remaining problem(until now) in the PKM technology has been the fact that all legs and actuators have to be mounted in some kind of platform or structure allowing it to resist the forces from each legs individually and in combination, resulting in a very heavy design preventing it from being agile and mobile.

Finally, after almost thirty years since the first PKM machines saw daylight, Exechon has developed a PKM machine that can maintain, or even increase, its stiffness and accuracy by totally eliminating the previous mandatory platforms and structures supporting the legs and actuators.

Exechon has solved this problem by connecting the outer gimbles of actuator one and three, eliminating the need of central support of these gimbles and at the same time making it possible to add on extra material in the centre, which was impossible in the platform design due to cable issues, resulting in increased stiffness.

This integrated one and three gimble also prevent actuator one and three from twisting in relation to each other (when a side force is applied) on the machine, resulting in increased stiffness and improved accuracy.

Further the outer gimble of actuator two has been turned ninety degrees eliminating a centre support for actuator two as well. This turned design also puts the holding points of actuator two right on top of the side structure, resulting in increased stiffness.

Overall the above patented design reduces the mass of a XT700S module with 3000kg, making it very suitable for “Self Adapting Parallel Kinematic Machines for Large Wing and Fuselage Assembly”.

CALIBRATION

To really make “Self Adapting Parallel Kinematic Machines for Large Wing and Fuselage Assembly” in combination with multiple hole drilling practical, it is crucial to find a way to calibrate the machines without using expensive and high tech equipment such as Laser Trackers and computerized adaptive systems.

Far more important is also the possibility to calibrate the machine tool vector, and not only the tool centre point, whish is a serious problem in most existing calibration systems.

Exechon has developed a system using a FARO Arm for automatic calibration. The machine is programmed in a pattern, letting the machine move to a number of points and repeats this pattern and points in multiple different tool vectors. The pattern can be adapted to an existing jig or fixture to avoid disassembly of any parts in the system during calibration.

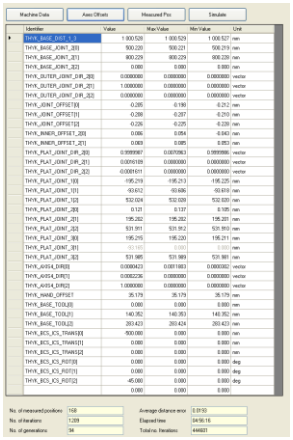

After collecting a selected number of x, y, z, and vector values, the values will be uploaded onto an external internet based calculation computer, which performs a massive amount of mathematical parameter calculations offline, and after 30 minutes a complete set of thirty-one (31) machine parameters and five (5) reference positions are ready to be downloaded and implemented into the machine, fully automated, resulting in a volumetric accuracy of around +/- 10 microns.

SIMPLIFIED ASSEMBLY

Another necessary item in “Self Adapting Parallel Kinematic Machines for Large Wing and Fuselage Assembly” is of course the assembly process itself. As earlier discussed, conventional assembly systems are far too complex and way too expensive to use in multiple hole drilling and assembly operations.

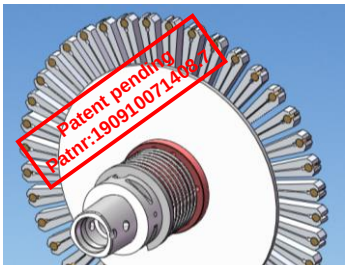

For this purpose Exechon has in cooperation with one of our Licensees developed a new simplified method to assembly fasteners in the new China Big Plane, using fastener “discs” that are loaded off-line, where jamming of feeders and other related problems doesn't effect the production nor the quality of the automated assembly.

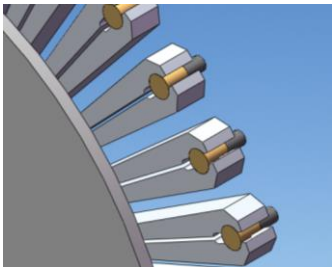

The discs are actually to be considered as tools, and are consequentially equipped with tool holders, and these disc tools are loaded into the tool magazine, either manually or automatically, and being seen as tools by the machine and its program, the assembly process is for sure simplified and guarantees a high up-time.

CROSS LASER

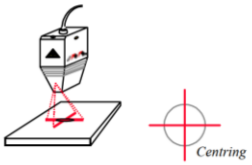

It has been a long lasting problem how to adapt multiple assembly heads to a unknown aero plane surface such as a wing panel or fuselage without using time consuming probing etc. To overcome this problem a new type of probing system was developed in cooperation with Boeing and Meta UK, a system combining two linear lasers into one laser head, a so called Cross Laser. The Cross Laser sends four points of measurements to the system which in its turn in a few seconds can calculate the accurate surface angle and position as well as hole and edge positions within 50 micron.

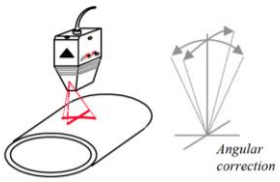

ORBITAL DRILLING

Some of the holes required to be drilled during assembly cannot be drilled conventional due to the risk of dilamination, which is an absolute no-no in automatic assembly, and so far the only good method to avoid this has been to use additional Orbital Drilling heads that further add on complexity, weight and cost to allready complex, hevy and costly systems. However, since just a few month back it is now possible to incorporate the Orbital Drilling process from Novator into the Exechon technology and achieve Orbital Drilling hole accuracy down to H6 without any additional mechanial equipment but just using the circual imterpolating capabillity of the Exechon technology.

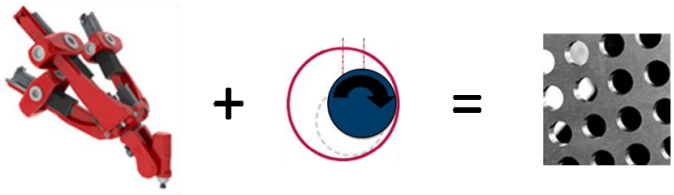

SELF ADAPTING PARALLEL KINEMATIC MACHINES FOR LARGE WING ASSEMBLY #1

Drilling multiple holes and assembly of multiple fasteners has become a nightmare requirement since more and more planes have to be manufactured in a shorter time.

The solution promoted by Airbus is “Multiple Hole Drilling & Assembly” which as earlier described is both technically and financially impossible with today’s large single head machines.

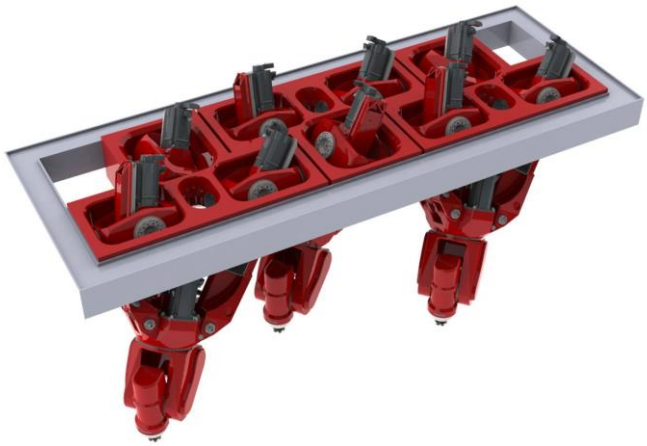

Exechon is currently participating in developing such a “Multiple Hole Drilling & Assembly” machine in cooperation with Airbus UK and the Manufacturing Technology Centre (MTC) in UK.

The system with consist of three parallel gantry mounted XT305S machines with 500mm stroke and traditional spindles with tool changers, and it will utilize all technologies earlier mentioned in this paper as well as a state of the art fixturing system developed by other parties within the project.

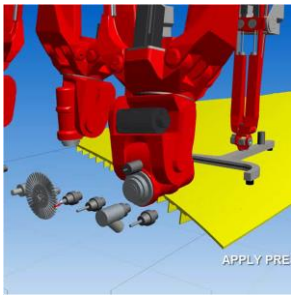

The process will be as following;

1. Positioning the gantry over the wing
2. The XT305S machines locate the surface and references using a permanently mounted cross laser.
3. The XT305S machines picks up selected tools from the tool changers.
4. The XT305S machines simultaneous drill and counter-sink all holes within their reach.
5. The XT305S machines also simultaneous perform Orbital Drilling of all holes requiring this type of operation within their reach.
6. The XT305S machines picks up vacuum cleaners from the tool changer and cleans all holes.
7. The XT305S machines picks up fastener disc and seals all holes.

8. The XT305S machines assemble all fasteners

9. Move the gantry to next position

SELF ADAPTING PARALLEL KINEMATIC MACHINES FOR LARGE WING ASSEMBLY #2.

For years discussions has been going on within the aerospace industry around mobile machine tools, and the Exechon technology has for the first time made it possible to utilize such a system.

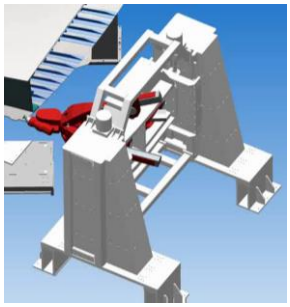

The system is designed and built in cooperation between Airbus UK, Queens University, and Güdel, both Exechon Licensees. The system is based on an Exechon module from Hwacheon, a Licensee in Korea, a structure with a z-travel from Güdel, and an Omni Move from Kuka Automation, and the system is designed to machine the root end in multiple jigs at Airbus.

The system has currently been verified at Airbus UK with exceptional results such as machining accuracy in one Exechon position of 20 microns and machining accuracies over the whole 4,5 meter root end of 40 microns.

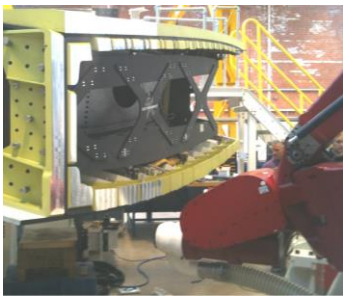

SELF ADAPTING PARALLEL KINEMATIC MACHINES FOR LARGE FUSELAGE ASSEMBLY #1

A new problem has occurred in assembly of aero plane structures due to the fact that fuselages are mainly manufactured in composite, which is very stiff and inflexible.

The problem is that it is virtually impossible to manufacture fuselages with a diameter of e.g. 6,5 meter, accurate enough to be able to mount two of them together end to end due to variations in diameter and ovality.

To solve this problem the ends of the fuselages have to be machined, and to build a traditional machine performing this task will require a huge structure with high accuracy and accompanied price tag.

Using a small light XT300S with a cross laser for self adapting capability, mounted in a non accurate structure, that in its turn is mounted on a high accuracy standard “Fibro” turn table, adapting its coordinate system to an average best fit of the fuselage, allows not only a low cost design, but also a optimized material removal that guarantee a minimum of material removal from the fuselage maintaining the structure integrity.

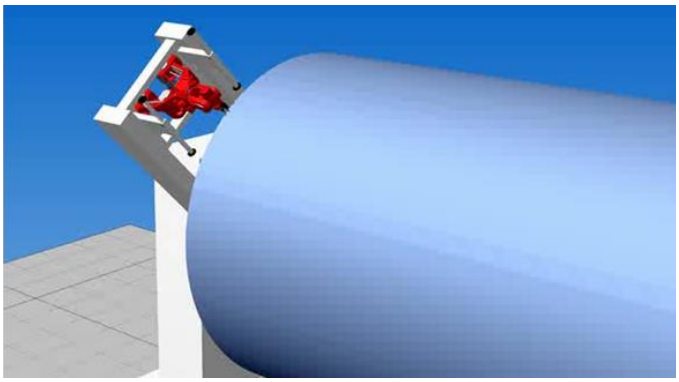

SELF ADAPTING PARALLEL KINEMATIC MACHINES FOR LARGE FUSELAGE ASSEMBLY #2

The next step in the process, mounting two fuselages together, normally require a huge machine structure with a very complex and heavy drilling and assembly head that can move around the fuselage joint with high accuracy.

Such machine, and especially the head, tends to become very complex with multiple integrated CNC functions like a drilling head, a sealing head, cleaning functions, and fastener assembly heads with multiple feeders, that all are normally associated with low uptime and a high price tag.

Instead we propose utilizing two small light XT300S using cross lasers for self adapting capability, mounted in a non accurate structure.

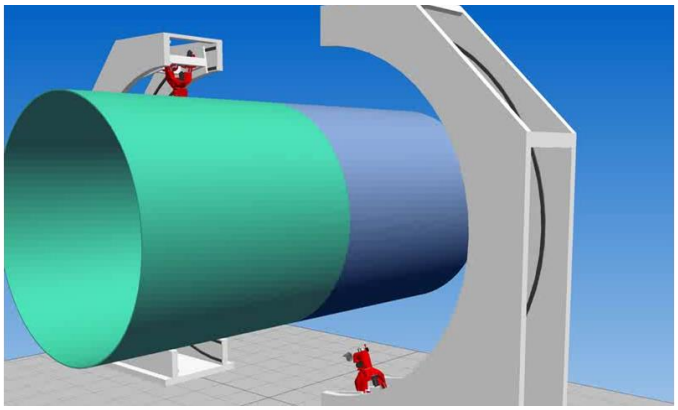

The process will be as following;

1. Positioning the two XT300S machines around the fuselage.
2. The XT300S machines locate the surface and references using a permanently mounted cross laser.
3. The XT300S machines picks up selected tools from the tool changer.
4. The XT300S machines perform simultaneous drilling and counter sinking all holes within the reach of the XT300S machines.
5. The XT300S machines also simultaneous perform Orbital Drilling of all holes requiring this type of operation within their reach.
6. The XT300S machines picks up vacuum cleaners from the tool changer and cleans all holes.
7. The XT300S machines picks up a fastener disc and seals all holes
8. The XT300S machines assemble all fasteners
9. Move the XT300S machines to next position

PORTABLE DRILLING & ASSEMBLY AUTOMATION

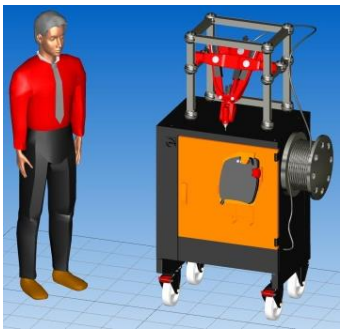

The future Exechon XMINI is a potable "machine tool robotics system" combining the flexibility and dynamics of articular arm robots with the accuracy and stiffness of CNC machines. This new patented light design gives these modules extreme mobility and, in combination with adapting technologies such as cross lasers and force sensors, it can perform accurate agile operations over very large areas without the use of accurate large expensive heavy duty structures.

The portable XMINI it's a new way of thinking but it's also easy to imagine the use of two to four XMINI machines in every wing and fuselage structure made for ever plane in the world ending up in hundreds of machines needed worldwide every year.

This small version of the Exechon PKM Systems is currently on an initial concept development stage with key users in the aerospace industry such as Airbus and Boeing. The concept is to develop a small in size and light weight PKM system that would be easy to position around aerospace parts that require complicated manufacturing processes that up to now require an extensive and expensive deployment of specialized jigs and fixtures that usually are used for the specific task without the ability of reuse or redeployment on other parts of a manufacturing line. For this reason the majority of these manufacturing processes are today 100% manual.

The Exechon Mini will be designed in such a way so that is light-weight but robust and accurate. The initial design specifies a mix of aluminium and composite (enhanced carbon fiber) parts, together with innovative support fixtures.

The XMINI will revolutionize a large number of existing manufacturing processes and will allow manufacturers to change custom made tooling manufacturing to flexible processes.

Procedures such like drilling and riveting of complex structures will be simplified with a use of a number of XMINI's that can be moved from one manufacturing station to another depending on volume and they will not be part specific.

CONTACT

Karl-Erik Neumann
CEO, Exechon AB
Sweden
+46 70 5680099
kalle.neumann@exechon.com
www.exechon.com

Time and Frequency Resource Allocation using Graph Theory in OFDMA Wireless Mesh Networks

Miri PRIESLER (MORENO)
Engineering Department, Ruppin Academic Center
Emek Hefer, 40250, Israel

and

Arie REICHMAN
Engineering Department, Ruppin Academic Center
Emek Hefer, 40250, Israel

ABSTRACT

A wireless network with a mesh topology works reliably and offers redundancy. In modern broadband wireless mesh networks that use MIMO and OFDMA techniques, the problems of time, frequency, and space resource allocations are different from a cellular system and more complicated due to system architecture and distributed control and management. This paper focuses on the resource allocation problem of the OFDMA system and we define the term of separability order. For simple topologies like the square grid configuration, the allocations are simple and an optimal solution can be shown, but for an arbitrary architecture we need advanced tools and we use Graph Theory tools to present two different algorithmic solutions, to allow frequency reuse.

Keywords: Wireless mesh networks, OFDMA, resource allocation, graph colouring, graph theory, graph algorithms.

1. INTRODUCTION

A wireless mesh network (WMN) [1,2] is a communications network made up of radio nodes organized in a mesh topology usually composed of mesh clients, mesh routers and gateways. The WMN enables rapid deployment with lower-cost backhaul and good coverage. The interest in these networks increases in parallel to the developments of cellular systems and has its own values. A wireless network with a mesh topology is reliable and offers redundancy. Broadband modern networks use multiple antennas at both transmitter and receiver (MIMO - multiple input multiple output) and multicarrier transmission techniques (OFDMA - orthogonal frequency division multiple access) [3].

The allocation of frequency resources in OFDMA WMN has unique characteristics due to WMN spatial architecture which is different from cellular network spatial architecture and due to the fact that the OFDMA channel can be split in sub-bands of subcarriers. Methods of dynamic sub-carrier assignment in OFDMA WMN are shown in [8-10] using cross-layer optimization taking into account interference among links and adaptive power allocation and admission control. In [12] the graph theory is used for resource allocations, in this paper the concepts are reviewed, and new methods and results are added.

2. RESOURCE ALLOCATION

Resources and Separation Order

The resources to be shared considered in this paper are:

- Time: The system may operate with time slots division, requiring network synchronization.
- Frequency: The frequency division can be among different OFDMA bands, *inter-band*, or among different sub-carriers in the same OFDMA band, *intra-band*. A group of subcarriers dedicated to some purpose, such as transmission for a specific user forms a sub-band.
- Space: Frequency reuse can be made using spatial separation:
  - Among geographically separated links.
  - Among different transmission directions using MIMO or directional antennas.
  - Among different reception directions using MIMO or directional antennas.

We define [4] the time frequency separation order (TF-SO) λ_{TF} as the number of combinations of time slots and frequency bands which give practical separation among such combinations (not according to frequency sub bands). If N_T is the number of time slots and N_{FB} is the number of frequency bands, then TF-SO is given by:

$$\lambda_{TF} = N_T \cdot N_{FB} \qquad \text{Eq. (1)}$$

For example, with four time slots and two frequency bands, the TF-SO is $\lambda_{TF} = 8$.

With multiple antennas, the spatial domain can be used to create additional degrees of freedom for communications. Utilizing multiple antennas may result in additional spatial channels. The TF-SO may be modified to include the space separation. Assuming that for each terminal, we have directional antennas that divide the space in N_{sS} sectors, we can extend the TF-SO to time, frequency and space separation order (TFS-SO) λ_{TFS}, according to the number of combinations of time slots, frequency bands, and angular directions that offer practical separation among such combinations. The TFS-SO is given by:

$$\lambda_{TFS} = N_T \cdot N_{FB} \cdot N_S \qquad \text{Eq. (2)}$$

However, since the number of angular directions of each terminal is not fixed, the separation varies with time. Therefore,

we must find an effective (average) TFS-SO factor with an effective number of sectors $N_{S.eff}$:

$$\lambda_{TFS.eff} = N_T \cdot N_{FB} \cdot N_{S.eff}. \quad \text{Eq. (3)}$$

Separation Rules and Separation Order Extension

The OFDMA should be combined with TDMA to allow connectivity among nodes in WMN. There are N_{FB} frequency bands of OFDMA and in each frequency band, N_{FSB} frequency sub-bands and N_T time slots of TDMA. In each slot, all frequencies may be used according to non-collision rules:

- A node may not transmit and receive in the same time slot in the same frequency band.
- All transmissions from a node to other nodes in the same time slot in the same frequency band should have different frequency sub-bands.
- All receptions at a node from other nodes in the same time slot in the same frequency band should have different frequency sub-bands. This includes intentional transmissions to this node as well as interferences, i.e. receptions from transmissions to other nodes received from transmitters in the node's area of reception.

The *intra-band* division does not give the same level of separation as different time slots and different frequency bands due to the additional constraints imposed. The extension of the notion of separation order that includes the effect of the sub-bands is denoted as *extended* separation order of time and frequency λ_{xTF}, or as *extended* separation of time, frequency and space λ_{xTFS}. For example for the case when each band has the same number of sub-bands N_{FSB}, the extended separation order is given by $\lambda_{xTF}=N_{FSB}\cdot\lambda_{TF}$ and $\lambda_{xTFS}=N_{FSB}\cdot\lambda_{TFS}$..

The meaning of the extended separation order is the number of combinations of time slots, frequency bands and frequency sub-bands (and of angular directions) and each such combination is denoted as a *resource element* (or briefly - *elements)*.

Perfect Square Grid Example

A perfect square grid serves as an example of resource allocation. We denote the node coordinates as (i,j), where i and j are integers.

Assuming that the communication range R is $1<R<\sqrt{2}$, then only the four closest neighbors can communicate directly, which defines a perfect grid graph.

Lemma The minimum number of resource elements, to be allocated on the edges of the grid, without causing disturbances, is $\lambda_{xTF}=16$.

Proof First regard any edge of the grid, the 6 edges adjacent to its end-vertices, and an additional parallel edge, that is located right beyond that edge. If any pair of these edges is allocated the same element, then the two edges would be in disturbance, therefore, to avoid disturbances, we need to set different elements on those 8 edges. Since every bi-directed transmissions on an edge must use two different elements, then we need to allocate 8×2=16 different elements on those edges. Therefore, we need at least 16 different elements for every disturbance-free allocation of elements on the grid.

To terminate the proof, we present a disturbance-free allocation of one element on every edge of the grid, using 8 different elements (16 elements when doubling the required elements per edge).

Allocation of elements on horizontal edges*:* For every i, i=0,1,2,3, we set the element i on the edges connecting the two coordinates (i mod 4, 0 mod 2) and (i+1 mod 4, 0 mod 2), and on the edges connection the two coordinates (i+2 mod 4, 1 mod 2) and (i+3 mod 4, 1 mod 2) .

Allocation of elements on vertical edges: For every j, j=0,1,2,3, we set the element j+4 on the edges connecting the two coordinates (0 mod 2, j mod 4) and (0 mod 2, j+1 mod 4), and on the edges connection the two coordinates (1 mod 2, j+2 mod 4) and (1 mod 2, j+3 mod 4) .

It is easy to verify that no pair of edges is in disturbance on this allocation, and thus, if the number of elements per edge is doubled, we get a non-disturbing allocation of 16 elements on the edges of the grid. □

The resource for a square grid is shown in Figure 1. The numbers 1 to 8 represents each two elements, one for each direction.

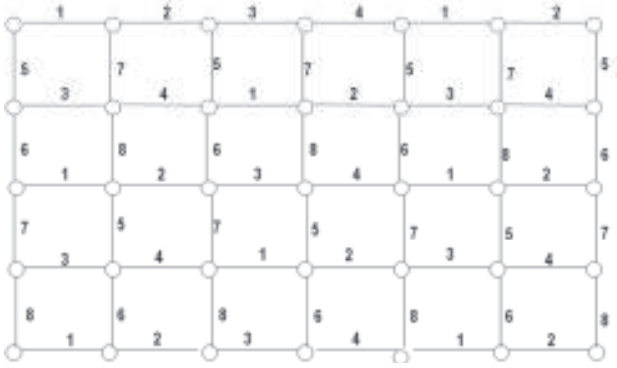

Figure 1. Optimal resource allocation for a square grid. Each of the numbers 1 to 8 represents two elements, one for each direction.

If the resource elements are combinations of time slot and frequency band there are no restrictions to allocations.

Often from practical considerations there is restriction to one frequency band. Therefore we have to use different time slots and may use sub division of the band into sub bands and limitations have to be taken into considerations according to the non-collision rules. For this case a solution will be described with four time slots and for sub-bands. We denote the two resource elements related to an horizontal link i as $\vec{i}$ and $\overleftarrow{i}$ and the two resource elements related to an vertical link j as $j\uparrow$ and $j\downarrow$. The active transmissions in each one of the four time slots are:

1. $\overleftarrow{1}$ and $\vec{2}$, $\overleftarrow{3}$ and $\vec{4}$
2. $\overleftarrow{2}$ and $\vec{3}$, $\overleftarrow{4}$ and $\vec{1}$
3. $7\uparrow$ and $8\downarrow$, $5\uparrow$ and $6\downarrow$
4. $8\uparrow$ and $5\downarrow$, $6\uparrow$ and $7\downarrow$

In each time slot there are four subband, which are the same subbands, e.g. $\overleftarrow{1}$, $\overleftarrow{2}$, $7\uparrow$, $8\uparrow$ occupy the same frequency subband. Therefore each node is transmitting in two time slots out of the four. The node with the links 1, 2, 8, 5, as an example transmits in slot 1: $\overleftarrow{1}$ and $\vec{2}$ and in slot 3: $7\uparrow$ and $8\downarrow$; slots 2 and 4 are used for reception. According to the links

connected to each node there are 16 types of nodes and each node type have a different template of operation.

3. Formal Resource Allocation Problem

In the rest of the paper we use Graph Theory methods and terminology [5,6,7], where each terminal, having a transmitter and a receiver, becomes a vertex, and the links become edges.

Let V be a set of topologically allocated vertices, and R be an upper bound on the distance between any two communicating vertices, i.e. if the distance between any two vertices does not exceed R, then they can communicate, and thus we connect them by an edge.

To avoid collisions, for every two vertices u, and v, different resources are being used to broadcast from u to v and to broadcast from v to u. Hence, there cannot exist simultaneous broadcasting from u to v and from v to u , and thus, for every slot of time, we may disregard the direction of the broadcasting, and use undirected graphs to describe the connections between the vertices of V. Therefore, the set of vertices, V, and the upper bound on the distance, R, induce an undirected graph $G = (V , E(V,R))$ were E denotes the set of edges connecting the vertices V within the distance R.

A resource allocation on G defines a set of *resource elements*, such that every edge of G uses one resource element of the set in each direction. A resource element stands for any combination of elementary resources: It can be regarded as a combination of time slots, band frequencies, sub-carriers, etc. Hence, it can represent pairs of the type {*time, band*}, {*time, sub-band*} etc.

The resource elements allocated on the edges of G must follow the following rules:

- For every vertex $v \in V$, all the simultaneous broadcasting from v, and to v, are mutually disturbing, and thus should be allocated by different resource elements.
- Moreover, if a vertex x transmits to a vertex y, then y is disturbed by the transmissions of x to other vertices, and it may disturb y to receive transmission from other vertices.

A more restrictive rule may be added to allow autonomous management of links between two nodes by the nodes it links by allowing the resources allocated to the link to be used in both directions according to the traffic between these nodes.

Therefore, the edges adjacent to x and the edges adjacent to y must all be allocated by different resource elements. We thus define two edges (u,v), and (x,y), with resource elements f_1, and f_2 respectively, to be *mutually undisturbed* if and only if they satisfy the following demands:

- Vertices *u, v, x,* and *y*, are all distinct, and
- Vertices u and v are not neighbours of vertices x, and y.

Obviously, if edges (u,v), and (x,y), are not mutually undisturbed, then they are *mutually disturbed*, and every pair of transmissions, set on this pair of edges, is also *mutually disturbed.*

Our goal is to allocate as few different resource elements as possible to the set of edges of the graph G, such that no two transmissions are mutually disturbed.

In the following two chapters, Chapter 4 and Chapter 5, we present two algorithms of two distinct approaches for solving this problem (however none of the algorithms is preferable). The first algorithm paints closed vertices (neighbours and neighbours of neighbours) with different colours, and allocates different resource elements to their edges. The second algorithm takes advantage of the radius of the *reach range* to allocate different elements to the edges in that range, while farther edges repeat using the same set of elements (and their vertices are regarded as being differently coloured).

4. First Resources allocation algorithm

The first algorithm, (A1), uses the Graph Theory term "Coloring of Vertices" to set elements only on edges that are "far enough" from each other.

Algorithm 1 (A1)

Input:

- A set V of topologically allocated vertices *V,*
- An upper bound on the distance R
- A set F of elements (Assume that F is large enough)

1) *Build the graph $G = (V,E)$ from V according to R (as suggested on the problem description)*
2) *Build the graph $G' = (E,E')$ from G such that for every $e_1,e_2 \in E$, $(e_1,e_2) \in E'$ if and only if e_1,e_2 are mutually disturbed.*
3) *Colour the edges of E by using as few colours as possible, such that the end vertices of every edge of G' are coloured differently. (Notice that even if the vertices of G' are randomly coloured properly, then every vertex is set by a colour that is different from the colours of its neighbours, and thus no more than $\Delta(G')+1$ colours are needed to colour properly the vertices of G' , where $\Delta(G')$ is the maximum degree of G' [5,6]).*
4) The colours of E in G' are the colours of E in G .

Output: A resource element on every edge of G .

Notice that every pair of edges, that was set by the same element, is mutually undisturbed, since G' was built accordingly

Obviously, if the graph G' is properly coloured by the minimum number of colours, then the algorithm may set as few elements as possible to the edges of G , since that colouring of G' ensures that the same elements are set properly as many times as possible. Unfortunately, the problem of properly colouring the vertices of an undirected graph with the minimum number of colours, is known to be NP-hard [11], that is, mathematicians believe that no polynomial time algorithm exists for solving that problem. We believe that this is also the status of our proposed Resources Allocation Problem. Therefore, we must settle with the random colouring of the vertices of G', that ensures the use of no more than $\Delta(G')+1$ colours. The result $\Delta(G')+1$ is a small enough number of elements to be set on the graph G .

The following Example, (E1), illustrates how Algorithm (A1) runs on a given undirected graph. Notice the two suggested colourings of E of G' in step 3: The first randomly uses the alphabetic names of E, and needs 10 colours to colour E

properly , while the second detects the existence of a triangle of G' with a "crowded" neighbourhood, (i.e. many edges are adjacent to the vertices of the triangle), and starts the colouring there, resulting the optimal 9 colours for the proper colouring of E. (Notice that the vertices of that triange - emphasized by yellow - and its neighbours, must all have distinct colours. Therefore, the 9 colours, needed to colour them, are the minimum number of colours in a proper colouring of E) .

Unfortunately, detecting maximum cliques (i.e. subgraphs of maximum number of vertices, where every pair of edges is connected by an edge), is also known to be NP-hard [11], therefore it is pointless to add the detection of crowded maximum cliques to the algorithm.

Example 1 (E1)

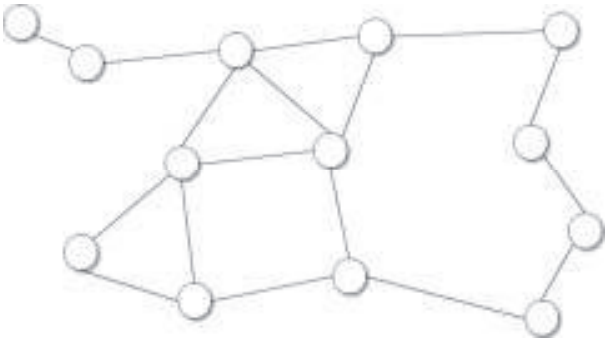

Figure 2. *Algorithm 1, step 1: The given graph G=(V,E)*

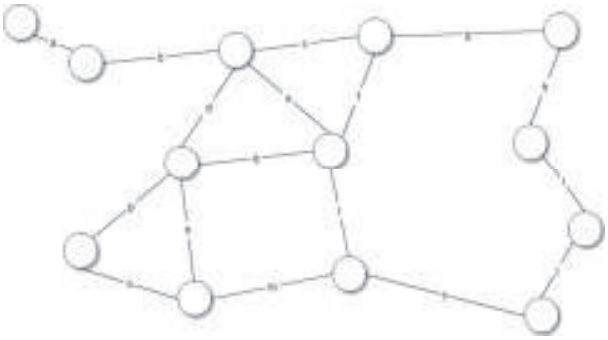

Figure 3. *Algorithm 1, step 2: Numbering the edges of G*

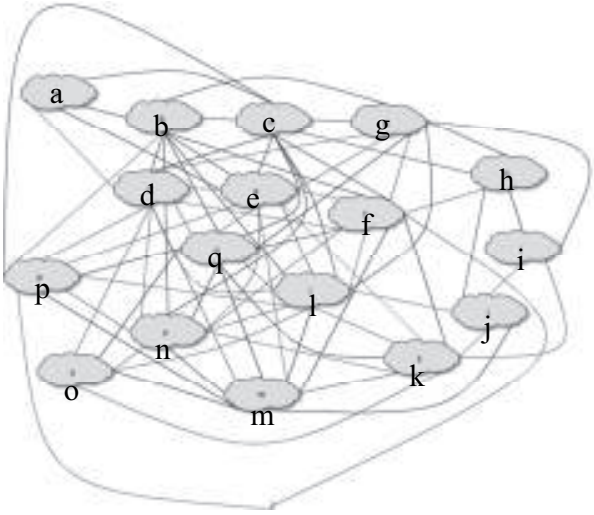

Figure 4. *Algorithm 1, step 2: The graph G'*

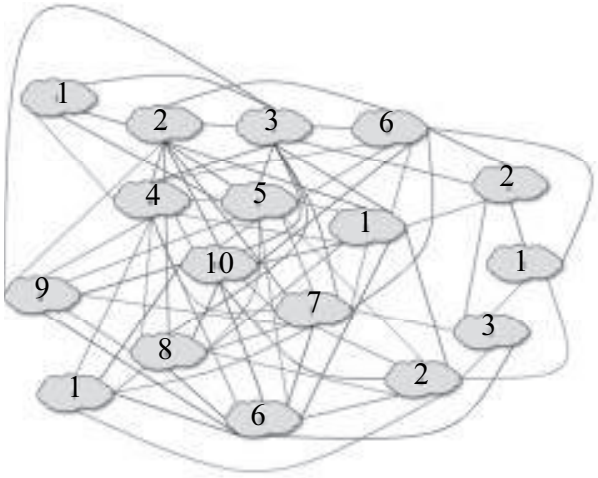

Figure 5. *Algorithm 1, step 3: Colouring E in G' in alphabetic order – Colouring with 10 colours*

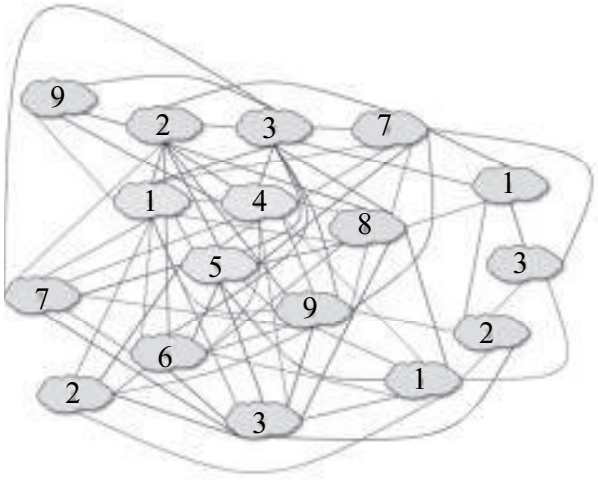

Figure 6. *Algorithm 1, step 3: Colouring E in G', starting with the emphasized triange and its neighbours – Optimal colouring with 9 colours*

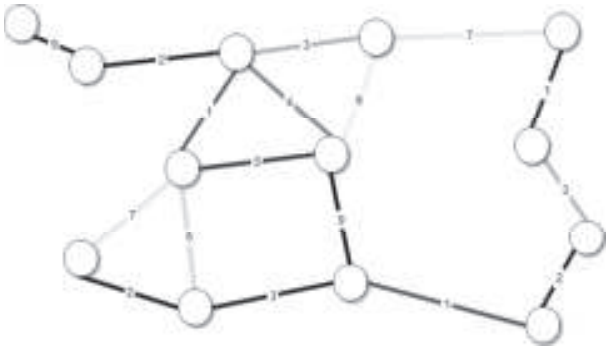

Figure 7. *Algorithm 1, step 4: The resulting allocation - Optimal colouring of E in G*

5. Second Resources Allocation Algorithm

Our second algorithm, (A2) , is a topological algorithm, that uses an algorithm we denote as *Common Elements Algorithm* (CEA), to draw as many non tangent circles of diameter R as possible, on the area of the graph G. Every two edges of different circles, cannot be mutually disturbed, and thus can be set the same element. Therefore, the same scope of elements can be set to the edges of each such circle.

Algorithm 2 (A2)

Input:

- A set V of topologically allocated vertices V ,
- An upper bound on the distance R
- A set F of elements (Assume that F is large enough)

1) Build the graph $G = (V,E)$ from V according to R (as suggested on the problem description)
2) As long as $E \neq \varnothing$,

a) Run the following algorithm, (CEA) , on G
b) Subtract the elements, being used by (CEA) of previous step, from F
c) Delete the edges, that received elements by (CEA) of previous step, from E
d) Delete vertices, that became isolated after the previous step

Output: The elements on all edges of G .

Following is the sub-algorithm that is used by (A2):

Common Elements Algorithm (CEA)

Input:

- An undirected graph $G=(V,E)$
- A set $F = \{f_1,f_2,....,f_r\}$ of elements (Assume that F is large enough)

1) As long as $E \neq \varnothing$,

a) Choose a random vertex $x \in V$,
b) Denote by B the area of the circle centered in x with the radius R
c) Denote by A the set of edges of E with at least one vertex in B
d) Set on each edge of A a different element from $\{f_1,f_2,\ldots,f_{|A|}\}$ (If sub-bands are used, then regard their vertices as being differently coloured) .
e) Denote by U the set of all end vertices of the edges of A
f) Denote by H the set of edges of E with at least one vertex in U
g) $V \leftarrow V\text{-}U$, $E \leftarrow E\text{-}H$

Output: Subgraphs $G_1=(V,H)$, and $G_2=(V,E\text{-}H)$, such that elements are allocated to the edges of H and no elements are allocated to the edges of $E\text{-}H$.

Notice that each iteration of (CEA) determines a new circle of diameter R, and allocates the edges of that circle, the same scope of elements as were set to the circles of the previous steps of that algorithm. Since two such circles are "far enough" from each other, no two edges, with a common element, are mutually disturbed.

Moreover, every call of (CEA) uses a different scope of elements, and thus two adjacent edges are allocated with different elements, and thus are not mutually disturbed.

The following Example, (E2), illustrates how Algorithm (CEA) runs on a given undirected graph.

Example 2 (E2)

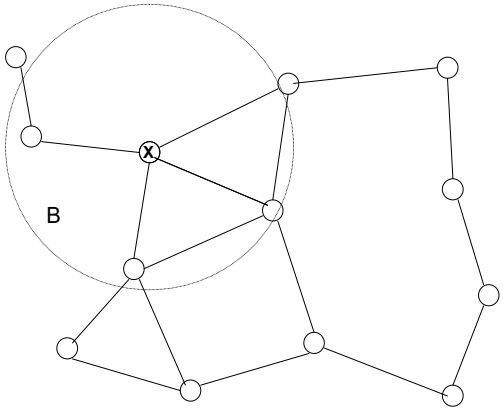

Figure 8. *Algorithm 2, steps a,b: The circle B around the centre x*

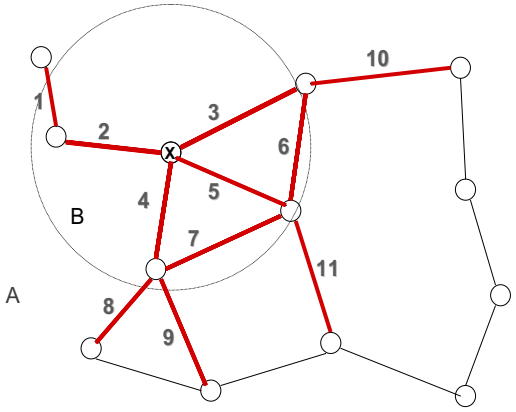

Figure 9. *Algorithm 2, steps c,d: The set A and the different allocations*

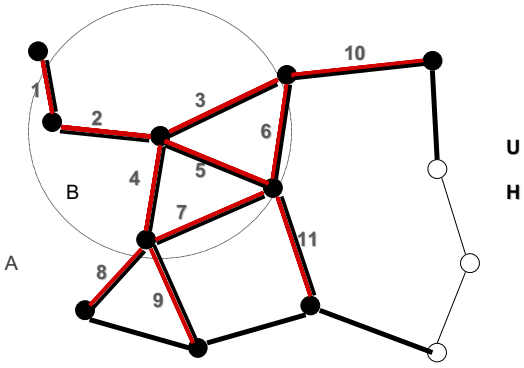

Figure 10. *Algorithm 2, steps e,f: The sets U and H*

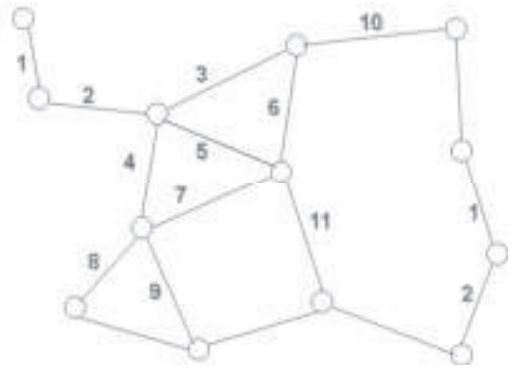

Figure 11. *Algorithm 2, results for first run of Algorithm CEA*

Figure 12. *Algorithm 2, results for second run of CEA*

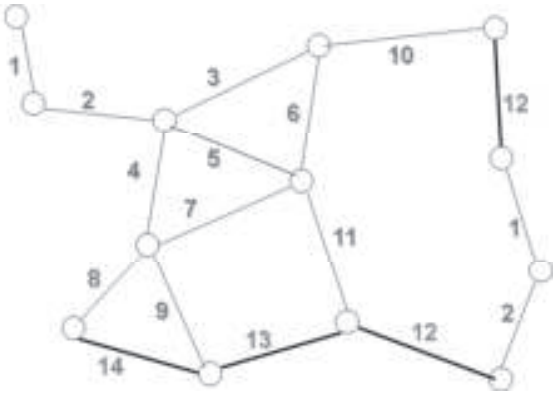

Figure 13. *Result of Algorithm 2 : Union of results of all CEA*

6. SUMMARY

The paper is focused on time, frequency and space resource allocations in WMN and defines the separation order of a system. The main contribution of the paper is in presenting algorithms, based on graph theory, that provide solutions to frequency and time resource allocations that can be used in various ways in OFDMA WMN.

As previously mentioned, the results of the algorithm can be used in several ways: One option allocates the same elements set of the form *{time, band}* to the edges of all the vertices with the same colour. Another option allocates the same combination of time slot and band, *{time, band}*, to all vertices coloured with the same colour, while their edges share the same set of sub-bands, for transmissions directed from the vertices to their neighbours. Therefore, each colour presents a different combination of a time slot and a band. Therefore, the first options sets pairs *{time, band}* to the edges, while the second option sets pairs *{time, sub-band}* to the edges of the graph. In both cases the pairs stand for the *elements.*

Note that each edge can be used to transfer to both directions, but not in the same time slot or not using the same band. Thus it should be allocated by two different elements. Therefore, regard every element *f* of the resulting algorithms, as a pair of elements *(f, f ')*, one for each direction of the edge.

Although Example (E1), on the first algorithm, results in the optimal solution for the graph of the example, these two algorithms are not necessarily optimal, but they result in a small number λ_{TF} of combinations of time slots and frequencies, i.e. a small number of pairs of the form *(time, frequency)*.

7. REFERENCES

[1] F. Akyildiz, X. Wanga, "Survey on Wireless Mesh Networks", **IEEE Radio Communications**, Sept. 2005.

[2] Ö. Oyman, J.N. Laneman, S. Sandhu, "Multihop Relaying for Broadband Wireless Mesh Networks: From Theory to Practice", **IEEE Communications Magazine**, Nov. 2007.

[3] D. Niyato, E. Hossain, "Radio resource management in MIMO-OFDM based wireless infrastructure mesh networks: Issues and approaches", **IEEE Communications Magazine**, vol. 45, No. 11, Nov. 2007, pp. 100-107.

[4] A. Reichman, A. Czylwik, "Broadband wireless mesh networks", **IEEE COMCAS 2011**, Nov. 2011.

[5] T.R. Jensen, B. Toft, **Graph coloring problems**, Wiley, 1994.

[6] R. Diestel, **Graph Theory**, Springer, 1991.

[7] T.H. Cormen, C.E. Leiserson, R.L Rivest, **Introduction to algorithms**, MIT Press, Cambridge, Massachusetts and McGraw-Hill, London, 1994.

[8] K. Karakayali, J.H. Kang, M. Kodialam, K. Balachandran, "Cross-Layer Optimization for OFDMA-Based Wireless Mesh Backhaul Networks", **IEEE Wireless Communications and Networking Conference,** March 2007, pp. 276 – 281.

[9] S. H. Ali, K. Lee, V.C.M. Leung, "Dynamic resource allocation in OFDMA wireless metropolitan area networks", **[Radio Resource Management and Protocol Engineering for IEEE 802.16], IEEE Wireless Communications, v**ol.14, No. 1, Feb. 2007, pp. 6 – 13.

[10] K. Thulasiraman, P., X, Shen, "Interference Aware Subcarrier Assignment for Throughput Maximization in OFDMA Wireless Relay Mesh Networks", **IEEE International Conference on Communications**, June 2009, pp. 1 – 6.

[11] M.R. Garey, D.S. Johnson, **Computers and intractability, a guide to the theory of NP-completeness**, San Francisco: W.H. Freeman and Company, 1979.

[12] A. Reichman , M. Priesler(Moreno), A. Czylwik, "Time and Frequency Resource Allocation in OFDMA Wireless Mesh Networks", **The 17th International OFDM Workshop (InOWo'12)**, Aug. 2012.

New Universally CAD System Usable Data Objects for Buildings, based on Universal Design and Required Spaces for Human Activities

The Design of Ergonomic and Economical Buildings can transform from Handicap Accessible towards Handicap Livable

Markku J. Rossi
Dept. of Electrical Engineering and Information Technology
Mikkeli University of Applied Sciences Ltd.
Mikkeli , Finland
markku.rossi@mamk.fi

Abstract—**The present design rules for designing the internal spaces for buildings taking into account Human Activities are very varied and can lead to insufficient spaces or economic losses related to over dimensioning. Three dimensional design objects for buildings have been mainly developed only for *stationary* furniture and appliances so that they can be used as Data Components in CAD systems. We propose that after measuring the 3D spaces (envelopes of volumes required) required for Human Activities such as washing a wheel chair patient in the shower the 3D Activity Spaces are transformed into 3D IFC Data Objects that can then be imported to the majority of the leading CAD systems related to designing buildings. The new Data Objects can then be fit to the internal spaces of the Handicap Accessible buildings. They answer the question " How much space is needed for Handicapped related activities ? ". We can achieve the optimal balance between the Universal Design functionality and the building cost. International co-operation in needed in specifying the series of movements for the activities by Health Care experts.**

Keywords-Universal Design; CAD systems; design rules; buildings; construction; 3D spaces; human activities; handicapped

I. INTRODUCTION

The CAD systems and wider Building Information Modeling (BIM) systems are quite efficiently used when designing all mechanical and electrical aspects of buildings both in construction and facilities. These include also the Building Services such as heating, ventilation, air conditioning, cooling, electrical systems and building automation. There are tens of CAD product families in wide usage and the three dominant CAD ecosystems have a high combined market share. In the UK in 2011, the three most sold 3D BIM systems had a combined market share of 65%. The CAD systems produce tens of different file formats for the designs. The conversion between the various formats and system versions has been a rather non-trivial task. Recently there has however been progress in interoperability related to 3D Data Objects representing e.g. appliances, mechanical building components and furniture. The standard ISO/PAS 16739:2005 describes so called IFC Objects (Industry Foundation Classes) [1]. The IFC specification is clustered by schemas (logical packages) of subsets of the information model and it is published as HTML based online documentation.

The IFC objects are supported by a large amount of CAD systems. The Tekla Corporation and its software product Tekla Structures supports the IFC standard [2] . The product both imports and exports IFC in .IFC and .xml file formats. In addition to Tekla, over 30 vendors of CAD systems support IFC.

Universal Design produces buildings and environments that are accessible to both people without and with disabilities. In the Health Care sector these design principles have been presented in the concept of Activities of Daily Living (ADLs). The new Data Objects proposed by us bring these design principles directly to the work environment of designing buildings. The Design for All concept (DfA) has the same principles than the Universal Design. In some countries, these activities are related to the term Barrier-free.

The problem formulation is a consequence of the co-operation between our University and the Finnish construction industry. The Construction Company U.Lipsanen Oy brought to our attention that more development is needed to get usable tools related to Universal Design and ADLs to the designers. The University responded with a solution after an internal invention report from a principal lecturer was analyzed and found to describe a new idea to solve the severe quality problem sometimes encountered in designs.

The Aalto University has published a thorough analysis and recommendations about the dimensioning and functionality of bathrooms suitable for residents that are using

mobility aids [5]. They present 2D simulated motion diagrams. There are however no links to CAD systems. The lists of matters that should be taken into account and the literature reference list of this publication are excellent sources of information for developing functionalities for CAD systems.

The Housing Finance Development Centre of Finland runs an electronic service providing regulations and recommendations for Universal Design related to Construction. First the inhabitant type is selected. The inhabitant can have one or several of the possible limitations. Then the room type of the building is selected. After this the service lists the relevant regulations and recommendations from five major domestic sources [6]. The service language is only Finnish at the moment.

II. THE PROCESS OF GENERATING NEW TYPE OF IFC DATA OBJECTS

The environment that defines the Needed Space for Activity includes the patient, the nurse or the caretaker and the equipment needed for the activity. The series of motions of the patient, the nurse and the equipment could be professionally designed by Health Care specialists.

The series of motions selected can be dependent of the physical abilities of the patient and of the nurse. It can also be dependent of the height of the persons and the weight of the persons. It is also dependent of the type of equipment needed. In the shower the external dimensions and the functionality of the wheelchair affect the optimal motions as well as the auxiliary equipment available in the shower. This leads to a need to specify professionally several alternatives of the series of motions, leading to a family of motion specifications for each activity. Because of several alternatives, there should be information related to the statistical probability of the occurrence of each alternative, preferably country by country. This probability would then be used for selecting the alternative most suitable to the construction design at hand. If the cost allows, the alternative simply with the largest dimensions can be selected.

The measurements for each alternative for each action can be conducted with stereo video camera equipment or with laser scanners of with both. Before this the motions of the activity have been specified so that the repeatability of the movements later based on following the specification is close to 100%.

The methodology of creating 3D models from photos taken from different angles around the subject is well known [3]. In this case three cameras at the directions of the three rectangular space dimensions are able to capture the motion envelope with a frame rate of only 2 frames per second.

The University developed a software concept in the beginning of 2012 for transforming 3D image files into IFC Objects that fulfill the IFC specification. Test transformations were performed and the generated IFC Objects worked the right way when having been imported to a CAD system.

During September 2013 the University starts a work package involving our ICT B.Econ. students for developing a software package for archiving laboratory videos, for finding the extreme dimensions of the videoed movement either automatically or semi-automatically, and for transforming the 3D objects related to the extreme space requirements into IFC objects.

A more recent technology, laser scanning is also viable for capturing motion envelopes. A modern laser scanner weighs only about 1.2 kilograms and measures up to distances of 30 m. The National Taiwan University used a combination of a scanner and a stereo camera to map buildings from inside [4]. The resolution of a typical indoor laser sensor is just enough for mapping also activity envelopes. The best scanning resolution available is typically of the order 30 millimeters. The persons cannot however be closer than 2 meters from the scanner during the measurement.

The differences of the new, proposed design process and the current design process can be seen from Figures 1 and 2.

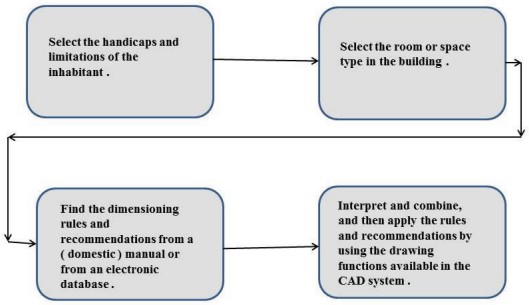

Figure 1. The current design process. Figure 2. The new design process.

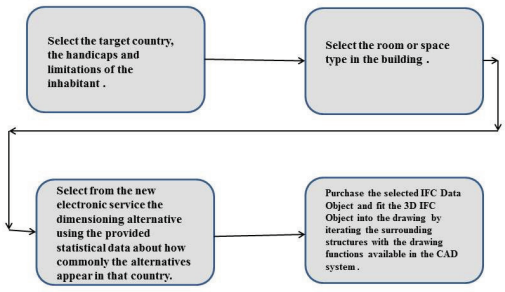

After the detailed 3D envelope of the activity has been calculated by the camera or scanner related software, it is also possible to simplify the surface by matching a combination of rectangular boxes and cylinders to the volume. The original surface details are not necessary when dimensioning the space of a room.

III. Ease of Use and Effectiveness

The work of interpreting the literary rules and recommendations, and integrating them into one set of rules and then applying them to the 3D structure under design can need a lot of effort at the moment. When testing the ARVI service [6], a case involving an inhabitant that uses a wheeled walker or rollator and when the room to be designed is the bathroom brought 86 hits to corresponding design rules and recommendations. It takes several hours for a typical designer to generate a combined design rule set from this kind of collection of rules.

We studied the effects of our new method to the work of architects by interviewing nine key architects in Finland. It appeared that the studies in Universal Design had been rather limited, less than 6 study weeks, at the Finnish Universities at least during the 70's. Many architects had developed their skills in Universal Design further after their graduation. The architects estimated that 60% of the architects that perform Universal Design do not remember the rule sets by heart, but refer to documentation. After a design has been released, over 50% of the designs have to be later revised because of accessibility reasons. The most interesting finding was that they estimated the level of efficiency increase in usage of work time to be 11 %. This gives a good ground to our commercialization efforts.

When comparing to the new IFC Data Object based design process the old one consumes more of designer's time. The rules interpretation phase can now be avoided and the cost of the ready IFC Object will be less than the time required for the rule interpretation would cost.

IV. Future Developments and Market Issues

The single, initial new IFC Objects correspond to one activity, one country and one set of dimensions of the involved persons and equipment. When the service company has accumulated a large number of IFC objects the combining of the activity cases can begin. An example of such a combination would be e.g. dressing of winter clothing and performing certain medical procedures in the same part of a room. This creates a large number of activity combinations but this is not a problem in the data management sense. The IFC Object can even show the required 3D spaces corresponding to different activities in different colors when the object is imported to the drawing and designing function of the CAD system. The University has plans to discuss with international partners to design a process that collects and actively promotes the generation of motion specifications of activities from different countries. When we will have a collection of specifications for the same action there is a possibility to head towards finding an international best practice for the action. When the best practice set of motions has been reached for an action, the dimensioning can still be country specific, but now depend only of the distribution of physical dimensions of the people in a particular country.

An important aspect would be to use only authoritative health care experts when specifying the motions. The building of a multinational process for this is a topic of new international research projects.

Our current project " Commercialization research for Value Add Data " mapped the nature of potential customers for collections of IFC objects. We took into account that not every registered designer is in business at the moment. From the interviews of the Finnish architects we got an estimate what proportion of designers are designing buildings that have requirements in Universal Design. In the market area Europe and Turkey we ended up to the following number estimates of potential customers :

- BA and B.Sc. level architects and engineers 315 000
- MA level architects 126 000
- Interior designers and industrial designers 2 000
- Building and construction companies with their own internal design departments 1 800 .

In addition, from the market area USA, Canada and Japan we recognized 286 000 potential customers.

Our common design process description was verified and completed by architect Asko Takala of Sivèn & Takala. The architects use hand drawn sketches, 2D views and 3D views. Once the design is in a CAD system, various types of presentations of the designs can be easily generated. We concluded that also 2D drawing objects representing the space required for human activities are necessary as well. It is straightforward to generate 2D versions of the 3D drawing objects.

The research topic at the moment is the best practices of marketing to these customer groups. The project will run until February 2014.

V. Intellectual Property

The corresponding Patent Application describing the design system has been filed by our University to the National Board of Patents and Registration of Finland in March 2013. An extension of the protection to the major markets is possible by the resources of a probable new service company. The University is interested in discuss-

ing with organizations that want to develop the commercialization of the concept.

The considered copy protection method of the IFC Objects is based on delivering the objects as parts of an executable file. The documentation asks to install the package to the particular workstation it will be used in. The program then finds out hardware or OS license specific information about the workstation. Then the pre-encrypted IFC object is further encrypted by using the workstation specific data as encryption keys. When the object is read from memory, it activates a two-phase decryption algorithm that returns the original IFC object to the CAD software. If the file is called with another computer, the keys are not right and the IFC file is not decrypted correctly.

ACKNOWLEDGEMENTS

The writer wishes to thank Mr. Matti Lipsanen of U.Lipsanen Oy for bringing the problem into our attention. I also thank our principal lecturer, Mr. Jukka-Pekka Selin for generating an internal invention report of the activity based 3D IFC Object principle. I also wish to thank the following architects for telling us estimations about the effects to the efficiency of the work processes : Marta Bordas Eddy (Tampere University of Technology / TUT) , Anna Helamaa (TUT) , Laura Mattila (Brunow & Maunula) , Tanja Röyhkiö (Puroplan) , Jonas Sillman (Sillman Digital) , Pirjo Sipiläinen (City of Helsinki) , Asko Takala (Sivèn & Takala) , Sampo Vallius (ARA) and Ira Verma (Aalto University) . This work was made possible by the funding of the European Regional Development Fund (ERDF) and TEKES (the Finnish Funding Agency for Technology and Innovation). The associated research project for commercialization is related to the ERDF activities of the region of South Savo in Finland.

REFERENCES

[1] International Organization for Standardization, "Abstract of Industry Foundation Classes (IFC2x) Platform Specification, in "Standards Catalogue", Electronic Publication, http://www.iso.org/iso/iso_catalogue/catalogue_tc/catalogue_detail.htm?csnumber=38056, accessed in November 2012.

[2] "Tekla Structures", in Tekla BIM Software. Electronic Publication, http://www.tekla.com/international/products/tekla-structures/Pages/Default.aspx , accessed in November 2012.

[3] M. Goesele et al. , "Multi-View Stereo for Community Photo Collections," , Proceedings of ICCV 2007, Rio de Janeiro, Brasil, October 14-20, 2007. 8 pp.

[4] K-H. Lin et al., "Mapping and localization in 3D Environments Using a 2D Laser Scanner and a Stereo Camera ", in Journal of Information Science and Engineering, Vol. 28, pp. 131-144, 2012.

[5] P. Sipiläinen, " Demands on dwellings for the elderly in home care ", PhD Dissertation, Aalto University, Department of Architecture, in Finnish, 176 pp. , ISBN 978-952-60-4225-1 , 2011.

[6] The Housing Finance Development Centre of Finland, " ARVI Database ", Electronic Service, at http://www.arvi.enef.net/ , in Finnish, accessed in December 2012. The username is arvi and the password is not required.

Computational Analysis of the 2415-3S Airfoil Aerodynamic Performance

Luis Velazquez-Araque[1] and Jiří Nožička[2]

[1]Department of Mechanical Engineering
National University of Táchira, San Cristóbal 5001, Venezuela
[2] Department of Mechanical Engineering
Czech Technical University in Prague, Prague 16607, Czech Republic

ABSTRACT

This paper deals with the numerical simulation of the two-dimensional, incompressible, steady air flow past an airfoil for a solar powered unmanned aerial vehicle (UAV) with internal propulsion system. This airfoil results from a NACA 2415 four digits family base airfoil modification [7] and has a propulsive outlet with the shape of a step on the suction surface. The analysis involved the airfoil's aerodynamic performance which meant obtaining lift, drag and pitching moment coefficient curves as a function of the angle of attack (AOA) for the condition where the engine of the UAV is turned off called the gliding condition and also for the blowing propulsive condition by means computational fluid dynamics. The computational domain has been discretised using a structured mesh of 188 x 200 tetrahedral elements. The RNG k-ε model is utilized to describe the turbulent flow process as it was followed in [5]. The simulations were held at a Reynolds number of 300000. Results allowed obtaining lift and drag forces and pitching moment coefficient and also the location of the separation and reattachment points in some cases by means of the wall shear stress on the suction surface as well as velocity contours and streamlines for both conditions at different angles of attack, from 0 to 16 degrees with the smallest increment of 4 degrees. Finally, results from both cases were compared and the influence of the propulsive flow on the aerodynamic characteristics of the airfoil has been analysed turning out that it improves significantly the performance of the airfoil reaching values up to 1,8 times in terms of lift at high angles of attack.

Keywords - lift; drag; pitching moment; unmanned aerial vehicle; CFD.

1. AIRFOIL TESTED

The 2415-3S airfoil (Figure 1), has been previously designed for the solar UAV focusing on several parameters of common commercial UAV's manufactures such as total wingspan, weight, flight velocity and others. It comes from a NACA four digits family airfoil, the NACA 2415 (Figure 2) [4]. It has an abrupt step on the suction side, located at 30% of the chord from the leading edge. This step simulates the blowing propulsive outlet of the wing in normal flight conditions. Since solar panels must be placed on the wings, it is possible to see the large and almost flat area for placing them past the blowing outlet.

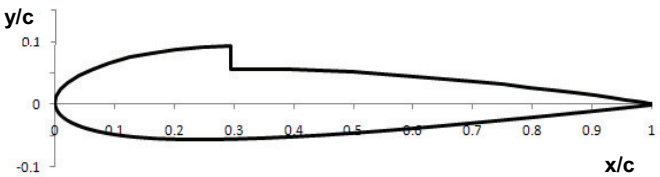

Figure 1. 2415-3S airfoil.

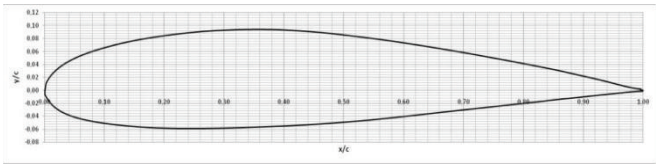

Figure 2. NACA 2415 airfoil.

2. COMPUTATIONAL DOMAIN

Something very important in this part is the choice of the domain, because it is formed by real borders such as the upper and lower surfaces of the airfoil and also by imaginary borders which enclose the external environment. The domain extends from 8 chord lengths upstream to 20 chord lengths downstream according to [1], an also 8 chord lengths for the upper and lower heights. The fluid flow simulated is air with a Reynolds number of 3.10^5. In Figure 3 it is possible to see the geometry of the domain for the 2415-3S airfoil.

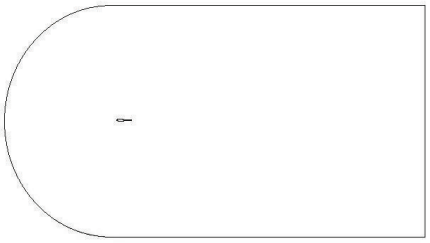

Figure 3. Computational domain for numerical simulations.

3. DISCRETIZATION OF THE DOMAIN

The geometry shown in Figure 3 is discretised using a structured mesh of 188 x 200 tetrahedral elements, this mesh has been also supplemented with very small elements in the vicinity of the surface of the airfoil forming a boundary layer with a grow factor of 1.2. References when creating the mesh were followed in [3], therefore the created mesh had a size change of 2.66 and an equisize skew of 0.348.

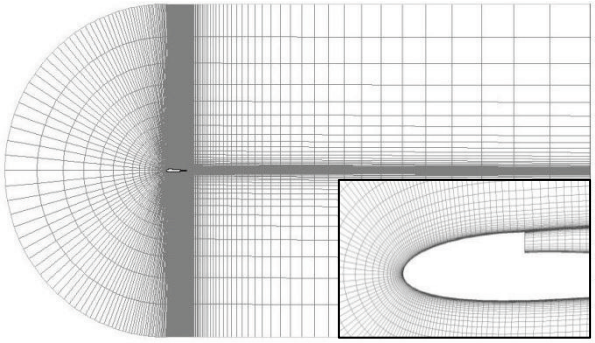

Figure 4. A mesh used for the numerical simulation.

The domain and the mesh were created using the commercial software GAMBIT, version 2.3. In order to obtain the lift and drag as a function angle of attack, single meshes were created for 0, 4, 8, 12 and 16 degrees and for every airfoil, thus there were created a total of 20 meshes (Figure 4).

Then, from the governing equations, the discretization of the domain and using the finite volume method based on finite elements, a discrete set of algebraic equations is set which solution is obtained as coupled, iteratively, using the commercial solver ANSYS FLUENT, version 12.0 using a scheme of second order upwind.

4. TURBULENCE MODEL

The *k-ε* model is derived from the Navier-Stokes equations and it is one of the simplest complete models of turbulence with two-equation models in which the solution of two separate transport equations allows the turbulent velocity and length scales to be independently determined. The standard *k-ε* model in ANSYS FLUENT falls within this class of models and has become very used for practical engineering flow calculations. It is a semi-empirical model. It is robust, economic, and presents reasonable accuracy for a wide range of turbulent flows. The chosen turbulence model was the RNG *k-ε*. The RNG (renormalization group theory) is an improvement of this model of turbulence because it provides an analytically derived differential formula for effective viscosity that accounts for low-Reynolds-number effects. Therefore it is more accurate and reliable for a wider class of flows.

5. BOUNDARY CONDITIONS

At the inlet it is specified the air absolute velocity magnitude and also its components; in this case the velocity is parallel to the horizontal axis, therefore it does not have any component in the ordinates. Concerning turbulence, it was also specified the turbulence intensity of 1,3 % in accordance to [2] and also the turbulent length scale. The upper and lower surfaces of the airfoil are set as walls. At the outlet it is specified the pressure as the atmospheric pressure. For the lateral walls of the domain they are set as symmetry.

6. GOVERNING EQUATIONS

Since this problem does not involve heat transfer nor compressibility the equation for energy conservation is not required, therefore the most important equations such as conservation of mass, momentum and the RNG *k-ε* turbulence model equations are used.

7. RESULTS AND ANALYSIS

Gliding Condition

In Figures 5 – 8, it is possible to see numerical lift coefficient (C_L) versus AOA, drag coefficient (C_D) versus AOA, C_L versus C_D and pitching moment coefficient (C_m) versus AOA for the 2415-3S airfoil for the condition where there is not flow through the blowing outlet. Curves from the original NACA 2415 airfoil have been included from [5] for further comparisons.

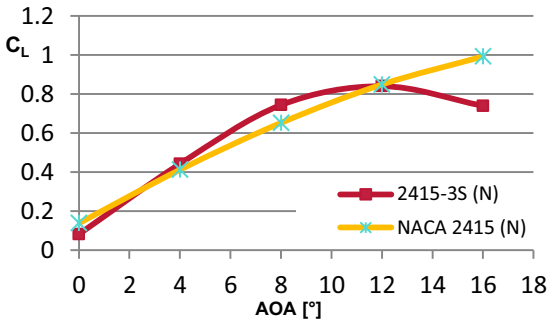

Figure. 5. Numerical lift coefficient for 2415-3S and NACA 2415 airfoils.

Concerning lift coefficient shown in Figure. 5, it can be observed the lift slope presented by the 2415-3S airfoil which was simulated at a Reynolds number of 310528 for a flow velocity of 20m/s, the stall region starts at 8 degrees of AOA with a stall point of C_L = 0,84 at 12 degrees of AOA, it is clear that the stall region starts at a lower AOA since the NACA 2415 presents the beginning of the stall region at 15 degrees. This airfoil at these conditions also presents higher values of C_L compared to the NACA 2415 between 4 and 12 degrees of AOA.

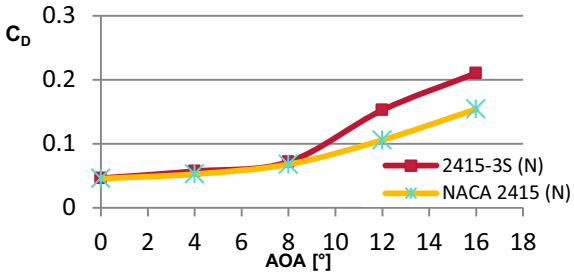

Figure 6. Numerical drag coefficient for 2415-3S and NACA 2415 airfoils.

In Figure 6 above, it is possible to see that the drag coefficient observed in the 2415-3S airfoil approaches to values similar to the NACA 2415 for AOA between 0 and 8 degrees. From this point, the values of drag coefficient increase rapidly. This behavior may indicate that the flow reattaches the airfoil surface after the step until 8 degrees of AOA, however this will be confirmed with the wall shear stress charts and streamlines which will be analyzed later. At 0 degrees of AOA both airfoils present a similar value of C_D around 0,05.

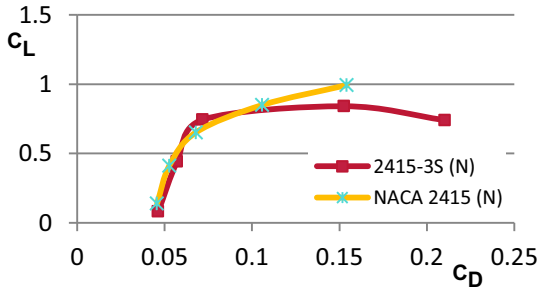

Figure 7. Numerical polar graph for 2415-3S and NACA 2415 airfoils.

The polar diagram shown in Figure 7 indicates that the airfoil 2415-3S has a good aerodynamic performance since it is very similar to NACA's 2415 from 0 to 10 degrees of AOA, however this performance decreases at high angles of attack, specifically from 10 degrees.

Concerning pitching moment coefficient at the leading edge, results shown in Figure 8 indicate that values of the 2415-3S airfoil present discrepancies but the behavior in general is similar to NACA's 2415 airfoil until 12 degrees of angle of attack.

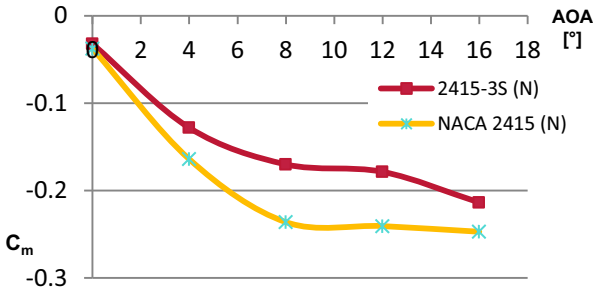

Figure 8. Numerical pitching moment coefficient for 2415-3S and NACA 2415 airfoils.

In Figure 9, it is possible to see the numerical wall shear stress on the suction surface along the chord line for the 2415-3S airfoil for the gliding condition; these images allow observing points of separation and reattachment of the flow. A shear stress is applied parallel or tangential to a face of a material. Any real fluids (liquids and gases included) moving along a solid surface will incur a shear stress on that surface. That is the reason why the wall shear stress is considered an indicative of separation of flow because when it is equal to zero, it means that the flow is not attached to the surface of the airfoil [6]. After this point, values of shear stress are different of zero and the separation region begins. In the case of reattachment of flow, it is noticed when the values of wall shear stress reach zero again, and the area between these two points is the separation region, in this region, the values of wall shear stress are negative, this can be seen if only the x-component of the wall shear stress is plotted but for a better observation, it was decided to plot the resultant wall shear stress, where all values are always positive.

It can be seen that the flow detaches at the location of the step at all AOA excepting at 16 degrees where the flow detaches before the step at 23 percent of the chord. At 0 and 4 degrees of AOA the flow reattaches after the step at locations of 56 and 62,5 percent of the chord, respetively. At 12 and 16 degrees of AOA the flow does not reattach to the surface of the 2415-3S airfoil.

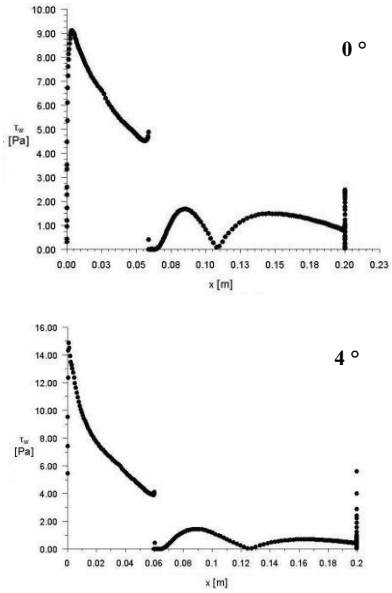

Figure 9. Wall shear stress of the 2415-3S airfoil at gliding condition for different AOA.

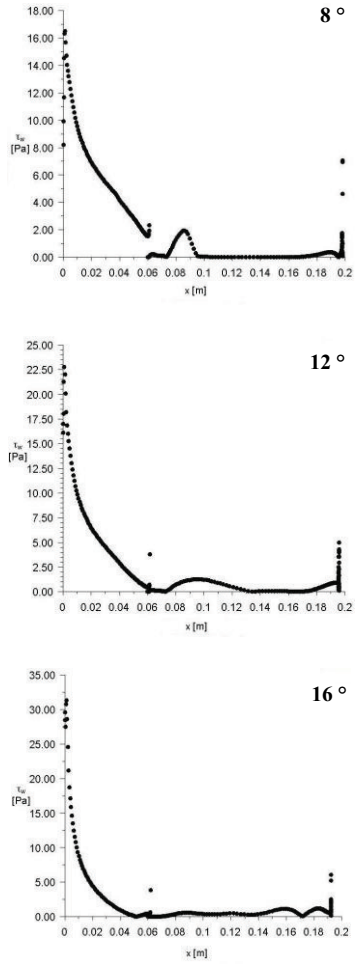

Figure 9. Wall shear stress of the 2415-3S airfoil at gliding condition for different AOA.

In Figure 10 it is possible to observe the flow field as velocity contours of the air flow past the 2415-3S airfoil. This is the first numerical graphical approach to the behavior of the air flow past the airfoil tested. Here it is observable the velocity changes in the selected domain; in our case the most important is to observe this phenomenon near the surface of the model. However these pictures do not show clearly the separation and reattachment points.

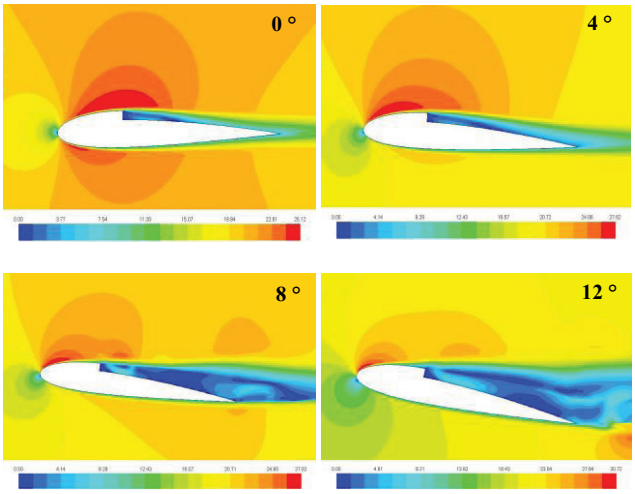

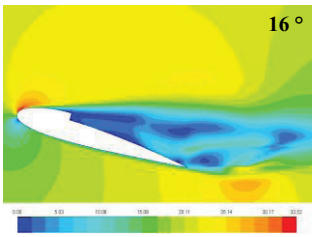

Figure 10. Velocity contours of the 2415-3S airfoil at gliding condition for different AOA.

Observing the flow fields for all AOA in Figure 10, it is possible to notice that for 8 degrees of AOA within the separation region, zones of high velocity which may indicate the presence of vortices due to the turbulence provoked by the high velocity of the flow and the sudden change in the geometry of the airfoil. This phenomenon will be observed in more detail below when analyzing the streamlines.

In Figure 11, it is possible to see the streamlines of the flow past the 2415-3S airfoil.

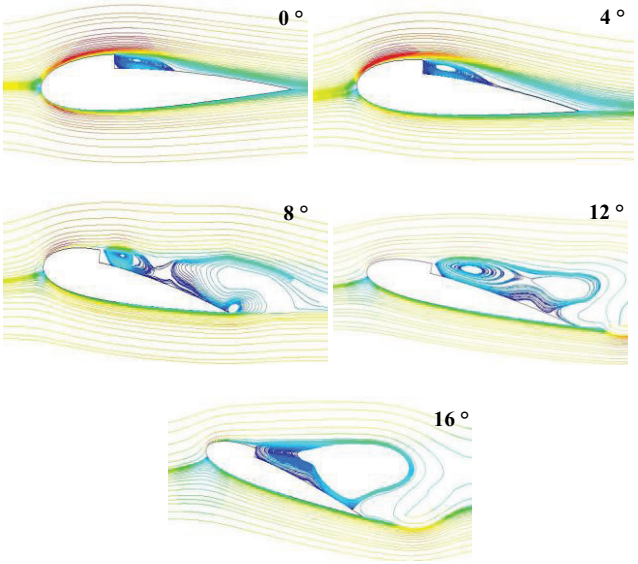

Figure 11. Streamlines of the 2415-3S airfoil at gliding condition for different AOA.

In Figure 11, it is observed that the flow is fully attached to the suction surface of the airfoil until the step where separation of flow occurs. This phenomenon occurs for almost all AOA. The spatial extension of the separation region can be detected by exploring the wall shear stress along the surface of the airfoil (Figure 9). Inside this region, it is possible to observe that the adverse pressure gradient causes a reversed flow and this becomes into a counter-rotating vortex. Then the flow reattaches again and remains in contact with the surface until the trailing edge, this reattachment was observed from 0 to 4 degrees of AOA. At 8 and 12 degrees of angle of attack, the flow does not reattach to the surface but in this case two vortices appear within the separation region due to the turbulences provoked by the high velocity of the flow. At 16 degrees of AOA, the separation region is huge but in this case it begins at certain distance before the step.

Propulsive Condition

In order to develop the new numerical simulation involving the blowing scenario, only one boundary condition was changed and it was the step which was not set as "wall" anymore but as "velocity inlet" and the value of this parameter was introduced as normal to the boundary, the introduced value was 30 m/s.

In Figures 12 - 15, it is possible to see numerical C_L versus AOA, C_D versus AOA, C_L versus C_D and C_m versus AOA for the 2415-3S airfoil for the condition where air at a velocity of 30 m/s flows through the blowing outlet. Previous curves of the 2415-3S for the gliding condition and curves of the original NACA 2415 airfoil have been included for further comparisons.

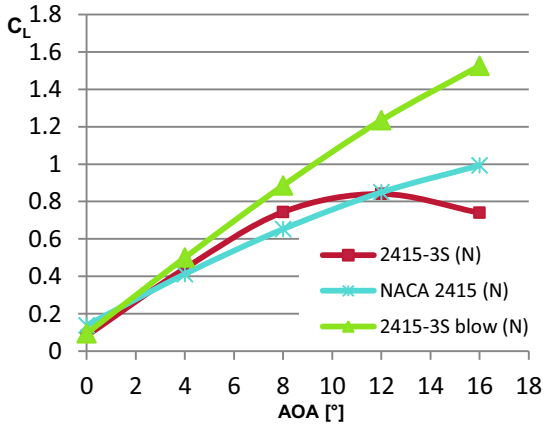

Figure 12. Numerical lift coefficient for 2415-3S airfoil for blowing and gliding conditions and NACA 2415 airfoil.

In Figure 12, the values of the lift coefficient for the 2415-3S at this new condition are similar to the ones for the gliding condition at very low angles of attack up to 4 degrees but from this point, the C_L increases rapidly and progressively with a higher slope and reaching values up to 1,5 times bigger than the original NACA 2415. The lift curve does not present a stall region in the range of studied angles of attack, what makes think that the flow is very attached to the surface of the airfoil for AOA even higher than 16 degrees. However this will be discussed when analyzing the wall shear stress graphs and streamlines.

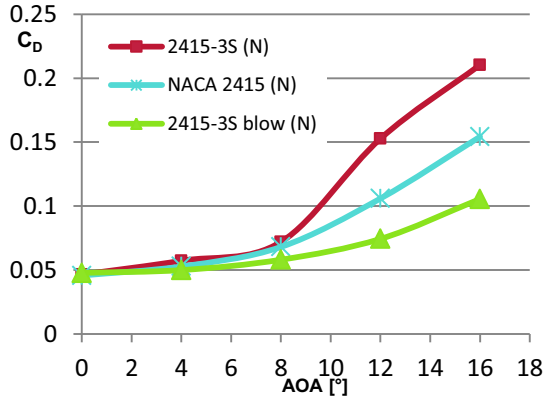

Figure 13. Numerical drag coefficient for 2415-3S airfoil for blowing and gliding conditions and NACA 2415 airfoil.

Concerning drag coefficient, shown in Figure 13, it is possible to see that values of C_D are low and similar for all cases at low angles of attack until 7 degrees, after this point the drag of the 2415-3S at the gliding condition increases rapidly and the drag of the original NACA 2415 does so but moderately. The C_D of the 2415-3S at the blowing condition increases as well but very moderately less that all other cases reaching a maximum of 0,1055 at the highest AOA, this indicates that the air blowing through the outlet does not exert a big influence on the drag

because the flow seems to be attached at every moment to the surface of the airfoil.

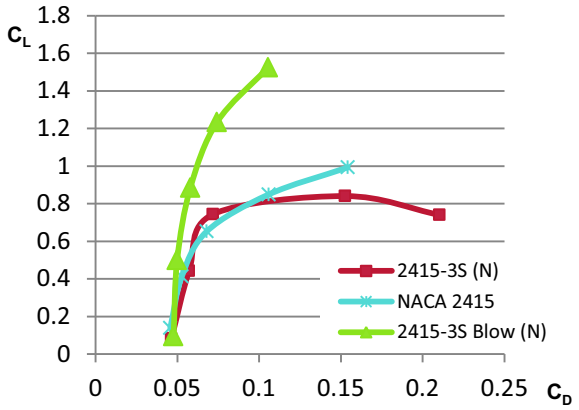

Figure 14. Numerical polar graph for 2415-3S airfoil for blowing and gliding conditions and NACA 2415 airfoil.

The polar graph shown in Figure 14 summarizes all the aspects previously observed in Figures 12 and 13. It is clear that the effect of blowing maximizes the aerodynamic performance of the airfoil and it can be seen in the polar curve for the 2415-3S which is completely concave, also for low angles of attack it is almost vertical, which indicates that the drag does not vary very much and the lift increases rapidly. Being the original NACA's 2415 aerodynamic performance the main goal during the modification of the airfoil, it has been greatly improved by the blowing effect.

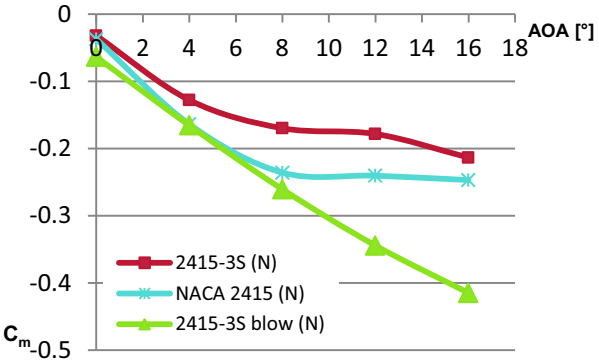

Figure 15. Numerical pitching moment coefficient for 2415-3S airfoil for blowing and gliding conditions and NACA 2415 airfoil.

Concerning pitching moment coefficient at the leading edge, results shown in Figure 15 indicate that the C_m for the 2415-3S at the blowing condition increases almost directly proportional to the angle of attack. Comparing to the NACA 2415 airfoil the behaviour is similar until 8 degrees of AOA where it stabilizes and the other still increases reaching a maximum of 0,415 in magnitude at 16 degrees of angle of attack.

In Figure 16, it is possible to see the numerical wall shear stress on the suction surface along the chord line for the 2415-3S airfoil under the blowing condition; these images allow observing points of separation and reattachment of the flow. It can be observed, according to the wall shear stress behaviour that the flow never detaches from the surface of the airfoil at any tested angle of attack, there is not present any separation region and high values of AOA could be reached without stalling. However it is important to note some aspects; the initial value of the wall shear stress at the leading edge, which is high and then decreases towards the location of the blowing outlet where a sudden rise is present in this point because of the flow through the outlet, reaching much higher values and then it decreases towards the trailing edge. Besides, the initial value of the wall shear stress at the leading edge increases with the angle of attack while the behavior after the step remains constant no matter the AOA.

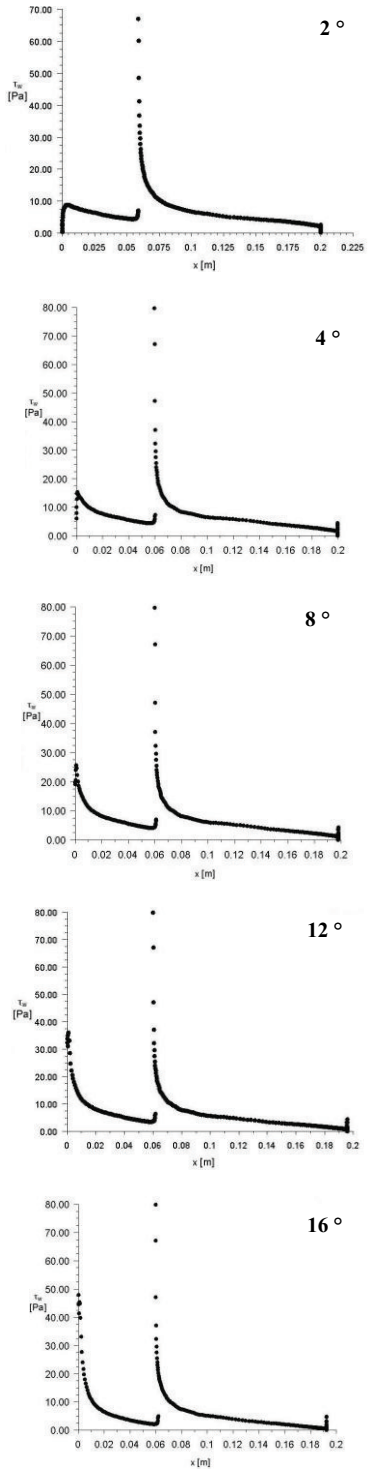

Figure 16. Wall shear stress of the 2415-3S airfoil at blowing condition for different AOA.

In Figure 17, it is possible to observe the flow field as velocity contours of the air flow past the 2415-3S airfoil under the blowing condition.

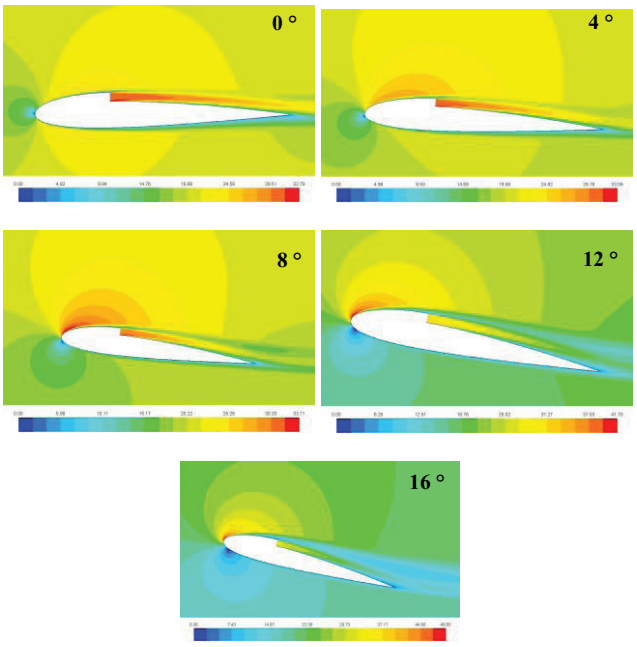

Figure 17. Velocity contours of the 2415-3S airfoil at blowing condition for different AOA.

Comparing the flow fields obtained for the blowing scenario in Figure 17 to the ones obtained for the gliding condition, it is possible to see the zone of highest velocity just next to the boundary called "blowing", and this is the locus of the propulsion. No presence of regions with a velocity of 0 m/s besides the stagnation point at the leading edge, therefore no regions of separation were observed at any angle of attack.

In Figure 18, it is possible to see the streamlines of the flow past the 2415-3S airfoil under the blowing condition.

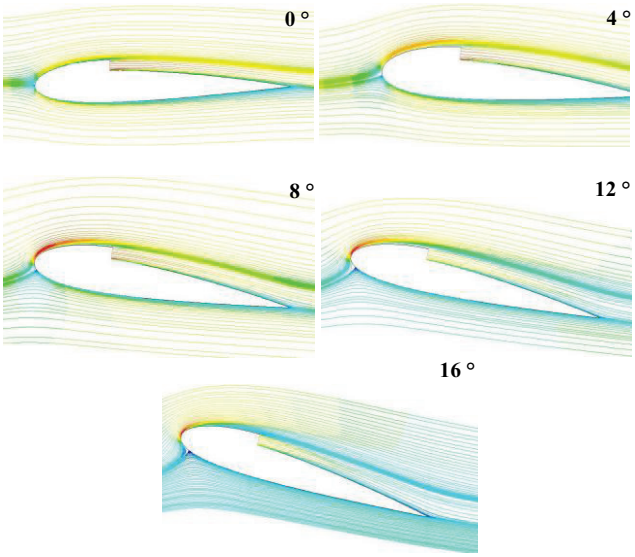

Figure 18. Streamlines of the 2415-3S airfoil at blowing condition for different AOA.

Concerning streamlines, it is possible to observe in Figure 18 the flow along the airfoil for the blowing scenario, where these ones look very well distributed, now next to the blowing outlet, streamlines are fully attached to the upper surface until the trailing edge, filling all the spots which are formed when there is not flow through the outlet. No vortices are present. Streamlines look parallel to the surface at every angle of attack, which helps to believe that much higher AOA's can be reached without approaching to the stall condition.

8. CONCLUSION

By means of the use of CFD it has been possible to obtain lift, drag and pitching moment coefficients and also the flow field of air past a new designed airfoil, the 2415-3S. It was also possible to obtain the location of separation and reattachment points in some cases for different angles of attack. Two conditions (gliding and propulsive) were analyzed through an exhaustive comparison, turning out that the aerodynamic performance of the airfoil increases at the blowing propulsive condition reaching values up to 1,8 times in terms of lift at high angles of attack.

9. REFERENCES

[1] Malan P., Suluksna K., Juntasaro E., Calibrating the γ-Re_θ Transition Model for Commercial CFD, in *The 47th AIAA Aerospace Sciences Meeting, 2009.*

[2] Nožička J., http://profily.fs.cvut.cz/, Laboratory of Department of Fluid Dynamics and Power Engineering of the CTU in Prague. Section Airfoils and Straight Blade Cascades.

[3] Rhie C.M., Chow W.L., Numerical Study of the Turbulent Flow Past an Airfoil with Trailing Edge Separation, *AIAA Journal*, Vol. 21, No. 11, 1983.

[4] Selig M.S., Lyon C.A., Giguere P., Ninham C., Guglielmo J.J., *Summary of Low-Speed Airfoil Data*, Vol. 2, Viginia Beach, SoarTech Publications, 1996.

[5] Rhie C.M., Chow W.L., Numerical Study of the Turbulent Flow Past an Airfoil with Trailing Edge Separation, *AIAA Journal*, Vol. 21, No. 11, 1983.

[6] Velazquez L., Nožička J., Numerical Simulation of the Fluid Flow past an Airfoil for an Unmanned Aerial Vehicle, in *The 22nd International Symposium on Transport Phenomena*. Delft, the Netherlands, 2011.

[7] Velazquez L., Nožička J, Kulhanek R., Oil and Smoke Flow Visualization past Two-Dimensional Airfoils for an Unmanned Aerial Vehicle, in *The 11th Asian Symposium of Visualization*. Niigata, Japan. 2011.

[8] Velazquez L., Nožička J., Vavřín J., Experimental Measurement of the Aerodynamic Characteristics of Two-Dimensional Airfoils for an Unmanned Aerial Vehicle, in *Experimental Fluid Mechanics 2010*. Liberec, 2010.

Emerging Trends, Technologies and Approaches Impacting Innovation

Dr. R. Cherinka, Dr. R. Miller, and Mr. J. Prezzama
The MITRE Corporation
4830 W. Kennedy Blvd., Tampa, FL 33609
Phone: 813-287-9457, Fax: 813-287-9540
rdc@mitre.org, drbob@widomaker.com, prezzama@mitre.org

ABSTRACT

As federal agencies seek innovative IT solutions to meet business demands, they face complex challenges. They must overcome organizational barriers, ensure their strategic technology delivers real value, and remain compliant with evolving standards and regulations. They need strategic technology investments and innovative solutions that are practical, measurable and achievable. Technology advances in cloud computing, social media/networking, mobility and information management are all evolving at a rapid pace. These technological trends, taken together, offer unprecedented access to information, people and even group sentiment, offering new ways to collaborate, connect producers to consumers to investors, and ultimately to innovate. With the specific emergence of social computing, an explosion of open innovation can be seen through the combination of gamification with crowdsourcing. This paper presents a study of approaches to foster open innovation, including the use of crowds and social media for continuous innovation. Specific examples are presented to highlight their use in "real world" environments and provide an assessment of applicability and challenges for implementation in large organizations.

Keywords: Innovation, Social Computing, Crowdsourcing, Crowdfunding, Gamification

1. INTRODUCTION

This paper presents a study of approaches to foster open innovation, including the use of crowds and social media for continuous innovation. Emerging trends and technologies that will have an impact on open innovation are introduced, as well as an examination of a brief evolution of innovation to understand attributes and patterns for its success and/or failure. The paper highlights specific examples of their use in "real world" environments and provides an assessment of applicability and challenges for implementation in large organizations.

With the emergence of social computing, an explosion of open innovation can be seen through the combination of gamification with crowdsourcing [6]. Within this combination, innovative applications use emergent game play rather that scripted play. Emergent games define the rules of play but not the outcome, allowing "players" to discover or invent solutions. Prediction markets are used to help scope solutions. We examine a number of recent examples that offer promising results, and can be considered as reference implementations for new business and/or acquisition models.

2. BACKGROUND

There are many sources in literature to study innovation and approaches that attempt to spark or recreate it on a continuous basis for success in business. Simply stated, innovation is about making a significant positive change [1]. Although Innovation stems from many sources, there are essentially six general patterns into which these sources tend to fall:

- *Hard work in a specific direction*: innovations come from dedicated people in a field working hard to solve a problem.
- *Hard work with direction change*: similar to above, but an unexpected opportunity emerges midway through the work.
- *Curiosity*: bright minds following their personal interests.
- *Wealth*: many innovations are driven by the quest for treasure.
- *Necessity*: driven by individuals in need of something they could not find otherwise.
- *Combination*: many innovations stem from any combination of the above.

There are also several challenges to innovation, related to idea generation and solution development, sponsorships and funding, scalability, customer outreach, competition and timeliness.

Understanding these patterns and challenges will help organizations to better prepare for considering new approaches to open innovation, and promoting a culture of awareness for creativity.

3. EMERGING TRENDS AND TECHNOLOGIES

New forces that are not easily controlled by information technology (IT) are pushing themselves to the forefront of IT spending [16]. Specifically, the forces of cloud computing, social media/networking, mobility, unified communications (UC), convergence and bring your own device (BYOD), and information management are all evolving at a rapid pace [10]. This evolution is largely happening despite the controls that IT normally places on the use of technologies [3]. The cloud offers new delivery styles and options that are industrialized in a value chain in which IT is only one part of that delivery. Social computing allows collaboration and a shift of behavioral patterns of users and the communities in which they work. Mobility offers new access channeled to applications and data and, at the same time, provides end users with a wide variety of choices of devices. UC is not necessarily a single tool, but a set of products that provides a consistent and unified user interface and user experience across multiple devices and media types, thereby enhancing collaboration opportunities. Finally, the concept of big data begins to forever alter the relationship of technology to information consumption. This can be seen as data, now coming from multiple federated sources and in both structured and unstructured forms, which must now be analyzed using new methodologies foreign to many IT departments. As Professor Jeff DeGraff of Michigan's Ross School of Business, and the executive director of the Innovatrium Institute for Technology once said, "Innovation has moved from an individual, organizational sport to a federation sport [10]."

It is important to understand the impact of this nexus of forces on the innovation process. These trends offer unprecedented access to information and people, offering new ways to collaborate, connect producers to consumers to investors, and ultimately to innovate.

4. APPROACHES TO INNOVATION

Approaches to innovation and its evolution throughout time has been studied and discussed throughout literature [26]. In his discussion of Innovation Models, Tidd discusses the five generations of

- *Linear*: need pull by existing markets and technology/process push, being the first two generations
- *Coupling*: producer/consumer interaction with cooperative feedback
- *Parallel*: supply chain linkages and consumer alliances
- *Network*: integration of systems and markets

Each of these models seeks to address the "sources of discontinuity" that is both the source and result of innovation. These include introduction of new technologies, creation of tipping points in public opinion and social attitudes, shifts in policy and regulation, emergence of new business models, and disruption resulting from unpredictable events. Each of these also may fail to address adequately these sources, the result being that innovation is thwarted or established organizations are blindsided. For example, in the Network model, parochial influences such as culture, education, economics and policy can limit the potential for innovation.

In this paper, we focus on new and/or emerging techniques, a potential sixth generation, that start to provide an example of evolution toward more open and continuous innovation. Some of these are highlighted below.

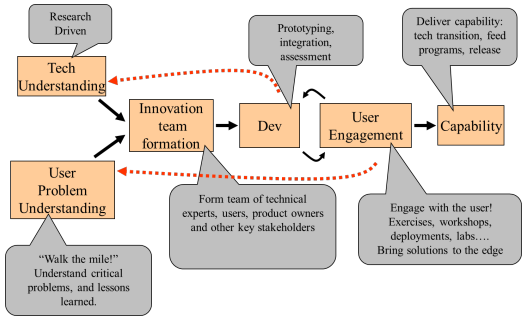

Figure 1. Agile Innovation Cycle with User Engagement

Agile Engineering Innovation Teams: Agile engineering attempts to spark innovation in the development of products or services [4]. The core principles of agile engineering present the notion of smaller time-boxed events, and the use of teams that contained diverse skills and represent all stakeholders associated with the problem at hand. As shown in Figure 1, this process relies heavily on a continuous agile cycle of plan-develop-feedback based on incremental prototyping and delivery [14]. The diversity of the innovation team is key to this approach, and often as a result, new ideas emerge from the users as they become engaged throughout this cycle.

Open Experimentation Events: Another approach that is becoming more popular with Government customers is to promote innovation with frequent and continuous engagement with users/customers of the product being developed. Some key variants of this approach include:

- *User-driven Field Experimentation*: Realistic Field exercises and test events that allow developers to have users operate and evaluate potential products.
- *User workshops*: Lighter-weight exploratory events that are "realistic enough" to set the proper context for developers and users to evaluate new research opportunities.
- *Multi-party engineering user engagements*: A formal evaluation and product acceptance event performed in conjunction with agile engineering processes.
- *Developer Environments and Testbeds*: Open integration and test environments that identify established standards and interfaces, and provide a common infrastructure to allow 3rd party developers to perform pre-integration of new capabilities.
- *Storyboarding and "Rock Drill" Brainstorming*: Open sessions between users, developers and project leaders using storyboarding and other brainstorming techniques to help define concepts and requirements.

Open Marketplaces: An outgrowth of the developer's testbed, the open marketplace provides a more comprehensive environment for developers to build capabilities in accordance with standards and platform requirements, and make them available through the marketplace for consumers to obtain and use. The "appstores" for mobile applications and desktop widgets are good examples.

In our experience, we have seen these techniques applied in a variety of large government projects with promising results. As a result, Government acquisition policies and processes are changing as open and continuous innovation and agile acquisition becomes the norm. With the increasing popularity and pervasive use of social computing, new approaches for innovation will continue to evolve and shape new ways of conducting business.

5. SOCIAL MEDIA AND CROWDS FOR CONTINUOUS INNOVATION

Social media is a means to an end, not the end itself. Social media enables mass collaboration, in which large and diverse groups of people who may have no preexisting connections pursue a mutual purpose that creates value [2]. Such a group is known as a collaborative community. It is through communities built around mass collaboration that allows an organization or project to enlist the interests, knowledge, talent and experience of everyone along its value chain, to create results that exceed those possible using traditional processes and small-group collaboration techniques.

In order for mass collaboration to be an effective tool, there are three key components that need to be effectively used together:

- *Social Media*: social media is an online environment created for the purpose of mass collaboration.
- *Community*: Communities are collections of individuals who come together to pursue a common purpose.
- *Purpose*: Purpose is what draws people together into a community.

Effectively, community is the people who collaborate, social media is how they communicate, and the purpose is why they communicate. At its heart, continuous innovation is about transforming ideas into products. As customers interact with those products, they generate feedback and data. The feedback is both qualitative (such as what they like and don't like) and quantitative (such as how many people use it and find it valuable). The products can be considered experiments; where the knowledge gained by the organization through these experiments is used to promote, influence and reshape future successful innovations and business models.

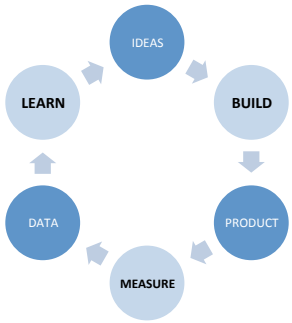

Figure 2. Build-Measure-Learn Loop

This innovation model can be simply visualized as a three-step process, depicted in Figure 2 [17]. The goal is to minimize the total time it takes to traverse this process.

Using this model, successful innovation teams must be structured correctly in order to succeed. Venture-backed and bootstrapped startups naturally have some of these structural attributes as a consequence of being small and

independent. For this to work in most organizations, however requires support from senior management to create the appropriate structures, based on several key attributes: scarce but secure resources, independent authority and autonomy to develop business opportunities, and a personal stake in the outcome.

It is also important to establish a platform for open experimentation. This platform should establish ground rules under which autonomous innovators can operate; how to protect the parent organization, how to hold entrepreneurial managers accountable, and how to reintegrate innovation back into the parent organization if it is successful. This *sandbox* for innovation should follow some key principles:

- Any team can create a true split-test experiment that affects only the sandboxed parts of a product or service.
- One team must see the whole experiment through from beginning to end.
- No experiment can run longer that a specified amount of time.
- No experiment can affect more than a specified number of customers.
- Every experiment has to be evaluated on the basis of a single standard of actionable metrics.
- Every team that works inside the sandbox and every product built must use the same metrics to evaluate success.
- Any team that creates an experiment must monitor the metrics and customer reactions while the experiment is in progress and abort or adapt as necessary.

Both developers and customers would work together in partnership in the sandbox, implementing the *build-measure-learn* loop through small iterations. Doing this continuously helps to cultivate an innovative culture throughout the organization and its partners.

The sandbox also needs to evolve into "ideagoras" or marketplaces for ideas, innovations, and for creative people to contribute [19]. This creates the crowdsourcing model that taps into millions of creative innovators, matching them to investors and customers. This allows organizations to "crowd-source" ideas – outsourcing difficult or lengthy tasks to the crowd, which can complete them more efficiently and cheaply than an in-house solution. "Crowd sourcing is the act of taking a job traditionally performed by a designated agent (usually an employee) and outsourcing it to an undefined, generally large group of people in the form of an open call [11]."

There are several ways to help define the crowdsourcing model beginning with crowd funding. This is the practice of on line "micro-lending" where entities can contribute small sums of money toward a common goal. Next is crowd wisdom. This can be thought of as on-line brainstorming events. Crowd creation is the third component. This can be seen in the open source development environment, where a problem is broken down into small manageable pieces, and the community utilizes spare cycles to solve the problem. Finally crowd voting is the idea of using the opinions of the masses to help define a particular course of action. Google takes this approach with their deployment of "Search" and the way their results are ranked [18].

Another dimension impacting innovation is the realization that creative people (aka. "Right brainers") need to be part of this continuous innovation. With the impact of an abundance of products, outsourcing of logical production of products to Asia, and the automation of redundant processes, it is becoming more important for businesses to find a competitive edge in order to innovate. Creativity is the key to gaining that edge [15]. For that reason, there is an ongoing movement to integrate the Arts and Design disciplines with STEM, thus promoting "STEAM" across Academia and Industry.

There are many examples of approaches based on social media, crowdsourcing and gamification that are starting to emerge. Some of these are highlighted below.

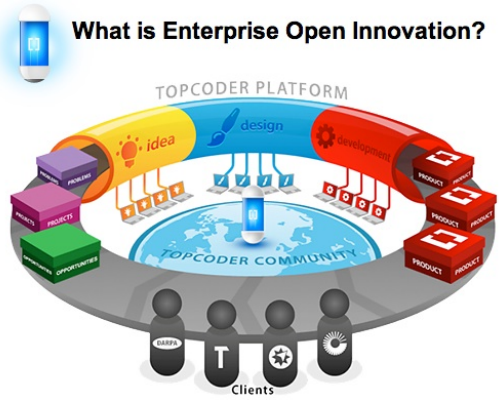

Figure 3. Topcoder Model

Topcoder: The "Topcoder" model, depicted in Figure 3 is based on users and/or investors publishing a need, challenge or problem that has to be addressed, and use crowdsourcing along with games/challenges to motivate creative and talented people to identify innovative solutions [21].

Kickstarter: The "Kickstarter" model is based on allowing individuals or groups with an innovative or creative idea

to post that idea as a project by creating a business/project plan, and use crowdsourcing to motivate investors (or anyone) to fund a project [9].

The major funding platform at the moment is Kickstarter [13]. Since it launched in April 2009, over 2.5 million people have used it to pledge over $389 million in funding for more than 74,000 creative projects. Of that, $333 million has gone to projects that met their targets and were ultimately successful.

Kickstarter is an all-or-nothing, no equity funding site. Innovators set a target for funding - be that $10 or $10,000,000 - and have to raise at least that much, or get nothing. The 'no equity' clause means that those who pledge money via Kickstarter do not get any share of the company. If the project fails, funders get nothing. If it succeeds, funders received the benefits originally specified by the project creator. This is done by setting up funding tiers of $1, $5, $10 and so on. Once a donor passes a tier, he or she gets the benefits associated with that tier. What Kickstarter doesn't allow is for users to get either a profit, or a share of the project they're funding.

Industry Collaboration Portals: This approach uses web-based collaboration platforms to create an environment for matching users to subject matter experts for the purpose of answering questions, brainstorming on challenging problems and sharing information about a topic of interest. The MITRE Industry Portals on Cloud Computing and Cyber Security are good examples [22].

Figure 4. Government use of competitions

Competitions and games to advance research or acquisition: An effective way to motivate crowds of innovators is to provide a challenging game or competition to achieve results. Similar to use of challenges in the Topcoder example, competitions themselves are an effective technique for maturing state-of-art research or for doing down-selects in an acquisition process. Figure 4 illustrates the Defense Advanced Research Projects Agency (DARPA) Grand Challenge, an experimental robotics competition used to further research in autonomous vehicles [7]. It also illustrates the Robotics Rodeo, a competition used by the United States Government Department of Defense to evaluate robotics solutions as a down-select process for awarding new contracts to vendors [12].

6. COMPLEXITY AND ARCHITECTURE

The forces of cloud computing, social media/networking, mobility and information management resulting in innovation that we see in the crowdsourcing model is typically being impressed upon systems that exhibit high levels of complexity. Complex systems are all evolving at a rapid pace. The cloud offers new delivery styles and options that are industrialized in a value chain in which IT is only one part of that delivery. Social computing allows collaboration and a shift of behavioral patterns of users and the communities in which they work. Mobility offers new access channeled to applications and data and, at the same time, provides end users with a wide variety of choices of devices. Finally, those characterized as having unpredictable behavior, fluid requirements, multiple competing stakeholders, and are susceptible to external pressures that can cause change across the entire system [20]. Complex Systems are constantly changing. They respond and interact with their environments – each causing impact on (and inspiring change in) the other, usually through bottoms-up disruption, not top-down orchestration.

New architectural paradigms are needed to expose opportunities for as well as the results of innovation via crowdsourcing approaches. The normal views are Operational (Business), Service, Information, and Technical. But these views do not address Innovation. In Figure 6 we provide a notional Architectural representation of generating an Innovation View via capturing and describing a set of innovation attributes.

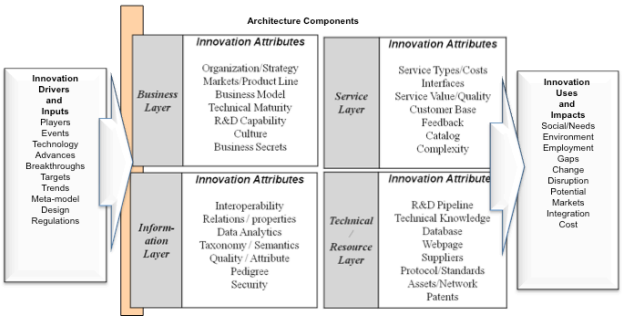

Figure 5. Notional Innovation View

An Innovation view would highlight those areas of the architecture that support (or are ripe for) innovation. The innovation view would also highlight how the architecture supports evolutionary aspects of the design.

7. CONCLUSIONS

Although emerging technologies and trends may be creating an environment conducive to innovation, there are several issues which can be seen as barriers to innovation becoming prevalent in today's society. First, is the need for more and better talent. Recent test scores and the number of graduates in science, technology engineering and mathematics (STEM), is not encouraging. [5] The students of today may not be prepared to be the innovators of tomorrow. Secondly, the availability of active research and development (R&D) programs in organizations can impede overall innovation. Finally, tied to the R&D "shortfall" is the actual availability of capital to fund innovation programs. As the US and many other countries cope with recession or other financial difficulties, innovation funding tends to be a lower priority [8]. For these reasons, it is even more important for organizations to look for creative and cost-effective ways to innovate.

This paper presents a study of several approaches to foster open innovation, including the use of crowds and social media for continuous innovation. It provides an assessment of applicability and challenges for implementation in large organizations. We have identified the most common barriers to true innovation as well as emerging technologies and trends which, we believe will fuel the spark of innovation in the near future. These technological trends, taken together, offer unprecedented access to information, people and even group sentiment, offering new ways to collaborate, connect producers to consumers to investors, and ultimately to innovate. We investigated the crowd-sourcing model and its potential value applied to commercial and government environments.

8. REFERENCES

[1] Berkun, S., *The Myths of Innovation*, O'Reilly Media, Inc., 2010.

[2] Bradley A. and M. McDonald, *The Social Organization*, Gartner, Inc., 2011.

[3] Cappuccio, D., *Ten Critical Trends and Technologies Impacting IT During the Next Five Years*, Gartner Symposium/ITxpo presentation, 21-25 October 2012.

[4] Cherinka, R. and R. Miller, *Agile Engineering of Scalable Enterprise-Level Capabilities*, World Multiconference on Systematics, Cybernetics and Informatics, 2008.

[5] Cherinka, P. Wahnish, J. Prezzama, *Fostering Partnerships between Industry and Academia to Promote STEM at the Secondary Educational Level, EEET Plenary Presentation, July 2012.*

[6] Cohen, L., *To the Point: Leverage the Power of the Collective Without Getting Lost in the Crowd*, Gartner Symposium/ITxpo presentation, 21-25 October 2012.

[7] DARPA, http://www.darpagrandchallenge.com/

[8] Davidson, John, Keystone Edge, , May 07, 2009, http://www.keystoneedge.com/features/jeffdegraff0507.aspx,

[9] Griliopoulos, D., *The Madness of Crowdfunding*, Maximum PC Magazine, pp 45-51, March 2013.

[10] Howard, C., *The Nexus of Forces Scenario*, Gartner Symposium/ITxpo presentation, 21-25 October 2012.

[11] Howe, Jeff, Crowdsourcing, *Why the Power of the Crowd is driving the Future*, http://www.crowdsourcing.com/.

[12] JIEDDO Robotics Rodeo Challenge, 2012, http://www.army.mil/article/83762/Robotics_Rodeo_highlights_advances_in_life_saving_technologies/

[13] www.kickstarter.com

[14] MITRE Technical Presentation, Warfighter Integration Technology Strategy, The MITRE Corporation, 2006.

[15] Pink, D., *A Whole New Mind*, Riverhead Books, Penguin Group Inc., 2006.

[16] Plummer, D., *Top Technology Predictions for 2013 and Beyond: Control Slips Away*, Gartner Symposium/ITxpo presentation, 21-25 October 2012.

[17] Ries, E., *The Lean Startup*, Crown Business, Crown Publishing, 2011.

[18] Sloane, P., *A Guide to Open Innovation and Crowdsourcing: Advice from Leading Experts*, Kogan Page Publishing, 2012

[19] Tapscott, D. and A. Williams, *Wikinomics*, Penguin Group Inc., 2008.

[20] Tidd, J., *Innovation Models*, Discussion Paper, Imperial College London, 2006.

[21] www.topcoder.com

[22] Metzger, Louis, MITRE Cloud Computing Portal, http://www.mitre.org/work/info_tech/cloud_computing/

The author's affiliation with The MITRE Corporation is provided for identification purposes only, and is not intended to convey or imply MITRE's concurrence with, or support for, the positions, opinions or viewpoints expressed by the author.

Two -Phase Partitioning Bioreactor for Anaerobic Biodegradation of High Spilled Crude Oil into Aqueous Media

Zainab Z. Ismail*
Department of Environmental Engineering, Baghdad University
Baghdad, Iraq

and

Ibtihaj A. Abdulrazzak
Ministry of Environment
Baghdad, Iraq

* Corresponding author (Z.Z. Ismail), Email: zismail9@gmail.com

ABSTRACT

A novel study was carried out to determine the potential of a Two Liquid Phase-Partitioning Bioreactor (TLPPB) inoculated with active mixed biomass to degrade high concentrations of crude oil in aqueous solution. Silicon oil was selected as the biocompatible solvent in contact with the aqueous-phase containing biomass. The performance of the two-liquid phase partitioning bioreactor (TLPPB) was evaluated under different initial concentrations of crude oil including 520, 1120, 2120, and 5290 mg /L. Complete biodegradation of crude oil was achieved within 15 days in this type of biphasic bioreactors. In comparison, the concentration of crude oil in a regular monophasic reactor dropped by 81% within 15 days, but remained incomplete for the duration of the experiments indicating that the organic phase, silicon oil significantly improved the process performance. This study confirms the potential of TLPPB for enhancing the transfer and subsequent biodegradation of immiscible crude oil in aqueous media.

Key words: Bioreactors, Crude oil, Biomass, Silicon oil, and Biodegradation.

1. INTRODUCTION

An extremely promising technology for the treatment of toxic organic contaminants has been developed based on the use of Two-Phase Partitioning Bioreactors (TPPBs) [1]. These TPPBs are especially interesting in such applications as they can enhance pollutant bioavailability to the microbial community [2]. Biodegradation of substituted phenols, VOC compounds, PAHs, xylene, butyl acetate, and other synthetic organic compounds were examined in TPPBs [3-5]. However, none of the previously reported studies related to TPPBs concerned of crude oil biodegradation. On the other hand, Oil pollution accidents are nowadays become a common phenomenon and have caused ecological and social catastrophes [6]. Beside accidental contamination of environment, the large amounts of oil sludge's generated in refineries from water oil separation systems pose severe problem because many of the treatment techniques are prohibitively expensive, or may be only partially effective [7]. The present study reports a new application of the biodegradation of crude oil using an aqueous-silicon oil two-phase system.

2. MATERIALS AND METHODS

Microorganism, culture media, and chemicals

A mixed culture collected from the bottom of an aeration basin at a local sewage treatment plant was acclimatized to crude oil. A high concentration of biomass was obtained by cultivating alicots (10 ml) of activated sludge samples in the rich culture media. This culture media contained 15 g/L peptone, 15 g/L prytone, and the mineral salt media (MSM) at pH 7.0. The composition of MSM (in mg/L) was $(NH_4)_2SO_4$ (100), K_2PO_4 (350), K_2HPO_4 (775), $MgSO_4$,$7H_2O$ (100), $CaCl_2$ (40), $FeSO_4$, $7H_2O$ (1), $MnSO_4$, H_2O (1), $NaMoO_4$ (0.21), NaCl (5000). All these chemicals were supplied as analytical reagent grade. Prior to use, the MSM were sterilized in an autoclave at 121°C for 30 min.

Crude oil samples were collected from a petroleum field in Basra city, Iraq. Silicon oil (Purity 99.99%) was obtained from Gainland Chemical Company, UK.

Culture conditions

Three different systems were used for the experiments: (1) the two-phase system contained silicon oil as the organic phase and the crude oil- contaminated aqueous phase with cultures suspension, (2) the cultures suspension in the oil-contaminated aqueous phase operated without an organic phase which were called one-phase and would highlight the potential of the two-phase process, (3) experiments operated as a two-phase system without culture (control system) to examine the possibility of crude oil reduction due to degradation, volatilization, and adsorption process.

Kinetic tests: single phase and two phases partitioning bioreactors

The biodegradation tests in this work were carried out in 500 mL-Erlenmeyer flasks as batch bioreactors. A set of 9 bioreactors were operated in this work, 4 reactors were operated as a monophasic system; each was filled with 450 ml of actual surface water collected from Tigris River as the aqueous phase. Four bioreactors were operated as a biphasic silicone oil/aqueous (1:2 v/v) system; each was filled with 300 ml of the actual surface water and 150 ml of silicon oil. Crude oil was alternatively provided at initial concentrations of 520, 1120, 2120, and 5290 mg/L respectively. The monophasic and biphasic reactors were then inoculated with 10 ml of enriched culture. The reactors were closed with rubber stoppers, and were magnetically stirred. The experiments were performed at 28±2ºC. A single reactor was operated as a biphasic reactor without cultures to examine the abiotic processes as mentioned in the previous section.

Monitoring of pH

The degradation of crude oil by microorganisms led to the production of acidic intermediates. This was confirmed by monitoring the pH every 24 h. However, extreme low pH conditions may inhibit the activity of the mixed cultures; accordingly adjustment of pH value to 7.0 was carried out in order to improve the overall effeciency of the process.

3. RESULTS AND DISSCUSION

Comparison of growth between biphasic and monophasic systems

Microbial growth was clearly detected in the inoculated reactors, with bacterial adhesion at the aqueous/organic interface being observed in the biphasic reactors. Lower growth rate was observed in the monophasic reactors for the entire experiment. Figs. 1 & 2 illustrate the SEM images for the biomass growth in the biphasic bioreactors before and after crude oil removal, respectively.

Kinetic tests

The presence of the silicon oil as the organic phase had a marked positive effect on the crude oil removal rate although almost similar crude oil concentrations profiles were observed for both, monophasic and biphasic bioreactors. However, complete crude oil degradation up to 100% in the two-liquid phase partitioning bioreactors (biphasic reactors) were observed

after 2 weeks regardless of the crude oil initial concentration.

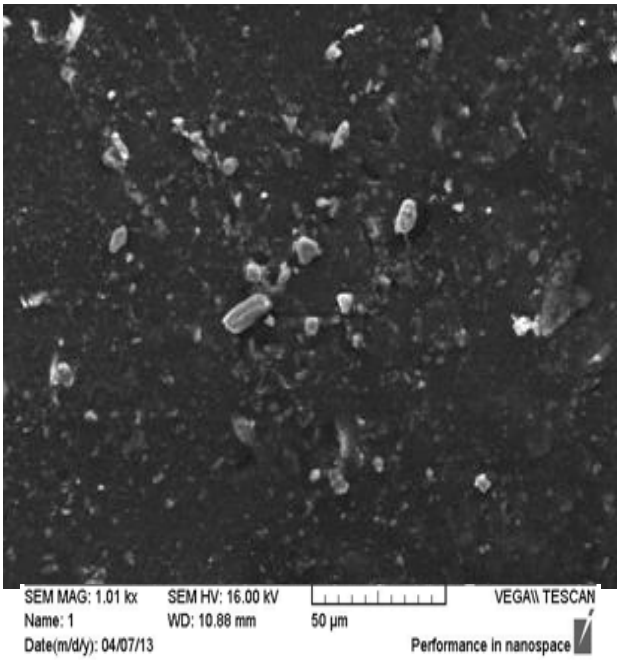

Fig. 1 SEM image for the biomass before crude oil removal in the biphasic bioreactor

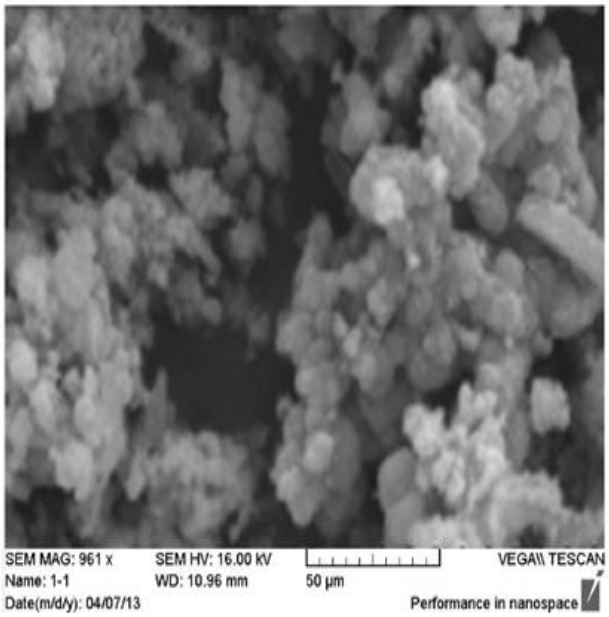

Fig. 2 SEM image for the biomass after crude oil removal in the biphasic bioreactor

In the monophasic bioreactors even after more than 6 weeks (data not shown graphically after 3weeks), the biodegradation of crude oil remained incomplete at the maximum of 80, 80, 85, and 95% for crude oil initial concentrations of 520, 1120, 2120, and 5290 mg /L, respectively (Figs. 3-6). These results indicate the role of silicon oil as the biocompatible solvent to enhance the biodegradation process of crude oil in aqueous media. Fig. 7 presents the biphasic bioreactors before and after the biotreatment and bio degradation of crude oil. However, results of the control reactor indicated the absence of abiotic processes effects since the concentration of crude oil remained constant.

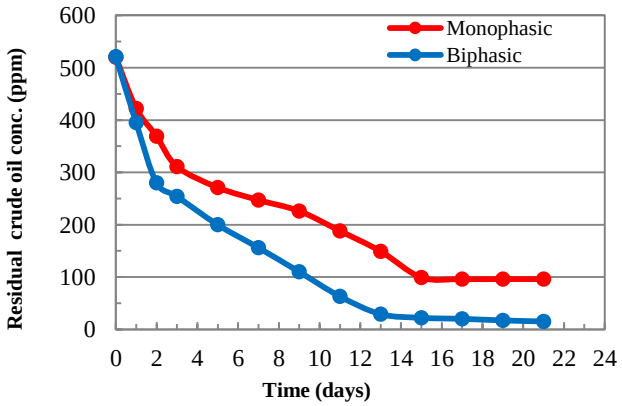

Fig. 3 Time plot of total remaining oil in monophasic and biphasic reactors at initial crude oil concentration of 520 ppm

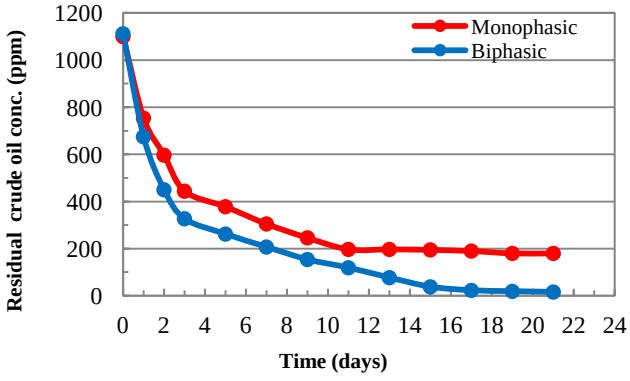

Fig. 4 Time plot of total remaining oil in monophasic and biphasic reactors at initial crude oil concentration of 1120 ppm

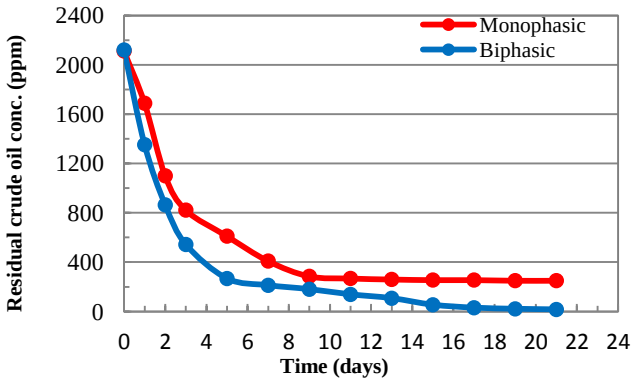

Fig. 5 Time plot of total remaining oil in monophasic and biphasic reactors at initial crude oil concentration of 2120 ppm

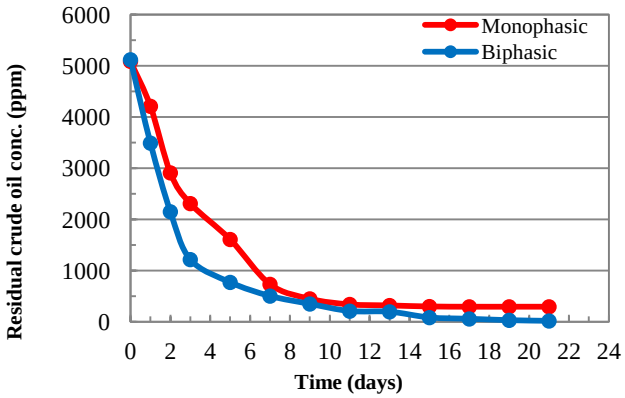

Fig. 6 Time plot of total remaining oil in monophasic and biphasic reactors at initial crude oil concentration of 5290 ppm

4. CONCLUSION

The biphasic aqueous-organic system effeciency has been demonstrated the complete biodegradation of crude oil up to 100% using mixed cultures. Experimental results revealed a promising method for the treatment of surface water contaminated with high concentrations of crude oil which could be released from accidental spills. The biphasic bioreactor significantly enhanced the biological removal rate of crude oil by continuous delivery of crude oil to microorganisms and reduced the inhibitory effect of crude oil on microorganisms.

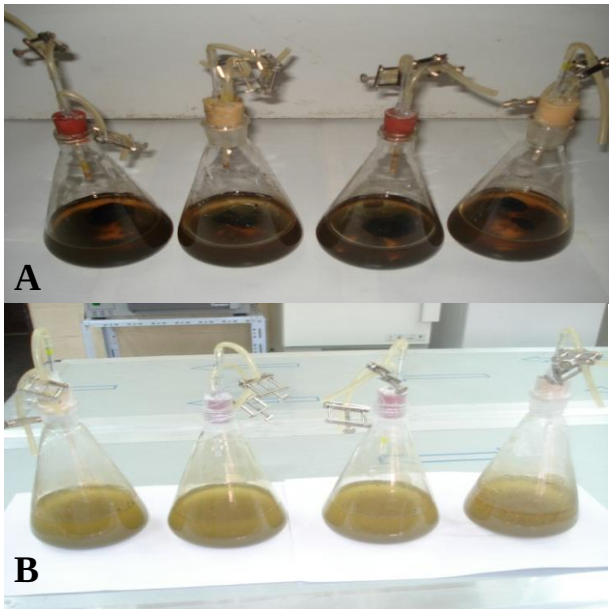

Fig. 7 Biphasic bioreactors, (A) before treatment, (B) after treatment

5. ACKNOWLEDGEMENT

This research was supported by the Ministry of Environment, Iraq.

6. REFERENCES

[1] A.J. Daugulis, "Two-phase partioniong bioreactors: a new technology platform for destroying xenobiotics" **Trends in Biotechnology**, Vol .19, 2001, pp. 457-462.

[2] R. Muñoz, S. Arriaga, S., Hernández, B. Guieysse, S. Revah, "Enhanced hexane biodegradation in a two phase partitioning bioreactor: Overcoming pollutant transport limitations", **Process Biochemistry**, Vol. 41, 2006, pp. 1614-1619.

[3] M.C. Tomei, S. Rita, D.M. Angelucci, M.C. Annesini, A.J. Daugulis, "Treatment of substituted phenol mixtures in single phase and two phase solid-liquid partitioning bioreactors", **Journal of Hazardous Materials**, Vol. 191, 2011, pp. 190-195.

[4] R-S. Juang, H-S. Kao, H-S, Z. Zhang, "A simplified dynamic model for the removal of toxic organics in a two-portioning bioreactor", **Separation and Purification Technology**, Vol. 90, 2012, pp. 213-220.

[5] R. Muñoz, E.I.H.H. Gan, M. Hernándze, G. Quijano, "Hexane biodegradation in two liquid-phase bioreactors: High performance operation based on the use of hydrophobic biomass", **Biochemical Engineering Journal**, Vol.70, 2013, pp. 9-16.

[6] K. Das, A.K. Mukherjee, "Crude-petroleum oil biodegradation effeciency of *Bacillus subtilis* and *Pseudomonas aeruginosa* strains isolated from a petroleum-oil contaminated soil from North- East India", **Bioresource Technology**, Vol. 98, 2007, pp. 1339-1345.

[7] N. Vasudevan, P. Rajaram, "Bioremediation of oil sludge contaminated soil", **Environment International**, Vol. 26, 2001, pp. 409-411.

Experimental Study on the Performance of a Fluid-Sloshing Type Energy Conversion System (FSECS)

Hsien Hua LEE

and

T.-Y. WU

Department of Marine Environment and Engineering, National Sun Yat-sen University
Kaohsiung, Taiwan 804

ABSTRACT

Recently, due to the dramatic requirement of petroleum from new developed countries, the price of crude oil reached skyrocketing height. Therefore, in this study, a new type of wave-energy converting system is developed and installed in an offshore platform structure to take the advantage of stronger motion of the platform subjected to waves. By utilizing the sloshing power of the fluid stored in an U-shape tube, the turbine of the electric power generator is driven and electricity can be generated. Some advantages are found from this system. Firstly, because the vibration in surge, heave and other motions of the platform induce the sloshing motion of fluid, the motion of the platform can be eased and the platform becomes more stable for the operation. Secondly, the power generated is a by-product of the platform operation, which aims to a self-content system for the power-supply in the platform. Thirdly, due to the simple structure and common material applied to the wave-converting system, the maintenance of the system is much easier compared to the others. From the testing results, it shows that with respect to various periods and amplitudes of the stroke in the experimental tests, the wave-power converting system can effectively generate electricity.

Key words: U-tube fluid-sloshing generator(UTPG), wave power conversion, actuator experiment, fluid-sloshing power generator (FSPG), fluid-sloshing power conversion system (FSPCS)

1. INTRODUCTION

As many developing countries rapidly emerged in the last two decades, the requirement for the supply of energy is more dramatic than ever. On the other hand, rapid increasing usage of the petroleum causes the green house effect and then the global warming as well so that natural caused disasters such as flooding, storming and deserting infertility induced from the rapid and large scale weather changes happened more often and caused larger casualties in last two decades. The storage of the petroleum is rapidly used up and yet, the requirement is continually increased more than ever. Searching for the substitution of petroleum is more intensive than ever now. Particularly, a recyclable, re-producible and more environmentally friendly energy or so-called green energy is under development in large scale [3].

An innovative idea by utilizing the sloshing power of liquid filled in a U-shape container to produce electric power is provided in this paper. Sloshing behavior of liquid in a pipe is similar to a flow that may quickly reverse its direction during alternate sloshing induced from tube vibration. Therefore, in this study a turbine system is selected due to its specialty that no matter which direction flow flows the turbine may maintain rotating in the same direction. This turbine system was developed by Gorlov and Darrieus [1, 2] for the power generator of sea flows or any flows that may change its direction. It was found that the efficiency of energy capture from the newly-developed turbine system is higher than traditional ones [5, 6].

After analysis, models of a U-tube sloshing-flow power converter were innovatively manufactured. A series of experimental tests were also designed and performed to obtain the influence of both dimensional parameters of the U-tube sloshing power converter and the environmental conditions. It is found from the experimental results that the newly developed system can successfully generate electricity. It is also found that parameters such as the amplitude and the period of the excitation of the U-tube that driving the flow-sloshing are closely related to the efficiency of the power converting system. The dimensional parameters of the U-tube flow-sloshing power converter must be carefully designed based on the application and environmental conditions.

2. THEORETICAL BASIS AND SYSTEM DESIGN

A typical U-tube is shown in Fig.1, of which the cross section of the tube can be any shape such as circular or square. Basic parameters of the U-tube will include the area of the

cross-section of the tube, the ratio between the height and the length of the tube and the water level filled in the tube. All of these parameters have influence on the performance of the U-tube system. It is assumed that the U-tube system is fixed on the main structure without any relative motions between them. When the main structure subjected to vibrations, the U-tube system will also shake along the structure in the same phase so that the water filled in the tube sloshes alternately along the U-tube while the water level is up and down in the vertical columns of the U-tube. It is noticed that the potential of the water varies alternately between two vertical columns when the water elevation of one column is over the other, respectively.

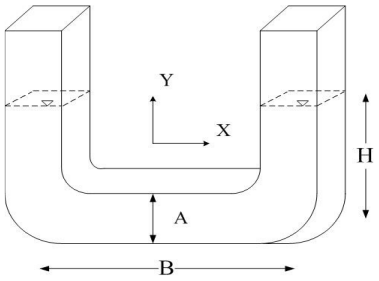

Fig. 1 A typical U-tube filled with liquid

Basic Theorems and Equation of Motion for Fluid in U-tube

As shown in Fig.1, the horizontal part of the tube between the center-line of vertical columns is B; the elevation of still liquid in the vertical column of the tube is H; the velocity and acceleration of fluid in the tube are $\dot{y}$ and $\ddot{y}$ respectively. The cross section area for the vertical column and the horizontal part of the U-tube are A_y and A_h respectively and a ratio between the vertical and horizontal cross section area is also defined as R. The horizontal velocity of the U-tube system induced by the motion of main structure is $\dot{x}$.

By applying Lagrange equation to the motion of the fluid in the U-tube when the fluid is driven by a horizontal velocity of the tube, the derivation to the fluid motion of kinetic energy and potential is written as

$$\frac{d}{dt}\left[\frac{\partial(P-U)}{\partial\dot{y}}\right]-\frac{\partial(P-U)}{\partial y}=Q \tag{1}$$

where the kinetic energy P from the fluid motion is defined as

$$P=2\left[\frac{1}{2}\rho A_v H(\dot{y}^2+\dot{x}^2)\right]+\rho A_h B\frac{(R\dot{y}+\dot{x})^2}{2} \tag{2}$$

and the potential energy U of the fluid is written as

$$U=\rho g A_v y^2 \tag{3}$$

It is also noticed that a non-conservative force Q the damping force exists when the fluid flows in the tube and it may be defined as

$$Q=-\frac{1}{2}\rho A_v h_d R^2|\dot{y}|\dot{y} \tag{4}$$

where h_d is the head loss coefficient of the fluid. Now the equation of motion of fluid in the tube is obtained from Lagrange equation [4, 7] through equation (2) and (3) as

$$\rho A_v[2H+B\cdot R]\ddot{y}+\frac{1}{2}\rho A_v h_d R^2|\dot{y}|\dot{y}+2\rho A_v g y=-\rho A_v B\ddot{x} \tag{5}$$

Design of the U-tube with Required Natural Frequency

Due to the fact that the best performance of a U-tube power generator is from a highest efficiency of energy capture from the rotation of the turbine, therefore to suit for various environments of the system, the very basic parameter of the system is the natural frequency and its relationship to the dimensional parameters. The frequency of the fluid f_w sloshing in a U-tube is obtained as

$$f_w=\sqrt{\frac{2g}{2H+B\cdot R}} \tag{6}$$

Based on the aspect of testing facilities such as the stroke and power of actuator system, the size of tank and stroke power of eventual testing for the practical application and some other limitations, the frequency of the U-tube with filled fluid of certain density is f_w =0.6Hz□0.66Hz and the testing period designed around the range of resonance is T=1.51sec□1.66sec.

3. EXPERIMENTAL MODEL AND TESTTING SET-UP

Turbine System Installed in A U-tube

According to pre-test analysis, several sets of turbine system were installed in a U-tube system, where the solidity ratio □ of the turbine area, number of turbines n and width of the turbine C are determined. A schematic view of the turbine and the generator device after its installation in a U-tube is shown in Fig.2.

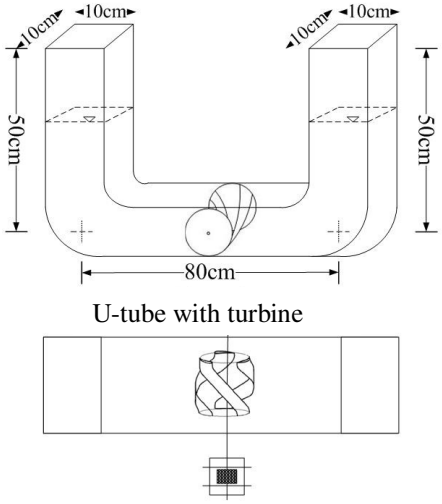

Fig. 2 Schematic view of turbine system installed in a U-tube (Lee and Wu 2009□

Experimental testing set-up

The test was performed in the structural testing lab, department of MEE, NSYSU, where a strong wall and strong floor system was in-built and additionally, an MTS hydraulic actuator of capability of 12 cm stroke and 30 Hz frequency along with signal amplifiers and data aquisition system were applied to the test.

Testing Parameters and Procedure

Parameters selected for the experimental test are basically the excitation amplitude induced from the stroke of actuator, period of the excitation and the natural frequency of the fluid that is determined from the relationship of fluid contained in the tube and the dimensional parameters of the tube as introduced in section 3. According to the parameters to be examined and their interrelations to be observed, totally 128 sets of tests were carried out in this part of experiment. Before performing the proposed sequence of the tests, a pre-testing run is necessary to re-correct the accuracy of measurement system.

3. EXPERIMENTAL RESULTS AND DISCUSSION

During the experimental test, the phenomenon to be investigated is analyzed through raw datum from data aquisition system. The phenomenon observed includes the velocity of flow, rotational speed of the turbine with and without the loading of power generator, the voltage, current and power rate generated by the generator. The parameters that may influence the results are set into various values, which include the solidity of turbine area, sloshing frequency of the fluid filled in the tube, the period and amplitude of excitation force.

Velocity of Fluid in the Tube without Generator Loading

Typical variation of the fluid flow in the U-tube during excitation is obtained and shown in Fig.3 and Fig.4, where due to sloshing motion, alternate velocity is observed. The maximum velocity of the flow can reach 2m/s. The sloshing flow is mostly in a stable vibrating pattern when the applied force to the U-tube system is a stable excitation. The influence of solidity of turbine area on the flow velocity is not positively related, but however, under same solidity of turbine area the rotational speed is positively related to the velocity of fluid flow.

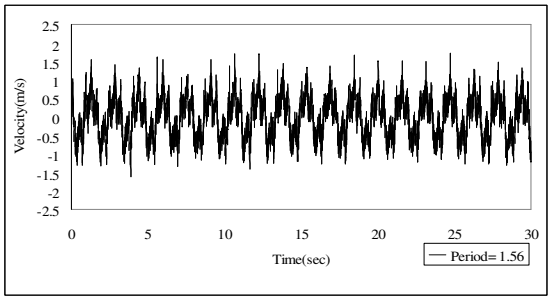

Fig. 3 Velocity of flow (T=1.56, solidity=0.3, amp.=90mm, f=0.66Hz)

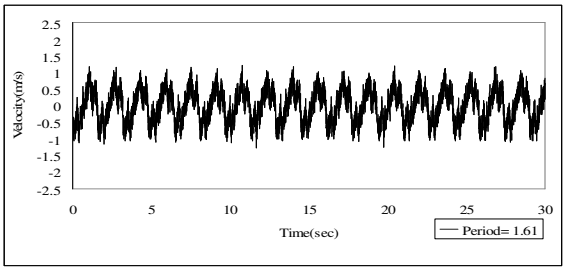

Fig. 4 Velocity of flow (T=1.61, solidity=0.3, amp.=90mm, f=0.66Hz)

Turbine Speed with Loading of Generator

Turbine of 0.3 solidity of turbine area: As shown in Fig.5 to Fig.8, where rotational speed of the turbine with loading of power generation is shown, when the solidity ratio of turbine area is 0.3, sloshing frequency of fluid is 0.64 and excitation period is 1.56 the maximum rotational speed of the turbine is 110 rpm. For the same solidity ratio of turbine area, when the sloshing frequency of fluid is 0.66 and excitation period is 1.66 the maximum rotational speed of the turbine is 89 rpm.

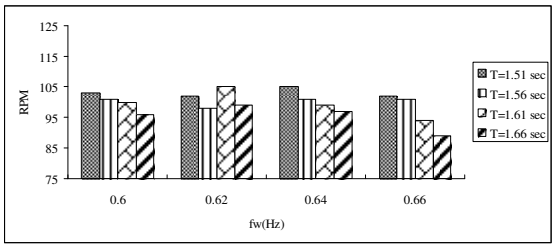

Fig. 5 Rotational speed of turbine under various fluid-frequency and excitation period (solidity=0.3, amp.=50mm)

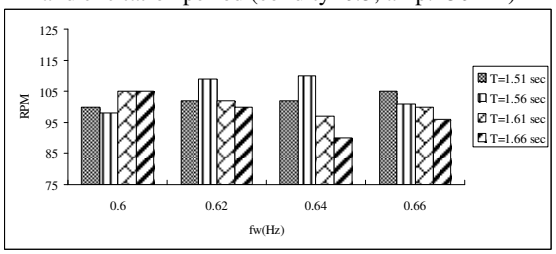

Fig. 6 Rotational speed of turbine under various fluid-frequency and excitation period (solidity=0.3, amp.=70mm)

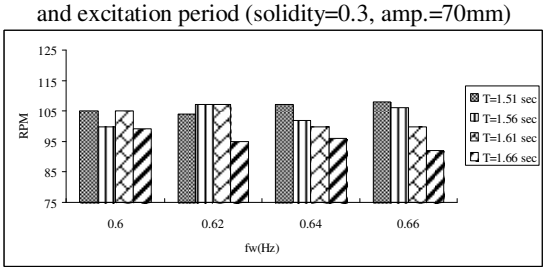

Fig. 7 Rotational speed of turbine under various fluid-frequency and excitation period (solidity=0.3, amp.=90mm)

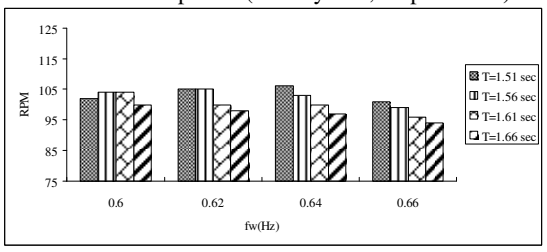

Fig. 8 Rotational speed of turbine under various fluid-frequency and excitation period (solidity=0.3, amp.=110mm)

Turbine of 0.3 solidity of turbine area: As shown in Fig.9 to Fig.12, where rotational speed of the turbine with loading of power generation is shown, when the solidity ratio of turbine area is 0.4, sloshing frequency of fluid is 0.66 and excitation period is 1.51 the maximum rotational speed of the turbine is 165 rpm. For the same solidity ratio of turbine area, when the sloshing frequency of fluid is 0.66 and excitation period is 1.66 the maximum rotational speed of the turbine is 98 rpm.

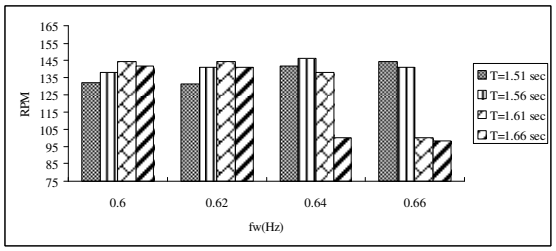

Fig. 9 Rotational speed of turbine under various fluid-frequency and excitation period (solidity=0.4□amplitude=50mm)

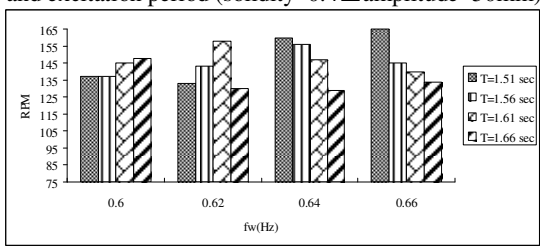

Fig. 10 Rotational speed of turbine under various fluid-frequency and excitation period (solidity=0.4□ amplitude=70mm)

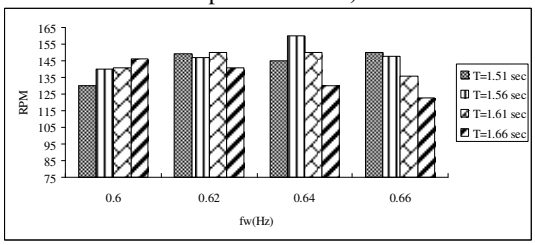

Fig. 11 Rotational speed of turbine under various fluid-frequency and excitation period (solidity=0.4□ amplitude=90mm)

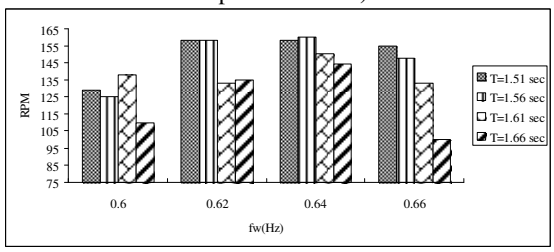

Fig. 12 Rotational speed of turbine under various fluid-frequency and excitation period (solidity=0.4□ amplitude=110mm)

Discussion and Analysis of the Results

It is noticed from the experimental results as were shown in the figures that the minimum speed of the turbine occurs when the amplitude of the excitation is 50mm, the fluid-frequency is 0.66Hz and the excitation period is 1.66 seconds. The maximum speed of the turbine occurs when the amplitude of the excitation is 70mm, the fluid-frequency is 0.64Hz and the excitation period is 1.56 seconds.

It is not necessary that the maximum speed occurs in the test

having the largest amplitude, but most testing cases have better performance for larger excitations for same testing model under same testing conditions. For larger solidity turbine system, the energy capture ability in terms of the rotational speed of the turbine is better. The performance of the system is strongly related to the relationship between the fluid-frequency and the period of applied excitation and the solidity ratio of the turbine.

4. CONCLUSIONS

In this study, a U-tube sloshing fluid power converting system was designed and tested in a structural laboratory with actuator excitation system. The testing parameters including the period and amplitude of excitation force, and the dimensional related parameters of the testing model such as the natural frequency of the designed model system, the solidity ratio of the turbine area. According to the experimental results, some conclusions are drawn as follows.

1. Under the same testing conditions such as same stroke amplitude and excitation period, the model of 0.4 solidity ratio of turbine has better performance than the one of 0.3 solidity ratio for the same design of natural frequency system.
2. The best performance of the system evaluated from the testing results is when the amplitude is level 2, the fluid frequency is level 4, excitation period is level 4 and solidity ratio is level 3.
3. Under the same testing conditions, model system of 0.4 solidity ratio of turbine area has a better performance that may be further improved if a more stable rotation for the turbine is obtained.

REFERENCES

1. Alexander N. Gorban, Alexander M. Gorlov, Valentin M. Silantyev（2001）,"Limits of the Turbine Efficiency for Free Fluid Flow" , *Journal of Energy Resources Technology*,Vol.123,pp. 311-317.
2. Alexander M. Gorlov（2001）, "Tidal energy", pp. 2955-2960.
3. Lee, H.H. and Jeng, Min-Liang （2001）"Feasible study on the floating type of wave power converter", Conference of Ocean Engineering,Taiwan, Proceedings, pp.451-456, Nov. 30-Dec.1, 2006.
4. Lee, H.H., Wong, S-H. and Lee, R-S. （2006）, "Response mitigation on the offshore floating platform system with TLCD", *Ocean Engineering -An Int. Journal*, Vol.33, pp.1118-1142.
5. Shiono, Mitsuhiro, Kdsuyuki Suzuki, Sezji Kiho （2002）, "Output characteristics of Darrieus water turbine with helical blades",*The Int. Society of Offshore and Polar Engineer*s, pp. 859-864.
6. Shiono, Mitsuhiro, Kdsuyuki Suzuki, Sezji Kiho （1998）, "The characteristics of Darrieus turbine for the tidal power", Elsevier Science LTD,1998.
7. Xue, S.D.,Ko, J.M.,Xu, Y.L.(2000), "Tuned liquid column damper for suppressing pitching motion of structures", *Engineering Structures*,Vol.23,pp. 1538-1551.

Automatic Flow Analysis for Human Blood at Low Shear Rate Range

Takamasa Suzuki, Hideki Yamamoto
Department of Chemical, Energy and Environment Engineering, Faculty of Environmental and Urban Engineering, Kansai University, 3-3-35, Yamate, Suita, 564-8680, Osaka, Japan
e-mail: yhideki@kansai-u.ac.jp

Kimito Kawamura
R&D Laboratories for Sustainable Value Creation, Asahi Group Holdings,ltd., 1-1-21, midori, Moriya, 302-0106, Ibaraki, Japan

Roberto Plasenzotti, Dominik Bernitzky
Core Unit for Biomedical Research, Medical University of Vienna, Waehringer Guertel 18-20 / AKH1Q, A-1090 Wien, Austria

Keywords: Flow property, Viscosity, Human blood, Rheometer, Flow curve

Abstract

A compact-sized falling needle rheometer with quick operation and automatic flow analysis has been developed for viscometry of human blood. The volume of a sample of blood only needs to be 4 mL and the measuring time is within 3 min. Measured flow properties of blood are evaluated as a flow curve showing the relationship between the shear stress and shear rate. Observed flow curves of the human bloods show three typical fluid regions, these are, the Non-newtonian fluid region for a low shear rate range, the transition region and the Newtonian fluid region for a high shear rate range. In normal male blood, the whole blood viscosity was 9.43mPa·s in the shear rate of 25 s^{-1}, 5.90mPa·s in the shear rate of 250 s^{-1}, and 5.77mPa·s in the shear rate of 500 s^{-1}(310K). The anticoagulated blood viscosity was 8.48mPa·s in the shear rate of 25 s^{-1}, 5.37mPa·s in the shear rate of 250 s^{-1}, and 5.21mPa·s in the shear rate of 500 s^{-1}(310K). These anticoagulated blood values were within the range of blood viscosity reported by other investigators. These show the shear rate dependency. More studies will be necessary to further explore these findings.

1 Introduction

The rheological properties of the blood is not only one of the important factors in the pathological diagnosis of the human body, but also basic data essential for analytical study of the change of fluid mechanics of the blood arising from the deterioration of the health condition. The rheological properties of blood are also important factors in pathological nexuses, but basic data of the viscosity of anticoagulated blood, especially non anticoagulated blood, are still lacking. In this context, the development of viscometry with high accuracy and quick operation, as well as the establishment of a data evaluation method by pathology are largely required. However, currently, there is little observed data of blood viscosity from measurement immediately after collection of a blood sample in comparison with the viscosity data of blood added with anticoagulant. [1-4]

In research so far, it was found that the flow properties of human blood are available for preventive medicine for blood dyscrasia, clinical medicine, health care, functional foods, or the inspection of the effects of medicines. Also, it was reported that the viscosity of human blood influenced the concentration of fibrinogen in the plasma and the hematocrit value, and that the viscosity of human blood could offer important information for myocardial infarction and cerebral infarction, etc. However, the measurement of the viscosity just after blood collection from a body is not so easy, and the accumulation of numerical data of the viscosity is not yet sufficient. Most of the measurements of blood viscosity were carried out using blood added with anticoagulant, and at present there is little measurement of blood without anticoagulant. Also, it is problematical that many different viscometers are applied to these purposes, and a standard method has not yet been determined; hence, the values differ according to the type of device.

The difficulties of flow analysis of blood come not only from an aggregation-dispersion phenomenon of red corpuscle cells, but also its transformation property, many interaction forces between corpuscle cells and blood plasma. Therefore, the establishment of exact viscometry for fresh blood is desired for further discussion about the relationship between blood disease and its flow properties.

In this paper, a compact-sized falling needle rheometer and a flow analysis method using this new device for fresh blood with anticoagulant have been developed, and the relationship between the apparent viscosity and physical properties of fresh blood has also been evaluated.

The theory of the presented viscometer is mainly based on the Stokes type of equation, and this is a kind of a falling body viscometer [5-9]. The viscosity of human blood can be measured with a small blood sample of about 3.5 cm^3 (total capacity is 4 cm^3) and with rapid operation within 2 min after taking a blood sample from the human body. The total scale of this compact-sized falling needle rheometer is downsized to about 1/30 the size of the previous apparatus [6]. A circular cylinder needle made of polypropylene is applied for the experiment, and its outer diameter and total length are 2 mm and 20 mm, respectively. This needle is also minimized at 1/5 that of a previous needle [6]. The density of the falling needle is controlled by the mass of a sinker enclosed in the needle tube. Flow analysis of the sample fluid is carried out using the needle's terminal velocity and the density difference between that of human blood and of a falling needle.

As stated above, the compact-sized falling needle rheometer is applied to the viscosity measurement of fresh blood before its coagulation. This paper is concerned with the development of a new rheometer for the measurement of flow properties of human bloods.

Fig. 1 Photograph of the compact-sized falling needle rheometer for measurement of fresh blood viscosity

2 Compact-Sized Falling Needle Rheometer with Automatic Operation

A schematic photograph of the compact-sized falling needle rheometer with automatic operation for measurement of blood viscosity is shown in Fig. 1. The schematic diagram of falling needle rheometer is illustrated in Fig. 2. The experimental apparatus consists of vertical double cylindrical vessels (one is a fluid vessel and the other is an insulating vessel cover) made of acrylic material (Fig. 2). The cap and bottom of the inner fluid vessel are made of Teflon. The inner fluid vessel for a blood sample is covered with the insulating vessel cover. The temperature of the inner fluid vessel is controlled at 310.15 K using a constant temperature air circulation system. This system is controlled by Peltier effect within an accuracy of 0.5 K. This constant temperature air is circulated in the space between the fluid vessel in the insulating cover. The diameter of the inner fluid vessel is 8.0 mm, and the height of the vessel is 90 mm. The total volume of the inner fluid vessel is about 4cm^3. A needle collector for the collection of the falling needles is connected to the bottom of the inner fluid vessel via a needle-fluid separator made of Teflon. The needle-fluid separator is a slender cylindrical tube, and its diameter is 2.2 mm, which is similar to the needle diameter (2 mm) shown in Fig. 2.

When a sample fluid (human blood) is introduced into the fluid vessel, the sample fluid does not leak into the space of the needle collector because the pressure in the needle collector is controlled at atmospheric pressure. After the operation of the first needle dropping automatically using needle falling system, the needle stopped at the bottom of the fluid vessel shown in Fig. 2 and is rapidly manually moved into the space in the needle collector by the guidance of a small magnet from outside the vessel. This movement of the falling needle from the bottom of the fluid vessel to the needle collector is important and indispensable for rapid measurement of fresh blood within 2 min. It was found in the preparatory experiment that the leakage of sample fluid into the needle collector from the fluid vessel is very little.

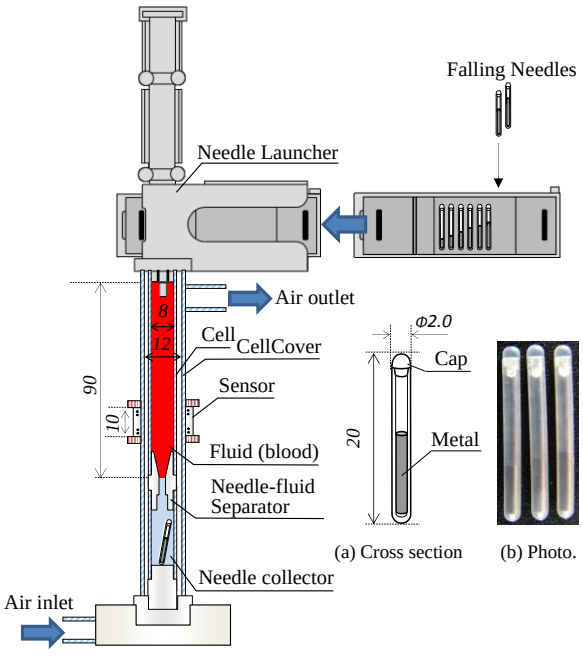

Fig. 2 Schematic diagram of the compact-sized falling needle rheometer for measurement of human blood viscosity

As each of the parts of the experimental apparatus such as the fluid vessel, the needle collector, the insulating vessel cover and a vessel stand shown in Fig.2 can be taken apart easily, the collection of falling needles after the experiment can be very rapid and easy. This experimental apparatus is considerably compact for measurement of the viscosity of human blood compared with previous apparatuses.

Table 1 Densities of falling needles used for viscometry of human blood

Needle No.	Density (10^3 kg·m^{-3})
1	1.101
2	1.116
3	1.142
4	1.181
5	1.233
6	1.366
7	1.497
8	1.618

The detail of the falling needle used in this experiment is also given in Fig. 2(a) and (b). This falling needle is a slender hollow cylindrical tube made of polypropylene. The diameter of the needle is 2 mm and its total length is 20 mm. The shape of both sides of each needle is hemispherical. Eight falling needles with different densities shown in Table 1 are used in this experiment. The density of each falling needle is controlled by the mass of a sinker (iron) enclosed inside the needle tube. This sinker is fixed at the bottom of the needle tube so that the center of gravity is at a lower position. The density is calculated by the volume and mass of each needle, and its uncertainty is estimated to be within ± 0.5x10^{-3}g·cm^{-3}. Table 1 shows measured needle densities used in the experiment, they are determined in consideration of average blood density (1.000g·cm^{-3} to 1.100 g·cm^{-3}).

In order to lead the falling needle to the center of the sample fluid, a needle inlet and needle launcher is equipped at the top of the fluid vessel. The needle launcher is a slender cylindrical tube as shown in Fig. 2. A pair of magnetic sensors is also installed at the middle part of the fluid vessel as shown in Fig. 2. The distance between magnetic sensors is 10 mm vertically. The passing time of each falling needle between magnetic sensors is automatically measured by a programmable controller manufactured by Sumitomo Metal Co., LTD. This magnetic sensor unit can be applied not only to clear liquids but also to opaque liquids. The programmable controller is connected to the personal computer via an amplification unit. It is possible to evaluate the falling velocity of each needle, and flow analysis such as a flow curve, apparent viscosity, and yield stress of the sample fluid can be measured automatically.

3 Experimental Method

Just after taking a blood sample from a vein, the blood is introduced into the fluid vessel shown in Fig. 2 and the top of the fluid vessel is covered with the Teflon cap in which the needle launcher is installed. This fluid vessel is equipped in the insulating vessel cover with two magnetic sensors. The vertical distance between the two magnetic sensors is 10 mm, and the fluid vessel is placed vertically on the vessel stand using a water level. Constant temperature air is circulated through the space between the fluid vessel and insulating vessel cover. The temperature of the fluid sample is kept at 310.15 K within an uncertainty of 0.5 K. Eight needles with different densities as shown in Table 1 are dropped down vertically in the sample fluid automatically using mechanical operation. The flow analysis is carried out using the observed passing time (terminal velocity) of the falling needles, needle densities, and blood density. Eight falling needles with different densities are used for measurement of the viscosity. Densities of blood are measured by the portable density/specific gravity meter (Kyoto Electronic Manufacturing Co., Ltd.) within an uncertainty of 10^{-4}g·cm^{-3}. The calibration of the presented falling needle viscometer is carried out using a standard liquid for calibrating viscometers. EDTA-2Na manufactured by Wako Pure Chemicals Co. Ltd., is used as anticoagulant material for blood.

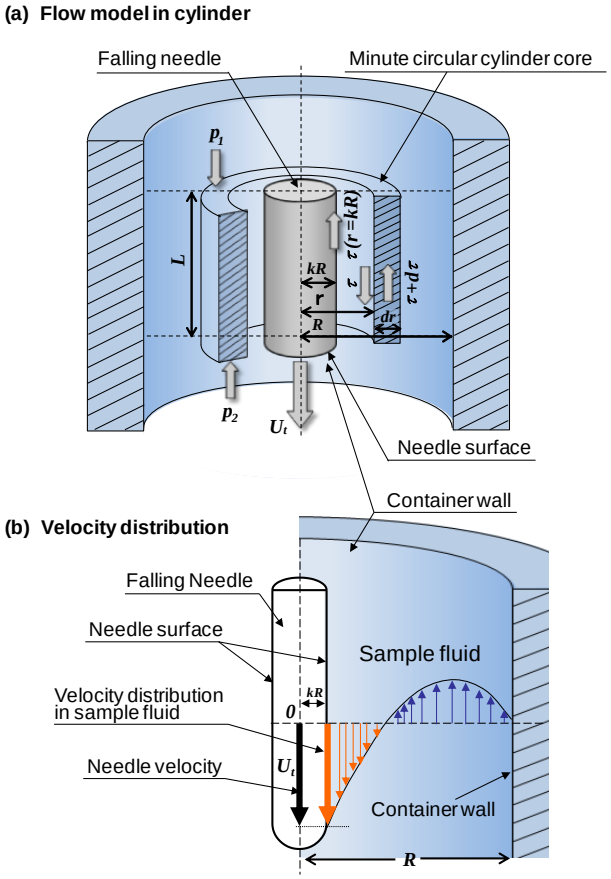

Fig. 3 (a) Flow model and (b) velocity distributions of the sample fluid in the fluid vessel of falling needle rheometer

4 Fluid Analysis using Compact-Sized Falling Needle Rheometer

Figure 3a and 3b show the model for flow analysis and velocity distribution in the compact-sized falling needle rheometer. This model is based on the flow analysis around the falling circular cylinder (falling needle) in the static fluid introduced into the cylindrical vessel. In order to apply this model to the motion of a falling needle and the mass transfer, the following four conditions are assumed.

(1) Fluid is an incompressible liquid.
(2) Slipping between the falling needle surface and container wall is negligible.
(3) Flow in the cylindrical vessel is laminar flow.
(4) The falling needle free-falls in the center of the vessel with a terminal velocity.

These assumptions and the constitution equation of fluid are used for flow analysis. This flow model can be applied for many types of constitution equations shown in Fig. 4. In this work, the constitution equations of Newtonian and non-Newtonian fluids are applied for blood analysis. The flow model of a falling needle in a static fluid according to the above assumptions is given in Fig. 3a. This model shows that the falling needle falls at a terminal velocity (U_t) in the static fluid introduced into the cylindrical fluid vessel.

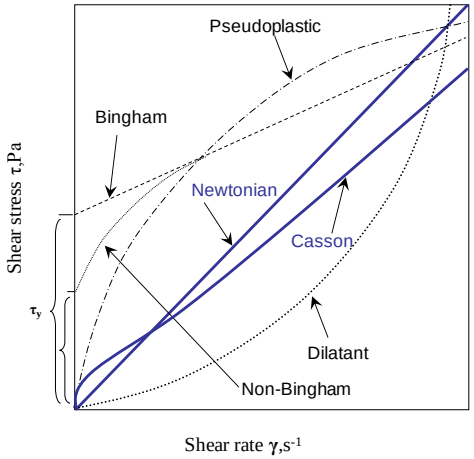

Fig. 4 Typical flow curves for Newtonian and non-Newtonian fluids

The fluid vessel diameter is R, and k is the ratio of the needle diameter to fluid vessel diameter.

The minute circular cylinder core shown in Fig. 3a is assumed as the fluid model for theoretical analysis. The inner diameter and outer diameter of this core are r and $r+\mathrm{d}r$, and the total length is L. The shear stresses on the inside and outside surfaces of the minute circular cylinder core are τ and $\tau+\mathrm{d}\tau$, respectively. The pressures at the top and bottom of the minute circular cylinder core are P_1 and P_2. When the falling needle falls at a terminal velocity in the static sample fluid, the momentums affected on four surfaces of the minute circular cylinder core shown in Fig. 3a are balanced with each other, and they are balanced while the needle is falling at the terminal velocity. Therefore, this force balance can be described by the following equation:

$$\mathrm{P}_1\left\{(r+dr)^2\pi - r^2\pi\right\} + 2\pi rL\tau = \mathrm{P}_2\left\{(r+dr)^2\pi - r^2\pi\right\} + 2\pi(r+dr)L(\tau+d\tau) \quad (1)$$

When $\Delta P = P_1 - P_2$ is less than 0, Eq.1 is arranged as follows:

$$\frac{1}{r}\frac{\mathrm{d}(r\tau)}{\mathrm{d}r} = \frac{\Delta P}{L} \quad (2)$$

Furthermore, while the needle falls at the terminal velocity in the sample fluid, the force balance of gravity, buoyancy, pressure and shear stress affected on the needle surfaces are given as

$$(\rho_\mathrm{s} - \rho_\mathrm{f})g\pi(kR)^2 L + \pi(kR)^2\Delta P = 2\pi kRL\tau_{(r=kR)} \quad (3)$$

In this equation, ρ_f and ρ_s are the fluid and needle density, respectively. The left-hand side first term of Eq.3 is the force of gravity and buoyancy, and the second term is the force of the pressure difference. The right-hand side term is the shear stress. This balance can be simply described by

$$(\rho_\mathrm{s} - \rho_\mathrm{f})g + \frac{\Delta P}{L} = \frac{2\tau_{(r=kR)}}{kR} \quad (4)$$

Figure 3b illustrates the velocity distribution of the sample fluid due to falling of the needle. The amount of fluid (Q) to transfer between the falling needle surface and the container wall due to falling of the needle can be calculated by

$$Q = 2\pi\int_{kR}^{R} ur\,\mathrm{d}r = \pi(kR)^2 U_\mathrm{t} \quad (5)$$

Figure 3b shows that the sample fluid around the falling needle is pulled downward with falling of the needle in the static sample fluid. On the other hand, the fluid near the container wall rises with the falling needle. The maximum velocity in the sample fluid is that on the needle surface. The maximum velocity is equal to that of the falling needle velocity. On the other hand, the velocity on the container wall becomes zero according to the above assumptions. Therefore, the boundary conditions of the velocity distribution can be described by

$$u_{(r=kR)} = -U_\mathrm{t} \quad (6a)$$

$$u_{(r=R)} = 0 \quad (6b)$$

In order to obtain the relationship between the shear rate and shear stress for the sample fluid, the Eqs. 2, 4, 5, 6a, and 6b and a constitution equation of the sample fluid are used simultaneously for flow analysis [6].

The constitution equation for a Newtonian fluid based on the law of viscosity is given by

$$\tau = \mu\left(\frac{\mathrm{d}u}{\mathrm{d}r}\right) = \mu\gamma \tag{7}$$

where μ is the viscosity, τ is the shear stress, and γ is the shear state. The viscosity of the fluid sample can be calculated by the following equation from combining Eqs. 2, 4, 5, 6a, 6b, and 7.

$$\mu = -\frac{(\rho_s - \rho_f)g(kR)^2\left\{(k^2+1)\ln k + 1 - k^2\right\}}{2(k^2+1)U_t} \tag{8}$$

As R and k in Eq. 8 are fixed values according to the size of the fluid vessel and falling needle, they are arranged by the following equation using the geometric constant G:

$$G = -\frac{2(k^2+1)}{(kR)^2\left\{(k^2+1)\ln k + 1 - k^2\right\}} \tag{9}$$

Therefore, the viscosity of a fluid can be simply described by

$$\mu = \frac{(\rho_s - \rho_f)g}{GU_t} \tag{10}$$

The shear rate of the sample fluid on the falling needle surface can be obtained from Eqs. 7 and 9 as

$$\gamma_{(r=kR)} = \frac{\mathrm{d}u}{\mathrm{d}r} = \frac{(k^2-1)U_t}{kR\left\{(k^2+1)\ln k + 1 - k^2\right\}} \tag{11}$$

The shear rate distribution for the radius direction can also be calculated by this equation.The shear stress of the sample fluid on the falling needle surface can also be described by the following equation by substituting Eqs. 8 and 11 for Eq. 7:

$$\tau_{(r=kR)} = \frac{(\rho_s - \rho_f)g(1-k^2)kR}{2(k^2+1)} \tag{12}$$

Equations 11 and 12 become fundamental data for flow analysis of the sample fluid. In this experiment, eight needles with different densities are used for the flow analysis. A flow curve of the sample fluid is obtained from the relationship the between shear stress and shear rate for eight needles [6].

5 Results and Discussion

5.1 Accuracy of the Falling Needle Rheometer

The accuracy and the reproducibility of the presented rheometer are ascertained by viscosity measurements of the standard liquid for calibration of viscometers manufactured by Nippon Grease Co., Ltd.(JS10 and JS20) and by Brookfield Co., Ltd.(NIST5 and NIST10). The standard liquids of JS10, JS20, NIST5 and NIST10 were chosen after careful consideration of the blood viscosity range (3.0 mPa·s to 7.0 mPa·s, $20s^{-1} < \gamma$). Flow curves of standard liquid show in Fig. 5 and comparison of measured values with standard value are given in Table 2. Good uncertainty within 1.0 % and reproducibility within ±1.0 % are confirmed by comparison with reference data (Standard liquids ; JS10, JS20, NIST5, NIST10).

Table 2 Comparison of measured viscosity of standard liquids for calibration of vicometers with standard values at 310.15K

Standard liquid	Viscosity[mPa·s]		Deviation[%]
	This work	Standard values	
JS 10	4.987	4.982	0.11
JS 20	9.006	8.963	0.48
NIST 5	4.705	4.70	0.12
NIST 10	9.211	9.30	0.95

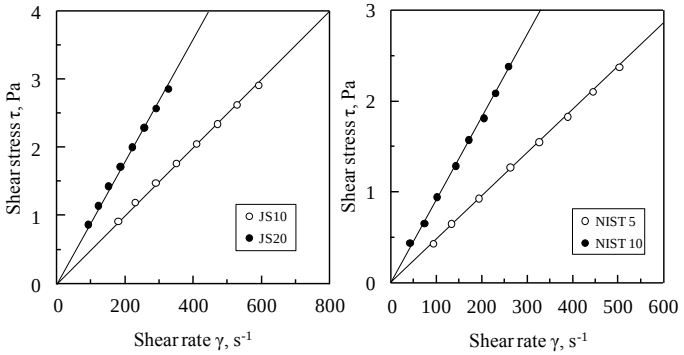

Fig. 5 Flow curve of Standard liquids at 310.15K
JS10, JS20: Standard liquid for calibration of viscometers
NIST5,NIST10: Brookfield Viscosity Standards are certified by methods traceable to the NIST

5.2 Flow Analysis of Human Blood

Flow analysis of fresh human blood was carried out using a compact-sized falling needle rheometer. Each result was evaluated as a flow curve, an apparent viscosity and hematocrit values. These rheological properties were compared between different blood samples.

In the experiment, fresh human brood of 20 cm^3 was taken from human veins, about 4cm^3 of whole blood was rapidly introduced into the fluid vessel without anticoagulant. The temperature of the fresh human blood was kept at 310.15 K using a constant temperature unit. The anticoagulant (EDTA-2Na) was added to the other blood (16 cm^3) for the purpose of comparison experiment and examination of blood component. Blood with anticoagulant was kept at 278.15 K and sent to a medical center for the measurement of the hematocrit value.

At first, the first needle was introduced into the needle launcher shown in Fig. 2, and the passing time of the needle between two magnetic sensors was measured by a programmable controller. After this operation, the falling needle stopped at the bottom of the fluid vessel and was rapidly moved into the space in the needle collector by the guidance of a small magnet from outside the vessel through manual operation. Next, the second needle was

also introduced into the needle launcher as soon as possible. When the final needle (eighth needles) was introduced into the needle launcher and the passing time was measured, the rheometric operation was finished. Densities of fresh human blood were measured by a portable density/gravity meter manufactured by Anton Paar., Ltd., within an uncertainty of 10^{-4} g·m^{-3} as soon as possible. Blood densities for males and females are listed in Table 3.

The experimental treatment of the fresh human blood without anticoagulant was carried out within 120 s except for the time needed for taking the blood (about 60 s), that is, the total time needed for this operation for each person was finished within 3 min.

The observed flow curve for male blood without anticoagulant was shown in Fig. 6-(a). This flow curve showed a linear relationship between the shear stress and shear rate in a high shear rate range (over 150 s^{-1}). However, non-Newtonian behavior (just like as Casson behavior) was confirmed in a low shear rate range (0 to 150 s^{-1}).

The observed flow curve of fresh blood showed the three typical fluid regions, that is, the non-Newtonian fluid region for the low shear rate range, and the transition region and Newtonian fluid region for the high shear rate range. Figure 6-(b) shows the flow curve of same person's blood with anticoagulant and a similar tendency with Fig. 6-(a) as non-Newtonian fluid was obtained. Casson behavior in the low shear rate range tends to differ with and without anticoagulant.

The observed flow curve for female blood with and without anticoagulant was shown in Fig.6-(c) and Fig.6-(d) under the same conditions. These flow curves also show a similar tendency with Fig.6-(a) and Fig.6-(b).

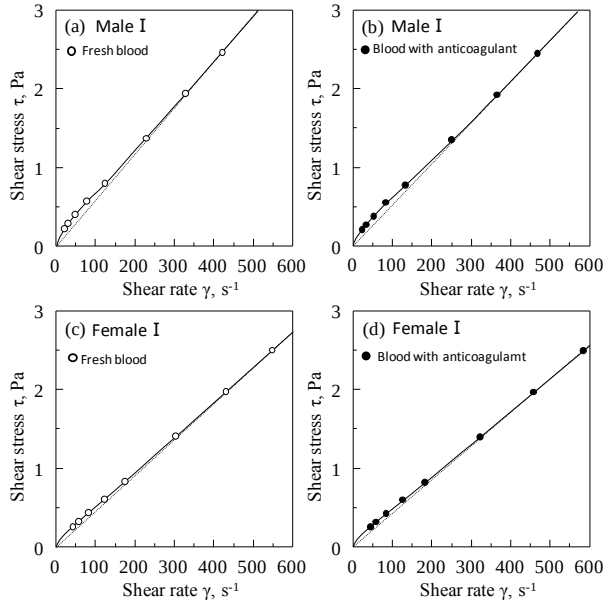

Fig.6-a Flow curve of fresh human blood for male without anticoagulant at 310.15 K

Fig. 6-b Flow curve of fresh human blood for male with anticoagulant at 310.15 K

Fig. 6-c Flow curve of fresh human blood for female without anticoagulant at 310.15 K

Fig.6-d Flow curve of fresh human blood for female with anticoagulant at 310.15 K

Figure 7 shows the relationship between the apparent viscosity and shear rate for human blood at 310.15 K, and the rheological parameters that were obtained are listed in Table 3. Figure 7 and Table 3 show a comparison between the flow properties of human blood with and without anticoagulant. Apparent human blood viscosity at low shear rate range shows higher value than that of high shear rate range.

Table 3 Comparison of apparent viscosity, hematocrit value and density of blood under the fixed shear rate ranges(<500s^{-1}) at 310.15 K

	Male blood Ⅰ		Male blood Ⅱ	
Shear rate* (s^{-1})	Fresh blood (mPa·s)	Fresh blood + anticoagulant (mPa·s)	Fresh blood (mPa·s)	Fresh blood + anticoagulant (mPa·s)
25	9.43	8.48	9.61	9.28
50	7.93	7.29	7.97	7.65
100	6.78	6.38	6.98	6.67
150	6.20	5.77	6.51	6.06
250	5.90	5.37	5.92	5.80
500	5.77	5.21	5.60	5.22
Density (10^3 kg·m^{-3})	1052.8	1053.3	1052.0	1053.4
Ht**		47.8		46.7
	Female blood Ⅰ		Female blood Ⅱ	
Shear rate* (s^{-1})	Fresh blood (mPa·s)	Fresh blood + anticoagulant (mPa·s)	Fresh blood (mPa·s)	Fresh blood + anticoagulant (mPa·s)
25	5.95	5.52	7.69	7.38
50	5.47	5.33	6.78	6.53
100	4.82	4.79	6.25	5.78
150	4.68	4.50	5.96	5.10
250	4.61	4.39	5.52	4.83
500	4.53	4.27	5.02	4.42
Density (10^3 kg·m^{-3})	1042	1043.2	1047.6	1048.7
Ht**		35.6		42.4

* Fixed shear rate ranges for all human blood measured in this work

**Hematocrit value: the volume percentage of red cells included in whole blood

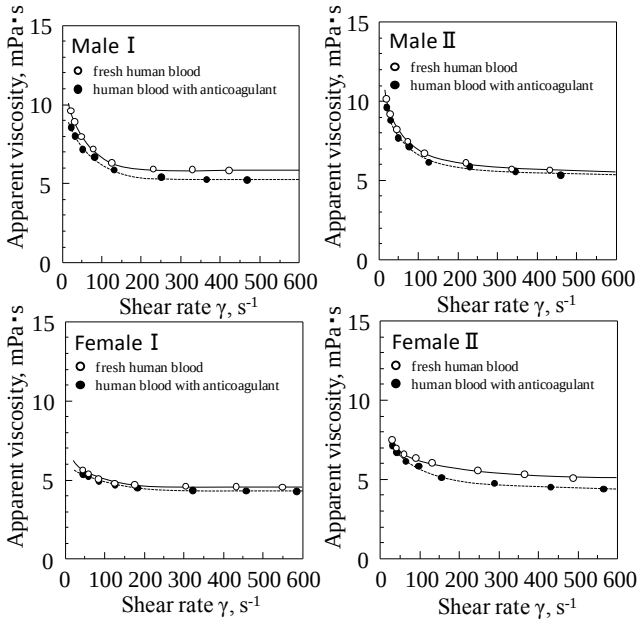

Fig.7 Relationship between apparent viscosity and shear rate for fresh human bloods at 310 .15K

In the case of the apparent viscosity with anticoagulant, the blood viscosity of human blood without anticoagulant was higher than that with anticoagulant. It is also found that blood viscosity and hematocrit value for male show a higher than those for female. Therefore fluid property of human blood was considered to be influenced by anticoagulant and blood component.

Table 4 shows the anticoagulated blood viscosity in normal subject was measured using Wells-Brookfield cone-plate viscometer (Model LVT-C/P) by other investigators [10-12]. Figure 8 shows the relationship between the apparent viscosity and shear rate for human blood with anticoagulant observed by FNR and literatures showing Table 3 and 4. Human blood with anticoagulant measured by FNR was similar range with previous works in literatures and these values show little higher value.

Table 4 Viscosity of normal human blood in various investigators

Investigator	Shear rate (s^{-1})	Blood viscosity (mPa·s)	
		Males	Females
Ditzel, J. (1968)	5.75	12.87±2.96	10.96±1.91
	11.5	9.65±1.91	8.78±1.22
	23	7.74±1.26	7.13±0.87
	46	6.24±0.87	5.87±0.59
	115	5.09±0.65	4.81±0.43
	230	4.58±0.56	4.36±0.36
	(Ht)	45.5±2.9%	42.3±2.2%
		Males	Females
Litwin, M.S. (1970)	5.8	12.3±2.1	8.9±1.4
	11.5	9.1±1.5	6.7±1.4
	23	7.0±0.9	5.5±0.6
	46	5.9±0.7	4.8±0.6
	115	4.8±0.6	4.0±0.4
	230	4.3±0.5	3.6±0.6
	(Ht)	46.4%	41.9%
		Males	Females
Hikoichi Fujinaga (1984)	11.5	8.74±0.31	7.34±0.27
	23	7.84±0.25	6.55±0.18
	46	6.68±0.14	5.64±0.12
	115	5.08±0.07	4.32±0.05
	230	4.33±0.04	3.72±0.04
	(Ht)	43.36±0.35%	37.64±0.37%

Figure 9 shows the relationship between the apparent viscosity for human blood for 20 person and hematocrit values that are the percentage of red cells included in whole blood. A linear relationship with the hematocrit values was obtained. However, this linearity of apparent viscosity shows down with increasing of hematocrit value. It was found that the viscosity for blood was closely connected with the hematocrit values.

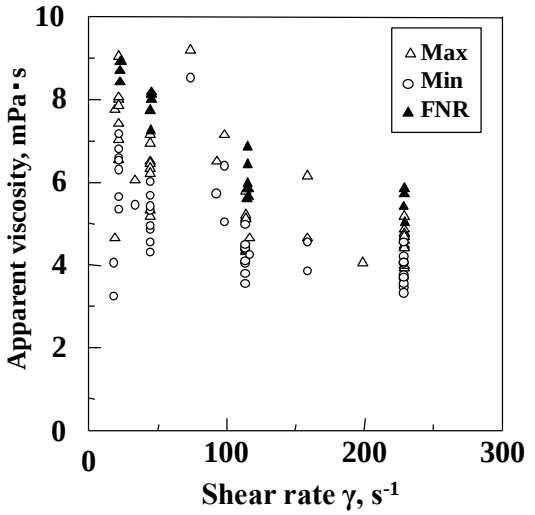

Fig.8 Relationship between apparent viscosity and shear rate for anticoagulated human bloods at 310 .15K

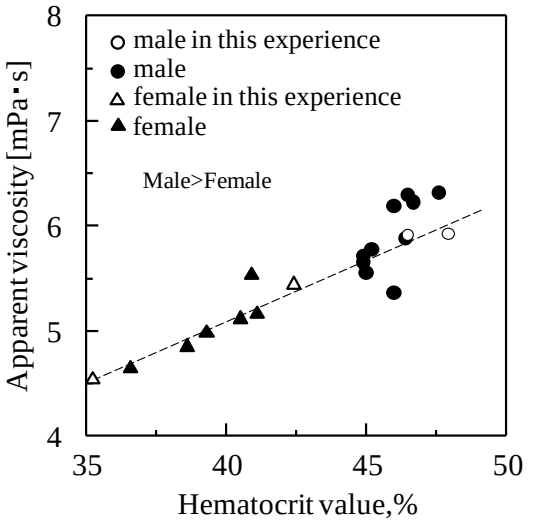

Fig.9 Relationship between average viscosity and hematocrit values of fresh human blood at 310.15 K

6 Conclusion

A compact-sized falling needle rheometer with quick operation and automatic flow analysis has been developed for the viscometry of human blood with anticoagulant. The volume of a fresh blood sample only needs to be 4 cm^3 and the measuring time is within 3 min after taking a blood sample from the vein. The measured flow properties of these bloods are evaluated as a flow curve, that is, the relationship between the shear stress (τ) and shear rate (γ). Observed flow curves of fresh human blood show the three typical fluid regions, that is, the non-Newtonian fluid region for the low shear rate range, and the transition region and Newtonian fluid region for the high shear rate range. Flow properties of blood such as the apparent viscosity (μ) are measured, and they are compared between blood with and without anticoagulant. It is found that the fresh human blood viscosity without anticoagulant shows a higher value than that without anticoagulant.

It is also found that blood viscosity and hematocrit value for male show a higher than those for female. The whole blood viscosity range measured by FNR were 5.95 mPa·s to 9.61 mPa·s in the shear rate of 25 s^{-1}, 4.61 mPa·s to 5.92 mPa·s in the shear rate of 250 s^{-1}, and 4.53mPa·s to 5.60 mPa·s in the shear rate of 500s^{-1}(310K). The anticoagulated blood viscosity range measured by FNR were 5.52 mPa·s to 9.28 mPa·s in the shear rate of 25 s^{-1}, 4.39 mPa·s to 5.80 mPa·s in the shear rate of 250 s^{-1}, and 4.27 mPa·s to 5.22 mPa·s in the shear rate of 500s^{-1}(310K). Human blood viscosity measured by FNR was within the range of human blood viscosity measured by rotary viscometer. A linear relationship between the hematocrit value, which is the volume percentage of red corpuscles in the human blood, and the apparent viscosity is observed for male and female blood. It is found that the compact-sized falling needle rheometer presented in this work is very useful for rheometry studies of fresh human blood with and without anticoagulant.

Nomenclature

d	needle diameter, m
f_e	yield stress of a Casson fluid, Pa
g	gravitational acceleration, m·s^{-2}
G	geometric needle constant, 1·m^{-2}
K	fluid consistency, Pa·s^{-n}
k	ratio of container to needle diameter
kR	needle radius, m
L	total needle length, m
n	fluid index
P_1,P_2	pressure of the upper and lower end of aminute circular cylinder, Pa
ΔP	pressure difference ($\Delta P=P_1-P_2$), Pa
Q	net flow rate of fluid pushed aside by the needle, m^3·s^{-1}
r	radius coordinate, m
R	container radius, m
u	velocity in the system length direction, m·s^{-1}
U_t	terminal velocity of a falling needle, m·s^{-1}
γ	shear rate, s^{-1}
μ	Newton viscosity, Pa·s
π	circular constant
ρ_f	fluid density, kg·m^{-3}
ρ_s	needle density, kg·m^{-3}
τ	shear stress, Pa
τ_y	yield stress, Pa

References

[1] E.W. Merrill, **Physiol. Rev**. 49, 863 (1969)
[2] M.F. Kiani ,A.G. Hudez, **Biorheology** 28, 65 (1991)
[3] H. Hartert, **Flow Properties of Blood and Other Biological Systems**, Pergamon Press, Oxford, New York & Paris, (1960),pp. 186-192
[4] P. Gaehtgens, **Biorheology** 17, 183 (1980)
[5] H.Yamamoto,K.Kawamura,K.Omura,S.Tokudome, **Int.J.Thermophysics**,31,2361(2010)
[6] H. Yamamoto, **J. Chem .Eng. of Japan** 25, 803 (1995)
[7] M. J.Davis, H. Brenner , **Phys. Fluids** 13, 3086 (2001)
[8] E.G. Wehbeh, T. J. Ui, R. G., **Phys. Fluids** 8, 645 (1993)
[9] J. A. Lescarboura, G. W. Swift, **AIChE J.** 14, 651 (1968)
[10] Ditzel .J, **Dan. Med. Bull.** 15, 49-53 (1968)
[11] Litwin MS, Chapman K, Stoliar JB., **Surgery** 1970, 67, 2, 342-345 (1970)
[12] H. Fujinaga, **Jpn.J.Hyg.** , 39 ,4 (1984)

Conflict Resolution and Concensus Development Among Inherently Contradictory Agents Using Fuzzy Linguistic Variables

Terrence P. Fries
Department of Computer Science
Indiana University of Pennsylvania
Indiana, PA 15705 USA

ABSTRACT

Decision making based upon the recommendations of multiple intelligent agents has become common in various applications. However, difficulty arises when the agents have quite different recommendations. Many methods have been proposed that attempt to resolve conflicting opinions multiple, heterogeneous agents in decision making. However, all of these methods require that the agents negotiate until they arrive at a consensus opinion. These do not provide for the cases in which the agents have contradictory opinions that cannot be compromised. In certain cases, agent opinions will conflict due to the nature of the agents' viewpoints. By forcing compromise or neglecting selected conflicting opinions, valuable information may be lost that adversely affect the decision. This paper proposes a method by which a consensus decision can be developed while not requiring that the individual agents abandon their opinions.

Keywords: Multi-Agent Systems, Consensus Development, Fuzzy Linguistic Variables, Fuzzy Aggregation, Fuzzy Ranking

1. INTRODUCTION

The use of multiple agents systems has become widespread for a variety of applications, including electronic business, communications, robot navigation, factory control, scheduling, human-computer interaction, and active networks providing customized packet processing. However, a problem arises when autonomous heterogeneous agents provide contradictory opinions. To address this, researchers have developed a number of methods for conflict resolution among agents [1-5]. The primary approach to conflict resolution is negotiation. These negotiation methods assume that the agents have some common ground on which to adjust their opinions to produce a compromise. This becomes problematic when the agents inherently have conflicting opinions due to their very nature. As an example, consider agents used to route packets in a wide area network. One agent may be concerned with producing the fastest transmission, while another agent has the goal of minimizing the cost of transmission. Inherently, these agents will likely produce contradictory recommendations due the difference in their goals. The opinions provided by both agents are valuable and must be considered in decision making regarding routing. Contradictory opinions cannot be discarded or compromised without losing essential information in the decision making process. However, negotiation methods would compromise the opinions of both conflicting agents. Therefore, alternative methods must be investigated to resolve conflicts without the loss of information.

The conflict resolution approach presented in this research involves the use of fuzzy sets to represent agent opinions. The fuzzy set representation allows the combination of disparate opinions without the loss of information. It also accounts for imprecision of data and incomplete data used by the each of the agents in forming an opinion. The conflict resolution and decision making approach assumes that agents with varying viewpoints will analyze the available data and provide a recommendation for each alternative. Decision making is a two-step process in which the opinions of all agents on a particular alternative are aggregated, or combined, and the resulting recommendations for each alternative are ranked for use in decision making.

Section II presents an overview of fuzzy set theory for those unfamiliar with it. In Section III, a method of developing a consensus among agents with disparate views is presented. Section IV provides a discussion of the effectiveness of the proposed approach and examples of successful implementations of the method presented here.

2. FUZZY INTELLIGENT AGENTS

Fuzzy Set Theory

In many real world situations, concepts cannot be clearly classified into one class, at the total exclusion of all

others. For example, the concept of "hot" cannot be defined using mathematical terms due to its varying interpretations by different people. Traditionally, membership of object *x* in a class, *A*, is expressed as a binary value using the membership function in Eq. (1).

$$\mu_A(x) = \begin{cases} 1 & \text{if } x \text{ is an element of set } A \\ 0 & \text{if } x \text{ is not an element of set } A \end{cases} \quad (1)$$

The membership function can also be expressed as a functional mapping which maps a set *A* to 0 or 1 as shown in Eq. (2).

$$\mu_A(x) \quad : \quad A \rightarrow \{0, 1\} \quad (2)$$

For example, if *x* is a temperature, then the membership function maps it to be either a member or not a member of the *hot* class. A problem arises in defining the membership function because people have differing opinions as to what temperature is hot. A person from the arctic may consider 30ºC to be a hot day, while someone from an equatorial region may not consider a day to be hot until it reaches 35ºC or higher. Fuzzy logic was introduced by Lotfi Zadeh [6, 7] to address such disparate opinions. A fuzzy set, or fuzzy class, is described by a membership function that defines a degree of membership of an object, *x*, in a set, *A*. The membership function provides a mapping to any real number in the range 0 to 1, inclusive, as shown in Eq. (3).

$$\mu_A(x) \quad : \quad A \rightarrow [0, 1] \quad (3)$$

The membership function may be shaped as a ramp, Gaussian, sigmoidal, or any other continuous function or the interval [0, 1]. The membership function for hot is shown in Figure 1. This would be defined as in Eq. (4).

$$\mu_{hot}(x) = \begin{cases} 0 & \text{if } a \le 25 \\ (x\text{-}25)/(x\text{-}35) & \text{if } 25 < x < 35 \\ 1 & \text{if } x \ge 35 \end{cases} \quad (4)$$

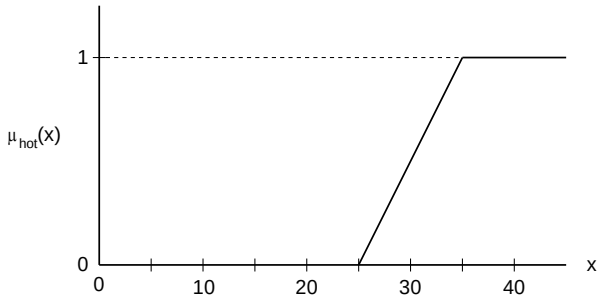

Figure 1. Fuzzy membership function for hot

For this membership function, a temperature of 25 has no membership (*x* value of 0.0) in *hot*, while 30 has a 0.5 degree of membership, and 35 has full membership (*x* value of 1.0). In a similar manner, linguistic variables such as hot, far, near, fast, and costly can also be expressed as fuzzy sets. This allows the expression of membership to employ linguistic variable that are much more understandable to humans who are developing and evaluating the applications.

Special Case Fuzzy Sets

Researchers have found it convenient to limit membership functions to a specific shape to simplify their use in a particular application. The most common membership functions are triangular and trapezoidal fuzzy sets.

A triangular fuzzy set has a triangular-shape convex membership function and is denoted by (*a*, α, β) and defined as where a is the center of the triangle and α and β define the left and right vertices, respectively, or the left and right spreads as shown in Figure 2. A triangular fuzzy number membership function is defined as

$$\mu_A(x) = \begin{cases} 1 - |a - x| / \alpha & \text{if } a - \alpha \le x \le a \\ 1 - |a - x| / \beta & \text{if } a \le x \le a + \beta \\ 0 & \text{otherwise} \end{cases} \quad (5)$$

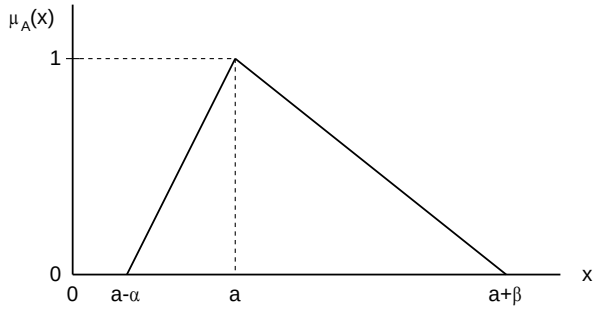

Figure 2. Triangular fuzzy number denoted by the tuple (a, α, β)

A trapezoidal fuzzy number (TFN) is a convex trapezoid denoted by the 4-tuple (*a*, *b*, *c*, *d*) where *a*, *b*, *c*, and *d* denote the critical points of the trapezoid as shown in Figure 3. The membership function of a trapezoidal fuzzy number is defined in Eq. (6).

$$\mu_A(x) = \begin{cases} (x-a)/(b-a) & \text{if } a < x < b \\ 1 & \text{if } b \le x \\ (d-x)/(d-c) & \text{if } c < x < d \\ 0 & \text{otherwise} \end{cases} \quad (6)$$

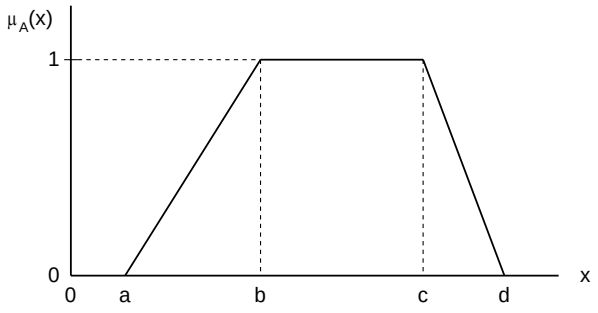

Figure 3. Trapezoidal fuzzy number (TFN) denoted by the 4-tuple (a, b, c, d)

Representing Fuzzy Opinions in Intelligent Agents

It has become common to represent agent opions in a multi-criteria decision making system using fuzzy sets [8-10]. For this research, agent opinions are assumed to be represented by trapezoidal fuzzy numbers (TFNs). TFNs were chosen because they reduce the computational complexity of numerical calculations required for aggregation and ranking of agent opinions. In addition, they provide membership functions that can express full membership (μ_A (x) = 1) for all or any portion of the universe of discourse, A, as desired. An agent's recommendation for a particular alternative can be expressed using the linguistic variables: *very unlikely*, *unlikely*, *possible*, *likely*, and *very likely*. These linguistic variable can be represented as TFNs as shown in Figure 4. Other sets of linguistic variables may also be used. For example, in a test case using multiple fuzzy agents for robot navigation (see Section IV), linguistic variables describing the direction of movement were used: *left*, *left-center*, *straight*, *right-center*, *right*, *back*, etc.

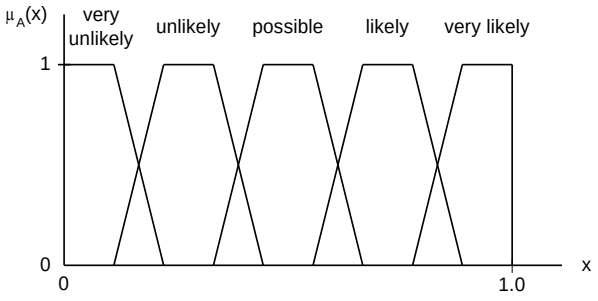

Figure 4. Representing agent opinions as linguistic variables using TFNs

3. CONFLICT RESOLUTION

In developing a consensus among intelligent agents, it is assumed in this research that a real time response is required. In many multiple agent applications, it is infeasible to wait long periods of time for decisions to be made. For example, the routing of data packets or access to critical information cannot wait for extensive computation. Therefore, a restriction is placed on the decision making process that it provide a real time response and, as a result, have limited computational complexity.

The conflict resolution and decision making approach presented in this paper assumes that agents with varying viewpoints will analyze the available data and provide a recommendation for each alternative. Decision making is a two-step process: (1) agent opinions are aggregated for a particular alternative are aggregated, or combined, and (2) the resulting recommendations for each alternative are ranked for use in decision making.

First, the recommendations of each agent for a particular alternative must then be combined into a single opinion on that alternative. Using the fuzzy recommendations, the aggregate opinion will be expressed in terms of a fuzzy number. Second, the aggregated recommendations for each alternative must be ordered so that the best one is selected based on the agent opinions. The best alternative is the consensus of the agents. The ordering of fuzzy numbers is not straight forward as with crisp numbers, such as 2, 5, and 8, due to the varying degrees of membership. Aggregation and ranking approaches are presented below for determining the best alternative based on the consensus of agent opinions.

Aggregation of Fuzzy Opinions

A number of aggregation approaches have been proposed [8-13]. Some aggregation methods require that the fuzzy opinions have some intersection so that they are not totally out of agreement. If the opinions do not have some agreement, the agents negotiate until they can arrive at a consensus. However, the agents assumed in this research may purposely have disparate recommendations due their divergent viewpoints. Other methods that have been proposed are computationally complex which violates the real-time response requirement. Therefore, none of these methods are appropriate.

Hsu and Chen [14] present an aggregation method using a similarity matrix that exhibits the similarities between the opinions of experts. The matrix operations are significantly faster than other approaches that rely on complex equations. However, Hsu and Chen require that all opinions for a particular option have a common intersection at some α-level cut. This research modifies

Hsu and Chen's aggregation method to allow opinions that do not intersect.

When at agent opinions for an alternative intersect at some α-level cut, the similarity matrix approach is used to aggregate the intersecting opinions. When there is no common intersection among agent opinions, weighted linear interpolation is used to aggregate the opinions for each alternative. Each agent, *i*, is assigned a rating, r_i. The most important agent is given a rating of 1 and the others are given ratings less than one in relation to their importance.

The degree of importance normalizes the ratings and is defined in Eq. (7).

$$w_i = \frac{r_i}{\sum_{i=1}^{n} r_i}, \quad i = 1,2,..,n \tag{7}$$

The aggregated fuzzy opinion for alternative *k* is formed as a TFN tuple (*a**, *b**, *c**, *d**) using the formulas in Eq. (8).

$$a^* = \sum_{i=1}^{n} w_i a_i$$

$$b^* = \sum_{i=1}^{n} w_i b_i \tag{8}$$

$$c^* = \sum_{i=1}^{n} w_i c_i$$

$$d^* = \sum_{i=1}^{n} w_i d_i$$

where

n	is the number of agents with opinions on alternative *k*
w_i	if the degree of importance of agent *i*
(a_i, b_i, c_i, d_i)	is the TFN opinion of agent *i* for alternative *k*

The resulting aggregated opinion, (*a**, *b**, *c**, *d**), can be defined as in Eq. (9).

$$\tilde{R} = \sum_{i=1}^{n} w_i (\cdot) \tilde{R}_i \tag{9}$$

where $(\cdot)$ is the fuzzy multiplication operator and $\tilde{R}_i = (a_i, b_i, c_i, d_i)$.

Ranking of Fuzzy Opinions for Decision Making

Once the opinions of the agents have been aggregated to produce a consensus opinion for each alternative, the best alternative must be selected. However, the opinions are expressed as fuzzy numbers and cannot be immediately compared. Researchers have proposed a number of methods for ranking fuzzy numbers [15-19]. Many fail to distinguish between fuzzy numbers with identical modes and symmetric spreads. While others cannot distinguish between fuzzy numbers with identical modes and symmetric spreads, thus, they favor numbers with larger spreads over smaller spreads. This is counterintuitive, since larger spreads indicate more uncertainty in the opinion. All but Nakamura's [19] method lack a mechanism to adjust favoritism toward larger or smaller spreads.

This research modifies Nakamura's [19] fuzzy preference function so that it can differentiate between fuzzy numbers with identical modes and symmetric spreads, and uses it to rank fuzzy opinions. Nakamura's approach compares each pair of fuzzy opinions using a fuzzy preference function which accounts for the Hamming distance of each fuzzy number and the to the fuzzy minimum and the fuzzified best and worst states. The pairwise comparisons are then used to rank the fuzzy opinions. The new fuzzy preference function compares each fuzzy opinion to an "ideal" fuzzy number which represents the case where the opinion is "very likely." This eliminates the problem Nakamura's method suffers when comparing fuzzy numbers with identical modes and symmetric spreads. Elimination of the pairwise comparisons significantly reduces the number of calculations required for Nakamura's method to n calculations for n nodes using the new method presented in this research. This research has shown that the order is reduced from $O(n^2)$ for Nakamura's method to $O(n)$ using the new method. The new method also simplifies the ranking of the opinions. Nakamura's method only provides preferences for pairs of fuzzy numbers, therefore, the preference function for each pair of fuzzy numbers must be evaluated. It is then necessary to evaluate all of the pairwise comparisons to provide a ranking. Since, in the new method, the fuzzy opinions are compared with a "very likely" fuzzy number, they all already ranked in comparison to this value and the process of determining the ranking based on pairwise comparisons is eliminated. The result of each fuzzy preference calculation for each node provides its ranking. The new fuzzy preference function comparing opinion A_i and the very likely mode, *V*, replaces the second fuzzy opinion with *V* and is defined in Eq. (10).

$$\mu_p(A_i,V)=\begin{cases}\dfrac{1}{\Delta_\alpha}[\alpha\ D(\underline{A}_i,\underline{A}_i\wedge\underline{V}) \\ \quad +(1-\alpha)\ D(\overline{A}_i,\overline{A}_i\wedge\overline{V})] & if\ \Delta_\alpha\neq 0 \\ 1/2 & if\ \Delta_\alpha=0\end{cases} \tag{10}$$

where

$$\Delta_\alpha=\alpha[D(\underline{A}_i,\underline{A}_i\wedge\underline{V})+D(\underline{V},\underline{A}_i\wedge\underline{V})] +(1-\alpha)[D(\overline{A}_i,\overline{A}_i\wedge\overline{V})+D(\overline{V},\overline{A}_i\wedge\overline{V})]$$

The notation $\bar{A}$ is the greatest upper set of A defined in Eq. (11).

$$\mu_{\bar{A}}(y)=\sup_{\{x|x\geq y\}}\mu_A(x),\qquad \forall y\in U \tag{11}$$

$\underline{A}$ is the greatest lower set of A defined in Eq. (12).

$$\mu_{\underline{A}}(y)=\sup_{\{x|x\leq y\}}\mu_A(x),\qquad \forall y\in U \tag{12}$$

$A_i\wedge V$ is the extended minimum defined in Eq. (13).

$$\mu_{A_i\wedge V}(z)=\sup_{\{x,y|x\wedge y=z\}}[\mu_{Ai}(x)\wedge\mu_V(y)],\forall z\in U \tag{13}$$

and $D(A_i,V)$ is the Hamming distance between A_i and V, defined by Eq. (14).

$$D(A_i,V)=\int_S|\mu_{Ai}(x)-\mu_V(x)|\,dx \tag{14}$$

The new fuzzy preference function can be simplified by showing that $D(A_i,V)$ when V is a TFN defined as (a, b, 1, 1). Therefore, if V is represented by (a, b, 1, 1), the revised new fuzzy preference function used to compare opinion A_i with the very likely mode, V, is defined as

$$\mu_p(A_i,V)=\begin{cases}\dfrac{1}{\Delta_\alpha}\alpha\ D(\underline{A}_i,\underline{A}_i\wedge\underline{V}) & if\ \Delta_\alpha\neq 0 \\ 1/2 & if\ \Delta_\alpha=0\end{cases} \tag{15}$$

where

$$\Delta_\alpha=\alpha[D(\underline{A}_i,\underline{A}_i\wedge\underline{V})+D(\underline{V},\underline{A}_i\wedge\underline{V})] +(1-\alpha)D(\overline{V},\overline{A}_i\wedge\overline{V})$$

4. CASE STUDIES

An agent-based diagnostic system utilizing fuzzy linguistic variables and the conflict resolution method described in the previous section has been implemented and tested. The diagnostic system was implemented for a manufacturing testbed consisting of two conveyors on which pallets are transported. The workcell had two robots that interact with the system and seven stations to simulate manufacturing processes including assembly, material handling, and inspection. The agents used in this diagnostic system were employed with expertise that considers recency of faults, frequently occurring faults, minimization of the resource cost to examine possible fault sources, mean-time-to-failure of components, and cyclic failures. The agent-based diagnostic system increased diagnostic accuracy, while reducing by an average of 91% the time to make a successful diagnostic determination [20].

A navigation system for a Pioneer 2-DX mobile robot has been implemented using the conflict resolution method presented in this paper. It uses autonomous agents that express their opinions using linguistic fuzzy numbers. This system reduced the total distance traveled by 18% over a similar system not using the conflict resolution method [21].

5. CONCLUSIONS

The conflict resolution method for multiple agent systems presented in this paper has been shown to perform well in several test applications. The approach allows the inclusion of disparate agent opinions in the consensus. Additional work is in progress on developing a method that allows implementation of various negotiation approaches without sacrificing the ability to retain and utilize disparate information.

6. REFERENCES

[1] R. Thangarjoo and H. C. Lau, "Distributed route planning via hybrid conflict resolution," *Proceedings of the IEEE/WIC/ACM International Conference on Web Intelligence and Intelligent Agent Technology*, pp. 374-378, September 2010.

[2] Q. Li, X. Cui, and X. Hu, "Conflict resolution winthin multi-agent system in collaborative design," *Proceedings of the International Conference on Computer Science and Software Engineering*, pp. 520-523, December 2008.

[3] E. Gonzalez, A. Perez, J. Cruz, and C. Bustacara, "MRCC: A multi-resolution cooperative control agent architecture, *Proccedings of the IEEE/WIC/ACM International Conference on Intelligent Agent Technology*, pp. 391-394, November 2007.

[4] A. Madureira, J. Santos, and N. Gomes, "Hybrid multi-agent system for cooperative dynamic scheduling through meta-heuristics," *Proceedings of the Interational Conference on Intelligent Systems Design and Applications*, pp. 9-14, October 2007.

[5] I. Letia and A. Groza, "Automating the dispute reolution in a task dependency network," *Proceedings of the IEEE/WIC/ACM International Conference on Intelligent Agent Technology*, pp. 365-371, September 2005.

[6] L. A. Zadeh, "Fuzzy sets," *Information and Control*, vol. 8, 338-353, 1965.

[7] L. A. Zadeh, "A theory of approximate reasoning," *Machine Intelligence*, vol. 9, pp. 149-194, 1979.

[8] L. Ai-Ping, J. yan, and W. Quan-Yuan, "A study on fuzzy operator in multicriteria decision systems," *Proceedings of the International Conference on Hybrid Information Technology*, pp. 380-386, November 2006.

[9] G. Wei and X. Wang, "Some geometric aggregation operators on interval-valued intuitionistic fuzzy sets and their application to group decision making," *Proceedings of the International Conference on Computational Intelligence and Security*, pp. 494-499, December 2007.

[10] Z. Xu and J. Chen, "On geometric aggregation over interval-valued intuitionalistic fuzzy information," *Proceedings of the 4th International Conference on Fuzzy Systems and Knowledge Discovery*, pp. 466-471, August 2007.

[11] R. Xu and X. Zhai, "Fuzzy opinion aggregation in group decision making environment," *Proceedings of the 4th International Conference on Fuzzy Systems and Knowledge Discovery*, pp. 301-304, August 2009.

[12] S. Ramalingam and D. Iourinski, "Using fuzzy functions to aggregate usability study data: A novel approach," *Proceedings of the International Conference on Information Technology and Applications*, pp. 415-418, July 2005.

[13] D. Stefka and M. Holena, "Dynamic classifier aggregation using fuzzy t-conorm integral," *Proceedings of the IEEE International Conference on Signal-Iamge Technologies and Internet-Based Systems*, pp. 126-133, December 2011.

[14] H. Hsu and C. Chen, "Aggregation of fuzzy opinions under group decision making," *Fuzzy Sets and Systems*, vol. 79, pp. 279-285, 1996.

[15] M. Almulta, K. Almatori, and H. Yahyaoui, "Possibility degree method for ranking intuitionalist fuzzy numbers," *Proceedings of the IEEE International Conference on Web Intelligence and Intelligent Agent Technology*, pp. 142-145, September 2010.

[16] Y.-C. Hung and S.-H. Ye, "The effect of combine Hopfield neural network and fuzzy ranking on e-learning system performance," *Proceedings of the IEEE International Conference on Advanced Learning Technologies*, pp. 611-613, July 2009.

[17] S. H. Siadat, A. Zengin, A. Marconi, and B. Pernici, "A fuzzy approach for ranking adaptation strategies in CLAM," *Proceedings of the 5th IEEE International Conference on Service-Oriented Computing and Applications*, pp. 1-4, December 2012.

[18] Z.-X. Wang and J. Li, "The method for ranking fuzzy numbers based on the approximate degree and fuzziness," *Proceedings of the 4th International Conference on Fuzzy Systems and Knowledge Discovery*, pp. 335-339, August 2009.

[19] K. Nakamura, "Preference relations on a set of fuzzy utilities as a basis for decision making," *Fuzzy Sets and Systems*, vol. 20, pp. 147-162, 1986.

[20] T. P. Fries, "Network Intrusion Detection Using an Evolutionary Fuzzy Rule-Based System," *Proceedings of the Conference on Systematics, Cybernetics and Informatics*, Orlando, FL, July 2011.

[21] T. P. Fries, "Autonomous Robot Navigation in Varying Terrain Using a Genetic Algorithm," *Proceedings of the Second IASTED International Conference on Robotics*, Pittsburgh, PA, November 2011.

Study on Integrated Risk Analysis Method and System Development With GIS Platform

Yi Liu, Shaobo Zhong, Hui Zhang, Rui Yang
Institute of Public Safety Research, Department of Engineering Physics, Tsinghua University, Beijing 100084, China

and

Lili Zheng
School of Aerospace, Tsinghua University, Beijing 100084, China

ABSTRACT

GIS-based case studies together with the software system were developed for the integrated risk analysis for dangerous chemical installations. A software system was developed with case-base, data-mining methods such as analytical hierarchy process (AHP), grey correlation analysis, fuzzy logic, neural network etc., and geographical information system (GIS) platform. The strong capabilities of spatial data manipulation provided by GIS facilitate the construction of case base. The design and implementation of the system are presented. Risk analysis was performed based on the developed system. With index-based method and case-data analyzing, risk analysis study was focused more on the factors of emergency response. Research results shows that the effect of emergency response should not be ignored in risk analysis study.

Keywords: Risk Analysis, Case Study, GIS platform, Emergency Response.

1. INTRODUCTION

Hazardous chemicals are referred to those chemical substances that are flammable, explosive, toxic, harmful, or corrosive. Hazardous chemical incidents may occur in the process of production, storage, transportation and use of hazardous chemicals, and may cause human casualty, financial loss, or environmental contamination. Risk analysis study has been given high attention for management of hazardous chemicals, preventing accidents, and reducing losses [1]. An integrated risk analysis should consider the inherent physical and chemical characteristics, the harm to health and environment, and the management and control status of those hazardous chemicals [2].

Cases are very useful data in risk analysis of hazardous chemicals. The main applications of cases include: estimating frequency of likely incidents, analyzing hazards of installations, providing support for case-based reasoning (CBR), and extracting indicator system. Case base creation and management in case-based systems have been recognized as the bottleneck that can determine whether a system will be successful or not [3]. In addition to providing support for CBR, cases themselves are also some typical samples and can be used in statistical analysis. With structured case data, an indicator system can be extracted from them by some data-mining methods such as analytical hierarchy process (AHP), grey correlation analysis, fuzzy logic, neural network etc. the indicator system are necessary basis in some indicator-oriented analysis methods of integrated risk analysis studies.

To execute integrated risk assessment based on cases, the first step is to create and maintain case base of chemical incidents. Some case information is available from books, Internet, electronic document etc. These multi-source data have various formats, media and are mostly textual. In these data, some general attributes of cases are recorded but they have informal, inconsistent forms. On the other hand, the geographical properties that are very important for their applicability in risk assessment are hardly recorded in these data. Furthermore, in an integrated risk assessment for hazardous chemical installations, the vulnerability analysis is a necessary component. It runs spatiotemporal process simulation of chemical incidents. Coupling the simulation results (spatial dispersion of hazardous chemical substances along with time) with the spatial distribution of population, environment and considering the chemical toxicity, health and environment vulnerability can be evaluated. Thus, a system that can help collect and manage cases of historical chemical incidents, chemical substances, population and environment distribution is required.

In this paper, a software system was developed with case-base, data-mining methods such as analytical hierarchy process (AHP), grey correlation analysis, fuzzy logic, neural network etc., and geographical information system (GIS) platform. Case studies are carried with the developed system and integrated risk analysis studies are performed.

2. GIS-BASED CASE-BASE SYSTEM

2.1 System Analysis

The system developed in this study include but not limited to the following functions.

(1) Case creation and maintenance for case-base

- Considering geographical properties

Based with Geographical Information Systems (GIS), basic spatiotemporal information is included in this system, such as river, road, resident, etc., and is capable for capturing, editing, storing, integrating, managing, analyzing, sharing, and displaying geographically referenced information[4]. Thus, each chemical incident case has spatial position related information that often has high impact on risk analysis.

- Case statistics, query, and collection

Case statistics, query are basic functions of case base. When a case base is built up, it may provide basic analysis functions, such as counting cases by type, querying cases by input conditions, or exporting the query results for further analysis. Case collection is a flexible function for users, which is to some extent similar to Wikipedia. One may input any kinds of case information with using this system and the system will collect the information as materials for creating new cases or modifying existing ones.

- Case presentation

For analysis and data mining, case is organized and saved in structured or semi-structured form. In this case, the cases can be expressed with varying forms in addition to textual format. Especially, with the help of computer graphics, multimedia techniques and GIS, a case can be presented through graphical or animated approaches that will be largely helpful for data mining and knowledge discovery.

(2) Chemical substances related data creation and maintenance

Not only the case base construction needs chemical substances related data, but also the vulnerability analysis requires physical, chemical or environmental parameters of chemical substances. The inherent characteristics of chemical substances are very important data for risk analysis as well as the application of this system.

(3) Model management

Simulation and calculation models for major dangerous chemical accidents such as leakage, explosion, and fire, etc. are developed in this system. The model results provide prediction of the accidents evolution and the spatial-temporal distribution of possible damage effect, which provides strong support for risk analysis. More over, through model analysis, incident scenarios can be reconstructed and extra data for cases obtained. These model data help for case modification.

4) Implementation of indicator-based risk analysis model

Many different methods have been developed to assess the risk for hazard materials such as Analytic Hierarchy Process [5], Fuzzy Synthetic Evaluation[6], Mont Carlo Method[7], Grey System Theory[8], Artificial Neural Network[9], Fault Tree Analysis[10], Beyesian Theory[11], Markov Model[12], *etc*.. The system developed in this study also provides factor analysis tools for developing risk analysis models. With cases and data established in the system, together with the data-mining models, one can easily set up an indexes system and verify its effectiveness and application. Furthermore, with some statistical methods, the weight for indicators can be determined with case data, which behaviors more objective instead of subjective.

2.2 System Design

The system includes three layers, presentation layer, business layer and data access layer, as shown in Fig. 1. Presentation layer stands for the computer-user interface, which is composed of .net window form controls, custom control (User control), third-party control library and ArcGIS Engine controls (which is provided by ArcGIS, they are intrinsically some C# wrapped COM components). Action refers to action objects that relate to interface events. The components in Business logic layer implement the business functions of the system. The current mainly implemented function include case management, chemical material management, indicator system construction and analysis, indicator system based risk assessment. Data access layer (DAL) implemented the generally used reading and writing operations of database and files.

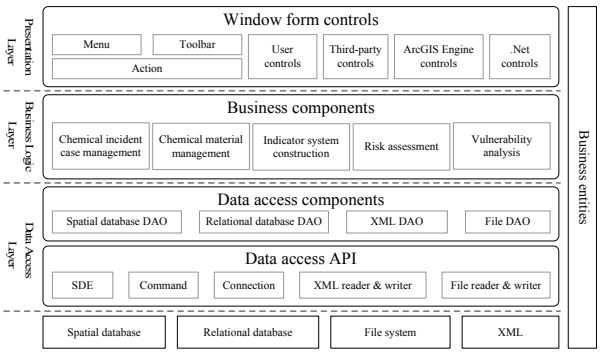

Fig. 1 The architecture of integrated risk analysis system for hazardous chemical installations

2.3 Database Design

For the integrated risk analysis, both the internal states and the external factors (such as ambient environment, rescue power etc.) should be considered. For hazardous chemical installations, the physical and chemical characteristics, e.g. the type, storage amount, materials of the container, are the internal factors determining the risk of the installation, and the terrain, residential situation, watershed, transportation, medical utilities, firefight power etc. are the external factors related to the risk of the installation. To make the case-base providing fundamental support for risk analysis, this study proposed a case structure, which perform as database in the system.

The basic information of a chemical incident has one-to-many relationship with other relevant information. For example, the affected zones by a chemical incident may have one or more. A chemical incident often involve in more than one kind of chemical materials. Nearby chemical installations around the incident position may be affected by the incident and cause potential sub-incident, which should be considered into risk analysis. Thus, the above factors should be stored in database, as shown in Fig.2.

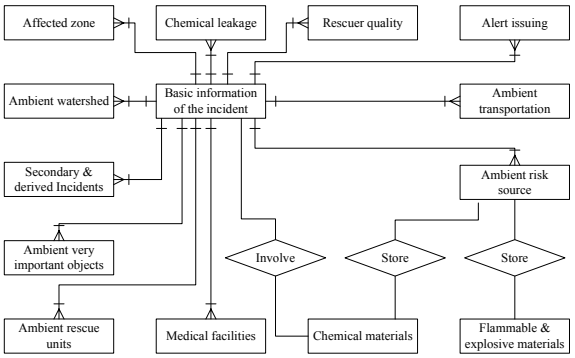

Fig.2 The E-R diagram of the system database

3. ILLUSTRATIVE APPLICATION: INTEGRATED RISK ANALYSIS

3.1 Case Study and Indexes Design

As commonly accepted, type and reserve are two of the most influential factors for risk of dangerous chemicals. For other factors besides inherent risk, the sub-accident risk and effect of emergency response are also very important and considered in this study. Cases study finds that the dangerous chemical accidents often cause sub-accidents, a typical example is the explosion accident of chemical plant in Jilin province, which caused large-scale water pollution in the Songhua River. In this study, we want to focus on whether and how the accident derivation and emergency rescue will affect risk level. Fig.3 shows the most often existed factors from fifty cases studies. The horizontal axis shows the first ten factors that most often appear in cases influencing the incident consequence. The vertical axis refers to the proportion of appearance frequency of each factor in all the studied cases to the amount of cases.

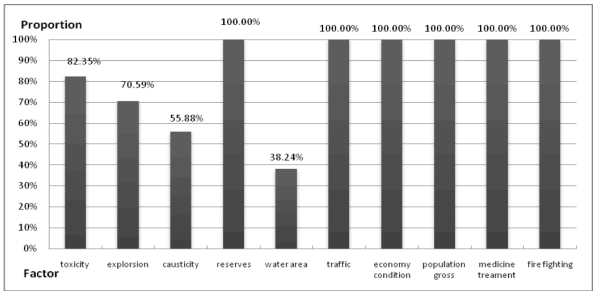

Fig.3 Influential factors from case study

Based on the result of Fig. 3, with the aids of the case study system developed above, the indexes for risk analysis of dangerous chemicals is designed as Table 1.

Detailed explanation of the indexes is as follows:

r_1 : Inherent Risk, refers to the inherent risk of the hazards, in despite of where and when it is, considering only the hazards category and the reserves in this study. The category refers to three characters of hazards with explosion possibility, causticity, and toxicity.

r_2 : Derived accident. It is find from case study that the dangerous chemical accidents often cause sub-incident, such as water pollution and traffic break.

r_3 : Circumjacent condition, considering economy and population here, which related to consequence of property loss and people casualty respectively.

r_4 : Emergency response, considering only emergency rescue action of medicine treatment and fire fighting team.

r_2 to r_4 are all geographical information related.

Definitions of other indexes are provided in Table 1. The indexes listed in Tab.1 may not be perfect. Each of the factors may consist of some more sub-factors. The reason that we select such indexes is that the basic data are obtained from accident cases study and thus is limited by cases. Another reason is that we want to focus on whether and how the accident derivation and emergency rescue will affect risk level. Thus to some extent a "simple" indexes helps to give deeper insight.

3.2 Weights of indexes

The weights of indexes are calculated with the system developed in this study. With the established case-base and data-mining methods such as analytical hierarchy process (AHP), grey correlation analysis, fuzzy logic, etc., it is not difficult to set reasonable weights for the indexes, as shown in table 2, where W_i denotes the weight of factor i.

3.3 Risk calculation

To calculate the integrated risk, several variables are defined. A general meaning integrated risk is denoted with R, and r represents the risk caused by each of the sub-factors, as the indexes shown in table 1. V is used to represent the comment value. Thus the integrated risk R is calculated with *eq*. (1),

$$R = \begin{cases} \sum_i r_i & if\ r_i\ has\ sub-level\ factors \\ \sum_i W_i V_i & if\ r_i\ has\ no\ sub-level\ factors \end{cases}, \quad (1)$$

where i represents all the factors that should be considered, and

$$r_i = \begin{cases} \sum_j r_{ij} & if\ r_{ij}\ has\ sub-level\ factors \\ \sum_j W_{ij} V_{ij} & if\ r_{ij}\ has\ no\ sub-level\ factors \end{cases}. \quad (2)$$

If the indexes have more levels, the calculation can be performed continually as

$$r_{ij} = \begin{cases} \sum_k r_{ijk} & if\ r_{ijk}\ has\ sub-level\ factors \\ \sum_k W_{ijk} V_{ijk} & if\ r_{ijk}\ has\ no\ sub-level\ factors \end{cases}, \quad (3)$$

and so on.

Table 1. Indexes design for risk analysis

Level-1	Level-2	Level-3
Inherent risk	Category (r_{11})	Explosion possibility (r_{111})
(r_1)		Causticity (r_{112})
		Toxicity (r_{113})
	Reserves (r_{12})	
Accident derivation	Water area pollution (r_{21})	
(r_2)		
	Traffic break (r_{22})	
Circumjacent condition	Economy (r_{31})	
(r_3)		
	Population (r_{32})	
Emergency response	Medical treatment (r_{41})	
(r_4)	Fire fighting team (r_{42})	

Table 2. Weights of indexes

W_1: 0.6205				W_2: 0.0569		W_3: 0.3226		W_4: 0.1813	
W_{11} : 0.4137			W_{12}:	W_{21}:	W_{22}:	W_{31}:	W_{32}	W_{41}:	W_{42}:
W_{111}: 0.2356	W_{112}: 0.0403	W_{113}: 0.1378	0.2068	0.0474	0.0095	0.0538	0.2688	0.0604	0.1209

In this study, the specific integrated risk is denoted by R_t, which composes R_1 and R_2. R_1 considers all the factors that will increase risk, and R_2 considers the factors that will reduce risk. And, the integrated risk R_t is calculated as

$$R_t = R_1 - R_2, \tag{4}$$

while

$$R_1 = \sum_{i=1}^{3} r_i, \quad R_2 = r_4, \tag{5}$$

R_1 and R_2 follow *eqs*. (1)-(3).

3.4 Results Analysis

To test the method developed in this study, another 34 typical accident cases are select. The accidents are divided into 4 levels according to the consequence seriousness of each accident, and are denoted with four different colors as red, orange, yellow and blue, as shown in table 3. The situation from each case is taken as basic data for risk analysis. That is, to assume the accident were not occurred and use the original conditions for risk analysis. Then, compare the result of risk analysis to the real accident consequence. The selected cases are numbered from 1 to 34 and the comparison is given in Fig.4. It can be found that the calculated risk values fit the level of the accident consequence level quite well. Cases with risk values more than 50 are mostly in red color, cases with risk values between about 35 to 50 cover the accidents of color orange and yellow, and those less than 35 mostly blue. If we set the risk level standard as table 3, the calculated risk results agree with the accident cases rather well.

In order to discuss the effect of emergency rescue action, the risk value to the selected cases is also calculated without considering of factors of emergency rescue action,

r_4. The result is shown in Fig.5. It can be found in Fig.5 that for all the cases, the risk values without r_4 are quite larger. This implies the important effect of emergency rescue in reducing risk, which should not be ignored. It also shows that it is difficult to clarify the risk value without r_4 to reasonable levels corresponding to the real accident consequence level, as shown in Fig.4 and table 3. This means if the effect of emergency rescue is ignored in the risk analysis, the results will to some extent lose reality.

Table 3. Risk level of selected cases

Accident level	I	II	III	IV
Representative Color	red	orange	yellow	blue
Risk level	I	II & III		IV
Risk value	⩾50	35~50		⩽35

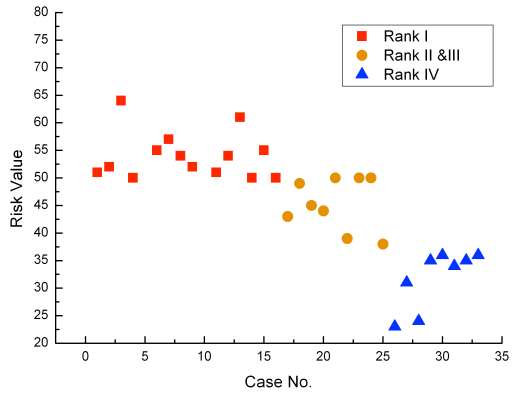

Fig.4 Risk analysis results of selected cases

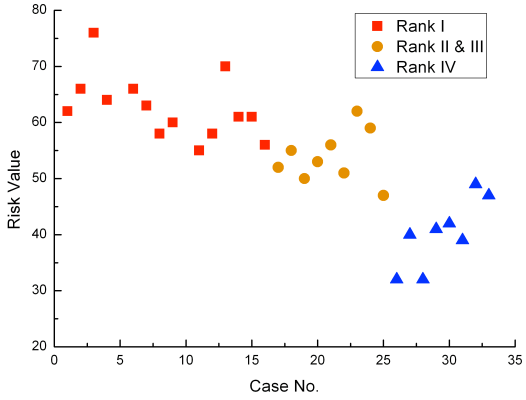

Fig.5 Risk analysis results of selected cases without factors of emergency rescue

4 CONCLUSIONS

Integrated risk analysis is very important work for effective prevention and control of chemical incidents. Scientific and practical risk analysis models provide strong support for the safety of chemical installations.

In this paper, a system framework of integrated risk analysis for dangerous chemical substances and installations is proposed. The business logic and the architecture of the system are analyzed and software system was developed with geographical information system (GIS) platform. Illustrative application of integrated risk analysis applying this system are performed and the results prove well. The risk analysis results indicate that the factors of emergency rescue play a significant role in reducing risk, and should not be ignored in risk analysis. Comparison of risk analysis results with and without factors of emergyency rescue shows that if the effect of emergency rescue is ignored, the risk analysis results may to some extent lose reality.

ACKNOWLEDGEMENT

Funded by National Natural Science Foundation of China (No. 70601015, No.91024032, No.91224008, No.70833003), Project of The National Science & Technology Pillar Program (No. 2011BAK07B02), Project of The Key Laboratory of Firefighting and Rescuing Technology of Ministry of Public Security (No.KF2011002).

REFERENCES

[1] Satty, T. L., and Kearns, K. P., Analytical Planning, Oxford, Pergamon Press.
[2] A. N. Paralikas, and A. I. Lygeros, A multi-criteria and fuzzy logic based methodology for the relative ranking of the fire hazard of chemical substances and installaions, Trans IChemE, Part B, Proc Saf Env Prot, vol, 83 , pp. 122-134, 2005.
[3] Chunsheng Yang, Robert Orchard, Benoit Farley, and Marvin Zaluski. Automated Case Base Creation and Management. Lecture Notes in Computer Science, 2003, 2718: 21-33
[4] K. Ohta,et al., Anaysis of the geographical accessibility of neurosurgical emergecy hospitals in Sapporo city using GIS and AHP, International Journal of Geographical Information Science, 21, pp. 687-698, 2007.
[5] Ernest H. Forman, Saul I Gass. (2001) The Analytic Hierarchy Process—An Exposition. Operations Research, 49, 4, 469-486.
[6] S. Bonvicini, P. Leonelli, G. Spadoni. (1998) Risk analysis of hazardous materials transportation: evaluating uncertainty by means of fuzzy logic. Journal of Hazardous Materials 62, 59-74.
[7] Mont Carlo Method: A.E.Ades, G.Lu.(2003)Correlations Between Parameters in Risk Models: Estimation and Propagation of Uncertainty by Markov Chain Monte Carlo. Risk Analysis. 23,6, 1165-1172.
[8] Grey System Theory: Mingzhi Mao, E.C. Chirwa.(2004) Application of grey model GM(1, 1) to vehicle fatality risk estimation. Technological Forecasting & Social Change. 73, 588-605.
[9] Artificial Neural Network: Raj Mohan Singh, Bithin Datta,and Ashu Jain. Identification of Unknown Groundwater Pollution Sources Using Artificial Neural Networks. Journal of water resources planning and management. 2004,506-514.
[10] Fault Tree Analysis: Faisal I. Khan , Tahir Husain.(2001) Risk Assessment and Safety Evaluation Using Probabilistic Fault Tree Analysis. Human and Ecological Risk Assessment. 7,1909-1927.
[11] Beyesian Theory: Chang-Ju Leea,*, Kun Jai Lee.(2006) Application of Bayesian network to the probabilistic risk assessment of nuclear waste disposal. Reliability Engineering and System Safety 91, 15–532.
[12] Markov Model: Karl N. Fleming. (2004) Markov models for evaluating risk-informed in-service inspection strategies for nuclear power plant piping systems.83, 27-45.

Design and Qualitative Assessment of Next Generation Hybrid Emergency Response Platform System for Landscape-scale Disasters

Yefeng MA
Institute of Public Safety Research, Tsinghua University,
Beijing, 100084, China

and

Hui ZHANG
Institute of Public Safety Research, Tsinghua University,
Beijing, 100084, China

and

Yi LIU
Institute of Public Safety Research, Tsinghua University,
Beijing, 100084, China

and

Rui YANG
Institute of Public Safety Research, Tsinghua University,
Beijing, 100084, China

ABSTRACT

Information and communication technologies (ICT) have made great contribution to support emergency management in dealing with earthquake, tsunami, flood, hurricane and many other disasters which are prone to cause landscape-scale catastrophe. Various information systems have been built to support information sharing, situation awareness, planning, communication, coordination, response and recovery. Such systems are usually designed to match with jurisdiction structures and emergency plans of the governments. For instance, National Incident Management System (NIMS) in USA is one example of such systems for comprehensive, nationwide and systematic approach to incident management. National emergency response platform (NERP) system in China is another example of such systems with similar functions. Chinese NERP is designed mainly based on centralized architecture and work effectively on earthquake, flood, fire, and industrial accident which only deal with one or a few government agencies [1]. Since in China government agencies run from central government to local counties, system can run very effectively. However, such system is not working well in disasters which require coordination between different government agencies. One the other hand, NIMS in USA can work well with disaster happening in a city. However, it is difficult to handle the problem requiring cooperation between different local governments. It is evident that if government structure in peace time and optimized government structure in disaster time is matched, response will be effective. If

there are different, it will be another disaster from government. Although training for joint command and emergency plans are helpful, it might still not enough for handling unexpected events. Adaption of government structure and information flow from peace time to disaster time is a great challenge. In this study, we look into the problems in Chinese NERP system and try to resolve information flow based on hybrid centralized system. In this way, coordination between government agencies and between government and general public will be more effective. Quantitative analysis will be conducted based on time response analysis for mass evacuation scenario.

With a centralized system, effective work relies on the ability to transmit accurate information to the centralized command and control center where information assessment and analysis are effectively conducted and public warning and various decisions can be made [2]. Decisions will then communicate back to local response agencies for execution. However, if disaster size becomes large such as Hurricane Katrina and Wenchuan earthquake, which are characterized as novel, unfamiliar, unprecedented and beyond the range of routine experience, the amount of information and corresponding communication tasks are astounding. Complicated and time critical situation presents great challenges for ICT system on processing large volume of information and supporting effective communication and coordination. In particular, problem becomes significant at the local level. As a matter of fact, in China, emergency management system at the local level is primarily used for collecting information and transmitting the information to higher level rather than organizing local response. They are waiting for decisions from the centralized command and control center. This is in part because of inadequate communication service as a result of inevitable damage by disaster. In this case, operational information system for organizing local response should be “light” enough to ensure rapid and adaptive implementation.

A hybrid centralized and decentralized ICT system is designed with basic functions of matching request and providing services directly in order to realize organized local response agencies in dealing with landscape-scale disasters. The function design of such system concentrates on five aspects: rescue support, medical support, supply support, transportation support and volunteer support. Under each function module, only two kinds of service will be developed: requesting (I have a need) and providing (I have an offer). The system is managed by the local command or ad hoc general headquarter. The user of this system is supposed to include affected people, governmental agencies, private sectors (such as supermarkets and companies), military and NGOs. The requesting service is primarily open to affected people and frontline responders. And the providing service faces to private sectors, higher-level responders and general public. In real situation, the affected area is large and usually divided into several small districts. The request will be first settled within each district. If request cannot be met, it will be handed to the ad hoc general headquarter which should make rapid decision to satisfy the request or not. If the request still cannot be met, the request will be turned to higher levels or to general public. In terms of function design, the rescue support is used for connecting different recuing forces including firefighter, police and military people and meeting their demands for equipment and personnel. The medical support part is used for deploying medical teams to where they are needed. The supply support part is for counting up the need for food, water, shelter and many other necessities and arranging the logistics. The transportation support part aims at coordinating transportation needs. And finally, the volunteer support part is used for organizing various NGOs and private sectors which have goodwill to offer help. This system will be not only applied as an operational system supporting quick decision-making for local responders, but also supported national emergency response system to improve situation awareness.

To quantify efficiency of developed hydride centralized and decentralized system, quantitative analysis is conducted to study the time response for mass evacuation scenarios. Various times are defined in Figure 1 based on

disaster evolution and system damage. When mass evacuation size increases and a number of districts are involved, required information processing and response times will be increased dramatically due to communication problems and delays. Quantitative analysis is conducted to compare the results from a centralized system, a decentralized system, and a hybrid system. Results are discussed. It is concluded that if the size is increased, hybrid system will be more effective and take advantages of centralized and decentralized system. In summary, developed hybrid information system aims at realizing two achievements. One is providing a specific platform to match the request and supply as quick as possible for local response. The other is quantified the deficiency and limitation of centralized NERP.

Key words: Hybrid, Information System, and Local Emergency Response

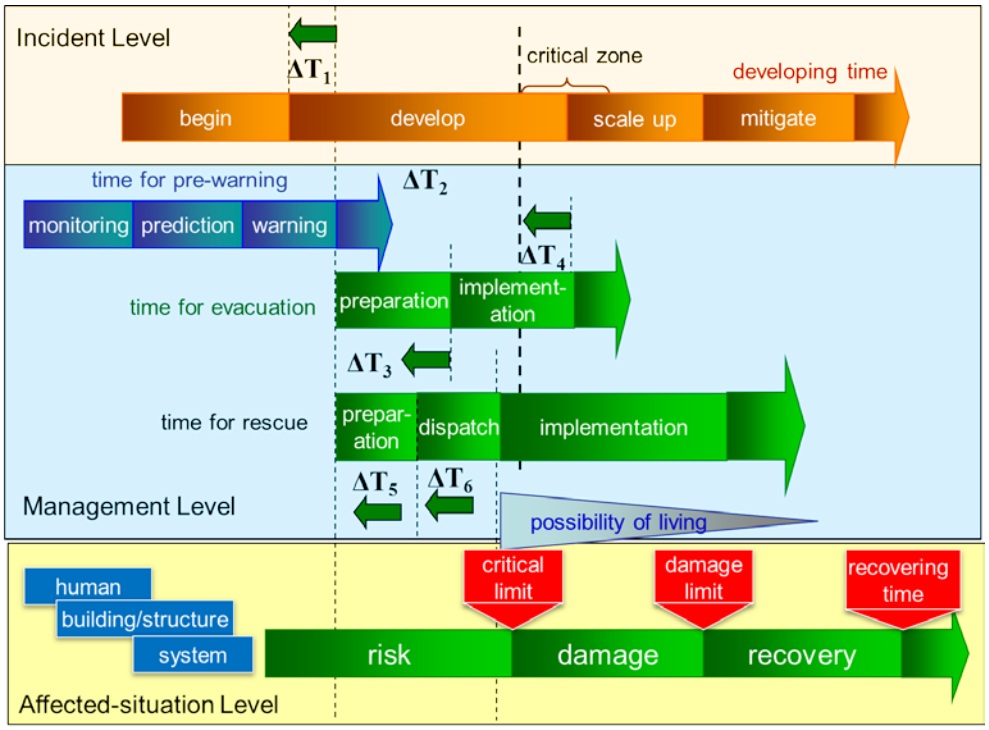

Figure 1. Schematic of Time Response for Mass Evacuation Scenario

REFERENCES

[1] W. Fan, "The design plan for Public Emergency Information System", **Informatization Construction**, No.09,2005, pp. 11-14. (in Chinese)

[2] H.B. Leonard, A.M. Howitt, "Organising Response to Extreme Emergencies: The Victorian Bushfires of 2009".**The Australian Journal of Public Administration**, Vol. 69, No.4, 2010, pp.372-386.

A Logic Block for Wave-Pipelining

Tomoaki SATO
Center for C&C, Hirosaki University
Hirosaki 036-8561 Japan

Sorawat CHIVAPREECHA
Faculty of Engineering, King Mongkut's Institute of Technology Ladkrabang
Bangkok 10520 Thailand

and

Phichet MOUNGNOUL
Faculty of Engineering, King Mongkut's Institute of Technology Ladkrabang
Bangkok 10520 Thailand

ABSTRACT

An FPGA (Field-Programmable Gate Array) device is selected in order to shorten the development life cycle of a processor. Using the FPGA is disadvantageous than using custom LSI (Large-Scale Integrated circuit) in terms of power consumption and operating frequency. That is, circuit design in the FPGA is required to design methods for high-speed and low-power operations. Wave-pipeline is one of a circuit design technique for high-speed processing and low power consumption. However, the design method has the problem of consuming a large number of logic blocks. To solve this problem, a logic block for wave-pipelining is proposed. The logic block is developed using 0.18-micron C-MOS (Complementary Metal–Oxide–Semiconductor) technology. A wave-pipelined adder which is made with the logic blocks is evaluated in the chip area. As a result, it is shown that the area of the adder which use the logic blocks is less than that of the adder without the logic blocks.

Keywords: FPGA, Wave-Pipeline, System LSI, Logic Bloc, Buffer, Timing.

1. INTRODUCTION

In recent years, the development life cycle of electronic devices is very short. Consequently, a processor and a system LSI (Large-Scale Integrated circuit) on the devices are similarly affected. In order to solve the problem, an FPGA (Field Programmable Gate Array) is used. The use of the FPGA improves the development life cycle and production cost in the case of low-volume production.

Evolution of semiconductor technology enables designing a large-scale circuit on the FPGA. The FPGA is used as the ASIC (Application Specific Integrated Circuit) of consumer devices as well as for prototyping of circuits. In recent years, a processor utilizing the reconfigurable features of the FPGA is realized. In spite of having such a feature, the designer of circuits in the FPGA needs circuit design techniques for high-speed processing and low power consumption.

One of the design methods, wave-pipeline [1] -[3] technique is used in the FPGA. The feature of the technique is a pipeline operation without a pipeline register. Conventional pipeline needs a pipeline register. The register always operates with clock signals. Thus, using registers is a cause of the power consumption. In addition, the operation frequency of conventional pipeline circuits depends on the critical path. Therefore, they significantly increase the processing time of the entire circuits.

On the other hand, wave-pipeline technique makes pipeline operations by timing adjustment. Buffer insertion is one of the methods of timing adjustment. Using this method is available on the FPGA. However, wave-pipelined circuits in the conventional FPGA are not assumed and consume a large number of logic blocks. In this paper, in order to solve this problem, the authors propose a logic block for wave-pipelining.

This paper is organized as follows. Section 2 presents the outlines of wave-pipeline. Then, Section 3 describes the logic block for wave-pipelining and evaluation of the logic bock is executed in Section 4. In Section 5, the conclusions are made.

2. WAVE-PIPELINE

Wave-pipeline is one of a circuit design technique for high-speed processing and low power consumption. Because wave-pipeline can be used at the gate level, circuit design on the FPGA can be used. In [4], a wave-pipelined multiplier on an FPGA was described. An application that uses wave-pipelined circuits has been developed in [5]. Currently, many wave-pipelined circuits are implemented on FPGAs.

It is to realize pipeline operations without using a pipeline register. Fig. 1 shows the overview of wave-pipeline and conventional pipeline. The important key words of wave-pipeline are D_{MAX}-path and D_{MIN}-path as shown in Fig. 1 (a). A clock cycle that influences the throughput of circuits is expressed by the following equation.

$$T_{CK} > (D_{MAX} - D_{MIN}) + T_{OV.} \quad (1)$$

Here,

T_{CK}: Clock cycle time,
T_{OV}: Overhead time.

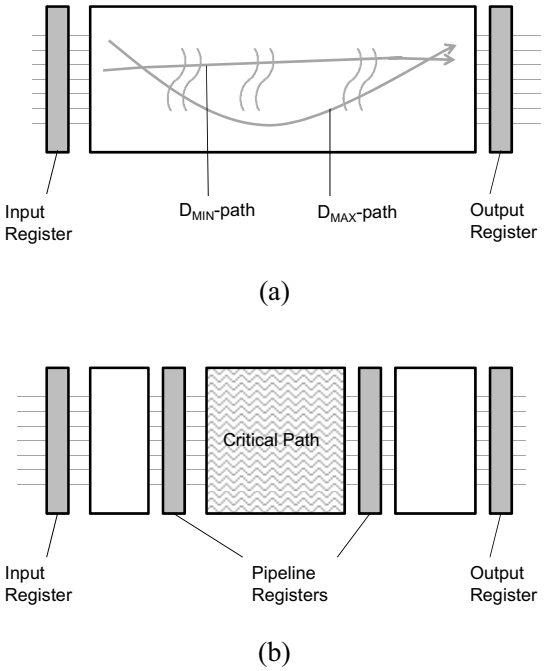

Fig. 1 Overview of Pipelines. (a) Wave-Pipeline (b) Conventional Pipeline.

According to Eq. (1), $D_{MAX} = D_{MIN}$ means the maximum speed of circuits at the gate level. Fig. 2 shows the diagram of wave-pipeline.

To approximate $D_{MAX} - D_{MIN}$ to 0, Adjustment of the delay time of D_{MAX} and D_{MIN} is needed. One of the methods of the adjustment is to insert buffers D_{MIN}-path. The methods can be used for the signal separation of multiplexing buffer.

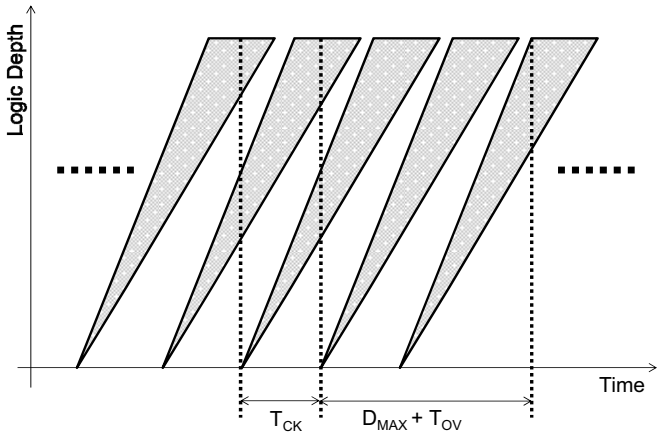

Fig. 2. Diagram of Wave-Pipeline

3. LOGIC BLOCK FOR WAVE-PIPELINING

In designing of wave-pipelined circuits, the insertion of buffers is used for timing adjustment. When designing a custom LSI, the insertion of buffers means to consume the area for the buffers. On the other hand, the insertion of buffers on an FPGA means a large number of logic blocks is consumed. That is, it means that the buffer insertion consumes large amounts of resources on the FPGA.

To solve the problem of consuming large amounts of resources on an FPGA, a logic block for wave-pipelining is proposed in this paper. The logic block is developed using a standard cell library. The library uses 0.18-micron C-MOS technology. To clarify the domination of the logic block, the areas of the wave-pipelined circuit of the logic block and that of a conventional logic block are compared.

Fig. 3 shows the conventional logic block. The conventional logic block consists of a LUT (Look up Table) and a flip-flop. The LUT is shown in Fig. 4 and a three-input LUT [6]. The function of the LUT and the flip-flop is switched by a selector. On the other hand, the logic block for timing adjustment is composed of several buffers. Those area and delay time are shown in Table 1 and Table 2, respectively.

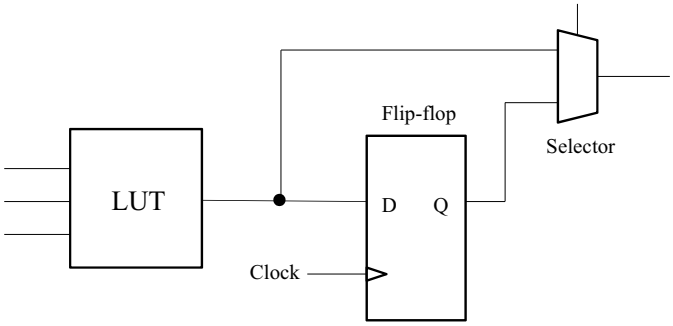

Fig. 3. Conventional Logic Block

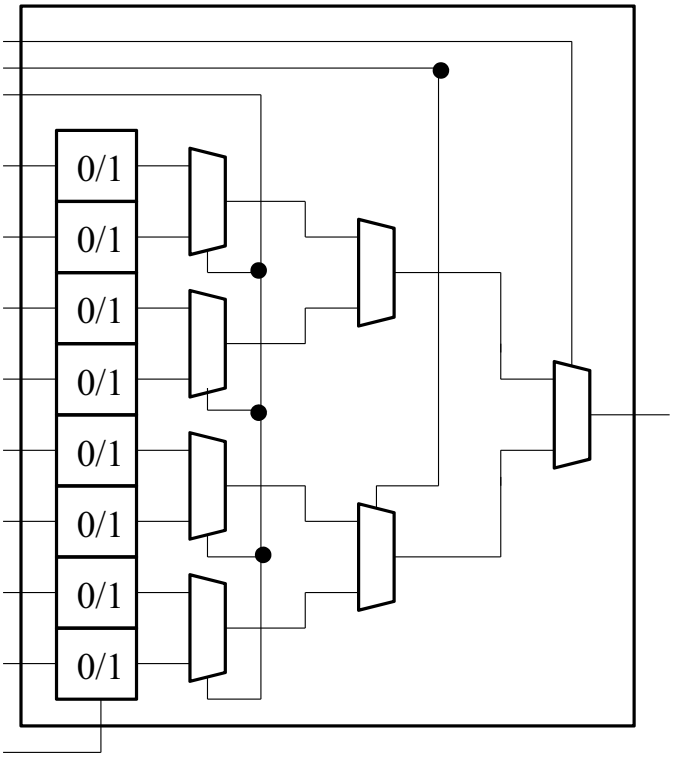

Fig. 4. Three-Input LUT

Table 1. Delay Times of Logic Blocks

Conventional Logic Block	0.84 ns
Logic Block for Timing Adjustment	0.85 ns

Table 2. Areas of Logic Blocks

Conventional Logic Block	997.4 μm^2
Logic Block for Timing Adjustment	148.5 μm^2

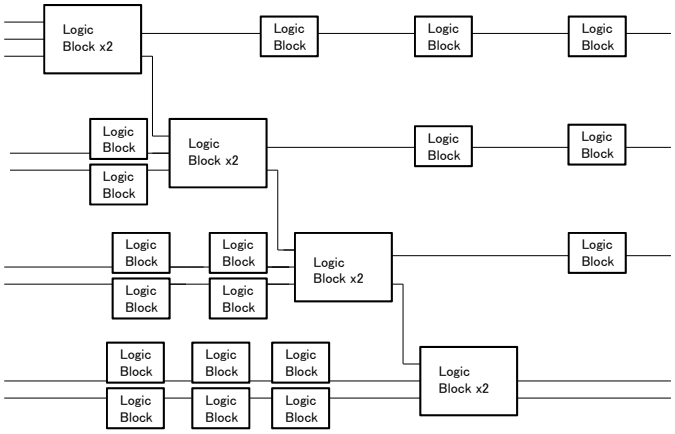

Fig. 5. 4-Bit Wave-Pipelined Adder (Only Using the Conventional Logic Block)

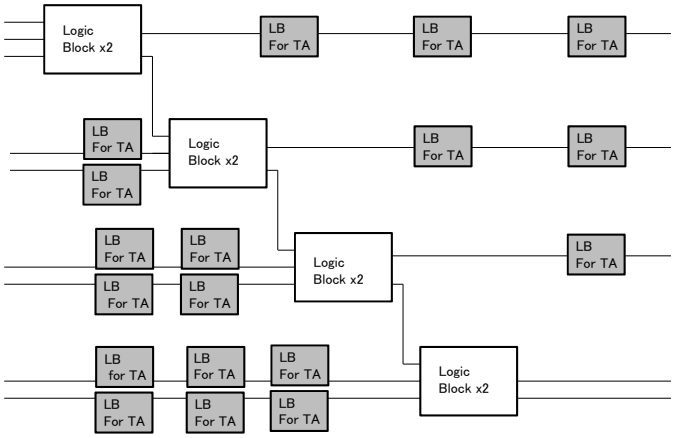

Fig. 6. 4-Bit Wave-Pipelined Adder (Using the Logic Block for Timing Adjustment)

4. EVALUATION

For the evaluation of areas, two 4-bit wave-pipelined adders are designed. Fig. 5 is the 4-bit wave-pipelined adder which is made of only the conventional logic blocks. And, Fig. 6 is the 4-bit wave-pipelined adder which is made of the logic blocks for time adjustment. The white coloured boxes are the conventional logic Block. The grey boxes shows the logic block for timing adjustment.

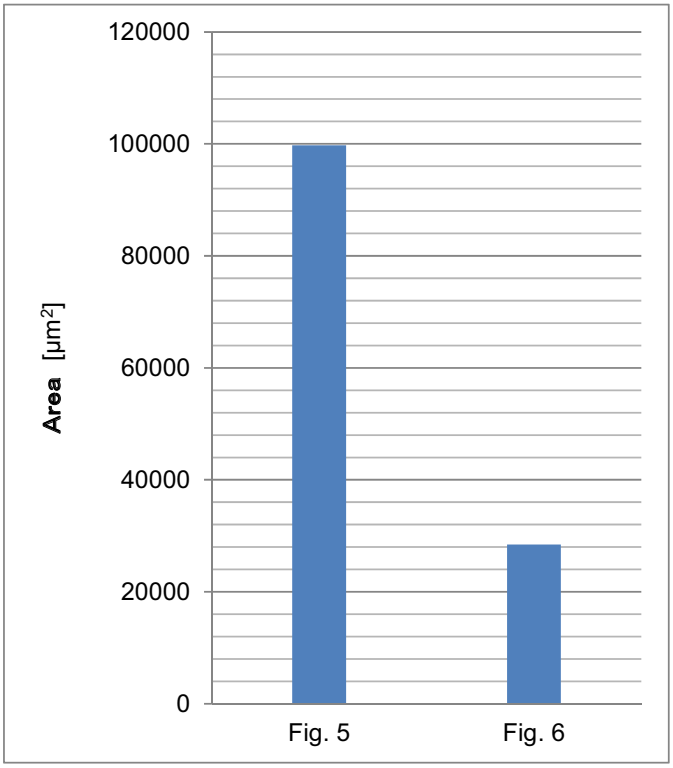

Fig. 7 Evaluation Results of Area Dissipations

Fig. 7 shows evaluation results of area dissipations. According to the results, using the logic blocks for timing adjustment makes a great decrease in the area of 4-bit wave-pipelined adder circuits. The area of Fig. 5 is 3.5 times the area of Fig. 6.

5. CONCLUSION

Wave-pipeline technique on an FPGA made the problem that is to consume a large number of logic blocks. In this paper, the authors have developed the logic block for wave-pipeline aimed to solve this problem. The developed logic block have been performed the comparative evaluation of area measurements. As a result, it has been shown that the use of the developed logic blocks enables reduced the area of wave-pipelined circuits.

The future works are the establishment of optimization techniques of timing adjustment of wave-pipelined circuits utilizing the reconfigurable features.

ACKNOWLEDGMENT

This work has been supported in part by VLSI Design and Education Center (VDEC), the University of Tokyo in collaboration with Synopsys, Inc. and KAKENHI Grant Numbers 21700064 and 25330149. The standard cell library used on this research was developed by Tamaru/Onodera Lab. of Kyoto Univ. and released by Prof. Kobayashi of Kyoto Inst. of Tech.

REFERENCES

[1] L. Cotton, “Maximum Rate Pipelining Systems,” **Proc. AFIPS Spring Joint Computer Conference**, pp. 581-586, 1969.

[2] F. Klass and M. J. Flynn, “Comparative Studies of Pipelined Circuits,” **Stanford University Technical Report**, No. CSL-TR-93-579, July 1993.

[3] W. P. Burleson, M. Ciesielski, F. Klass, and W. Liu, “Wave-Pipelining: A Tutorial and Research Survey,” **IEEE Trans. on Very Large Scale Integration (VLSI) Systems**, Vol. 6, No. 3, pp. 464-474, Sept. 1998.

[4] I. B. Eduardo, L. Sergio and M. M. Juan, "Some Experiments About Wave Pipelining on FPGA’s," **IEEE Trans. on Very Large Scale Integration (VLSI) Systems**, vol. 6, no. 2, pp. 232-237, 1998.

[5] T. Sato and M. Fukase, "Reconfigurable hardware implementation of host-based IDS," **Proc. of APCC 2003**, vol. 2, pp. 849-853, 2003.

[6] S. Brown and Z. **Vranesic, Fundamentals of Digital Logic with VHDL Design,** Mc Graw Hill, 3 edition, 2009.

Study on Multi-dimensional Scenario-space Method for Case-Based Reasoning

Yi Liu, Yulin Feng, Hui Zhang, Rui Yang
Institute of Public Safety Research, Department of Engineering Physics, Tsinghua University, Beijing 100084, China

and

Lili Zheng
School of Aerospace, Tsinghua University, Beijing 100084, China

ABSTRACT

Case based reasoning (CBR) is a popular problem solving method. A case based reasoning cycle always contains four processes: retrieve, reuse, revise and retain (the four REs). This paper presents a multi-dimensional scenario-space (MDSS) method, which makes CBR more efficient. The four REs cycle using MDSS is also discussed in the paper.

Keywords: Multi-dimensional Scenario-space, Case based reasoning, the four REs cycle.

1. INTRODUCTION

Case based reasoning, more commonly known as CBR, is a problem-solving paradigm, which is growing rapidly in the past several years. Case based reasoning is often used to utilize the specific knowledge of past experience so that problems can be solved by adapting solutions from similar cases which were successfully dealt with in the past. In addition, case based reasoning is also an approach to incremental, sustained learning since well solved cases are retained so that more cases can be available for future problems.

A case based reasoning cycle always contains four processes, retrieve, reuse, revise, and retain, also known as "the four REs" [1]. For each process, some more steps should be taken according to the specific problem:

The retrieve process is aimed at case matching. In this process, cases in the existing case library or case management system would be thoroughly searched in order to find some previous cases that can match for new problems. Since hardly two cases could be exactly same, retrieving may sometimes be pretty difficult in defining 'similarity'. Similarity thresholds on some aspects of the case always have to be set in order to define 'sufficiently similarity', which can make the searching process much easier. In this way, the retrieving process always ends with a set of cases instead of one "best match" case. After some cases being retrieved, the following process is the reusing process, which aimed at better using of knowledge and experiences from retrieved cases. If a "best match" case found, reusing would be pretty easy since the existing solution can be adopted directly. However, it is often the case that only part of the existing solution can be beneficial, and adaptations are essential. The revision process is mainly meant for learning from incorrect or even failed cases. In this process, errors should be found and corrected using some domain-specific methods according to the new problem itself. This process always requires through understanding of the cases and strong mathematical base are also required since adjustments can be quite complex. Last but not least, cases should always be retained after the former three processes; no matter the problem solving procedure is a success or a failure. By learning from successful solutions, the case library can be enlarged; when failures occur, the case may also be retained to prevent the decision maker from making the same mistakes.

In applying case based reasoning in practice, some considerations need to be taken in advance, like how to evaluate the similarity between two cases, how a best match can be derived, how to make full use of an existing solution, etc. Some work has been done to deal with such problems. Lao, A. (2009)[2] proposed ontology-based similarity measurement to retrieve the similar sub-problems that overcomes the synonym problems on case retrieval. Chen, Y.-J. (2009)[3] developed a mechanism for ontology-based distributed case-based reasoning using characteristic of ontology and a proposed multistage algorithm, to effectively support knowledge retrieval within the virtual enterprise environment. Guo, Y. (2013)[4] proposed an intelligent case retrieval method by integrating ontology technology into case based reasoning system.

This paper is aimed at developing a multi-dimensional scenario-space method in case based reasoning to make it more efficient for reasoning. By applying this method, the existing case libraries can be transformed as a digitized database in which the relationships between cases as well as cases themselves can be formatted and quantified, and so that more convenient and compatible for reasoning.

2. MDSS METHOD

2.1 Definition of MDSS

When talking about a specific case, aspects, which are either common or specific, should be taken into consideration. Take corporation risk evaluation system as an example, the consultancy institutions always need to investigate the corporation's capital and debt amount, business volume reputation, the number of employee etc., and then give a report based on the analysis. Since corporations in the same industry always have some characteristics in common, a case library may need to be established after some period of time for future reference, which may help improve the efficiency. However, the question lies that what factors should be recorded and how to properly and efficiently record them.

In a Multi-Dimensional Scenario-Space (MDSS) system, a case may be defined as a point in a multi-dimensional space where the factors, say capital, debt, etc. are served as the coordinate axises. As for factors like the reputation of the company, which is a non-quantified evaluation, the ratings given by some rating agencies like Standard & Poor's or Fitch may be concerned, while variables in the domain of 0 to 1 may be defined according to the rating in order to measure the reputation. As for other factors like the number of employees, the numbers may vary a great deal between corporations, which can make it difficult to define the coordinate unit. For example, the number of employees in corporations like Microsoft Corporation can be some 100,000, while for some newly established corporations, the number can be only about 100. In this situation, some modifications like logarithmic transformation may be essential.

By applying the multi-dimensional scenario-space system in case based reasoning, a case can be presented as a point in the multi-dimensional space while the similarity between cases can be measured as the distance between them. In addition, two or more cases may be used together for more accurate matching. Take a two-dimensional system as an example. Every case can be defined as a point, say (X_j,Y_j) for the j^{th} case. Since any point can be represented as the weighted average of three points, which are not in a line, the new case can always be found a match, which is either a single case or a combination of two or more cases.

It may be difficult for a high-dimensional scenario-space system, say a 10-dimensional space, in which at least 10 previous cases should be involved to ensure that new cases can be represented. However, as time going on, the capacity of the case library can be increasing so that cases can be more precisely represented.

2.2 Retrieving with MDSS

While by applying the multi-dimensional coordinate system, this can be relatively easier. Since the previous cases are all transformed into points in the system, the norms can surely be used. The Euclid Norm is used here due to its popularity. Case A, rather than case B is said to be more similar to case C can be represented if the Euclidean distance between A and C is smaller than the distance between B and C.

In an N-dimensional space, the Euclidean distance can be written as:

$$d_{1,2} = \sqrt{\sum_i (X_{1i} - X_{2i})^2} \quad (1)$$

Thus, A is more similar to C than B if $d_{A,C} < d_{B,C}$; which means that cases which are closer to the new point can lead to better accuracy.

When searching for cases that are 'sufficiently similar' to the new case, we may look for some threshold d_m previous cases whose Euclidean distance from the new case is no greater than d_m will be chosen. In choosing d_m, some factors should be taken into consideration. To begin with, accuracy need to be ensured to some degree, which means that d_m shouldn't be too large. In addition, d_m shouldn't be too small, either. When d_m is quite small, only a few cases can be found from the case library, which may limit the number of possible solutions, thus making the decision maker in a difficult situation. Taking above into consideration, the compromise between accuracy and number may always be made. For some industry, like the aviation industry, which have strong demand for accuracy or when the case library is large enough, accuracy can be put in first place in choosing the threshold. While for a small case library or in some situations which doesn't care too much about the precision, like choosing the appropriate amount of food for family raised oxen and sheep, d_m may be larger so that more reference can be found.

2.3 Reusing with MDSS

Since every case can be defined as a specific point in the space, some mathematical methods can be used in the multi-dimensional scenario-space system. This paper presents a method of reusing existing cases with matrix operations, which is helpful for decision making

For an n-dimensional coordinate system, N cases may be collected from the case library to form a $N \times n$ matrix. Assuming that enough cases can be derived from the case library, i.e. N>n, then choose n cases which are not corrected to each other in order to form a $n \times n$ matrix **C** whose rank is *n*. Therefore we may have

$$det|\mathbf{C}| \neq 0 \quad (2)$$

Here we still take the corporation risk evaluating system as an example. For the n cases, the result of the evaluation, say risk level can be formed into a vector named as **r**. Therefore, the evaluation process can be defined as a function **f** which satisfies the following equation:

$$f(\mathbf{C}) = \mathbf{r} \quad (3)$$

Here **f** is defined as a liner function for simplifications, as for a n-dimensional space, the function can be regarded as a $1 \times n$ vector named as **A.** Thus, the equation can be written as

$$\mathbf{AC} = \mathbf{r} \quad (4)$$

Since the results have already been in the library, **C** and **r** are both known conditions and **A** can be derived as:

$$\mathbf{A} = \mathbf{rC}^{-1} \quad (5)$$

To make the equation above meaningful, C should not be any singular matrix while the assumption that the rank of **C** is n can satisfy this.

For a new case, which can be represented as some coordinate $\mathbf{X} = (X_1, X_2, \ldots, X_n)$, the result, say the risk level can be derived as follows:

$$Result = \mathbf{AX} = \mathbf{rC}^{-1}\mathbf{X} \quad (6)$$

Which is an explicit model for case based reasoning where C stands for the case library, A is for the method of reusing the cases while 'Result' is derived based on previous results which are named as **r**.

3. FUTURE RESEARCH

3.1 Revising with MDSS

In case based reasoning, failures may always be met, multi-dimensional scenario-space system is no exception. When a failure happens, mistakes made due to careless, like calculation errors, should first be corrected. Then, the whole decision making cycle should be examines and revised to prevent the decision makers from making the same mistake.

As is stated in the previous session, case based reasoning can be defined as a function. However, the function cannot work well in all cases. According to equation (5), the function is derived based on **r** and **C**, which stand for the result and condition of the chosen cases. Some questions related to case choosing process should be asked:

(1) Is the similarity evaluation method defined properly?
(2) Are the cases chosen properly?
(3) Is the accuracy level meeting the accuracy requirements?

After that, the function itself should be examined. Here we present a linear function, while in reality, the situations may be much more complex so that the polynomials, hyperbolic functions or some other functions should be used. Since no function can be suitable for all cases, the revision process should always be accompanying the case based reasoning decision process.

3.2 Retaining with MDSS

The multi-dimensional scenario-space system is also very open since the dimension can always be enlarged, even when it becomes a complex giant system.

For a three-dimensional corporation risk evaluating system, where the overall risk is originally defined with the capital amount, debt amount and reputation, when someday a new case showing that the potential risk is also strongly related to the number of employees, then it can be a fourth coordinate axis for the new four-dimensional coordinate system. For the existing cases, which have been defined as a point in the three-dimensional space, can be transformed to the four-dimensional space simply by adding a coordinate. Cases that lack related information may be defined as 0 in the new coordinate axis, or be removed from the case library since accuracy can be more important in some situations.

New cases should be always retained since cases in the long past may not be useful in the future since the world is changing day and day, no matter success or failures. Sometimes, new cases may indicate a new trend, which shows that some existing coordinating axises are of little use in the future. While by learning from the failures, mistakes can be avoided. What' s more, in multi-dimensional scenario-space system, a failing case can also be represented as a point in the system, cases which are very close to the failures should be carefully used or even abandoned directly.

4 CONCLUSIONS

This paper presents a multi-dimensional scenario-space system in case based reasoning for decision-making support, in which cases can be transformed to a quantified database, which makes the process more efficient. In the retrieving process, the multi-dimensional scenario-space system may help to define similarity and 'sufficient similarity'; in the reusing process, this paper presents a new method using matrix calculation since the cases can be defined as points in the multi-dimensional coordinate system; in the revising process, the multi-dimensional scenario-space system makes it more convenient for checking the errors and make some revision; while in the retain process, new cases can be kept for future reference as well as future revision which may start a new cycle. By applying the multi-dimensional scenario-space system in case based reasoning, the decision making process can be more efficient and more convenient.

ACKNOWLEDGEMENT

Funded by National Natural Science Foundation of China (No. 70601015, No.91024032, No.91224008, No.70833003), Project of The National Science & Technology Pillar Program (No. 2011BAK07B02), Project of The Key Laboratory of Firefighting and Rescuing Technology of Ministry of Public Security (No.KF2011002).

REFERENCES

[1] A. Aamodt, E. Plaza (1994); Case-Based Reasoning: Foundational Issues, Methodological Variations, and System Approaches. AI Communications. IOS Press, Vol. 7: 1, pp. 39-59.

[2] Chen, Y. -J, Chen, Y. -M, & Su, Y. -. (2009). An ontology-based distributed case-based reasoning for virtual enterprises. Paper presented at the Proceedings of the International Conference on Complex, Intelligent and Software Intensive Systems, CISIS 2009, 128-135.

[3] Guo, Y., Peng, Y., & Hu, J. (2013). Research on high creative application of case-based reasoning system on engineering design. Computers in Industry, 64(1), 90-103.

[4] Lau, A., Tsui, E., & Lee, W. B. (2009). An ontology-based similarity measurement for problem-based case reasoning. Expert Systems with Applications, 36(3 PART 2), 6574-6579.

[5] Vladimir Kurbalija, Mirjana Ivanovic, Zoran Budimac: Case-Based Reasoning Framework for Generating Wide-Range Decision Support Systems. 273-279.

Design Next Generation Emergency Platform System based on Cloud Computing

Yi Liu, Yefeng Ma, Hui Zhang, Yi Liu, Rui Yang,
Institute of Public Safety Research, Tsinghua University
Beijing, 100083,China

and

Lili Zheng
School of Aerospace ,Tsinghua University
Beijing, 100083,China

Keywords: Cloud Computing, Platform, System, emergency respond, decision making

Emergency platform system has been routinely used to response various natural and man-made disasters happened in China since 2008 including Sichuan Earthquake. The emergency platform system is capable of providing CRITICAL services for general public and decision makers including 8 functions such as Crisis prediction and early warning, Risk analysis and damage monitoring, Intelligent operational planning, Training, Integrated emergency management, Command & control, Assessment of response, and Logistics. Events driven strategically emergency plans from scenario analysis are developed to form the base plans for disaster response. In China, major planning scenarios across 4 areas such as natural and man-made disasters, industrial accidents, health emergency, and social security are being developed. Target Capability List (TCL) is being created. Critical information and decision making elements should be acquired effectively at various key stages to guarantee the success of the operations. Critical information comes from four areas: disaster evolution and damage monitoring domain, social network domain, behaviors domain, and decision support domain. To support such system, emerging information technology such as cloud computing will be ideal tools for applications. In this abstract, feasibility of emergency-cloud emergency platform is discussed and key elements and framework design are provided. Figure 1(a) shows the general structure and functions of the emergency-cloud platform and Figure 1(b) is workflow of such system to support on-demand service for emergency plan and decision making.

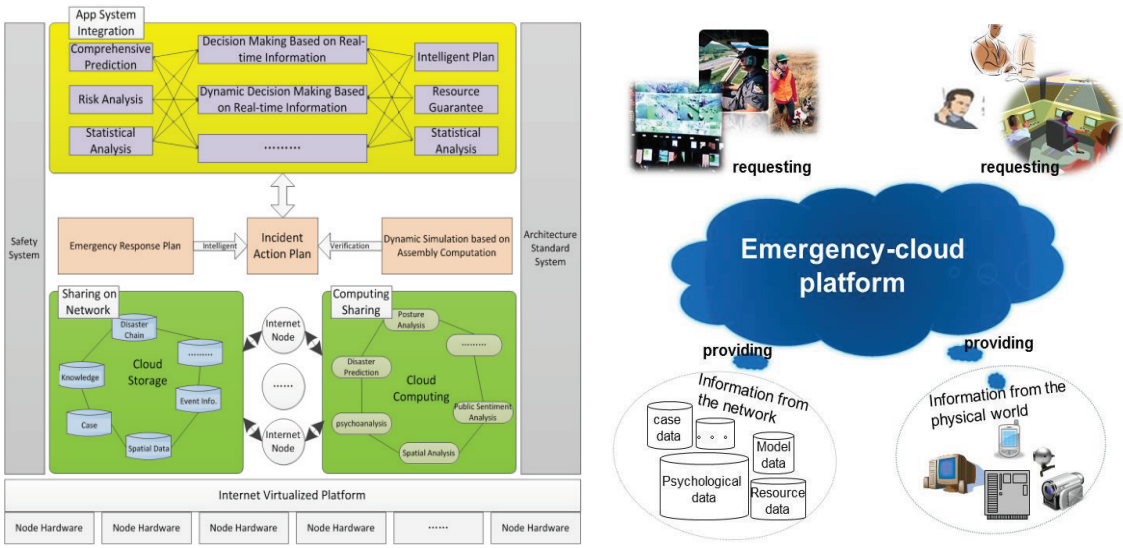

Figure 1(a) General structure and functions of the emergency-cloud platform and (b) workflow of such system to support on-demand service for emergency plan and decision making

Newly developed emergency-cloud system is a service supported platform consistent with the rule of request-answer. It supports emergency information flow and resource management in two dimensions: function and application dimensions. The emergency-cloud system should be able to deal with traditional and unexpected events in both dimensions considering the life cycle of the disaster. In order to achieve the goal of emergency respond on real-time and online. Emergency-cloud merges emerging technologies such as cloud computing, the internet of things, high-performance computing and various decision models to response crisis in uniform and intelligent ways and to meet the demand in emergency management. These processes require the implementation of service in the emergency-cloud. The architecture of emergency-cloud is shown in Figure 2.

The architecture of emergency-cloud includes various layers such as physical resource, cyber information collection, emergency-cloud computing platform, emergency-cloud services, emergency response sub-clouds, cloud interface and users. All the levels of emergency-cloud listed could provide technical support from bottom to up, and answer the calls from top to down to support real-time online decision making. Description of each layer can be summarized as follows

Physical resource and information collection layer: Through the ways of information gathering and physical perception of the internet of things, real-time monitoring in the physical and cyber world could be accessed. The information collection layer stores massive heterogeneous data of the events as well as decision-supporting information in the dispersed state; the information collection layer could provide accessible support for the network management of resources along with the balanced configuration of emergency-cloud.

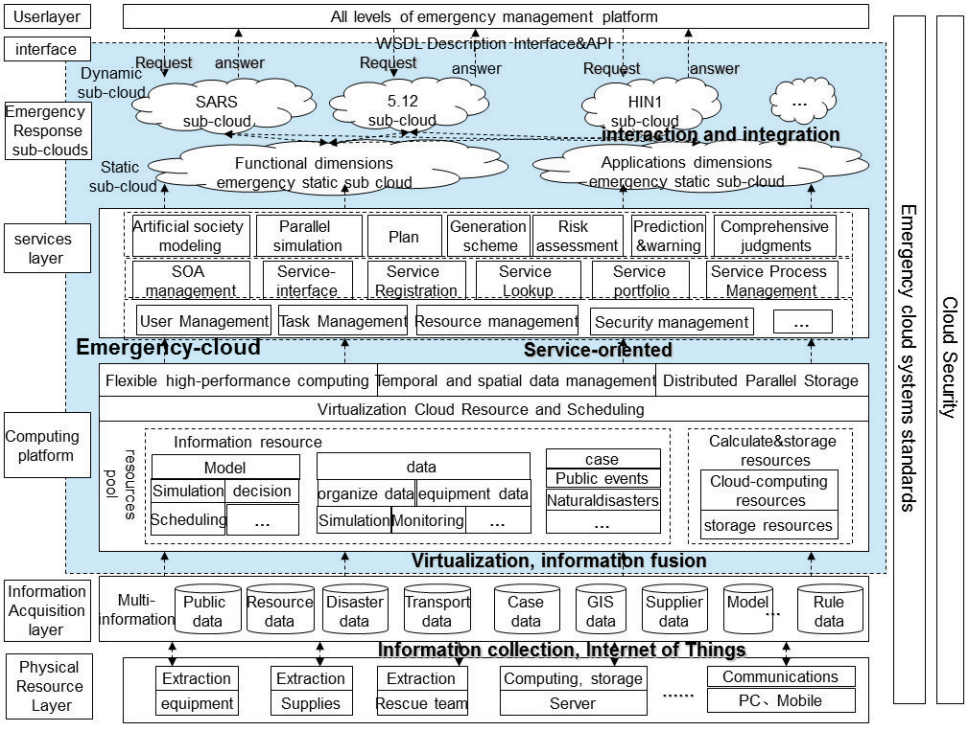

Figure 2. The architecture of Emergency-Cloud

Emergency-cloud computing platform layer: This layer includes resource pool and virtualization of cloud resource management and scheduling module. The emergency-cloud resource pool could realize the collection and merge the big data using virtualization and semantic web. The emergency-cloud resource pool also uses the unified classification management to provide support for functional needs. The decision-support resources such as flexible and high-performance computing, spatial data management and storage, distributed paralleling storage, as well as cases and models for the applicable service of upper emergency-cloud could be provided by virtualization and scheduling technology.

Emergency-cloud service layer: This layer transforms the emergency-cloud resources into emergency-cloud services by using the precise semantic service packaging technology, and managed and published the service by unified services registered facilities. Emergency-cloud service layer includes services for emergency applications which are transformed from the demand of specific emergency business decision, such as artificial social modeling, parallel simulation, plan management, scheme generation and service for emergency management such as SOA component management, service interface management, service registration, the process combination management. The services for system management include the cloud user management, resource management, task management, security management and etc.

Emergency response sub-clouds layer: This layer includes static and dynamic sub-clouds. The static sub-cloud is responded to function and application dimensions. The dynamic sub-clouds establish to response the requirements of various incidents. By dynamically matches the contingency cloud services, which are based on precise semantics. The dynamic sub-clouds give requestor supporting by providing timely and efficient cloud services.

Cloud interfaces and user layer: By standardized service

access, cloud interface layer will provide service delivery interface to the emergency management platform of all levels of government or various areas of expertise. By terminal access the emergency-cloud services, different levels of users are able to perform emergency duties.

In summary, the existing emergency response platform system is reviewed and the demand of new emergency platform was analyzed. Feasibility and framework design are discussed.

REFERENCES

1. Bohu Li, Lin Zhang, Shilong Wang (2010) Cloud **manufacturing-new service-oriented networked manufacturing mode**. Integrated Manufacturing Computer Systems, 1, 1-7.
2. Kenji E. Kushida，Jonathan Murray ，John Zysman (2011)**Diffusing. the Cloud: Cloud Computing and Implications for Public Policy**. Journal of Industry, Competition and Trade.September 209-237.
3. Victor A. Banuls, Murray Turoff, Starr Roxanne Hiltz(2012)**Collaborative scenario modeling in emergency management through cross-impact,** Technological Forecasting & Social Change 1579–1602.

Can SideBySide be Adapted to use Generative Codes to Create a more Creative Tool for the Physical Environment?

Pauline de Souza
Department of Art and Design, School of Art and Digital Industries, University of East London, United Kingdom, E16 2RD.

Abstract

SideBySide an ad-hoc multi-user interaction with handheld projectors developed by Ivan Poupyrev, Karl D.D. Wilis, Scott E. Hudson and Moshe Mahler sets out to track multiple independent projected images by using device mounted cameras and hybrid visible infrared light projectors. The infrared process uses invisible marker tracking based on a augmented marker system to locate potential visual images. The system was created to enable people to share content in their folder and overlap these images once they are projected. Individuals find images from other sources and place them in their folders. The images are not produced by the individual.

My research, which is a work in process, looks at SideBySide from a different perspective. Using generative algorithmic system can provide a more creative visual processing and engagement that is more participatory than the present software used by SideBySide. This paper looks at how generative computer vision base detection techniques can be used in interactive media. Generative codes can produce augmented reality and one existing prototype is Konstruct which works on iphones. The Konstruct marker is placed in a physical space and the iphone is held up in front of it. Voice activation changes the size of the work and there is a paint brush that is controlled by movement of the head. A menu helps to control the colour palette and size of the paint brush. However, this approach is limited for professional creative people who need a more interactive device. Augmented reality offers a more immersive environment than QR codes.

Keywords: SideBySide, Generative Codes, Augmented Reality Markers, Interactivity and ArTag.

Introduction.

Augmented reality is a strategic system that interacts with our living environment on different levels but is full potential as a functional tool still needs to be explored. The development of SideBySide provides an opportunity to see how augmented reality can be directed into other directions. My research into this area is motivated by reconsidering how the handheld computing device of SideBySide can be used as a tool in a different way. It relates to my interest in generative codes, art and design involvement in the creative environment. It relates how creativity ideas are produced, shared and allow interactive participation.

Software used by the SideBySide system depends on static images. It does this by combining infrared and visible imagery. These images which are loaded into red and green channels of an Open GL frame buffer. A separate monochrome image from the red and green channel is loaded into a blue channel using Open GL's additive blending mode. Next the channels are combined in real time using the graphic processing unit (fig.1)

Fig.1. SideBySide Software Ivan Poupyrev.

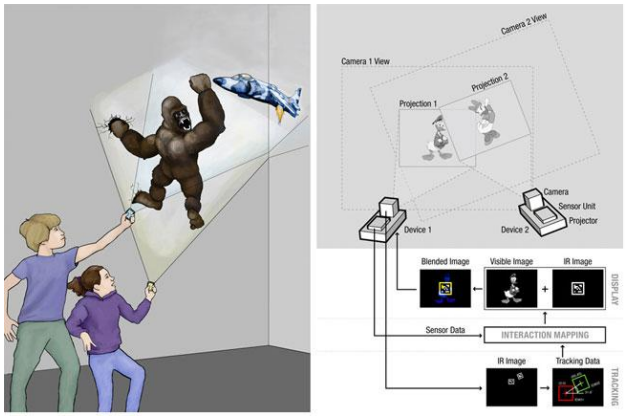

Generative codes enable images to change. They can be static or mobile. This flexibility provides a more creative practitioners. Some artists are already working with generative codes with designers while other artists are working independently. What are usually produced are images on a

computer interface that might allow some participation between the artist and user. Genomixer made in 2002-03 by Stanza is an example of an art work using generative code (fig.2). Genomixer is a human geonome sequence that uses the artist blood to create DNA profiles. The user can cross reference all the code genome sequences to make different variables of the artist. Even though it is possible for the user to have an interactive involvement the creative process is always pre-determined by the artist and the user is more an objective user than one who engages with a creative process on a different level. Artist sometimes share files via p2p systems which allow other creative professional practitioners to work together on the computer.

Fig. 2. Stanza, Genomixer in-touch 2002-03.

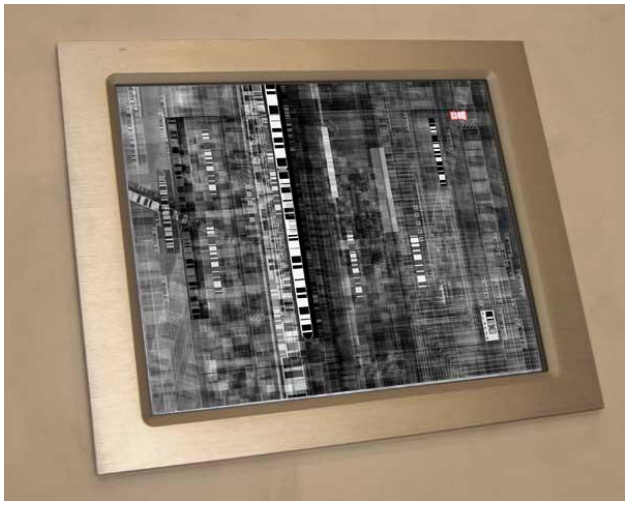

The software for Konstruct is different. The Konstruct app prototype designed by James Alliban shows the possibility of generative augmented reality codes. It has only been designed for iphones using 3Gs and 4Gs devices running on IOS4 or above. It requires the user to down oad an augmented marker (fig.3).

Fig. 3. Konstruct James Alliban 2012.

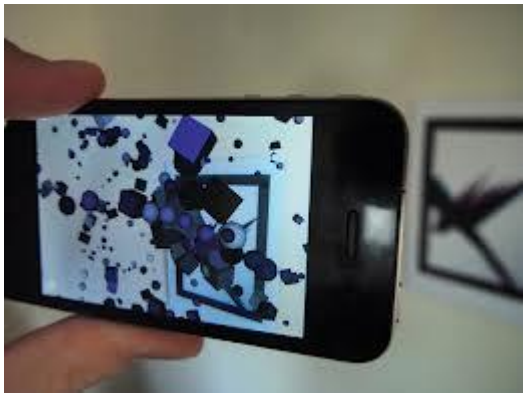

Konstruct provides a selection of shapes that the user can creative (fig.4). Unlike, SideBySide, it provides a colour palette settings. It offers a random scale and scatter settings, minimum and maximum setting including a frequency setting for the augmented image that appears in the physical environment.

Fig.4. Konstruct. James Alliban 2012.

Konstruct works in the exterior and interior environments 9figs.5-6). However, the limited selecting abstract pre-determinded shapes and noise sensitivity does not make it an ideal tool for professional creative practitioners. The problem with noise sensitivity relates to the accuracy of the augmented marker. The registration of the augmented reality marker detection process needs to be accurate and noise sensitivity errors are difficult to control. Also creative practitioners will need different files to enable them to create the types of work that they do.

Fig.5. Konstruct, James Alliban 2012.

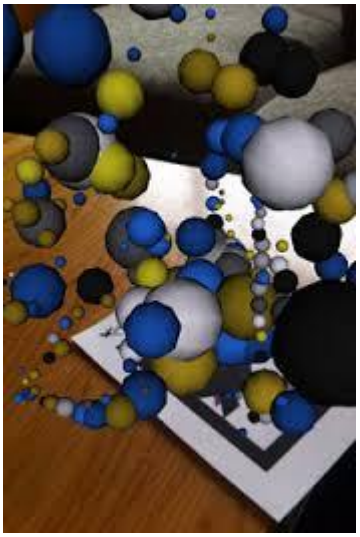

Fig.6. Konstruct, James Alliban 2012.

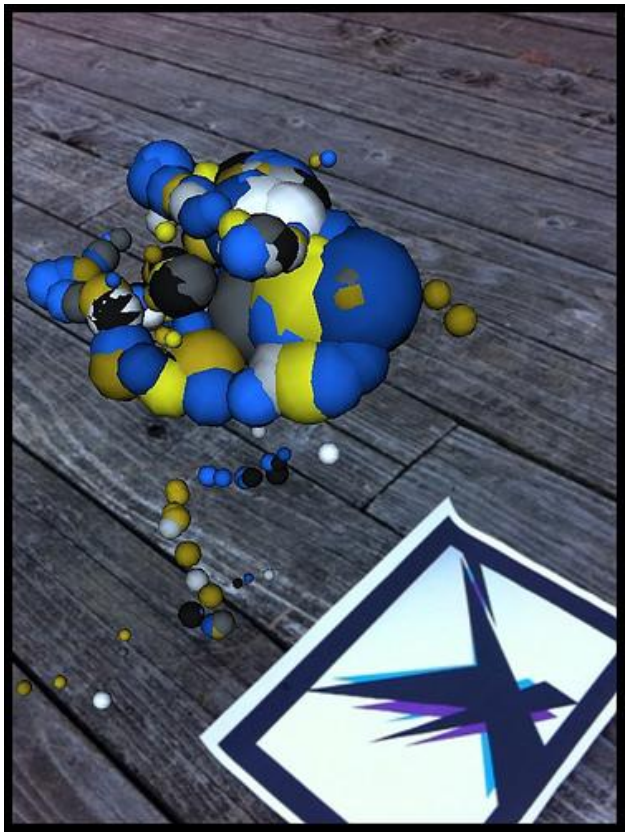

To change SideBySide into a tool that can use generative augmented reality codes another system is needed. This has to be a meta-programming system which allows generative augmented reality codes to write generative augmented reality codes. Various parsers support different schema languages and parsers that work with Java XML offers potential experiments for generative augmented reality code which can write generative augmented reality code. Digital assest exchange is essential and a validation tool makes it possible to write a detailed content specification for documents. Equally the Document Object Model provides a more interactive form, link and image elements that works in Java XML. The focus has to be on a parser that allows user/server/user/user-server/server-user to send information over the network. This has to be adaptable and enable information to be sent back and forth. This is how professional creative practitioners exchange ideas, develop and create ideas.

Augmented reality markers move away from the two dimensional surface projection of SideBySide. They produce an image that is more formed in the physical environment. Network operating parsers and applications need augmented markers because they are important for the distribution of the augmented reality images. ArTag already exists and is a useful augmented marker as it does not have the same problem as ArToll Kit another augmented marker used by people who are interested in augmented reality images. ArTag's detection process is based on a pixel edge approach. ArTool Kit depends on a marker vertification and identification process that uses a correlation system that causes high false positive and marker confusion rates.ArTag combines segmented edge pixels into quadrangle groups creating a homogenous form where the augmented marker's interior can be sampled. ArTool Kit has a processing time which is influenced by the size of its library. In ArTool Kit's augmented marker every feature vector must be correlated with every prototype vector in the library. ArTag's identification marker does not use an image matching library system and the identification process is much faster than ArTool Kit. Another problem ArTool Kit has to deal with is lighting. Different lighting prevents ArTool Kit detection working correctly. The marker has to be modified to perform local thresholding, a single image requires different thresholds and multiple detection processes have to take place. ArTag's augmented marker can cope with different lighting.

ArTag's augmented marker has been produced to deal with error problems. It does this by using 36 binary symbols 946 binary symbols can also be used) consisting of black and white cells formed into a grid. The identification process uses a 36 sequence encoded as 10 bit sequence based at the four corners of the marker. What is left are 26 redundant sequence bits that detect error, ensure that correction takes place and provides opportunity for uniqueness that the identification process using the four corners of the marker allows. The ArTag's augmented marker only uses one sequence in the decoding process. ArTag's augmented maker's time and spatical synching is more useful because the detection of the image including its framing is rendered simultaneously on each display which depends on good network communication. The spatical synching enables the master and local dimensions to be adaptable. The master dimensions are defined by the total width and height of pixels in the interior space of the marker. The local dimensions are based on the width and height of an individual display within the master dimension. ArTag's augmented marker is not too dense which increases the distance where data can be collected (fig.7).

Fig.7. ArTag Augmented Markers.

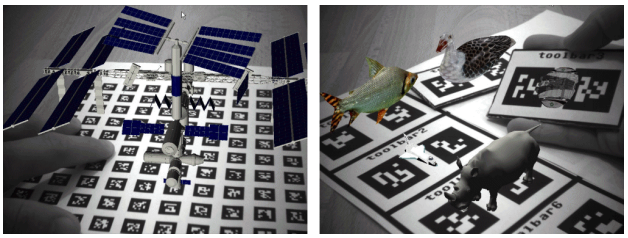

The positive elements of ArTag's augmented marker has been taken further by Martin Hirzer in his essay "Marker Detection for Augmented Reality Applications" (2008). The detection process of ArTag has been converted into a line detection process that still uses the pixel edge detection method. The line detection process does not process all the pixels in an image. The augmented marker grid consist of widely spaced horizontal and vertical scan lines. The error adaption in the ArTag's marker is also used and this allows the line detection process to be flexible to create other scan lines. By using a gradient system all detected lines are extended into full length lines which are grouped into quadrangles. The grouping uses a RANSAC (Random Sample Consensus) system which allows the image to be divided into smaller sections and are processed

consecutively. Similar to ArTag's augmented marker the line detection system has to be accurate when searching for the marker's edge to ensure the marker's corner points can be located.

Concluding that with a software system that can allow generative augmented reality codes to rewrite generative augmented reality codes, with the production of augmented markers that allows for multilayering and prevents misreading of augmented markers, that can use an adaptive random sample detection process SideBySide can be adapted to make a different tool for professional creative practitioners. This work is still in process.

1. Martin Hirzer, **Marker Detection for Augmented Reality Applications** (Tug-Company Graphic) 2008.
2. Ivan Popyrev et al, **SideBySide** (Disney Research Centre) 2011.

Experimental Testing of Ceramic Cutting Inserts at Irregular Interrupted Cutting Process

Robert CEP, Adam JANASEK, Jana PETRU, Ondrej DUPALA
Department of Machining and Assembly, Faculty of Mechanical Engineering
VSB - Technical University of Ostrava
17. listopadu 15/2172, 708 33 Ostrava - Poruba, Czech Republic
robert.cep@vsb.cz, adam.janasek@vsb.cz, jana.petru@vsb.cz, ondrej.dupala@vsb.cz

Abstract

The principle aim of this investigation is to test two types of ceramic cutting insert and compare their ability to withstand the simulated load by shock. Design, construction and application of ceramic cutting tools are one of the most important research topics in the field of metal cutting and advanced ceramic materials. The ceramic tools are increasingly utilized in industries and their mechanical properties have superior performances. It is efforts to develop more cost-effective ceramic tool for machining processes. Our experiments are conducted on a special preparation for longitudinal turning. The preparation can test a different type of material, and is limited only by cutting speed. The main goals of the tests will be contribute to the wider usage of these cutting materials in interrupted machining at "Balanced method" or "Unbalanced method" and demonstrate the effect of the time delay between individual beats. The irregular beats will be generated in the different time delays, which will have a clear impact on the thermal beats and mechanical shocks.

Keywords: Ceramic; Insert; Turning; Tool Wear; Machining.

Introduction

Surface roughness and dimensional accuracy play an important role in the performance of a machined component. In actual machining processes, however, the quality of the workpiece (either roughness or dimension) are greatly influenced by the cutting conditions, tool geometry, tool material, machining process, chip formation, workpiece material, tool wear and vibration during cutting [1], [2], [3] and [4]. The high-quality product with longer tool life may be achieved by proper selection of machining parameters and by direct monitoring of cutting process.

The current production techniques are carefully designed and are based on a decades of experience, research and development. Nowadays is effort to use the cutting tool with maximum performance during its lifetime because the machining operations used at manufacturing may be affected on several parameters.

The aim of this work is to test mechanical, thermal shocks and ability to withstand the simulated load of the ceramic cutting edge by these shocks. These shocks cause the damage, fracture or abrasion. The phenomenon can be studied not only at interrupted cutting but also at uninterrupted. The continuous cutting leads to fluctuate of the main cutting force. The choice of the right cutting tool is critical for the highest machining achievement. Vibration generated in machining induces the early termination of tool life.

Current efforts in the cutting technology are concerned with the high speed machining of highly resistant material, developments in equipment and tool material are significant improvement. Ceramic also provide the only way to work economically the hard machinable alloys in the aerospace industry [5, 11]. In an increasing number of machining applications, the right insert for the job is very difficult to choose. The ceramic cutting insert starts to be a very popular for his high productive at milling and turning applications. Their application in metalworking has a lot of benefits as improved cutting performance, tool life, reduction in the costs and simplified changeover.

Longitudinal Turning Test at Cyclic Stress

The experiments are conducted on a special preparation at longitudinal turning which was constructed at Department of Machining and Assembly, Technical University of Ostrava. Special preparation for tests is clamped to the lathe chuck and it is supported by the modified point which is established in tail stock sleeve. The basic construction consists of special cylinders which are milled four mortises, see Figure 1.

The preparation can test a different type of material, and is limited only by cutting speed. In general, the preparation was used only for testing by four slats variant but this process did not show mechanical, thermal shocks at unbalanced cutting process so we could not studied dependence of unbalanced and balanced method. For this reason, the main aim is to prove the impact of the time delays between shocks.

If the tool is not in constant cutting process, we can talk about the interrupted cut. The cause of cyclic stress is the cutting phase which involves heating of cutting edge and its subsequent cooling at the finishing of the cut process. It is a variant of the four, three, two and one shock per one revolution. Usually, we are talking about cyclic stress. The measured number of shocks to tool wear determines the tool life or lifetime period of ceramic cutting insert. Nowadays, these tests are an essential part of the development of the new

tools, evaluating their lifetime period and cutting power.

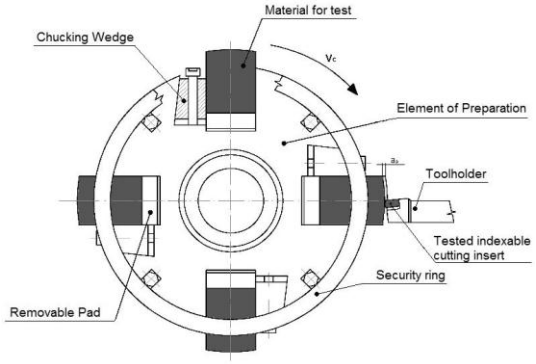

Figure 1. Scheme of Preparation for Slide Turning [6]

A series of turning test were conducted without any coolant in TOS Trenčín, type SN 55 turning lathe. The experiments were carried out using the cutting conditions shown in Table 1. Each test was started with a new cutting insert and machining was stopped at a certain interval of time and was tested at a constant temperature of 20°C.

Table 1. Experimental Conditions

Revolution, n [rev]	520	360
Cutting speed, v_c [m/min]	425	294
Feed, f [mm/rev]	0.20	
Axial depth of cut, a_p [mm]	1	

At four and two slats method, we are talking talk about "Balanced method" and it is able to use a high revolution and the cutting speed. At the four slats method, inserts are exposed to four shocks per revolution and there is not such a large thermal and mechanical shocks as two slats method, where is cooling phase, between mesh and therefore creates the thermal shock. At three and one slats method, we are talking about "Unbalanced method". It was necessary to change the cutting parameters, which was reduced revolution and cutting speed. When you try to maintain the same cutting parameters as "Balanced method", was created a large tremble and vibration, could be a huge risk of machine damage.

Work Material and Cutting Tool

Greanleaf HSN-100 insert is the latest in engineered silicon nitride-based cutting tools. Advanced materials combined with unique processing techniques give HSN-100 superior toughness and high cutting speed capability. HSN-100 is well suited for the turning and milling of all classes of cast iron. It is an outstanding performer in ductile, malleable, nodular and other difficult to machine irons. [7]

TaeguTec AB 2010 insert has wide range of high technology ceramics grades from excellent wear resistant high alumina grade to silicon carbide whisker reinforced ceramics grade. The ceramic grade has very good performance in the machining of hardened steel, cast iron and heat resistant super alloy. Shiny gold is colored ceramic with excellent wear resistance. Comparable to low CBN grade in machining of hardened steel. Hardened steel, Alloy steel, Tool steel, Case hardened steel. Coating improves tool life 50% than uncoated grade. [8]

Cutting geometry for tool testing from cutting ceramics was chosen with regard to ISO 3685 standard - Tool Life Testing of Single Point Turning Tools (ISO 3685, 1990). All types of indexable cutting inserts, that we will be tested, have a normalize shape SNGN 120716 T02020 and will be attached to the tool holder CSRNR 25x25 M12-K.

The material used in the experiment was medium carbon steel, type C45 (material No. 1.0503, DIN C45, AISI 1045). The chemical composition and mechanical properties are listed in Table 2 and 3. Carbon steel C45 was chosen on the basis that is a reference material for the class of machinability 14b.

Table 2. Mechanical Properties in Normalized Condition

Mechanical properties	Proof stress Rp 0.2 [MPa]	Tensile strength Rm [MPa]	Elongation A5 [%]	Hardness [HB]	Elastic modulus E [GPa]
C45	325	630 - 780	17	207 - 255	211

Table 3. Chemical Composition (in weight %)

C	Si	Mn	Cr	Mo	Ni	V	W	Others
0.46	max. 0.40	0.65	max. 0.40	max. 0.10	max. 0.40	-	-	(Cr + Mo + Ni) = max. 0.63

Experimental Results and Discussion

The limit value of 6000 shocks was determined on the basis of previous testing experience in terms of time and material demands. [9, 12]

The Table 4, Table 5, Table 6 and Table 7 shows the tool wear on tool face and tool flank. The photo of inserts was taken on Intracomicro microscope at 4x magnification.

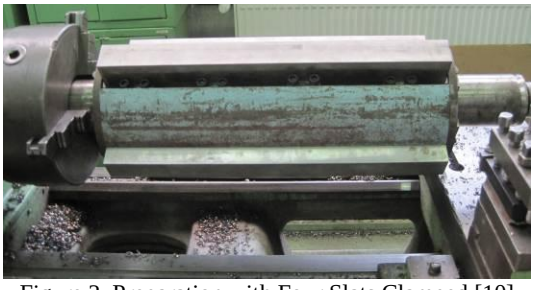

Figure 2. Preparation with Four Slats Clamped [10]

At four and two slats method, we are talking talk about "Balanced method" and we are able to use a high revolution and the cutting speed. At the four slats method, inserts are exposed to four shocks per revolution and there is not such a large thermal and mechanical shocks as two slats method, where is cooling phase, between mesh and therefore creates the thermal shock.

At three and one slats method, we are talking about "Unbalanced method". It was necessary to change the cutting parameters, which was reduced revolution and cutting speed. When you try to maintain the same cutting parameters as "Balanced method", was created a large tremble and vibration, could be a huge risk of machine damage.

Measured Data

Table 4. Measured Values for Four Slats Variant

n = 520 [rev], v_c = 425 [m/min], a_p = 1 [mm], f = 0.2 [mm/rev]

4 slats	**Greenleaf HSN 100**				**Taegutec AB 2010**			
No.	*l* [mm]	*Ra* [µm]	*Rz* [µm]	*R* [-]	*l* [mm]	*Ra* [µm]	*Rz* [µm]	*R* [-]
1	222	1.26	6.1	4440	294	1.6	6.6	5880
2	234	1.24	5.9	4680	288	1.58	6.1	5760
3	220	1.34	5.7	4400	292	1.62	6.2	5840
4	220	1.28	5.8	4400	264	1.68	6.4	5280
5	248	1.24	5.9	4960	276	1.65	5.9	5520
Average	**228.8**	**1.27**	**5.88**	**4576**	**282.8**	**1.63**	**6.24**	**5656**
Standard deviation, u_A	5.4626	0.0186	0.0663	110	5.6426	0.0178	0.1208	113
Tool face								
Tool flank	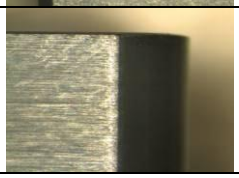							

Table 5. Measured Values for Three Slats Variant

n = 360 [rev], v_c = 294 [m/min], a_p = 1 [mm], f = 0.2 [mm/rev]

3 slats	**Greenleaf HSN 100**				**Taegutec AB 2010**			
No.	*l* [mm]	*Ra* [µm]	*Rz* [µm]	*R* [-]	*l* [mm]	*Ra* [µm]	*Rz* [µm]	*R* [-]
1	400	1.29	6.2	6000	400	1.4	6.6	6000
2	400	1.37	6.8	6000	400	1.28	6.2	6000
3	400	1.34	6.4	6000	400	1.39	6.3	6000
4	400	1.36	6.3	6000	400	1.36	6.4	6000
5	400	1.42	6.9	6000	400	1.34	6.5	6000
Average	**400**	**1.36**	**6.52**	**6000**	**400**	**1.35**	**6.4**	**6000**
Standard deviation, u_A	0	0.0211	0.13928	0	0	0.0214	0.0707	0
Tool face	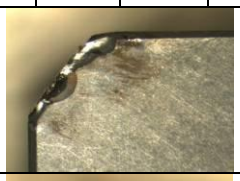				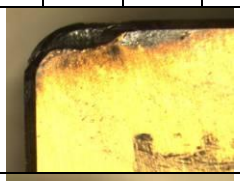			
Tool flank	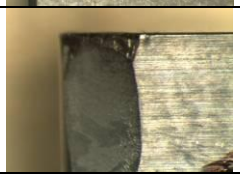				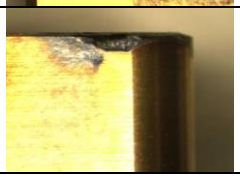			

Table 6. Measured Values for Two Slats Variant

n = 520 [rev], v_c = 425 [m/min], a_p = 1 [mm], f = 0.2 [mm/rev]

2 slats	**Greenleaf HSN 100**				**Taegutec AB 2010**			
No.	*l* [mm]	*Ra* [µm]	*Rz* [µm]	*R* [-]	*l* [mm]	*Ra* [µm]	*Rz* [µm]	*R* [-]
1	198	1.24	6.2	1980	420	1.39	6.50	4200
2	218	1.28	6.4	2180	525	1.4	6.80	5250
3	298	1.3	6.3	2980	600	1.36	6.2	6000
4	354	1.26	6.2	3540	592	1.38	6.4	5920
5	268	1.27	6.1	2680	600	1.37	6.5	6000
Average	**267.2**	**1.27**	**6.24**	**2672**	**547.4**	**1.38**	**6.48**	**5474**
Standard deviation, u_A	28.0114	0.010	0.051	281	34.8247	0.0071	0.097	349
Tool face								
Tool flank					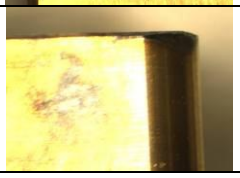			

Table 7. Measured Values for One Slat Variant

n = 360 [rev], v_c = 294 [m/min], a_p = 1 [mm], f = 0.2 [mm/rev]

1 slat	**Greenleaf HSN 100**				**Taegutec AB 2010**			
No.	*l* [mm]	*Ra* [µm]	*Rz* [µm]	*R* [-]	*l* [mm]	*Ra* [µm]	*Rz* [µm]	*R* [-]
1	1200	1.42	6.7	6000	1200	1.58	6.70	6000
2	1200	1.39	6.5	6000	1200	1.59	6.60	6000
3	1200	1.4	6.6	6000	1200	1.60	6.50	6000
4	1200	1.38	6.5	6000	1200	1.62	6.70	6000
5	1200	1.37	6.6	6000	1200	1.60	6.60	6000
Average	**1200**	**1.39**	**6.58**	**6000**	**1200**	**1.60**	**6.62**	**6000**
Standard deviation, u_A	0	0.0086	0.0374	0	0	0.0066	0.0374	0
Tool face	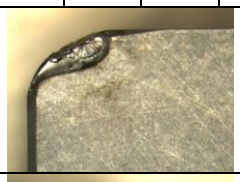							
Tool flank					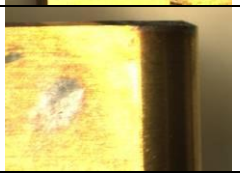			

Comparison for Different Number of Slats

Figure 3 shows the comparison of two ceramic cutting inserts at "Balanced method" of machining. When we are compared two manufacturers at four slats method it can be seen that Greenleaf HSN 100 withstood 4576 shocks and Taegutec AB 2010 withstood 5656 shocks what is a higher number. Taegutec AB 2010 is more suitable for interrupted cutting under given cutting condition and at "Balanced method".

If we are comparing the same, but at two slats method, can be seen that Greanleaf HSN 100 withstood only 2672 shocks and Taegutec AB 2010 withstood 5474 shocks. This difference is more considerable. The two slats method has a longer cooling phase, between mesh and therefore creates the thermal shock.

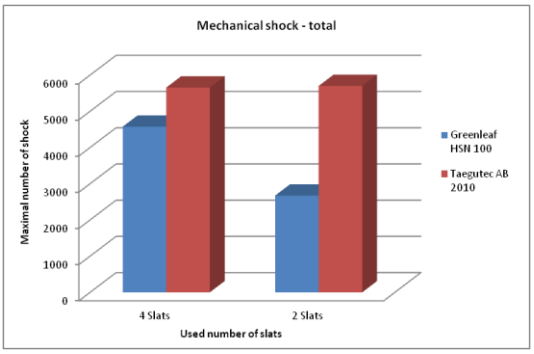

Figure 3. Total Number of Shocks at "Balanced Method"

Figure 4 shows the comparison of two ceramic cutting inserts at "Unbalanced method" of machining. It was necessary to change the cutting parameters, which was reduced revolution and cutting speed. When we try to maintain the same cutting parameters as "Balanced method", was created a large tremble and vibration, could be a huge risk of machine damage.

During the "Unbalanced method", the inserts withstood the maximal number of shocks and we could not to evaluate due to small revolution and cutting speed. This phenomenon is caused by relatively small cutting parameters for ceramic material. Unfortunately, the technical limitation of the machine have not allowed to test at higher cutting parameters. Thanks to the results showed below we can say the inserts are suitable for interrupted cutting at these parameters n = 360 [rev], v_c = 294 [m/min], a_p = 1 [mm], f = 0.2 [mm/rev]. Our next research question involves using the same cutting parameters as in previous case and for this reason we have to use a turning lathe with bigger foundation to avoid to trembling and vibration.

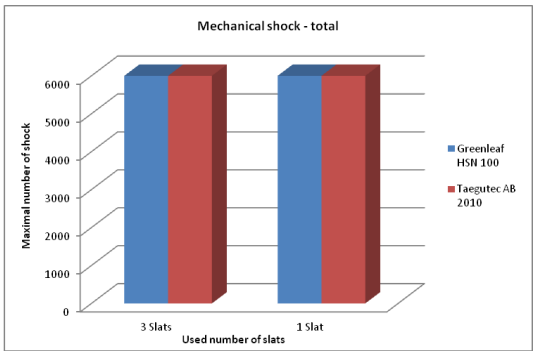

Figure 4. Total Number of Shocks at "Unbalanced Method"

The value of average roughness (*Ra*) and ten-point mean roughness (*Rz*) for tested indexable cutting inserts is represented by Figure 5 and 6 and also presents the difference which is caused by different number of clamped slats.

During "Balanced method" can be said that Greenleaf HSN 100 reached the better results than Taegutec AB 2010 for both of tested parameters. This result is opposite than at testing of the maximal number of shock.

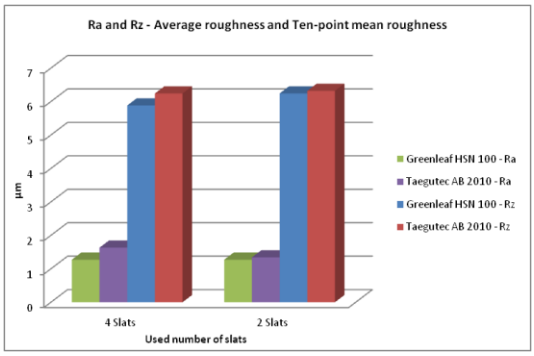

Figure 5. Average Roughness and Ten-point Mean Roughness at "Balanced Method"

During "Unbalanced method" is not possible come to the conclusion because the measured values did not reached linear relationship as previous case.

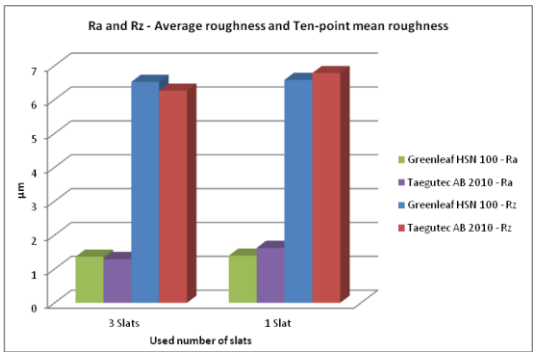

Figure 6. Average Roughness and Ten-point Mean Roughness at "Unbalanced Method"

Conclusion

Nowadays, a higher production rate with required quality and low cost is the basic principle in the competitive manufacturing industry. However, prolonged tool life means lower wear rate that implies a better understanding of the tool wear mechanisms during cutting processes.

The aim of this work is to test two ceramic cutting inserts at interrupted cutting by two methods "Unbalanced method" and "Unbalanced method". During the "Unbalanced method" are created longer gaps between the shocks and is created cooling phase which is connected with thermal load.

The experimental results based on the present conditions may be summarized as follows.

- at "Balanced method" when we are compared two manufacturers at four slats method it can be seen that Greenleaf HSN 100 withstood 4576 shocks and Taegutec AB 2010 withstood 5656 shocks what is a higher number. Taegutec AB 2010 is more suitable for interrupted cutting under given cutting condition.
- at "Balanced method" when we are compared two manufacturers at two slats method, can be seen that Greanleaf HSN 100 withstood only 2672 shocks and Taegutec AB 2010 withstood 5474 shocks. This difference is more considerable. The two slats method has a longer cooling phase, between mesh and therefore creates the thermal shock.
- during the "Unbalanced method", the inserts withstood the maximal number of shocks and we could not to evaluate due to small revolution and cutting speed. This phenomenon is caused by relatively small cutting parameters for ceramic material. Unfortunately, the technical limitation of the machine have not allowed to test at higher cutting parameters.

The results were not been testify about the influence of thermal and mechanical shocks enough. For this reason will be suitable to do testing for more type of inserts at different cutting speed and also different feed rates. This will be the main aim one's effort to finish this problematic in future. In the next research will be suitable to cancel our limitation by the maximal number of shocks but it brings a high demands on the testing price. Generally, the price question is the most important factor of each research at this modern time.

References

[1] V. Solaja. Wear of carbide tools and surface finish generated in finish turning of steel, in: Proceedings of the First International MTDR Conference, Vol. 2, 1958/1959, pp. 40-58.

[2] E.J.A. Armarego; R.H. Brown. The Machining of Metals, Prentice-Hall, Englewood Cliffs, NJ, 1969.

[3] X.D Fang. Experimental investigation of overall machining performance with overall progressive tool wear at different tool faces Wear, 173 (1994), pp. 171-178.

[4] M.C. Shaw. Metal Cutting Principles, Oxford University Press, New York, 1984.

[5] Silva, R.F.; Gomes, J.M.; Miranda, A.S. and Vieira, J.M. Resistance of Si_3N_4 ceramic tools to thermal and mechanical loading in cutting of iron alloys. [online]. No. 168 [cit. 2013-01-05]. Available from: http://repositorium.sdum.uminho.pt/bitstream/1822/1534/23/1.pdf

[6] Reiner, Jan. Testing of ceramic cutting tools by the simulator for interrupted cutting : diploma thesis" Ostrava : Department of Machining and Assembly, Faculty of Mechanical Engineering, VŠB – Technical university of Ostrava, 2009. pp. 73.

[7] Greenleaf global Support. GREENLEAF CORPORATION. [online]. [cit. 2012-07-08]. Available from: http://www.greenleafglobalsupport.com/wcsstore/Greenleaf/upload/docs/CeramicGrades.pdf

[8] TAEGUTEC. *TaeguTurn.* [online]. [cit. 2012-05-06]. Available from: http://www.taegutec-india.com/redirect.asp?URL=http://www.taegutec.co.kr/main.asp?CountryID=1

[9] Cep, Robert; Janasek, Adam; Valicek, Jan and Cepova, Lenka. Testing of Greenleaf ceramic cutting tools with an interrupted cutting. *Tehnički vjesnik: Portal znanstvenih časopisa Republike Hrvatske*. 2011, Vol. 18, No. 3. ISSN 1330-3651.

[10] Zalesak, Marek. Influence of Thermal and Mechanical Shocks on Edge Condition at Interrupted Machining. Ostrava: Department of machining and assembly 346, Faculty of Mechanical Engineering, VSB - Technical University of Ostrava, 2012, pp. 56. Head of diploma thesis: Cep, Robert.

[11] Čep, Robert; Neslušan, Miroslav; Barišić, Branimir. Chip Formation Analysis During Hard Turning. *Strojarstvo*, 2008, vol 50, No. 6, pp. 337-345. ISSN 0562 - 1887.

[12] Čep, Robert. Proposal and Verification of Cutting Tool Tests at Interrupted Machining. Ostrava, 2010. pp. 119. Habilitation thesis. Department of machining and assembly 346, Faculty of Mechanical Engineering, VSB - Technical University of Ostrava.

The 5th International Multi-Conference on Engineering and Technological Innovation: IMETI 2012

July 09th - July 12th, 2013 – Orlando, Florida, USA

Title: Modelling and Thermal Analysis of Steam Turbine Blade For Supercritical Parameters

PROF. M.B.MAISURIA
SARDAR VALLABHBHAI NATIONAL INSTITUTE OF TECHNOLOGY
SURAT-395007, GUJRAT, INDIA.

ABSTRACT

Increase in price of crude oil and natural gasses has led to use coal as a fuel for power generation. With coal as a fuel it is necessary to utilize it for reasonable power generation cost and acceptable emissions which extends application opportunities for wide implementation of supercritical (SC) steam cycle.SC technology provides not only stable and high quality electric power but also contribute to reduction of CO2 emissions and general adverse impact to the environment.

In super critical cycle the turbine inlet pressure and temperature are increased to achieve the higher efficiency. To allow these increases various design measures has to be considered. In steam turbines blade is a one of the important components. Blade converts kinetic energy in to mechanical (i.e. rotational) energy. So blade needs more rigorous design practice compared to those in sub- critical steam cycle where pressure and temperature at inlet are lower.

In this paper purpose is to simulate two different types of blades with same supercritical parameters and discuss different results like distribution of turbulent intensity, distribution of total pressure, velocity variation between blades.

Keywords: Steam Turbines(STs),Supercritical parameter, Cylindrical Profile, F3Dimensional Blade Profile, Turbulent intensity, Absolute velocity.

1 .INTRODUCION

Climate change concerns and the rising price of coal are driving the power generation market toward more efficient cycles than the conventional subcritical steam plant. Steam turbines (STs) need to operate at substantially higher pressures and temperatures in the supercritical (SC) and ultra-supercritical (USC) domain. The SC steam plant design is rapidly becoming the preferred option for many owners, given its cost-effective use of coal, an abundant domestic fossil fuel. Concurrently, there is an ongoing push to reduce stack emissions of all pollutants and to capture CO_2. The future will, without a doubt, lead to the increased use of USC technologies. While the definition of SC conditions is straightforward, the meaning of USC is subject to interpretation. SC is a thermal cycle with a main steam temperature of less than 1,112 °F (600 °C) operating at pressures between 218 and 272 bars.

The initial step in this development process is thermodynamic cycle optimization, followed by an effort to increase ST overall efficiency by improving the high pressure (HP) and intermediate pressure (IP) modules. Higher steam temperatures in particular as well as increased steam pressure, will significantly improve thermal cycle efficiency.

The trend in advanced ST design is to achieve greater standardization in the number of modules and their sizes as a means of reducing cost and accelerating schedule. The thermodynamic performance of the ST, more than

any other power plant component, determines overall power plant efficiency. Future development of high efficiency advanced ST at advanced USC conditions is largely dependent on the parallel development of advanced materials and super-alloys capable of withstanding the extreme working environments both in terms of corrosion resistance and their creep rupture strength.

Beside of material selection, the appropriate USC ST design and configuration is mainly determinate by unit output rating, LP ST back-pressure, number of reheats and other
Special requirements (e.g. process steam extraction).

The blades of an ST are the components that receive the most attention. Blades convert the heat energy of the steam to mechanical energy and new design of profile of blade is main issue in advanced ST design. Significant efforts are invested to optimize blade design, which has a direct and powerful effect on HP and IP modules efficiency.

In conventional cylindrical profile of blades profile section of the blade profile along height is same. There is no twisted of profile, it is like straight cylinder so it is called as cylindrical profile. In F3Dimensional Blade profile section of blade profile twisted and also bowed, in this blade the shape of the blade is like a banana and bowed. It is customary to use a fully developed 3-d design, accounting for all blade profile losses, leakage losses, and other secondary effects.

In the investigation, analysis is carried out on cylindrical and F3Dimensional blade by using CFD software. With the help of this analysis the pressure distribution between two blades is obtained. It also gives pattern of turbulence intensity which provides the idea about secondary losses between two blades.

2. MODELING AND THERMAL ANALYSIS OF STEAM TURBINE BLADES

The purpose of the CFD pre-processor operations is to create and mesh that represents a section of the flow environment surrounding an individual blade.

For modelling and meshing of the 3D blade GAMBIT 2.4 modelling software was used and also we can give the boundary condition in this software.

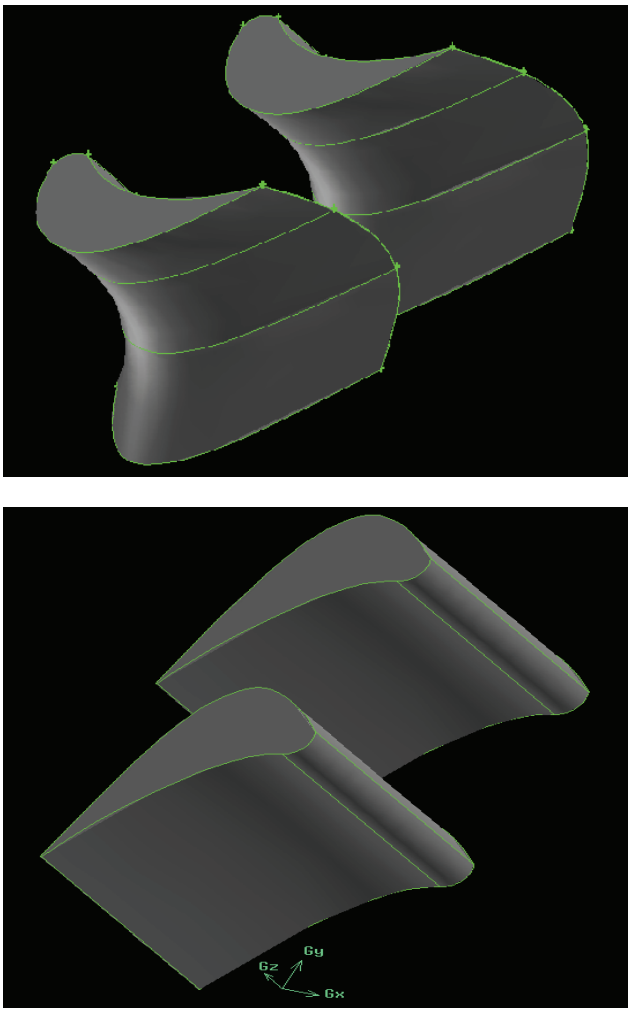

Fig 1: Model of Fully 3D Design Blade and Conventional Cylindrical Design Blade

A CFD pre-processor generated volume is meshed according to standard pre-processor meshing technique. We can mesh the volume without notification by means of the Tat/Hybrid or Stair step volume meshing techniques. According to various trial and experiments it is found that obstructed mesh does not provide the accurate solution of many CFD problems, so the most preferable mesh for complex geometries is only the structured mesh. It will give better results and converged solution with lesser processing time.

After completing boundary condition in GAMBIT 2.4, we can import all these boundary condition in the fluent 6.3 as a mesh file.

3. RESULTS

Variation of Turbulence Intensity

The turbulence intensity is shown in figure on cross section plane at top and bottom. Distribution of turbulence intensity on different planes along the flow path is shown in figure.

It is observed that turbulence intensity at the entire locations inlet to outlet increasing.

In the 3Dimensional blade the turbulence intensity is at one point between two blades is between 1.83×10^3 to 1.97×10^3 and in the cylindrical blade the turbulence intensity is between 2.26×10^3 to 2.57×10^3 .Where the condition of steam applied same in both blades. The turbulence intensity in cylindrical blade is more than 3Dimensional blade. So the secondary losses in cylindrical blade are also more than 3Diimensional blade.

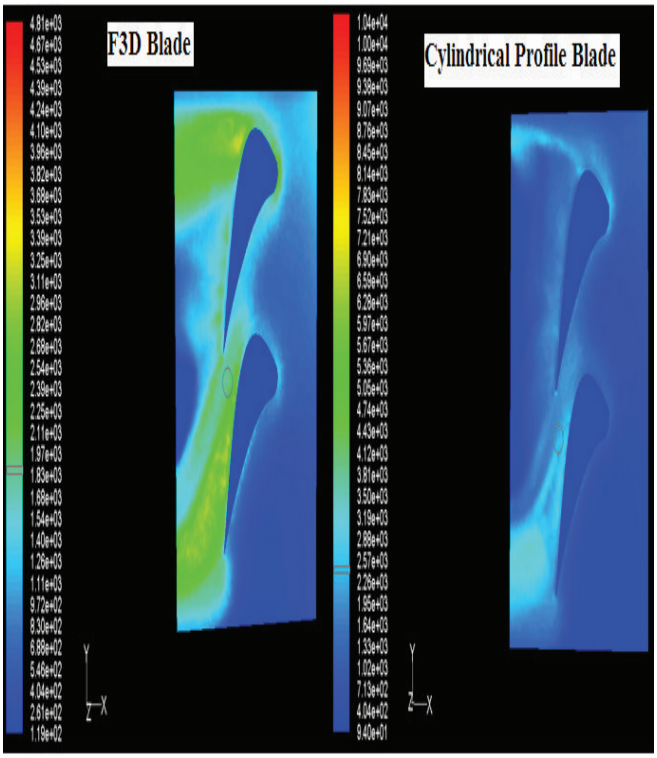

Fig 2: Variation of the Turbulence Intensity (%) at the top plane

In figure no.3 shows the variation of turbulence intensity at cross section area of bottom plane. Distribution of turbulence intensity on different planes along the flow path is also shown in figure. It is observed that the turbulence intensity is increasing along flow path.

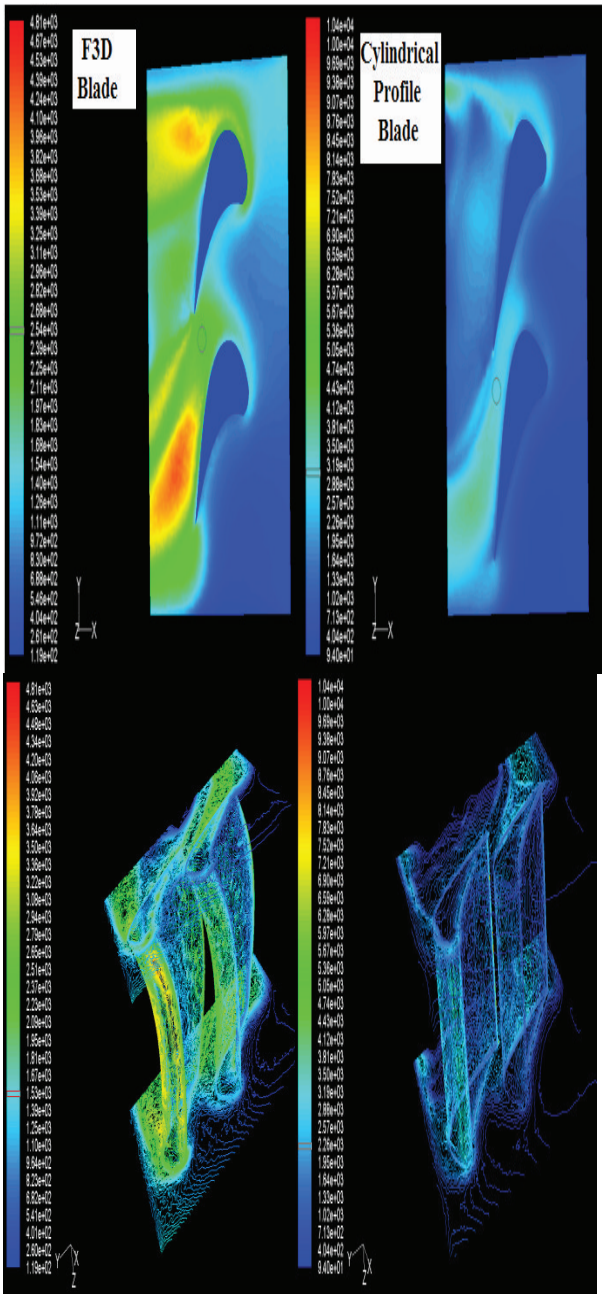

Fig 3: Variation of the Turbulence Intensity (%) at the Bottom plane

Variation of total pressure

Distribution of total pressure along the blade path is shown in figure. The pressure variation along both the blades are shown in the figure. The results of pressure variation are also different because the profile of both the blades is different. Therefore the secondary losses and profile losses are reduced in the 3Dimensional blade.

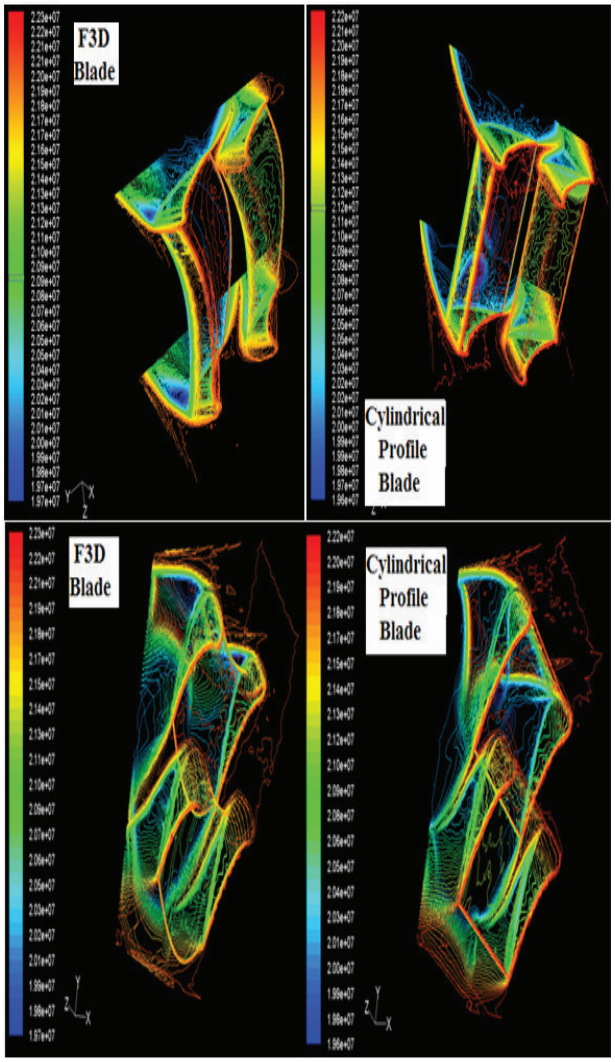

Fig 4: Variation of Total Pressure

Variation of absolute velocity

The absolute velocity is shown in figure. It is observed that absolute velocity values decrease near outflow.

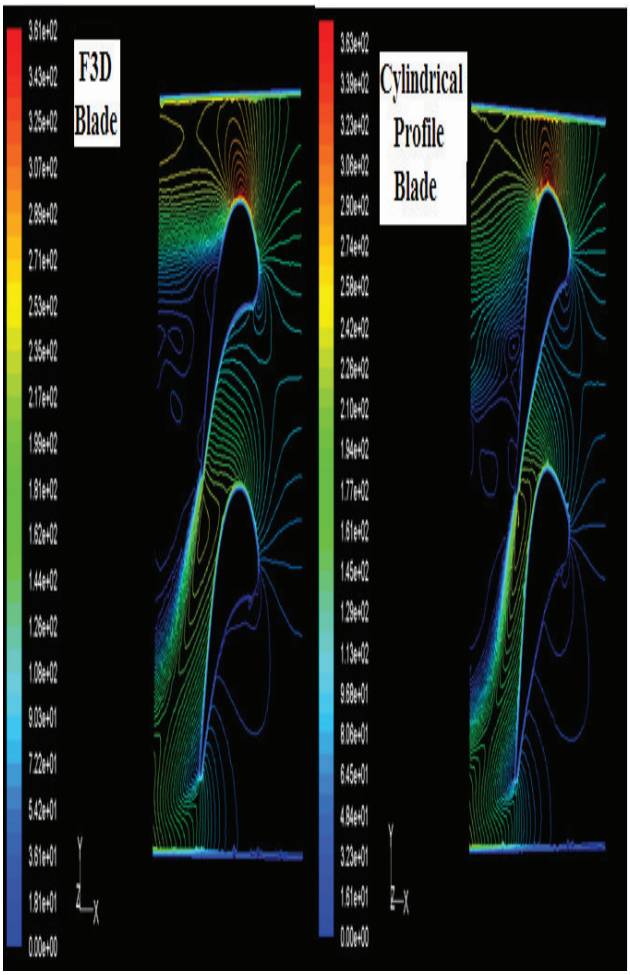

Fig 5: Variation of Absolute Velocity

4. CONCLUSION

From the result of these two blades performance, it can be decided that the fully 3Dimensional reaction blades are good. The secondary losses and profile losses are reduced in fully 3 dimensional reaction blades. Because of the blades are short, relatively large end wall losses occurs at the hub and the shroud. By modifying the conventional cylindrical design in to fully developed 3-D design and bending and twisting the blade at hub and tip, a stage efficiency can be improved by approximately 3%.

If the integral shroud blades are used in place of riveted blades, it will be considered good improvement in design of steam turbine. Height of root is also increased in the

last stage blade in L.P. turbine for reducing the centrifugal force on the blade.

REFERENCES

[1] Oeynhausen H., A. Drosdziok, and M. Deckers. "**Steam Turbines for the New Generation of Power Plants**," VGB Kraftwerkstechnik 76, 1996.

[2] Drosdziok A."**Steam Turbines**" [in German] BWK 50, 1998.

[3] R.Yadav "**Steam and gas turbine**", Central Publishing House Allahabad, 2003

[4] Lakshminarayan B. **Fluid Dynamics and Heat Transfer of Turbo machinery**."John Wiley, New York, 1996.

[5] Mathis D.M. fundamentals of turbine design. In "**Handbook of turbo machinery**" (E. Logan, Jr., Ed.).Marcel Dekker, New York 1994.

[6] A. *Stodola*, ***Steam and Gas Turbine***, Peter Smith, New York, 1945.

[7] **Steam Power plants new wave of super criticality**; M.R. Susta IMTE AG power consulting engineers, Switzerland and P. Luby, INGCHEM, Slovak Republic; Powergen Europe 2002.

[8] **Supercritical Systems**, P.Luby, INGCHEM, Slovak Republic; Modern Power Systems, August 2003.

[9] EIA **international Energy outlook**; 2007.

[10] **Advanced steam turbine technology for High Efficient Ultra-Supercritical Power Plants**; M.Deckers, A.Wichtmann, W.Ulm; Siemens AG Power Generation & Siemens Westinghouse Power Corporation; Germany-USA; China Power 2005

[11] BP **Stastical Review of World Energy**; June 2008

[12] **Proven Advanced Ultra –Supercritical Technology for Future clean and Efficient US Coal Fired Power Plants** ;R Baumgartner & J.Kern,Siemens Westinghouse Power Corporation USA; S.whyley &p.j. Melling, Misui Babcock Energy ltd.,USA;Coalgen 2005.

[13] Church Edwin F."**Steam turbines**", revised edition, McGraw –Hill book Company lnc, London, 1987.

[14] C.W.Elston and R. Sheppard, "**First commercial Supercritical pressure steam**
Turbine built for philo,"ASME paper no. 55 A 159, 1955.

[15] C.B.Campbell, C.T.Frank, and J.C. Spaks"**The edddystone Super pressure Unit**, "ASME paper no.56 -156, 1956.

[16] R.Blum and J.Hald,"**Benifit of Advanced Steam Power Plants**,"pp.1009-1016 in proc.Materials for Adv. Power Engg.2002,J.Lecomte-Beckers,M.cartonn,F.schubert and P.J,Ennis,Eds ,Forschungszentrum ,Julich,GmbH,2002.

[17] Advanced **Clean Coal**; EPRI; S. Dalton; May 2007.

[18]D.V.Thornton and K.H.Meyer,"**European High Temperature Materials Development for Advanced Steam turbine**, "ibid,pp.349-364.2003

[19]K.Miyashitha,"**Overview of advanced steam plant development in Japan**"pp.17-30 in Proc. Inst.Mech.Eng.Conf.Advanced Steam Plant, London, 1997.

[20] R.D. Hottenstine "**An investigation of the role of super nine material in supercritical plant development** ,"Parsons Infrastructure and Technology Group,Inc.,Position Paper PZ-401-03,1999.

Influence of strengthening effect on machinability of the welded Inconel 625 and of the wrought Inconel 625

Jana PETRŮ, Tomas ZLÁMAL, Robert ČEP, Marek PAGÁČ, Martin GREPL
Department of Machining and Assembly, Faculty of Mechanical Engineering
VSB - Technical University of Ostrava
17. listopadu 15/2172, 708 33 Ostrava - Poruba, Czech Republic
jana.petru@vsb.cz, tomas.zlamal@vsb.cz, rober.cep@vsb.cz, , marek.pagac@vsb.cz, martin.grepl@vsb.cz

Abstract

The article deals with the comparison of the different properties welded and wrought Inconel 625. The benchmark and the object of solution was to determine the size of hardening surface layer in the process of machining Inconel 625. The main aim was to determine the appropriate method of comparison of the both materials and to confirm design trial with the practical tests. Based on the measured values were evaluated experimental tests and measures proposed to rectify the problem of strengthening.

Keywords: Inconel; Machining; Turning; Machinability; Strengthening

Introduction

With the increasing share of oil extraction on the seabed, requirements increase for component life of drilling rigs. They operate in extreme conditions therefore require high technical and technological processing. The increasing depth, pressure, and the presence of salt indirectly affect from which the material will produce these components. Thanks to its positive properties is material Inconel one of the most widely used materials in the salty marine environment. Examples of use aren´t only machine parts for mining equipment, but also the cladding of submarine cables and their attachment to the seabed.

Due to the technological demands of machining Inconel, required accuracy and the resulting quality of the machined part is not always easy to satisfy customer´s requirements. Inconel is very hard workable. By spill machining has material tendency to elastic deformation and so to intensive firming. Worsened machining of Inconel associated with extreme strengthening of surface of material strongly influences consumption of cutting tools, it overloads power of lathe and especially isn´t allow to use the advanced high-speed turning which is common with other steels.

Material Inconel 625 is due to the high strength, excellent structure, excellent resistance to oxidation and corrosive environment of one of the most widely used materials for a wide range of extremely stressed components. However during processing of the material by conventional cutting operation occurs to the elastic deformation where the surface layer after machining is intensively strengthened. Hardening and its influence is generally manifested worse machinability and lower resulting quality of the machined surface. Worsened machinability welded Inconel associated with the extreme strengthening surface significantly affects the machining process. Due to the high consumption of cutting tools and higher demands on compliance with the guaranteed quality machined surfaces and overloading of the machine entered the company V-NASS request to review the process of machining Inconel 625 welded compared with wrought Inconel 625. [1]

Work hardening

The nickel alloys have an austenitic matrix, and like the austenitic stainless steels, works harden rapidly. The high pressures developed between the tool and workpiece during cutting or grinding produce a stressed layer of deformed metal on the surface of the work. The deformation causes a hardening effect that retards further machining. The stresses in this deformed layer not only affect the mechanical properties of the workpiece but also can caused distortion of parts that have small cross sections. One method of reducing work hardening during machining is to work harden the material prior to machining, by cold working. Cold-drawn, stress-relieved material is always preferred for machining, particular when the smoothest finish is desired. Hot-rolled material is next best while annealed material is least desirable in most applications. The best finish is produced on age-hardenable alloys by machining them in the aged condition. Because the high strength and hardness of aged material prevent heavy cuts, rough machining is done before age hardening. Solution annealing usually improves machinability of age-hardenable alloys by dissolving hard phases. A second method of minimizing work hardening is employing careful machining practice. Sharp tools with positive rake angles, which cut metal instead of cut must be sufficient to prevent burnishing or glazing. Tools should not be allowed to rub the work, either because of improper clearance or by being allowed to dwell in the cut. [2]

INCONEL alloy 625

Inconel alloys are corrosion and oxidation resistant and therefore are well suited for usage in extreme environments. When heat is applied to Inconel it forms a protective oxide layer through passivation. Inconel retains strength over a wide temperature range, an advantage for high temperature applications.

Depending on the alloy, Inconel's high temperature strength is established either by solid solution strengthening or precipitation strengthening. [3] INCONEL nickel-chromium alloy 625 (W.Nr. 2.4856) is used for its high strength, excellent fabricability (including joining), and outstanding corrosion resistance. Service temperatures range from cryogenic to 1800°F (982°C). Strength of INCONEL alloy 625 is derived from the stiffening effect of molybdenum and niobium on its nickel-chromium matrix; thus precipitation-hardening treatments are not required. This combination of elements also is responsible for superior resistance to a wide range of corrosive environments of unusual severity as well as to high-temperature effects such as oxidation and carburization. The properties of INCONEL alloy 625 that make it an excellent choice for sea-water applications are freedom from local attack (pitting and crevice corrosion), high corrosion-fatigue strength, high tensile strength, and resistance to chloride-ion stress-corrosion cracking. High tensile, creep, and rupture strength; outstanding fatigue and thermal-fatigue strength; oxidation resistance; and excellent weldability and brazeability are the properties of INCONEL alloy 625 that make it interesting to the aerospace field. The outstanding and versatile corrosion resistance of INCONEL alloy 625 under a wide range of temperatures and pressures is a primary reason for its wide acceptance in the chemical processing field. Because of its ease of fabrication, it is made into a variety of components for plant equipment. Its high strength enables it to be used, for example, in thinner-walled vessels or tubing than possible with other materials, thus improving heat transfer and saving weight. [4]

Preparation of the samples

For the comparison, the firming effect is important the design and preparation of the test samples on which measurements will be carried out. The experiment used two samples, one from welded and the second from wrought Inconel 625. For a sample, see fig. 1 a layer of Inconel 625 welded on the surface of the base material. This layer of weld material has a specified thickness of 1/8" (3.2 mm) and is designed as a two-layer weld due to the prescribed concentration of Fe at the surface. For the second sample was used forged from Inconel 625.

Fig. 1. Sample with welded Inconel 625

Test samples were machined a side cutting tool during longitudinal turning to the desired diameter 80 mm and then subjected to prescribed tests for determining the intensity of reinforcement. Machining has taken place in predetermined conditions with cutting speed $v_c = 150$ m.min^{-1}, depth of cut $a_p = 1$ mm and feed f by values given in the Table 1.

Tab.1. Values for measuring displacements hardening surface layer

Section [5mm]	Feed f [mm]	Section [5 mm]	Feed f [mm]
1	0.01	5	0.07
2	0.02	6	0.10
3	0.03	7	0.15
4	0.05	8	0.20

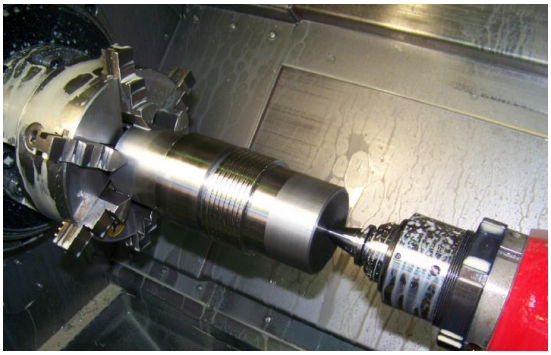

Fig. 2. Machining of test sample

Determination of hardening intensity

During machining leads to hardening of the surface layer of the workpiece and at this time when the tool is in the cut and separates chip from the machining material. At this phenomenon occurs due to the pressure of the tool on the workpiece for tamping surface layer behind the blade tool (tertiary deformation). In the train of this come hardened surface layer with very small thickness. This hardened layer has during subsequent machining negative effect on the tool head. It is exposed to higher loads where there is tool attends to wear out or change its geometry

due up edge formation. For the determination the intensity of hardening the surface layer of the weld and wrought Inconel 625 was selected method compared by Vickers. Measurements were performed on a machine AMH43 for automated hardness testing with different loads. For objective findings hardness surface layer was chosen load 50 g in which there was the least penetration (perforation) of the measuring indenter via a compacted layer. To eliminate errors that might occur during the measurement were performed on all three feeds scars.

Results of the measured hardness values reinforced with layers wrought Inconel

Tab. 2. Measured values at 50 g load

Distance [mm]	Hardness HV	Distance [mm]	Hardness HV	Distance [mm]	Hardness HV
2	569	17	525	32	434
2.5	580	17.5	525	32.5	434
3	574	18	520	33	435
7	591	22	487	37	429
7.5	585	22.5	492	37.5	431
8	591	23	492	38	426
12	564	27	476	40	426
12.5	564	27.5	473	**Min**	**426**
13	559	28	472	**Max**	**591**

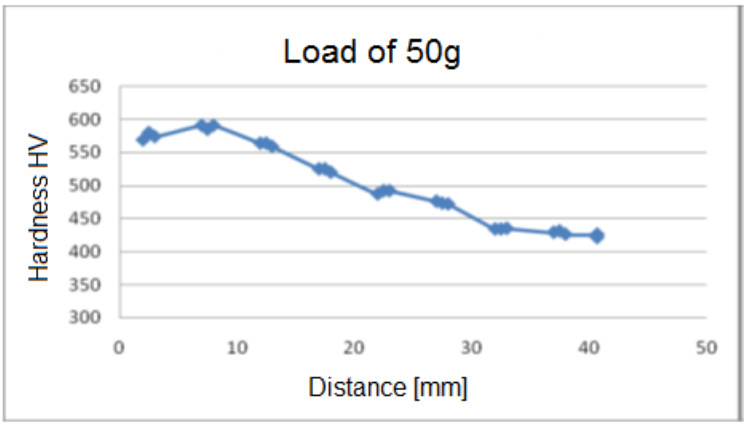

Graph 1. The measured values of hardness of reinforced layer by Vickers

Results of the measured values of hardness of reinforced layers welded Inconel:

Tab. 3. Measured values at 50 g load

Distance [mm]	Hardness HV	Distance [mm]	Hardness HV	Distance [mm]	Hardness HV
2	580	13	558	27.5	493
2.5	580	17	513	28	491
3	584	17.5	516	32	484
7	587	18	513	32.5	485
7.5	592	22	495	33	487
8	587	22.5	497	37	487
12	561	23	493	**Min**	**484**
12.5	558	27	494	**Max**	**592**

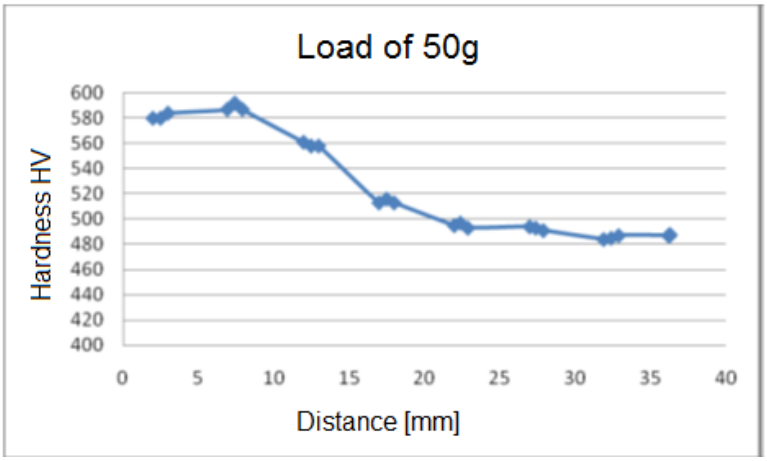

Graph 2. The measured values of hardness reinforced layer by Vickers

Evaluation of the measured values

From the graphs can be seen that the values of hardness HV decreases proportionally with increasing feed. This effect was most noticeable between feeds 0.02 mm and 0.15 mm. From this it is evident that the greatest hardening formed at lower feed rates and gradually decreased with increasing feed rate. The comparison of the two graphs shows that the difference in hardness of the weld and wrought Inconel 625 using low values feeds is negligible. In improving the feed value occurred anticipated decline and changes in hardness of machined surfaces of materials. Inconel 625 weld hardness remained constant and decreased with increasing feed already very slowly. The wrought Inconel 625 occurred due to increasing feed remain a significant decrease in the hardness of the machined surface see graph 3.

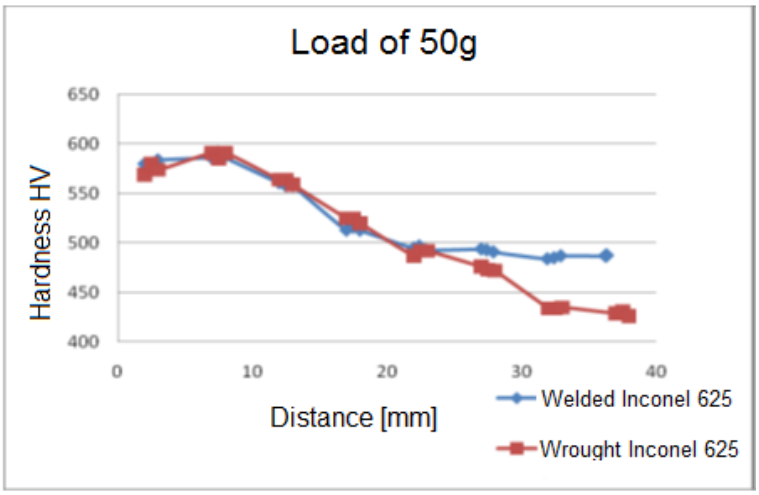

Graph 3. Comparison of hardness HV welded and wrought Inconel 625

From the measured values of surface hardness of machined material showed that in the processing of low feed doesn´t show the difference of hardness surface layer welded or wrought Inconel 625. The difference occurred until the value of the displacement of 0.1 mm, the hardness of the surface layer welded Inconel 625 remained approximately constant. While the wrought Inconel occurred with increasing feed value to continue reducing the hardness. The difference between the hardness of the surface layers of welded and forged Inconel 625 was at machining feed rate 0.2 mm equal to 55 HV.

Conclusion

In machining Inconel 625 at low feed rates in completion comes substantial hardening of the surface layer. This is undesirable if it must be so hardened surface layer re-machined. This phenomenon usually occurs at the surfaces with narrow tolerance dimension where the machine operator a few chips closer to the mean diameter tolerance. Working so hard coating material has led to a reduction in the life of cutting tools, inserts higher consumption, greater risk of failure to close tolerance dimensions and thus to degraded surface of the workpiece. The aim was to eliminate the formation of undesirable hardening

surface layer. The solution was the choice of appropriate cutting conditions, material removal strategies (more roughing chips with one finishing chip). It was conditional rigidity machine-tool-workpiece, higher precision of machine and with debugged CNC program.

References

[1] Sandmeyer Steel Company: Stainless Steel Plate [online].[cit. 2012-12-18]. *Nickel Alloy*. Available from WWW: <http://www.sandmeyersteel.com/nickelalloy-properties.html>.

[2] Specialmetals.com [online]. c2009 [cit. 2012-12-18]. *Machinig Special Metals Corporation Products*. Available from WWW: <http://www.specialmetals.com/documents/machining.pdf >.

[3] WES Hardmetal Engineering [online]. c2011 [cit. 2012-12-18]. *INCONEL*. Available from WWW: <http:// http://www.wesltd.com/divisions/hardmetal/html/InconelMaterial.html>.

[4] Specialmetals.com [online]. c2009 [cit. 2012-12-18]. *Machinig Special Metals Corporation Products*. Available from WWW: <http://www.specialmetals.com/documents/Inconel%20alloy%20625.pdf>.

[5] PETRŮ, J.; GREPL, M.; ZLÁMAL, T. *Design of Dural Alloy Machining Technology Using CNC Machines. In Progressive Methods in Manufacturing Technologies*, Czech Republic, Perná 3 – 5th november 2011. Ostrava : VŠB-Technical Univerzity of Ostrava, Department of Machining and Assembly. p. 85-88. ISBN 978-80-248-2502-1.

[6] NOVÁKOVÁ, J.; PETŘKOVSKÁ, L.; BRYCHTA, J.; ČEP, R.; OČENÁŠOVÁ, L. Influence of High Speed Parameters on the Quality of Machined Surface. In *World Academy of Science, Engineering and Technology WASET 2009, Volume 56, ICMAME 2009, International Conference on Mechanical, Aeronautical and Manufacturing Engineering, Singapore 26. – 28. August 2009. Singapore:* World Academy of Science, Engineering and Technology, Singapore, p. 274-277. ISSN 2070-3720.

[7] PETRŮ, J.; ČEP, R.; GREPL, M.; PETŘKOVSKÁ, L. Effect of High Feed Milling on the Microstructure and Microhardness of Surface Layer. In *Annals of DAAAM for 2011 & Proceedings of the 22nd International DAAAM Symposium, 23-26th November 2011, Volume 22, No. 1, Vienna, Austria*, Published by DAAAM International Vienna, Vienna, 2011, p. 999 – 1000. ISBN 978-3-901509-83-4.

[8] STAHL, J. E. *Metal Cutting Theories and Models.* Published by Lund University, Sweden 2012, p. 590. ISBN 978-91-637-1336-1.

[9] DAVIS, J. R. *Surface hardening of Steels.* Published by ASM International, United States of America, 2002, p. 364. ISBN 978-0-87170-764-2.

Decision Analysis of Supply Chain Resource Integration and Optimization in Mass Customization by the Fourth Party Logistics*

Jianming Yao
School of Business, Renmin University of China,
Beijing, 100872, China

And

Zhenzhen Zhao
School of Business, Renmin University of China,
Beijing, 100872, China

ABSTRACT

A new problem about the supply chain resource integration and optimization in mass customization (MC) by the fourth party logistics (4PL) is analyzed in this paper. On this basis, a dynamic and multi-objective optimization model and an algorithm are set up for the decision optimization of the supply chain resource integration in mass customization by 4PL. The optimization model and the algorithm can not only reflect the operating requirements for the special resource integration process in mass customization, but also reflect the thought of solving the key contradiction in mass customization and give consideration to the characters of 4PL operation in the supply chain. The application feasibility of the model and algorithm are validated is also pointed out in this paper.

Keywords: Decision Analysis, Supply Chain Resource Integration, Optimization, Mass Customization, Fourth Party Logistics.

1. INTRODUCTION

How to deal with the contradiction between mass production effect and customized demand is the key problem on mass customization (MC) [1]. With the development of supply chain management, we can probe a new way to solve this problem through the excellent character of supply chain resource integration, allocation and optimization. However, the supply chain resource integration in mass customization has special characters, mainly reflected in the random information of customer orders and the outstanding collaborative benefit and risk conflictions which will cause many complicated contradictions in supply chain operation [2, 3]. Therefore, how to settle these problems is most important in implementing mass customization.

In recent years, the successful operation of the fourth party logistics (4PL) has gradually demonstrated that it is an effective mode to integrate, allocate and optimize the complicated resources of supply chain reasonably, efficiently and flexibly [4]. Especially, 4PL have great superiorities in coordinating different kinds of supply chain co-operators' benefits and risks in the operation. Therefore, 4PL is a better method to settle the problems of the random information of customer orders and the outstanding collaborative benefit and risk conflictions in MC and the effective way is to integrate the different resources of the supply chain and allocate the MC tasks to them. The implementation of this process needs mathematic optimization method.

However, there are no effective quantitative methods to guide the integration practices and especially there are lack of analyses on quantitative integration process about the supply chain resource in MC by 4PL up to now which will inevitably limit the superiorities of 4PL application in mass customization.

Based on our early relative achievements about the supply chain operation in MC and the supply chain resource integration in 4PL mode, see Reference [2-4], this paper set up a dynamic and multi-objective optimization mathematic model about the decision optimization on supply chain resource integration in mass customization by 4PL from the view of systemically balancing and quantifying the supply chain.

In order to solve the optimization problem, this paper also set up an algorithm for the decision optimization of the supply chain resource integration in mass customization by 4PL. The optimization model and the algorithm can not only reflect the operating requirements for the special resource integration process in mass customization, but also reflect the thought of solving the key contradiction in mass customization [2] and give consideration to the collaborative benefits and risks in the supply chain.

2. ASSUMPTIONS

We assume that the total production stages for MC is K and let k (k =1, 2, ..., K) denote the index of each stage. We use t as an independent time variable and use t_k denote the starting moment at the kth stage.

* This research is supported by National Natural Science Foundation of China (71072148).

In the 4PL resource integration scheme, the core enterprise can select the suitable moment t_k to implement supply chain resource integration and MC task allocation.

Let N_k denote the total number of the cooperators (including the number of the core enterprise's production/working groups taking part in the related production) at the kth stage. In following analysis, we use 'nodes' instead of 'cooperators'. Let r (r = 1, 2, …, N_k) denote the index of the node at the kth stage. Let (kr) denote the index of each node. All these nodes will join in the supply chain resource integration and MC task allocation process by 4PL.

Reference [3] pointed out that the key problem of MC to solve is to satisfy the different customized demands with the scale production efficiency. As for a manufacturing supply chain, it is to make the system's comprehensive profits maximum on the premise of rationally realizing the production efficiency to different orders. Obviously, these constitute a contradictory body. To relieve these dominant contradictions in the dynamic scheduling and to show the effects of the scope economy in MC, we put forward the idea of the time threshold based on the elementary classification of the stochastic orders. The main idea of the time threshold is that the core enterprise should put forward a time horizon to wait dynamically for other orders' coming by weighing all factors in the supply chain system when it has received any order in the scheduling. At the same time, to promote the customized service level maximally and realize the approximately full customization, we also given an idea of the secondary classification of orders based on the time threshold. The main contents of the secondary classification are as follows: Definition 1, the orders received by the enterprise during the time threshold whose parts will be made by the unique designing and machining technology are named Special Order (SO); Definition 2, the orders besides SO are named General Order (GO); Definition 3, the orders that should be given the highest priority to operate to fit the urgent delivery date of customer are named Rush Order (RO) which are not restricted by the time threshold.

We can see that, on one hand, the idea of the secondary order classification contains completely the customized qualities of products, which can be reflected by the physical characters of products and be corresponding to the classification of GO and SO and also contains the customized delivery date of products which can be corresponding to the classification of RO; on the other hand, it contains completely the realization of the production efficiency in the supply chain scheduling in MC which can be reflected by the complexity of the production process, be corresponding to the classification of GO and SO and can be reflected by the same time production lot corresponding to the definition of the time threshold. So, to plan and optimize the supply chain resource integration and MC task allocation based on the order classification by the time threshold is a good idea to satisfy the different demands of the customer with the higher production efficiency. This is the key way to relieve the first dominant contradiction.

The existence of the rush orders and special orders may make it more complicated and difficult to handle the supply chain resource integration and MC task allocation. But as a real meaning customized system, to greatly satisfy the customer demands is necessary. And only on this base can the excellent service brand be set up gradually and can the supply chain cooperative relationships develop and last greatly and long. At the same time, to reduce the rush orders and the special orders gradually will be the objective for the enterprises to get by reform and process reorganization. Here, we will introduce the idea of the time threshold and the order classification into the supply chain resource integration and MC task allocation process to determine the decision optimization adjustment moment.

For the order information, let N_O denote the total number of the orders received by the core enterprise during the time threshold T_0. Let G denote the number of the production categories divided by the starting stages of the different sub-tasks of the orders at moment t_k and let h (h =1, 2, …, G) denote the index of each production category.

Let M_g (g =1, 2, …, G) denote the total number of the order categories divided by the order classification described above in the hth production category at moment t_k and let i (i =1, 2, …, M_g) denote the index of each order category. Let N_m (m =1, 2, …, M_g) denote the number of the total orders in the ith order category at moment t_k and let j (j =1, 2, …, N_m) denote the index of each order. Finally, let (hij) denote the index of each order after the above division.

When the tasks of (hij) are produced by (kr), we assume the relations as follows: Let $T_{D.hij}$ denote the delivery date; let $T_{kr.hij}(t_k)$, $C_{T.kr.hij}(t_k)$, $T_{ext.kr.hij}(t_k)$ and $C_{ext.kr.hij}(t_k)$ denote respectively the production time and cost (not including the extra inventory time and cost), the extra inventory time and cost; let $T_{exp.kr.hij}(t_k)$ and $C_{exp.kr.hij}(t_k)$ denote the expected production time and cost determined by the core enterprise; let $C_{\Delta\tau.kr.hij}(t_k)$ denote the extra inventory cost per unit time and define $C_{ext.kr.hij}(t_k)=T_{ext.kr.hij}(t_k)\ C_{\Delta\tau.kr.hij}(t_k)$. Let $T_{\Delta.k+1,r.hij}(t_k)$ denote the acceptable absolute value of the difference between the actual production time and the expected production time for (kr) producing the tasks of (hij) when it is operated at stage (k+1, r).

To set the constraints, let $A_{dem.k.hij}(t_k)$ and $Q_{sta.k.hij}$ denote respectively the spare production capacity demand and the production quality demand of (hij) to the kth stage. Let $A_{sup.kr.hij}(t_k)$ denote the spare production capacity supply of (kr) to (hij). Let $Q_{kr.hij}$ denote the production quality supply of (kr) to (hij). At the same time, let $\varepsilon_{kr.hij}(t_k)$ denote the profit preference of (kr) to (hij), let $U_{kr}(t_k)$ and $U_{min.kr}(t_k)$ denote respectively the profit preference satisfaction degree of (kr) and its minimum, let $U_{SC}(t_k)$ denote the overall satisfaction profit of the supply chain system and let $\phi_{kr}(t_k)$ ($0\le\phi_{kr}(t_k)\le1$) denote the contribution factor of (kr) to $U_{SC}(t_k)$ (when all the nodes achieve their maximum satisfaction profit and all $\phi_{kr}(t_k)$ equal 1, $U_{SC}(t_k)$ will be maximum ideally). Assume that the financial compensation is needed when the delivery date exceed the due date by accidents. So, let β denote the delayed delivery tolerance parameter and let β_{max} denote the maximum of β which will be jointly determined by the core enterprise and other cooperators. Assume that if (hij) is operated at (kr), then $\delta_{kr.hij}(t_k)$=1, otherwise $\delta_{kr.hij}(t_k)$=0.

3. OPTIMIZATION MODLE

We set up a 0-1 programming model as follows.

The optimization objective functions are

$$\min_{\max \text{ PROD profit}} Z_1 = \sum_{k=1}^{K}\sum_{r=1}^{N_k}\sum_{h=1}^{G}\sum_{i=1}^{M_g}\sum_{j=1}^{N_m}\{[(C_{T.kr.hij}(t_k)+T_{ext.kr.hij}(t_k)C_{\Delta\tau.kr.hij}(t_k))$$

$$+\varepsilon_{kr.hij}(t_k)T_{kr.hij}(t_k)]\delta_{kr.hij}(t_k)\} \quad (1)$$

$$\min_{\max \text{CUST profit}} Z_2 = \left| \begin{matrix} T_{\exp.kr.hij}(t_k) - \\ (T_{kr.hij}(t_k) + T_{\text{ext}.kr.hij}(t_k)) \end{matrix} \right| + \beta \quad (2)$$

$$\min_{\max \text{MC profit}} Z_3 = \left| \sum_{j=1}^{N_m} \delta_{kr.hij}(t_k) - N_m \right| \quad (3)$$

$$\max_{\max \text{SC profit}} Z_4 = U_{\text{SC}}(t) = \sum_{k=1}^{K} \sum_{r=1}^{N_k} \phi_{kr}(t_k) U_{kr}(t_k) \quad (4)$$

subject to

$$\sum_{h=1}^{G} \sum_{i=1}^{M_g} \sum_{j=1}^{N_m} A_{\text{dem}.k.hij}(t_k) \le \sum_{r=1}^{N_k} A_{\text{sup}.kr.hij}(t_k) \quad (5)$$

$$T_{\text{D}.hij}(t) \le \sum_{k=1}^{K} \sum_{r=1}^{N_k} (T_{kr.hij}(t_k) + T_{\text{ext}.kr.hij}(t_k))\delta_{kr.hij}(t_k) \le (1+\beta) T_{\text{D}.hij}(t) \quad (6)$$

$$\left| T_{\exp.kr.hij}(t_k) - (T_{kr.hij}(t_k) + T_{\text{ext}.kr.hij}(t_k)) \right| \le T_{\Delta.k+1,r.hij}(t_k) \quad (7)$$

$$\sum_{r=1}^{N_k} \sum_{h=1}^{G} \sum_{i=1}^{M_g} \sum_{j=1}^{N_m} \delta_{kr.hij}(t_k) = N_{\text{O}} \quad (8)$$

$$\sum_{r=1}^{N_k} \delta_{kr.hij}(t_k) = 1 \quad (9)$$

$$U_{kr}(t_k) \ge U_{\min.kr}(t_k) \quad (10)$$

$$Q_{kr.hij} \ge Q_{\text{sta}.k.hij} \quad (11)$$

Where $0 \le \beta \le \beta_{\max} < 1$; $k = 1, \ldots K$; $r = 1, \ldots, N_k$; $h = 1, \ldots G$; $i = 1, \ldots, M_g$; $j = 1, \ldots, N_m$.

In the model, Constraint (5) describes the spare production capacity demand relations. Constraint (6) reflects the delivery constraints of the customized production. Constraint (7) assures that each production stage of the same customized product at different stages will continues smoothly. Constraint (8) assures that all orders received during the time threshold must go through all the production stages. For the orders whose tasks may not participate in some stages in practice, we make them through the virtual stages to replace. Constraint (9) assures that each task will be completed by its corresponding cooperators and there will not be any duplicated production to one task. Constraint (10) assures that the supply chain's collaborative relations are built on the satisfaction of the cooperators' profit preferences reaching their acceptable levels. Otherwise, they may not accept the resource integration and task allocation. Constraint (11) assures the quality demand of MC.

4. MEANING OF OPTIMIZATION

Equation (1) addresses optimizing the production cost of MC and its outstanding feature is the introduction of the profit preference factor.

Equation (2) addresses optimizing the punctual deliveries of the customized products. From system opinion, when the actual production time is closer to its expected value, the deliveries to the customers can be better guaranteed. In addition, the smaller the value of β, the higher the level of the punctual delivery service is.

Equation (3) addresses optimizing the scale production. The value of Z_3 is smaller the better. Because the division of N_m is based on the order classification ideas discussed above and the direct aim of the ideas is to alleviate the key contradiction in MC, which is also the goal of Equation (3). When the spare production capacity of (kr) is greater than N_m needed, the tasks of N_m can be completed by one or more cooperators at the same stage. Obviously, the scale production effect of the former is higher than latter. But, the same as analyzing the profit preference, the decision result will be determined by the profit situation of the subjective and objective collaborative production.

Equation (4) addresses optimizing the supply chain's overall profit on the premise that every cooperator can achieve its own satisfaction level.

These four objective functions influence and restrict each other. The ultimate objective of the model is to reflect the levels of alleviating the dominant contradictions. It also illustrate that the supply chain resource integration and task allocation in MC by 4PL is a typical multi-objective optimization problem. In alleviating two dominant contradictions, we must consider a comprehensive optimization solution for these multiple objectives at the same time. Therefore, we choose four aspects including the customized production cost, the production time, the scale production effect and the production capacity congestion as the optimizing goals which are closely related to the micro-level of the solution operation in order to realize the application of our alleviation ideas.

5. OPTIMIZATION ALGORITHM

The above 0-1 programming model is a typical NP-hard problem. Currently, there are not very effective solution methods for linear 0-1 programming problem, such as the knapsack problem. Especially, when the optimization objective is nonlinear, the solving difficulty is even greater. In general, the genetic algorithm and bionic approach are the primary methods to solve such problems.

In this paper, we use an improved ant optimization algorithm to solve the optimization problem, for it has more advantages [5] has been widely used in combination optimizations, dynamic routing and scheduling problems [6]. Certainly, there is possibility to develop other algorithm to solve the problems in this paper, but till now, ant algorithm is the best one. For example, fish swarm algorithm is another bionic method, but it is more complex, need long time computation and is difficult to balance the parameter relations among much more points to be sought in the optimization network although it has more advantages in global search. Meanwhile, a major problem is that it is difficult to bring multi-attribute optimization objectives in solving the multi-objective optimization. So, it is difficult to comprehensively deal with the problems in this paper by fish swarm algorithm.

However, as shown in the former text, there are much more new operating characters and complexities in the supply chain resource integration and task allocation in MC compared with

the general operation problems such as JSS and FSS. In order to make the algorithm rational and suitable, we must develop the general ant algorithm.

Suppose that a supply chain network at the moment of resource integration and task allocation adjustment is composed of the source node, object node and cooperator nodes. The stage division of the network will be determined dynamically by the practical production circumstance of the several orders at the moment t_D.

In the running of algorithm, ants will move from the source node to the object node through the network and die then. As the ants can't return, the pheromone [5] of different roads will be determined intelligently by the different cooperators' production parameters. The structure of the algorithm is as follows.

First, we consider the structure of the ants and the forbidden nodes. To realize the algorithm we adopt the special method to make ants. That is: we make two-step division to the ant classification. The first step is to classify the ants by the orders' production classification. Each order class is corresponding with an ant classification; the second is to classify them by the beginning stage of the production in the same order classification, and the different beginning stages are corresponding with the different ant classes. Suppose at moment t_D, the number of the order classes that should be made the resource integration and task allocation adjustment is n and the index of the different beginning stages in every classification is m_i (i=1,2,…n). Then, the number of the ant class at moment t_D is $\sum_{i=1}^{n} m_i$ and every ant class is signified as A_{ij}(i=1,2,…n;j=1,2,…m_i). For each ant class, we set the forbidden nodes according to its allowable field.

Then, the probability to select the different paths should be determined as follows.

Firstly, we decide the attraction probability of the paths to ants. Given M_{ij}* is the allowable field of A_{ij} at t_D. The set of cooperator r(r=1,2,…R) at stage k(k=1,2,…K) is signified by $M_{ij.kr}$*. As one of the optimization objectives is to minimize the production cost, the quantity (signified by $\pi_{ij.kr}^{(1)}$) of the remained pheromone by ant class A_{ij} is in the inverse ratio of the production cost when they passing through $M_{ij.kr}$*. Then the attraction probability of class (1) for cooperator r to A_{ij} at stage k can be described as:

$$P_{\mathrm{A}}^{(1)} = \pi_{ij.kr}^{(1)} / \sum_{r=1}^{\mathrm{R}} \pi_{ij.kr}^{(1)} \tag{12}$$

At the same time, let the expected production time limit (expected production delivery date) of A_{ij} to kr is T_E. Considering the dynamic character of the supply chain's cooperative relationship, some cooperator should make a competitive bidding according to its own production process because of its probable cooperative relations with the other supply chain networks at the same time. Then let its competitive bidding delivery date be T_S and let $T_\Delta = \left|T_E - T_S\right|$. We can learn that to realize the punctuality of the customized production and the connections of the different production stages, the smaller T_Δ is, the better it is. Certainly, some times the quantity of T_Δ has the relation with the production cost which should be weighed by the supply chain system. Let $\pi_{ij.kr}^{(2)}$ denote the pheromone quantity which is inversely proportional to T_Δ that ant class A_{ij} left when they pass through node kr. So the attraction probability of class (2) for cooperator r to A_{ij} at stage k can be described as:

$$P_{\mathrm{A}}^{(2)} = \pi_{ij.kr}^{(2)} / \sum_{r=1}^{\mathrm{R}} \pi_{ij.kr}^{(2)} \tag{13}$$

Secondly, we decide the exclusion probability of the paths to ants. Scholar Navarro Varela et al. [7] has given the idea that the pheromone of the same ant class will attract each other and that of the different class will exclude. So, in order to solve the production congestion, we set the exclusion probability of the paths to ants. Let $\psi_{pq.kr}$ denote the quantity of the remained pheromone by non-A_{ij} ant class at kr, then the exclusion probability of it to A_{ij} can be described as:

$$P_{\mathrm{R}} = \psi_{pq.kr} / \sum_{r=1}^{\mathrm{R}} \psi_{pq.kr} \quad (p=i,q\neq j;p\neq i,q=j;p\neq i,q\neq j) \tag{14}$$

Thirdly, we decide the probability of the ants to select paths. Let the probability of A_{ij} to select path kr be:

$$P_{ij.kr} = \alpha P_{\mathrm{A}}^{(1)} + \beta P_{\mathrm{A}}^{(2)} + \gamma(1 - P_{\mathrm{R}}) \tag{15}$$

In Eq. (15), α,β,γ($0<\alpha,\beta,\gamma<1$;$\alpha+\beta+\gamma=1$) are the parameters for the algorithm and they can reflect the expected weight relations between the attraction and exclusion probabilities.

We also need to determine the update rule of the pheromone. Different from the traditional algorithm, the ants in this paper only have one-way motion character, so the algorithm should update the pheromone at every production node automatically. Here we use Φ to denote all the former $\pi^{(1)}$, $\pi^{(2)}$ and ψ to simplify the indications and the update rule is:

$$\begin{aligned} &\Phi(t+1) = \Phi(t) + \Delta\Phi(t,t+1) \\ &-\xi\Phi(t) = (1-\xi)\Phi(t) + \Delta\Phi(t,t+1) \end{aligned} \tag{16}$$

where $\Phi(t)$ and $\Phi(t+1)$ denote respectively the pheromone quantity remained at the node at the t^{th} and the $(t+1)^{\mathrm{th}}$ batch, $\Delta\Phi(t, t+1)$ denotes the pheromone quantity left at the $(t+1)^{\mathrm{th}}$ batch and ξ($0<\xi<1$) denotes the volatile coefficient of the pheromone.

6. ALGORITHM STEPS

In supply chain resource integration, when the adjustment moment comes, we operate the algorithm to adjust dynamically the assignments of the production tasks among the supply chain cooperators. Because there are many complex cooperative and competitive relations among the cooperators, it is difficult to find the exact optimization solution. In practice, we can weigh in several aspects (e.g., the production cost and production delivery date in this paper) and put forward an expected satisfaction level before scheduling. When the algorithm convergence makes every optimizing index reach its corresponding level, the algorithm can be over. The steps are:

STEP 1. The core enterprise determine the resource integration and task allocation adjustment moment.

STEP 2. When the algorithm begins, we judge the order classification according to the description and set up the ant

classification, then determine the allowable fields for them.

STEP 3. Set the expected production delivery date T_E, set the production cost of all kinds of MC production class corresponding with the different kinds of ant class A_{ij} at different production stages. Determine the relations between T_Δ and the remained pheromone of all kinds of ants by the way of sampling and analyzing the present data.

STEP 4. Determine the expected satisfaction level of every optimization index such as the production cost and delivery date according to the historical experience and the data on-the-spot.

STEP 5. Set and adjust the value of α, β, γ and ξ.

STEP 6. Generate ant batch t (in the beginning, t=1) at source node and there are kinds of ant class in every batch. Let the number of the ants in every class be x times as much as the number of the corresponding kinds of orders ($3<x<10$ is quietly suitable for the small supply chain network). Make the ants move to the object node and die when they arrive. Update the pheromone at every node according to the rule and then let $t=t+1$.

STEP 7. Account the ant number passing every node in every batch. Make the judgment of whether the ant number of selecting every node has become stable. We can judge the stable state by comparing the number of the ants selecting one node in this batch with the former batch to see if there is no obvious change, or by observing the number of the ants that always changes in a small scope during the recent several batches.

Then, we give the assignment of MC tasks to different cooperators according to the number of the ants distributed at the different nodes, calculate the optimizing level of all kinds of indexes and judge if they have reached the satisfaction level. If yes, we can stop the algorithm and turn to step 8, otherwise turn to step 6.

STEP 8. Output the algorithm result and make the resource integration and task allocation implementation according to it.

Here, we should also pay attention to several issues.

Firstly, if the move of the ants can't reach the stable state even they have passed all batches, we should adjust the values of all kinds of parameters to a larger range, which means we should turn to step 5.

Secondly, if every index can't reach the satisfaction level even if the algorithm has run in a long time, we should revise the expected satisfaction level, which means we should turn to step 4.

Finally, when the algorithm reaches the stable state, the problems of production congestion at some nodes are disappeared, and even if the quantities of the attraction pheromone at these nodes are larger, the ant current through these nodes will not increase. It is owed to the role of the exclusion probability.

7. VALIDATE RESULT

We validate the reasonability and feasibility of the above model and ant algorithm in the optimization decision of the supply chain resources integration in MC by 4PL through a case study and simulation.

8. CONCLUSIONS

This paper explores a quantitative method about the supply chain resource integration in MC by 4PL mode and presents an integration optimization and MC task allocation model and an algorithm to reflect the mechanism of quantification. Obviously, there are many and complex dominant factors which play a decisive role in the integration decision optimization and it is need to give more deep, detailed and refined analyses to their operational characters and rules.

The model and algorithm set up in this paper are based on the integration quantitative theories and methods in 4PL mode. They not only reflect the complicated characteristics of the supply chain resource integration in MC production process but also merge the solution methods of several important relations into the integration optimization process.

The quantitative method of the resource integration optimization in MC by 4PL in this paper can reflect the complex diversity of the supply chain resources to be integrated in 4PL, can reflect the different resource demands for different MC customer and can reflect the resource integration demands for supply chain system and every resource individual. It can clearly describe the complex relationships between the subject and object in the supply chain resource integration in MC; easily balance the relationships among multi-objectives of integration from the angle of subjective and objective system strategy; easily solve the special problems (such as the congestion problem) in the actual operational level. In addition, the model and algorithm are also transition bridges from the integration optimization theories and methods to the practice.

The integration mode of the supply chain resource in MC by 4PL belongs to the frontier of supply chain management field. In future study, we should give more attention to the complicacy of the dominant factors. Especially in different production or service industries, it is most important to grasp this principle. Meanwhile, it need more depth analysis about the complex relations among various factors to guide the integration practice of 4PL with better integration strategy and to exploit more advantages in integrating supply chain resources in MC by 4PL.

9. REFERENCES

[1] R. Duray, P. T. Ward, G. W. Milligan, "Approaches to mass customization: configurations and empirical validation", **Journal of Operational Management**, Vol. 18, No. 6, 2000, pp. 605-625.

[2] J. M. Yao, "Scheduling Optimization of Cooperator Selection and Task Allocation in Mass Customization Supply Chain Based on Collaborative Benefits and Risks", **International Journal of Production Research**, Vol. 51, No. 8, 2013, pp. 2219-2239.

[3] J. M. Yao, "Supply Chain Scheduling Optimization in Mass Customization Based on Dynamic Profit Preference and Application Case Study", **Production Planning & Control**, Vol. 22, No. 7, 2011, pp. 690-707.

[4] J. M. Yao, "Decision Optimization Analysis on Supply Chain Resources Integration in the Fourth Party Logistics", **Journal of Manufacturing Systems**, Vol. 29, No. 4, 2010, pp. 121-129.
[5] E. Bonabeau, M. Dorigo, A. G. Theraul, "Inspiration for optimization from social insect behavior", **Nature**, Vol. 406, No. 1, 2000, pp. 39-42.
[6] J. Bautista, J. Pereira, "Ant algorithms for a time and space constrained assembly line balancing problem", **European Journal of Operational Research**, Vol. 177, No. 3, 2005, pp. 2016-2032.
[7] Varela, "Ant colony optimization for virtual-wavelength-path routing and wavelength allocation", **Proc. Conf. evolutionary computation**, Washington DC, USA, 1999, pp. 324-337.

Set of Elements, parameters and considerations to get the successful inclusion of the Smart Grids in Colombian Power Systems

J. Silva, A. Ospino, M. Balbis
Universidad de La Costa
Barranquilla, Atlantico,50366,
jsilva6@cuc.edu.co

***Abstract*— this document is a synthesis of those parameters, considerations, elements and systems that must be implemented if the objective is based on the inclusion of smart grids in the Colombian electrical system. This paper defines the changes of the traditional figure of the electrical energetic chains that includes generators, transmission, distributors, retailers and users to introduce the new concept of ProUser[1]. This new term generates a change in the electrical chain and it will be become bidirectional and decentralized in operation.**

Keywords—Smart grid; descetralized system; bidirectional; ProUser;

I. INTRODUCTION

This paper presents the explanations of those aspects that have to be considered when is talked about Smart grids and that also many times is being confused with the use of telemetric and automatic system. For that reason must be formally defined for Latin America and Specific for Colombia a structured definition. Also can give the line to follow for the interconnected system to overcome and introduce the smart grids successfully.

In this document is related the following aspect: (2) a formal definition for Smart Grids focused on the purpose projected for Spain which introduce the term in the electric market chain. (3) The elements that have to be included in the electrical system to could reach the Smart grid definition. (4) After that is defined the possible Electrical Energetic Chain that satisfies the bidirectional orientation of the ProUsers with the system, the changes that will be produced in the electrical energetic chain if is desired to include smart grids in the Colombian system and the purpose of a distributed system market in energy consume but automatically controlled by telemetric systems. Finally, it is presented the road to follow if is desired a successful inclusion of smart grids in Colombia.

This paper does not desire to generate controversy on the real meaning of the composed word "smarts grids", the objective is to identify what is the real definition of the term, the elements that must be included to make reference about them and to emphasize that the surveys that have been doing in Colombia are just the first step that is defined in the fourth section of this paper.

II. FORMAL DEFINITION FOR SMART GRIDS

This section presents the formal definition based on the first applications of the term defined in Europe and after that are presented the objectives wanted to be reached.

A. Definition

An Smart Grid or a smart system to distribute energy is defined as the integration of elements that allow the optimization of the energy production and distribution using automatic system that are able to ensure economic energy, sustainability, lower losses, high levels of quality, reliability, security and flexibility, integrating distributed system generation to the energy chain that can be renewable and cheaper or wasted in the case of non – renewable energy that is produced in the figures of cogeneration or self-generation. [2]

The diagram box that is showed in Figure 1, represents the formal characteristic that must be included in a design of a smart grid and they are defined as follow:

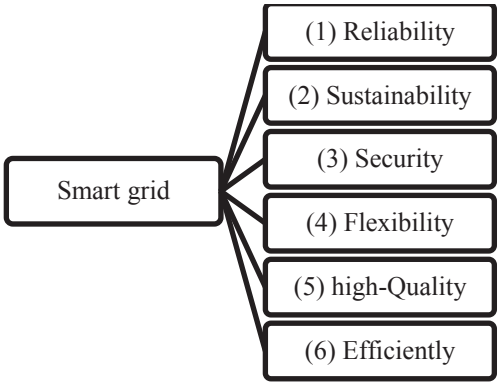

Figure 1. Inclusion of the last propieties that must be considered in a smart distribute energy system.

1) Reliability: As the actual definition, it is the probability that the system could be able to operate completely[1] if one of its elements is not in operation due to a contingence or programmed event of maintenance. The reliability must be defined and structured in a smart grid, for each one of its elements and project the availability of it in a defined period of time. The global system must be able to operate in a higher condition of contingence. It makes reference when more than two elements of the system go out from normal operation. (There must be a probability of operation higher that the criteria N-2 elements).

2) Sustainability: This term is the most ambitious because it mean completely autonomy. The energy of the generators must be controled efficiently and the centraliced system have

1 ProUser: It is the term that integrates the criteria used in EEUU and Europe to include the figure of Users that could generate with renewable energy in most of the cases.

to have in realtime the capacity of supply of all the generator (included: Conventional and distributed system generators that are available to conect to the network).

3) Security: As the actual definition of security it must be focused on ensure the the continuity of the suminister of energy to the users that are connected to the electrical system.

4) Flexibility: To be able the system to commute its elements to secure the energy suppy. [4]

5) High-Quality: This make reference to be in rule with the current regulation of energy quality. The users of the system must be certified with the normative to avoid the inclusion of losses or quality problems int the network. [4,9] Also the distribution agent must be in rule with the respect normative that implies that all their system have to be in rule with the normative[2]. [4]

*6) Efficiently:*Smart grids are focused also in production, transmittion and final use of the energy that is necesarry, reducing losses, mitigate the downtime operation of machines, optimize the system and develop culture and stregaties to save energy in all the energetic chain. Many efficient process are focused in tecnological changes due to the actual condition of their electric and mechanical equipments. [1] For example an air-cooling system for each one of the offices in a building, could be replaced by a core cooling system for all the building. In Colombia has started the implementation of the ISO 50001[3] and have been introduced the RETIQ[4] and RETILAP[5] that contribute to inprove the eficience of the system. Smart grids will be measured also efficiently and they must be designed taking into acount this aspect.

B. Objetive of smart grids

According to the definition and the properties that were defined previously, many authors and entrepreneurs that are working in this topic consider eight objectives to include smart grids in all the electrical chains around the world. They also impact in the reduction of the pollutant emissions of $C0_2$ that many processes of the industry and the electric generation are causing and they are resumed as follow:

1) To strengthen the grid implementing automation to obtain an optimal operation and reduce techinal losses and gain reliability, security and flexibility.

2) To optimizate the interconetion with renewable energy systems to minimize the cost of the energy and improve sustainability.

3) To developing decentraliced schemes to introduce the implementation of distributed generation.

4) To produce new techological forms of energy storage, focused in alternative system generation in which the energy is not as stable as the conventional system and must be storaged before it use.

5) To develop a change in the electrical market due to the inclusion of new figures of generation system And to encourage those users that produce and use efficiently the energy.

6) To become the demand management of the energy in a real-time management.

7) To include into the electrical market new figures of consumption, for example the electric vehicle.

8) To reduce peaks of the daily demand respect the conventional energy generation. It is said that this peaks will be assumed by the introduction of the new figures of distributed system generators.

III. ELEMENTS NEEDED FOR SMART GRIDS

According to the orientation of the document it is noticed that Colombia is not going to be ready for this system during the following years but it could be reached if are implemented strategies that could benefit the progress of smart grids.

The actual model of the energetic chain must be modified to could include successfully the smart grids. In this section will be defined those elements.

A. ProUser

In the new model is needed to be modified the term of user for many cases in which will be projected to include new types of distributed system generation or the case of the electric vehicle. This new element became the electrical system chain bidirectional due to it could supply and in other case consume energy from the interconnected system. [3]

This user must be regulated and controlled systematically and in real–time with the aim of detect how much energy it consume, in which periods register the highest consume of energy and define its sustainability in percentage values.

The overcrowding of ProUser could be the solution to the reduction in the use of conventional energy system, in hours where the daily demand is the highest of the day. Gradually, the ProUser could become own sustainable during this periods of the day using its own energy generated.

A ProUser is basically an integration of consume and production of energy based on the term distributed system as is shown in figure 2.

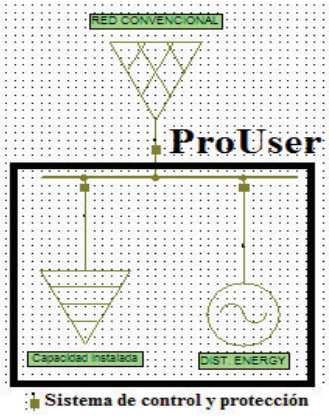

1 Completely: This means that all the users or charged can receive the energy from the system.

2 For Colombian case the normative NTC 5000 (Quality of the electric power) and the STD IEEE 519

3 ISO 50001 is the standard energy management.

4 RETIQ is the technical regulations for labeling

5 RETILAP: is the technical regulation for lighting and street lighting

Figure 2. Single line representation of a ProUser.

B. Renewable Energy

As is represented in represented in figure 2 and as is expressed in the definition of a Smart Grid, this type of energy in most of the cases has to be renewable. The use of renewable energy has to increase in Colombia and more modern systems than JEPIRACHI have to be developed and installed. [3, 8]

The table I and II, enumerate the range of wind and solar intensity respectively in many regions around Colombia according with the established in the UPME[1].

TABLE I. WIND POTENTIAL IN COLOMBIA [2]

Wind speed (m/s)	Place with wind potential (place - department)
igual o superior a 5 m/s durante todo el año	Galerazamba-Guajira
	San Andres – Archipielago de San Andres
	Gacheneca - Boyacá
Entre 4 a 5 m/s durante todo el año	La religiosa - Huila
	Providencia – Archivielago de San andres
	Riohacha – La guajira
Rangos entre 4 – 5 m/s existentes en algunas epocas del año	Villa Carmen - Boyacá
	Obonuco – Nariño
	Cúcuta – Norte de Santander
	Ábrego – Norte de Santander
	Urrao – Antioquia
	Bogotá - Cundinamarca
	Barranquilla - Atlantico
	Soledad – Atlantico
	Santa Marta - Magdalena
	Achique - Tolima

TABLE II. SOLAR POTENTIAL IN COLOMBIA [2]

REGION	Energy kWh/m^2/year
Caribe	4015
Orinoquia	1643
Amazonia	1551
Andina	1643
Pacifica	1278

C. Automatic control system

The control system must be changed due to the bidirectional action of the new term introduced as ProUser. The system has to be measured and controlled from a centralized point that allows the demand management in real-time and that will be able of act in the presence of faults or contingencies. [9]

D. Telemetry system

This terminology has created controversy in its implementation because is confused with smart grids and it is important to highlight that the telemetry it in this moment the form to control the user based on a control and communication system where measurement is stored directly from the system installed in the cabling. [3]

The telemetry system used in this moment is in one direction due to the type of chain that is currently handled. The telemetry system required must be directional and able to sense the flux direction according to the type of user the telemetry system would have been programmed in different manners. [3]

IV. ELECTRICAL ENERGETIC CHAIN MODIFICATION

This section finally defines a purpose to follow in order to get in operation a system based on a smart technology. Figure 3, represent the unidirectional consume chain in the electric system. [6, 7]

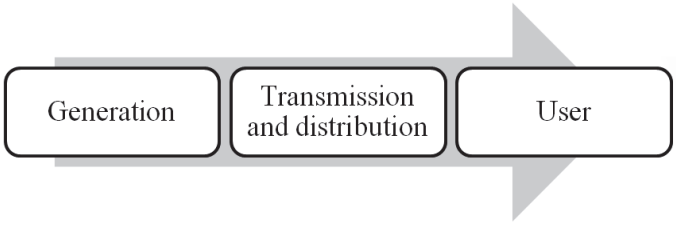

Figure 3. Actual system direction (Unidirectional) of the chain of energy consume

A. Scheme including smart grids

The diagram showed in figure 4, is the objective when Smart grids started to be included in the national grid system. There is noticed the bidirectional lines orientation between electrical grid and those proUsers. The bidirectional lines orientation means that the figure ProUser could provide energy to the electrical grid according to the needs and requirement of the grid. This includes a bidirectional control and a new implementation of a new programming of telemetric system.

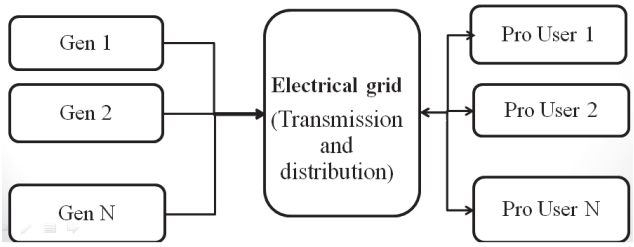

Figure 4. System purposed for smart grids acording. (Bidirectional between Pro Users and Electrical grid)

B. The road to reach the desired market

According to this survey and in phase with the opinion of the researchers that have been working in this topic, it is still generating a question: *What should be done to include successfully smart grids?"*

The answers to this question are basically good management of investigations and the support of the state to obtain the inclusion of all the parameters presented in section II. [3] The following scheme responds to the possible road to follow and take the same line of implementation as is being doing in EEUU and EUROPE. This scheme is divided in five phases:

1) The first phase: responds to the investigations and researches to obtain a technological improve and must be oriented and supported by the state. The state have to stimulate and promote the researches and development of these

1 UPME: Mine and Energy planning unit in Colombia

technologies due to they are not mature, they are just in test as this is happing with the wind energy park (Jepirachi). These phase implicate that the state must me more constant if it wanted to reach the projections that many researchers are proposing. The telemetry also has to be tasted in a bidirectional system.

2) The Second Phase: implicate the successfully development of each one of the elements that need to be technological mature in the first phase and once finished they must be standardized with the aim of promote its production massively.

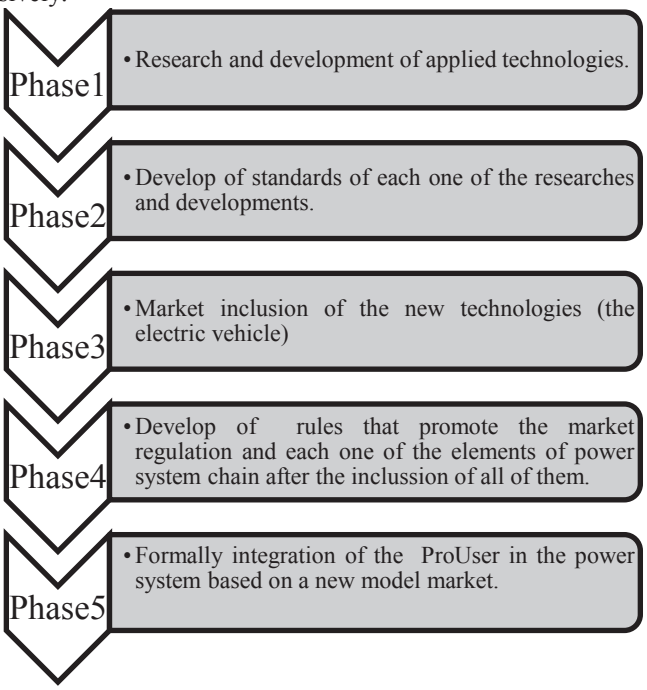

Figure 5. Scheme line to include the smart grids in the power system

3) The third phase makes reference to the inclusion of the technologies developed and standardized into the power system as is the case of the electric vehicle.

4) The fourth phase: will be reached until the inclusion of all the elements that integrates the smart grids and they have to be tested during their operation. This period could be called as a *"taste period for smarts technologies"* and after that there must be a regulation of all these elements and specify their restrictions and objectives in the chain.

5) Finally, the fifth phase is the inclusion of the smart users or ProUsers that will be able to interact with the market and be self-sustaining.

V. CONLUSIONS

As an outcome of this survey was to focus the lector in which of the phase is Colombia and that the concept of Smart Grid could be understand for everyone with the aim of focus all the researches into the same line. Also it is important to take into account the participation of the state that will be the promoter of this implementation and will guide to integrate all the elements that are needed.

It cannot be talked about smart grid if there only renewable system that is being applied because this is just one element of smart grids. It cannot be confused telemetry with smart grid basically because the telemetry is just control and measurement and will be also just an element of smart grid. It cannot be consider a home automation that could include renewable energy as a Smart Grid. They are only a possible ProUser figure.

All these elements that were mentioned are needed and must be developed and implemented successfully for that reason Colombia will be working in Smart Grid but this is the global line of investigation that integrates: Renewable systems, efficiency, URE, power system, control and automation and economy energy management.

REFERENCES

[1] A. Sinha,, S.Neogi, "Smart grid initiative for power distribution utility in India" IEEE press. India. 2011.

[2] D. Diaz. "Esquema de incorporación de las Smart Grids en el sistema de potencia Colombiano. Universidad Pontifica Bolibariana. Colombia. 2011.

[3] Energia y Sociedad. "Smart grids: redes eléctricas inteligentes". España. Marzo de 2010.

[4] E. Heiskanen, K. Matschoss. "Exploring emerging customer needs for smart grid applications" Germany. IEEE Press. 2011.

[5] G. Tang, "Smart grid management & visualization", smart power management system. Graceroce International Corporation. Toronto, Canada. IEEE press. 2011.

[6] J. Morales, A Gomez "La red inteligente: ahorro energético y telecomunicaciones. Convergencia con la red eléctrica y desarrollo sostenible" L&M Data Communications S.A. October 2006.

[7] M. Hashmi, K. Mäki "Survey of Smart Grid Concepts, Architectures, and Technological Demonstrations Worldwide". IEEE . Finland. 2011.

[8] Observatorio Industrial del Sector de la Electrónica, Tencologías de la Información y Telecomunicaciones. "Smart Grids y la evolución de la red eléctrica. Centros tecnologicos de españa". Madrid España. Diciembre de 2011.

[9] W. Mendoza, S Fujji "Smart grids tecnologia y tendencias: integración con sistemas SCADA/EMS/DMS," Decimo tercer encuentro regional iberoamericano de CIGRE. Operación y control de sistemas. 2009.

AUTHORS INDEX